AERODYNAMIC PASSIVE CONTROL SYSTEMS OF THE SPACE OBJECTS ORBITAL MOTION

ANATOLII ALPATOV, ERIK LAPKHANOV, OLEKSANDR PALII

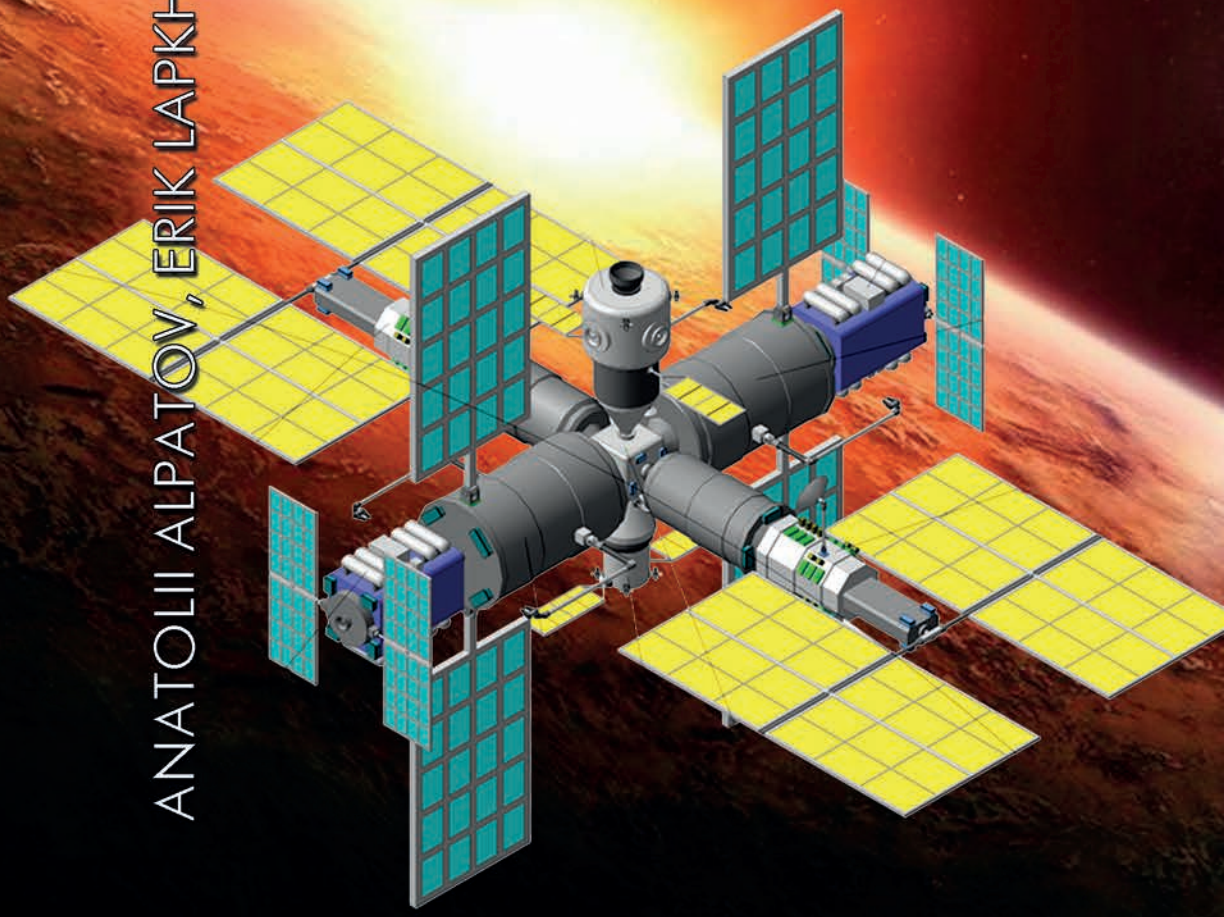

STATE SPACE AGENCY OF UKRAINE
NATIONAL ACADEMY OF SCIENCES OF UKRAINE
INSTITUTE OF TECHNICAL MECHANICS

ДЕРЖАВНЕ КОСМІЧНЕ АГЕНТСТВО УКРАЇНИ
НАЦІОНАЛЬНА АКАДЕМІЯ НАУК УКРАЇНИ
ІНСТИТУТ ТЕХНІЧНОЇ МЕХАНІКИ

АНАТОЛІЙ АЛПАТОВ, ЕРІК ЛАПХАНОВ, ОЛЕКСАНДР ПАЛІЙ

АЕРОДИНАМІЧНІ СИСТЕМИ ПАСИВНОГО КЕРУВАННЯ ОРБІТАЛЬНИМ РУХОМ КОСМІЧНИХ ОБ'ЄКТІВ

ПРОЄКТ
«УКРАЇНСЬКА НАУКОВА КНИГА
ІНОЗЕМНОЮ МОВОЮ»

КИЇВ
АКАДЕМПЕРІОДИКА
2024

ANATOLII ALPATOV, ERIK LAPKHANOV, OLEKSANDR PALII

AERODYNAMIC PASSIVE CONTROL SYSTEMS OF THE SPACE OBJECTS ORBITAL MOTION

PROJECT
«UKRAINIAN SCIENTIFIC BOOK
IN A FOREIGN LANGUAGE»

KYIV
AKADEMPERIODYKA
2024

https://doi.org/10.15407/akademperiodyka.527.172
UDC 629.78.076
A53

Reviewers:

M.D. KOSHOVYI, Professor of the Department of Intelligent Measurement Systems and Engineering at the National Aerospace University named after M.E. Zhukovsky "Kharkiv Aviation Institute", Doctor of Technical Sciences, Professor

O.V. GOLUBEK, Professor of the Department of Cybersecurity and Computer-Integrated Technologies at Oles Honchar Dnipro National University, Doctor of Technical Sciences

V.P. POSHYVALOV, Deputy Director of the Institute of Technical Mechanics of the National Academy of Sciences of Ukraine and the State Space Agency of Ukraine for Scientific Work, Doctor of Technical Sciences, Professor

Approved for publication by Institute of Technical Mechanics of the National Academy of Sciences of Ukraine and the State Space Agency of Ukraine (September, 14, 2023, Protocol No. 7)

The publication was funded within the framework of the Targeted Complex Program of the NAS of Ukraine "Scientific Bases of Functioning and Providing for Conditions for the Development of the Scientific and Publishing Complex of the NAS of Ukraine"

Alpatov A.P.

A53 Aerodynamic passive control systems of the space objects orbital motion / Anatolii Alpatov, Erik Lapkhanov, Oleksandr Palii; National Academy of Sciences of Ukraine, State Space Agency of Ukraine, Institute of Technical Mechanics. — Kyiv: Akademperiodyka, 2024. — 172 p.

ISBN 978-966-360-527-2

The monography considers the features of the design of space aerodynamic systems for passive control of spacecraft. One of the purposes of using this technology is the deorbiting of space debris fragments from working orbits. The classification of the aerodynamic deorbiting system has been proposed. Classes of aerodynamic systems are divided according to various criteria such as: the degree of stiffness of the aerodynamic element, according to the method of forming the aerodynamic deorbit system, according to the modularity of the design of the aerodynamic element, into groups using the transformation of the design elements of the object, depending on the type of material, etc.

For scientific and engineering workers working in the field of rocket and space technology, as well as for graduate students and students of relevant specialties.

UDC 629.78.076

ISBN 978-966-360-527-2

CONTENTS

CHAPTER 6

SPECIALIZED INFLATABLE AERODYNAMIC SYSTEMS

ABBREVIATIONS

ADS — aerodynamic deorbiting system
AE — aerodynamic element
AOCS — attitude orbital control system
ASS — aerodynamic shading systems
BNS — ballistic and navigation support
BRF — body reference frame
CFS — thin-walled film shell
COM — centers of mass
DS — deployment system
EDSTS — electrodynamic space tether system
EMF — Earth magnetic field
FMI — flexible multi-impact
FSD — fragment of space debris
HDC — hibrid deorbiting system
IRVE — Inflatable Re-Entry Vehicle Experiment
IS — inflation system
LBS — load-bearing structure
LCP — liquid crystal polymer
LEO — low Earth orbit
LGC — Local geodetic coordinates
LTP — The local tangent plane coordinates
LV — launch vehicle
LVLH — Local Vertical Local Horizontal Reference Frame
MLI — multilayer material for isolation
MLSO — modular large-sized space objects
MMOD — micrometeoroid and orbital debris
NASA — National Aeronautics and Space Administration
OGRF — Orbital General Reference Frame

PBD — pneumatic braking device
PTFE — polytetrafluoroethylene
RAAN — the right ascension of the ascending node
RDV — Russian Descending Vehicle
SBRF — Spacecraft Body Reference Frame
SBSLS — space-based shading and lighting system
SC — spacecraft
SCR — spacecraft-receiver
SCT — spacecraft transmitter
SD — space debris
SDO — space debris object
SIP — space industrial platform
SS — storage system
SSC — service spacecraft
STW — Orbital Associated Upper Reference Frame
TP — technological process

PREFACE

The rapid creation of new space technologies and the active development of space around the Earth over the past half century have led to the accumulation of a significant number of objects of man-made origin in Earth's orbits. In turn, a significant number of these space objects of man-made origin do not function, and hence form the so-called space debris (Alpatov, 2012). The main sources of space debris, as a rule, are the upper stages of launch vehicles and spacecraft at the end of their active lifetime or in case of premature failure. Also, the sources of space debris are debris that has been formed as a result of the collision of space objects (for example: the collision of the artificial satellites of the Earth «Kosmos-2251» and «Iridium 33» in 2009) or the explosion of a space object (high-energy explosion of the artificial satellite of the Earth «Nimbus-6» on May 1, 1991). Based on this, the American astrophysicist Donald Kesler revealed the possible consequences of the rapid increase in fragments of space debris in orbits as a result of the collision or destruction of space objects into a large number of fragments. This effect shows the possibility of an avalanche-like increase in fragments of space debris, which is the result of a «chain reaction» of collisions, as a result of which some orbits may even be unusable (Kessler, 2010). The growth dynamics of the number of cataloged space debris objects (SDO) and their fragments, which is published quarterly in the analytical reports of the National Aeronautics and Space Administration (NASA), shows that as of November 2019, about 14,800 space debris objects have been cataloged in near-Earth orbits (The Orbital Debris Quarterly News, 2020). Also, it has been determined that the greatest concentration of space debris is observed in low, close to circular, Earth orbits up to 2,000 km high, as well as in geosynchronous and high elliptical communication orbits within 20,000 km in the range of inclinations of 50...60° (Alpatov, 2017a, Alpatov, 2019a).

Today, there are two methods of near-Earth space protection from pollution, which consists of the active and passive means

used for SDO deorbiting (Lapkhanov, 2019a; Palii, 2012; Dron, 2014; Alpatov, 2018; Alpatov, 2019b). Space propulsion systems and electromagnetic systems are among the active launch vehicles that spacecraft are equipped with (Lapkhanov, 2019, Palii, 2012). The principle of operation of such systems is based on creating a braking pulse for the space vehicle, after the end of its lifetime, to reduce the altitude of the orbit and further burning in the dense layers of the atmosphere. The advantage of using these systems is the speed of operation and the presence of a significant number of experimental confirmations of successful deorbiting. However, propulsion and electromagnetic systems require the presence of fairly significant reserves of fuel and electrical energy on board the space vehicle for their operation and the efficiency of the orientation and stabilization systems, which is difficult to ensure after the end of the lifetime. Other subspecies of active systems are service spacecrafts (SSC) with contact and non-contact removal methods (Lapkhanov, 2019a; Alpatov, 2018; Alpatov, 2019b). However, the application of SSC is a rather complex, multi-stage and energy-consuming task that requires significant resources for its implementation and increases the cost. Based on this, the beneficial effect of SDO removal with the help of SSC may not always exceed the total costs associated with the use of SSC, which calls into question the absolute expediency of this method.

In turn, passive means practically do not require fuel and on-board energy for their operation. Known passive means under development are aerodynamic systems (ADS) (Lapkhanov, 2019a), (Alpatov, 2015; Alpatov, 2017b; US patent for invention — 6830222…, 2004), electrodynamic space tether systems (EDSTS) (Myshchenko, 2018; Myshchenko, 2017; Myshchenko, 2020) and plasmadynamic devices with magnetic braking systems (Kawashima, 2018; Shuvalov, 2018; Shuvalov, 2016; Lapkhanov, 2019b). A characteristic feature of the functioning of these systems is the creation of a braking force due to an increase in the ballistic coefficient of the spacecraft. However, despite the almost complete absence of fuel and on-board energy consumption for operation, passive means also have their drawbacks. Thus, for EDSTS, there are difficulties with deployment and stabilization of the relative position of the tether, aerodynamic deorbiting systems are exposed to atomic oxygen and factors of outer space, which can damage the shell or sail element, and plasmodynamic devices have not been tested in outer space. In addition, when using the listed systems, the deorbit time is quite significant, and the maximum altitude of use is 900—1000 km, which may not be suitable for all orbits.

Based on this, a new concept has appeared, which consists of creating a hybrid means of deorbiting, which combines the advantages of several existing active and passive means of deorbiting. The use of such an approach expands the limits of the effective use of existing deorbit systems. For example, in (Dron', 2019a), the creation of a hybrid propulsion-aerodynamic system has been proposed, which allows for the minimization of fuel consumption for the deorbited SDO from high orbits. In the research paper (Pfisterer, 2011), a hypothesis has been put forward about the possibility of using electromagnets to stabilize aerodynamic sailing elements to maintain the maximum value of the ballistic coefficient of the spacecraft.

CHAPTER 1

ANALYSIS OF SPACECRAFT OBJECT REMOVAL SYSTEMS FROM LOW-EARTH ORBITS

1.1. The problem of near-Earth space pollution

The problem of the growing amount of space debris is one of the main global environmental threats facing humanity. According to data from the US NASA, as of April 2023, about 16000 man-made space debris (SD) objects have been cataloged (The Orbital Debris Quarterly News, 2020). The main sources of SDO are the upper stages of launch vehicles (LV) and spacecraft (SC) after the end of the lifetime. According to the generally accepted classification, SDO are divided into three categories: small, medium and large (Table 1.1) (Lapkhanov, 2019a).

In 1987, the American astrophysicist Donald Kessler revealed the possible consequences of an uncontrolled increase in SDO in orbit due to the collision of two large objects (The Orbital Debris Quarterly News, 2020). Later, this effect was named in honor of the scientist «Kesler effect» and showed the possibility of an avalanche-like increase in SDO due to a «chain reaction» of collisions, as a result of which some orbits may even be unusable (Kessler, 2010).

Every year, the risk of implementing the described scenario increases. After the first recorded collisions of active spacecraft with space debris (Alpatov, 2012), considerable attention has been paid to this problem. Thus, aerospace agencies from all countries began to develop recommendations aimed at preventing the creation of new space debris from new launch campaigns, thus making the problem global. However, according to (The Orbital Debris Quarterly News, 2020), there are already a large number of threatening SDO objects in Earth's orbits, the deorbiting of which is necessary to prevent the Kessler scenario.

Thus, the highest density of SDO is observed in low Earth orbit (LEO) (Fig. 1.1).

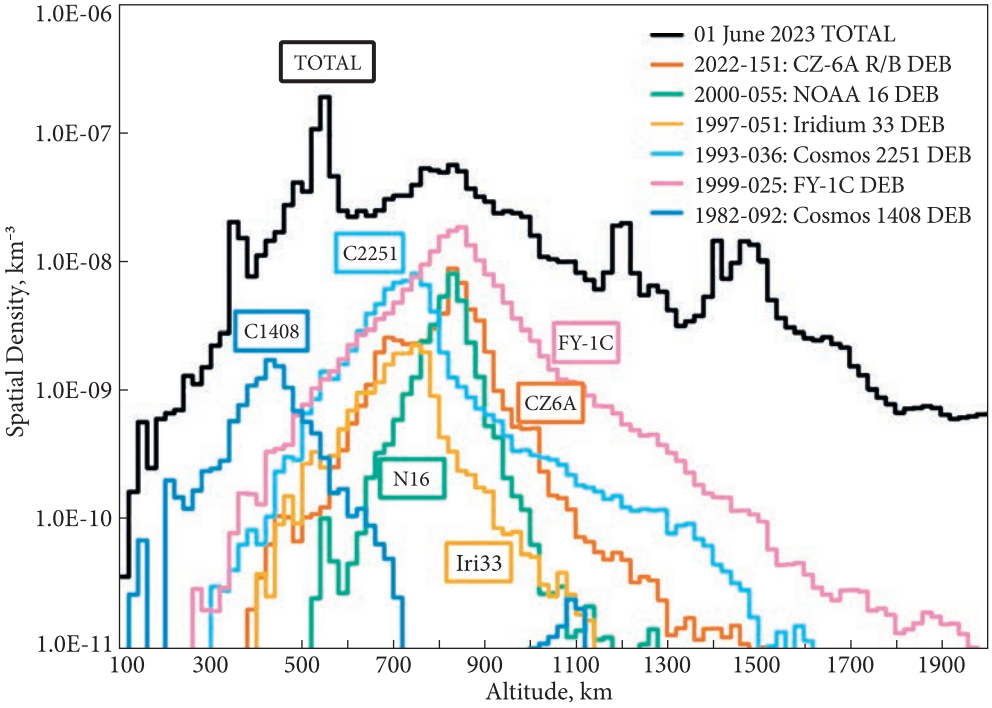

Fig. 1.1. Distribution of SDO density at the LEO altitudes

Table 1.1. **Classification of space debris objects**

Classifier	Category		
	Small	Medium	Large
The largest diameter, m	<0.01	0.01—0.1	>0.1
Possible consequences of a collision	Possible damage	Partial / complete destruction	Complete destruction
Protection possibility	Possible	Impossible	Impossible
Observability	Unobservable, forecasts derived from statistical models are being used	Partially monitored	Monitored
Estimated number	>100 million	Ca. 500 000	>21000
Share of mass from the total mass of OSD	Not established	5%	95%

From the distribution of the SDO mass density, the most polluted regions of the LEO are located at altitudes from 500 to 1000 km. SDO deorbiting from the given altitude range can be carried out using both an active method and a passive method of deorbiting. Passive methods involve the use of existing physical fields or the external environment to reduce the SDO orbit altitude and with subsequent combustion in the dense atmosphere. At the indicated altitudes, from 500 to 1000 km, the force of aerodynamic braking and the effect of plasmodynamic braking (Lorentz force) can be used to remove the SDO (Lapkhanov, 2019a, Myshchenko 2018; Myshchenko, 2017; Myshchenko, 2020; Kawashima, 2018; Shuvalov, 2018; Shuvalov, 2016; Lapkhanov, 2019b). Active methods are based on the creation of an artificial impact on the object of space debris, or the use of an additional resource of the spacecraft's propulsion systems.

1.2. The current state of development of active systems for the space debris objects removal from working orbits

Active means of SDO removal are based on the use of SSC or additional resources of spacecraft propulsion systems for removal from working orbits after the end of the shell lifetime period (Palii, 2012, Lapkhanov, 2019a).

The notion of «SDO remove» will be understood as a part of the deorbiting process, during the initial transfer of SDO to orbits where the term of lifetime corresponds to the requirements.

Means of removal involving the use of SSC can be divided into two groups:

- contactless means of removing space debris objects, based on contactless impact (generating of ion beam, laser, etc.) from the SSC side on the SDO with the absence of direct mechanical connection (Alpatov, 2019b, Bombardelli, 2011; Alpatov, 2016a; Bombardelli, 2012; Khoroshilov, 2017; Khoroshilov, 2018);
- contact means of SDO removal, using mechanical contact of SSC to SDO (mechanical manipulators, nets, cable systems, etc.) (Alpatov, 2013a; Shan, 2018; Pelton, 2015; Xin, 2011; Yoshida, 2004; Han, 2015; Moody, 2016; Wormnes, 2013; Benvenuto, 2015; Patent for invention US8979034, 2015; Dudziak, 2015).

Without the use of SSC, active removal systems use an additional resource of the spacecraft's propulsion systems, or, if necessary, the spacecraft are equipped with additional propulsion systems for generating a braking pulse. In turn, to solve such a problem, various types of propulsion systems can be used, such as liquid, solid fuel and electrojet rocket propulsion systems. The use of such systems has a rather deep scientific and practical justification, because it has been a topic of research in space science and technology since its inception. The principle of operation of such systems is based on the formation of a braking pulse, the vector of which is directed in the opposite direction to the main vector of the spacecraft's motion. In this case, the amount of spacecraft motion per turn decreases and the spacecraft begins a gradual descent to a certain altitude of the orbit, where its lifetime meets the requirements (Lovell, 2004). It should be noted that when using

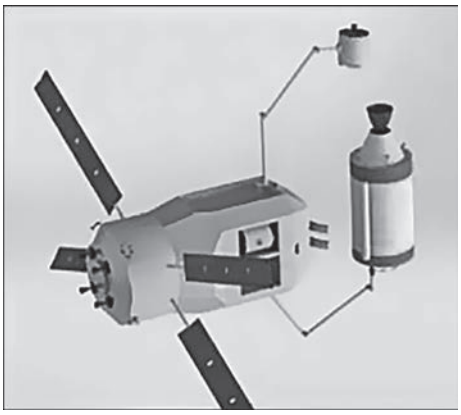

Fig. 1.2. An example of the manipulator development for capturing the upper stages of launch vehicles

Fig. 1.3. An example of the special nets development with a cable connection for capturing SDO

active propulsion means for SDO removal, the process of deorbiting is carried out in a fairly short period of time. However, it should be noted that for this it may be necessary to have a significant amount of fuel on board the spacecraft to form a braking impulse, as well as on-board energy to provide the necessary orientation. Ensuring the reliability of the main systems of the spacecraft, the functioning of which is necessary for the implementation of this removal method, after the end of the lifetime, also causes additional difficulties. Thus, when designing such a class of removal means, it is necessary to take into account the redundancy of the main systems of the spacecraft, which leads to additional costs. Otherwise, when using the main systems of the spacecraft, the shell lifetime period must be determined taking into account the deorbit period, which can reduce the time of the spacecraft's useful operation. Based on this, it can be concluded that the advantages of using active propulsion systems are speed and deep scientific and practical justification. Thus, in the presence of SDO, which poses a significant danger to functioning spacecraft in orbit with a high density of spacecraft, it can be quickly removed with the help of propulsion systems in a fairly short period of time.

In turn, active means involving the use of SSC have a much larger range of effective applications. The use of contact removal means on SSC (Alpatov, 2013a, 2019b; Shan, 2018; Pelton, 2015; Xin, 2011; Yoshida, 2004; Han, 2015; Moody, 2016; Wormnes, 2013; Benvenuto, 2015; Patent for invention US8979034, 2015;, Dudziak, 2015) can allow solving two main tasks of clearing the near-Earth space: transfer of SDO to burial orbits and transportation of SDO to appropriate processing complexes within the framework of the concept (Alpatov, 2013b, , 2018). However, as shown in (Lapkhanov, 2019a), when using a grip with a rigid connection, such as mechanical manipulators (Fig. 1.2), there can be significant difficulties in capturing rotating SDO.

Taking this into account, another method of capture using a flexible connection has been proposed. Systems with a flexible connection include special

catching nets (Fig. 1.3) (Benvenuto, 2015) and harpoon systems with cable tugs (Dudziak, 2015).

It is rational to use this class of active contact systems for tasks of SDO transportation (Alpatov, 2013b, 2018) or tasks of transfer to burial orbits. However, when analyzing the possibility of using tugs with cable ties, difficulties have been also revealed that may arise during further practical implementation (Lapkhanov, 2019a). Thus, when transporting SDO with the help of SSC with a cable connection, a necessary condition is to ensure stable movement of the connection after turning on the SSC thruster. In addition, the activation and operation of the SSC thruster can lead to longitudinal oscillations of the cable system and excite the angular movement of the SDO, which can affect the stability of the link movement. The occurrence of such oscillations can occur in the case of significant leverage between the point of attachment of the rope and the SDO center of mass and lead to entanglement of the rope itself. An impulse effect on the cable system when the SSC engine is turned on can also lead to a dangerous convergence of the SSC with the SDO and their subsequent collision.

Thus, control difficulties in ensuring the necessary stabilization of SSC-SDO connections when using active contact systems and insufficiently complete scientific and theoretical substantiation of the possibility of their mass use create difficulties in assessing the effectiveness of these means of SDO removal. At the same time, this class of systems can be a fairly effective technology to solve the problems of the concept (Alpatov, 2013b, 2018), but it requires significant refinements for further practical implementation.

It should be noted that contactless active removing systems are also widely discussed among aerospace scientists. The most well-known example of systems for active non-contact SDO removal from low Earth orbits (LEO) is the space «shepherd with an ion beam» system, which was studied in the LEOSWEEP project (Alpatov, 2019b, 2016a; Bombardelli, 2011, 2012; Khoroshilov, 2017, 2018).

The concept of the «shepherd with an ion beam» is based on the use of the flow of ions as a means of transmitting a power pulse from the SSC to the SDO (Alpatov, 2019b, Bombardelli, 2011, 2012). According to the conducted studies (Alpatov, 2019b), the force transmitted by the ion beam from the SSC to the upper stages of the Cyclone 3 and Cyclone 4 launch vehicles is about several mN, which can be compared to the thrust of space microjet propulsion systems. In [30], with the help of computer simulation, it has been calculated that the speed of SDO removal from the ranges of LEO, with an altitude of 600—700 km is about 1 km per day, and taking into account the reduction of SDO, it increases. Taking into account these characteristics (Khoroshilov, 2018), the time of transfer from an altitude of 640 km to an altitude of 340 km of the 1575 kg SDO was about six months. Also, it was shown (Alpatov, 2019b, Khoroshilov, 2017, 2018) that during the period of SDO removal, there is a theoretical possibility of maintaining the robustness of controlling the position of the SSC relative to the SDO and maintaining the permissible accuracy of pointing the ion beam at the SDO. Thus, the

possible advantages of SDO removal (Alpatov, 2019b) with the help of a space «shepherd with an ion beam» can be emphasized in the following points:

- the relatively small mass of the SSC, which is 10% of the mass of the SDO (however, it is worth emphasizing that this condition is valid only for SDO weighing more than 1.5 tons);
- lack of direct contact with the SDO;
- the theoretical possibility of multiple use under certain conditions.

However, SSC with an ion beam also has many certain disadvantages, which makes this system quite complex and increases its cost:

- the operation of SSC requires a ground flight control center to adjust the trajectory and position relative to the air traffic control system, which requires additional costs;
- significant costs of on-board electrical energy, taking into account costs for compensation of the ion beam action;
- the structural complexity of the system, which requires significant costs for the creation of a high-tech system — a beam ion gun.

Considering the listed advantages and disadvantages of the « shepherd with an ion beam» concept, it can be concluded that it has certain high indicators according to some efficiency criteria (Alpatov, 2019b), but is very costly and unattractive from an economic point of view. In turn, the use of «shepherd with an ion beam»refers to fairly fast methods of SDO removal from LEO, which has a high reliability of SSC in comparison with contact capture systems. Thus, with a possible hypothetical further practical implementation, the «shepherd with an ion beam» is recommended to be used in orbits with a critical level of contamination, for SDOs that are already in orbit and are not equipped with on-board removal systems (stages of launch vehicles, large fragments of the spacecraft, etc.).

1.3. Analytical review of passive space debris deorbiting systems

Passive removal methods include aerodynamic inflatable and sailing systems, solar sails, electrodynamic cable systems, and electromagnetic devices.

1.3.1. Aerodynamic deorbit systems

The harbingers of the creation of ADS were inflatable space aerodynamic systems. This class of space systems is used in spacecraft designs and its inflatable elements. For example, frames for the deployment of solar batteries, antenna surfaces of space telescopes, frames for straightening the panels of a solar sail, and rods for carrying scientific instruments to great distances from the spacecraft.

An example of an inflatable space aerodynamic system is the «Echo» spacecraft (Fig. 1.4) (The Echo-I…, 1964). Echo-1 spacecraft has been designed as an

Fig. 1.4. Echo inflatable satellite

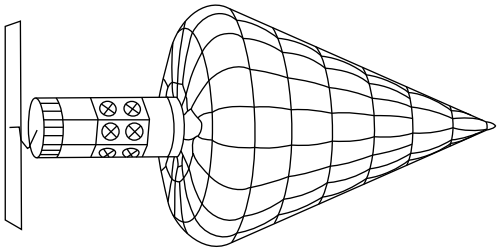

Fig. 1.5. Inflatable satellite «Misty»

experimental, spherical, radio broadcasting station to operate in a circular orbit around the Earth to establish worldwide communication. The spacecraft has been made of a polyethylene terephthalate polymer film with a thickness of $1.27 \cdot 10^{-5}$ m, with an external coating of an aluminum layer $2.2 \cdot 10^{-7}$ m thick. The thin layer of aluminum performed two functions: reflection of the incident signal, because aluminum has a reflection coefficient greater than 0.97 in the frequency range of 400—10000 MHz, and protection of the polymer film from the impacts of ultraviolet radiation.

Inflatable systems are used to ensure low visibility of the spy satellite «Misty» (Fig. 1.5) (US Patent No. 5345238, 1994). To shield the satellite, it is proposed to use an inflatable device in the shape of a cone, which is made of a synthetic polymer film of the Kapton or Mylar type ≈1 mm thick, covered with an electrically conductive reflective material, usually a thin layer of gold or aluminum. The suppression of the spacecraft signature includes additional mechanisms:

- an inflation device (contains a powder-like agent that turns into gaseous form under the influence of solar radiation);
- a substance of a special chemical composition that covers the inner walls of the case, which hardens under the impact of ultraviolet radiation and gives the structure the necessary rigidity;
- preparations for degassing and dehydration of an inflatable cone;
- mechanisms to change the orientation of the cone relative to the spacecraft.

Before the spacecraft launch, the film cone is tightly folded in a sealed container and it is deployed using a special mechanism after the satellite is launched into orbit. Under the impact of solar radiation, the powdered agent turns into a gaseous state and gradually inflates the film. The film takes a given conical shape, which is fixed by hardening a special composition applied to its inner walls. As a result, a strong and light structure of the given configuration is formed.

In recent years, several projects of inflatable space antennas have appeared. The frame of such an antenna can be made in the form of an inflatable torus, to which reflective and auxiliary surfaces made of synthetic films are attached. At the same time, both surfaces form a closed volume, the creation of excess pressure

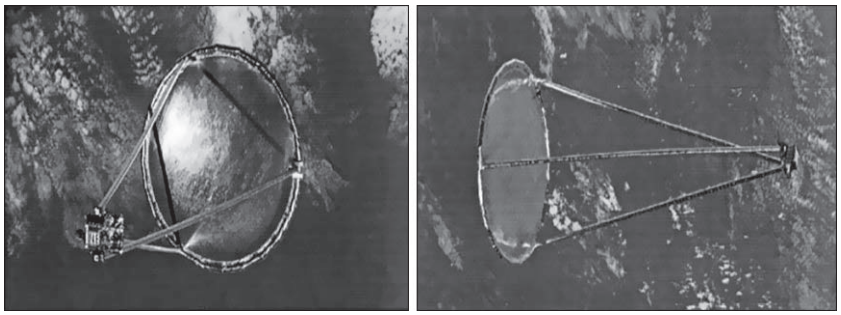

Fig. 1.6. Inflatable antenna deployed in orbit

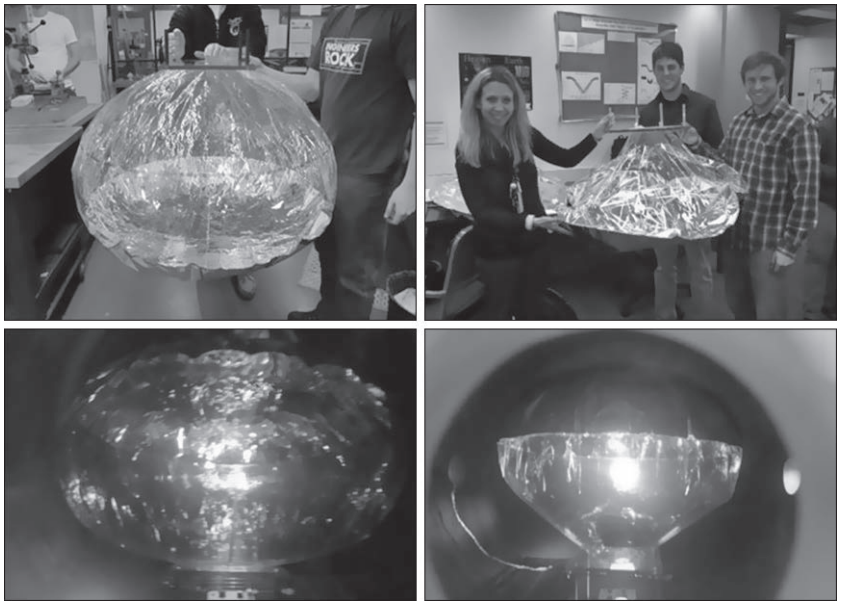

Fig. 1.7. Project of inflatable antenna for CommCube-1 spacecraft

in which provides surface tension. The irradiating device is attached to the torus using a system of braces.

To the reflecting surface, made of metallized film and having the shape of a paraboloid of rotation or a sphere, a grid of quartz threads can be attached to maintain geometric dimensions and reduce temperature deformations.

Inflatable structures of space antennas cause their very compact stacking and are characterized by a small ratio of the structure mass to the area of the mirror deployment, equal to 0.15 to 0.25 kg/m^2. However, in the manufacture of inflatable structures, technological difficulties arise since the frame has closed cavities, so the seams must provide high tightness, which during the operation of a space antenna of a similar design must accurately withstand the pressure ratio the torus and inside the main volume of the antenna.

The main disadvantage of inflatable space antennas is that when they are pierced by meteoroid bodies, they lose their efficiency. However, inflatable space antenna designs may be widely used in the future if they are designed and built using formable and self-curing materials with appropriate characteristics.

An example of the use of inflatable aerodynamic systems is the space experiment of deploying an inflatable antenna in orbit (Freeland, 2014). The experiment has been carried out as part of the Space Shuttle STS-77 mission. The antenna with a diameter of 14 m (Fig. 1.6) was fixed on three sliding supports 28 m long, fixed on the satellite.

Initially, the entire structure was placed in a compact transport container measuring about 2 × 3 × 1 m, and its weight was 60 kg. The internal pressure in the antenna was about 0.003 mm Hg. Art. The experiment tested the procedure for deploying (inflating) the antenna from the container and the possibility of using it for its intended purpose — for transmitting or receiving signals.

Inflatable space antennas have found application on space vehicles of the CubeSat class. An example is the inflatable antenna (Fig. 1.7) for the CommCube-1 spacecraft (Babuscia, 2013).

For the tests, two Mylar antennas have been made, one of which, when inflated, resembled a cone in shape, the other a cylinder. After determining the optimal assembly method for each variant, the researchers were able to fit the antenna (and some benzoic acid) into 10 cm3. In a vacuum chamber, where benzoic acid turned into a gaseous state and filled the antenna, the developers tested the electromagnetic properties of the inflatable device. The cylindrical inflatable antenna worked a little better.

In (Lindell, 2006) describes the intention of NASA by the forces of the Langley Research Center, the Mechanical Analytical Society, the Douglas firm, and other partners to develop the mock-up shown in Figure 1.8, structurally very similar to the Russian Descending Vehicle (RDV) from the Demonstrator PBD to work out within the framework of the IRVE (Inflatable Re-Entry Vehicle Experiment) technology of RDV with an inflatable braking device.

US specialists recognize that aerodynamic screens of inflatable construction have advantages over traditional rigid brake screens. Their use allows you to save the volume under the LV fairing for placing the payload, increase its mass, not limit the size of the screen to the available volume under the fairing, etc. One of the last development stages of the IRVE project to date includes a flight experiment that took place in August 2009. The launch of the model RDV with PBD was carried out with the help of a launch vehicle, which raised the model to an altitude of about 210 km.

At this altitude, the mock-up RDV with PBD (PBD mass — 40 kg) was separated from the LV and it began its free fall. During the fall, the PBD was opened and inflated. The model entered the atmosphere at a speed of about 1700 m/s (Mach number ≈5). 20 minutes after launch, the RDV crashed in the Atlantic Ocean.

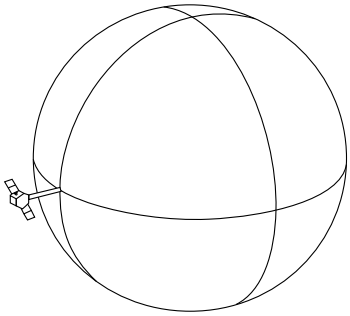

Fig. 1.9. Device for orbital lowering of space objects

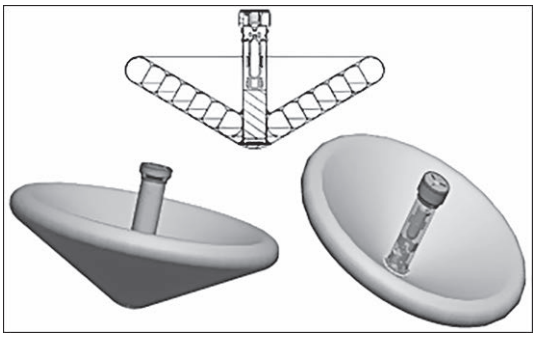

Fig. 1.8. Project «IRVE»

At orbits up to 2000 km, the atmosphere exerts an impact on the spacecraft motion, in turn, the atmosphere exerts a significant braking effect for space systems with high values of ballistic coefficients at altitudes up to 700—800 km. Under normal conditions, due to the relatively small cross-section of the middle, the impact of atmospheric flux is insignificant and the force of the aerodynamic perturbation does not create the necessary braking effect to deorbit the SDO from orbit. As a result, a number of methods have been proposed to increase the characteristic area of the SDO, the main of which is the use of inflatable aerodynamic deorbit systems (Alpatov, 2015, 2017b; US patent for invention № 6830222…, 2004), (Rasse, 2014; Roddy, 2016; Andrews, 2011; Viquerat, 2014; Patent of Ukraine for invention № 109318, 2015; Patent of Ukraine for invention № 113747, 2017; Patent of Ukraine for invention № 109194, 2015), which are deployed due to the use of special inflation and aerodynamic systems sailing film systems deployed using special mechanical devices and combined (US patent for the invention № 6550720; Gloyer, 2002; Patent of the EU for the invention № EP1989112; Dupuy, 2010; Patent application for the invention No. WO2012092933; Maesen, 2007; Roberts, 2002; Alhorn, 2010, 2011; Anderson, 2011; Sinn, 2012; Wolanski, 2012; PW-SAT2…, 2014; Williams, 2017; Sproewitz, 2017; Visagie, 2015; MMA Design…, 2013; Stohlman, 2014).

Inflatable aerodynamic deorbit systems. The accumulated experience of creating inflatable space aerodynamic systems served to create the ADS. ADS can be divided into groups:

1) ADS based on single or grouped shells;

2) film frame and non-frame constructions of ADS, which are deployed;

3) ADS with the use of space object structural elements to reduce the term of their ballistic existence;

4) active ADS.

Aerodynamic deorbit systems based on single or grouped shells. The system given in (US patent for invention № 6830222…, 2004) (Fig. 1.9) serves as an example of the use of single shells in the creation of an ADS.

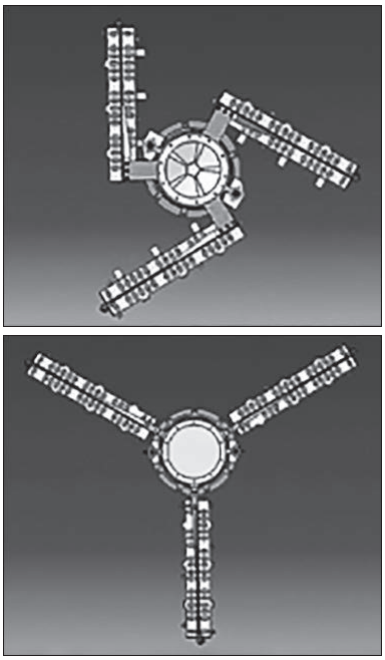

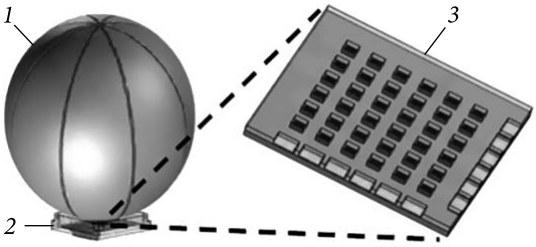

Fig. 1.11. NASA Proposed Inflatable Retraction System for 1U, 2U, 3U CubeSats. *1* — inflatable mini balloon, *2* — packaging device, *3* — control board

◀

Fig. 1.10. IDEAS mechanical design for inflatable ADSs

The proposed ADS is made in the form of an inflatable sphere made of a soft elastic shell. Inflation of the shell allows for an increase in the cross-sectional area and accordingly increases the strength of the aerodynamic resistance, which will lead to a gradual decrease of the spacecraft to the dense layers of the atmosphere. This system will make it possible to increase the ballistic coefficient of the deorbited object by two orders of magnitude. The casing is expected to be inflated using on-board gas reserves. This system is attractive from the point of view of simplicity and technical realizability, however, it has significant disadvantages that are revealed under the influence of space factors, in particular SF. Thus, if SF gets into the shell, the formation of a hole, violation of the shell sealing, loss of its shape and a sharp decrease in its efficiency are possible.

The development of inflatable aerodynamic systems for deorbiting the SDO (Fig 1.10) is one of the most researched issues in modern aerospace science and industry. Thus, thanks to the achievements obtained in the course of the IDEAS project, several optimizations have been determined for the inflatable aerodynamic deorbit systems of spacecraft from orbit at the end of the period lifetime. Based on the IDEAS building blocks, research has been conducted to achieve a better ballistic ratio (deployment area / system mass) for inflatable ADSs and to integrate panel placement constraints.

One of the main aspects of the mechanical design of IDEAS for inflatable ADSs is the modularity and scalability of the main components, for convenient placement on all types of spacecraft, as well as ease of stacking and layout (Fig. 1.14) (Rasse, 2014).

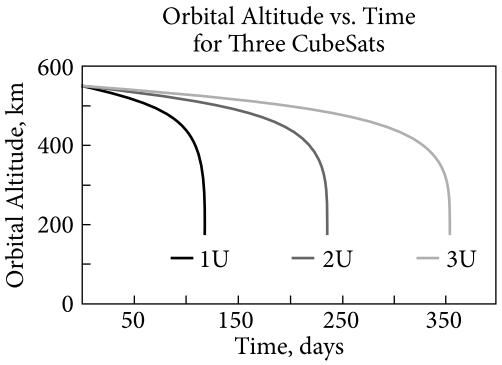

Fig. 1.12. The time of removal of cubesats 1U, 2U, 3U from orbit using a system with an inflatable mini balloon with a diameter of 1 m

Fig. 1.13. Inflatable ADS with protection of the SC from damage during reentry

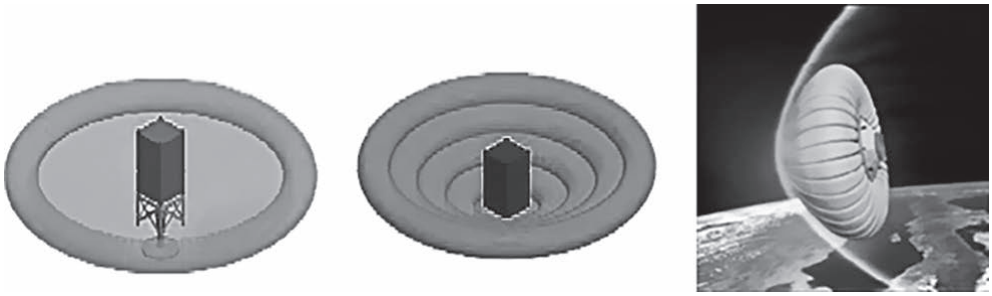

Thus, for NASA's 1U, 2U, and 3U cubesats, a system is proposed that includes an inflatable mini balloon, a packaging and deployment device, as well as an electronic control unit for the inflatable ADS (Fig. 1.11) (Roddy, 2016). The inflatable balloon consists of thin metalized polyamide films such as Kapton® HN, consisting of several lenticular crystals that form the spherical shape of the balloon and a subsystem package suitable for spacecraft integration.

When calculating the deorbit time from an altitude of 550 km to 180 km using this inflatable ADS for cubesats 1U, 2U, and 3U, we have obtained results that significantly exceed the requirements for the deorbit time of spent spacecraft in 25 years (Fig. 1.12).

It is worth noting that when conducting additional research on increasing or decreasing the diameter of the mini balloon, the lead time has changed significantly, proportional to the size of the inflatable ADS. It has been also established that this system can be designed to carry the entire range of small satellites (<180 kg) from orbits up to 1000 km high within the required time of 25 years.

In connection with the value of the materials used for the spacecraft creation, as well as the possibility of their secondary processing and use, the task of preserving spent spacecraft when they are deorbited from orbit has arisen. Thus, an approach has been proposed, which consists of the use of an inflatable ADS, which allows not only to remove the spacecraft from orbit, but also to preserve it from burning in the dense layers of the atmosphere and from destruction upon impact with the Earth, using the principle of a kind of «cocoon» and a damper (Fig. 1.13) (Andrews, 2011).

This system is designed as a stand-alone device that can be launched automatically by the spacecraft on a command basis or initiated after the end of its lifetime to accelerate deorbiting. Deployment is initiated by a latch mechanism that releases four spring-loaded hinged walls that slide apart to allow deployment and inflation of the torus. The choice of the shell material has been made taking into account the tests of several inflation mechanisms.

The cone consists of a high-temperature and high-strength commercially available fabric coated with a high-temperature flexible ablation coating. The tori consist of a thin-walled inflatable balloon that is sewn into a high-temperature fabric casing at a deployable base. The cone is attached to the heat sink, which is located at the end of the shock-damping mechanism. The system is planned to be tested on a CubeSat 3U class spacecraft.

The next deployable inflatable ADS consists of a cylindrical inflatable mast that serves as a support structure for the 10 square meter sail used in the InflateSail 3U cubesat demonstrated in the QB50 mission (Viquerat, 2014). In the unfolded state, the inflatable mast has a length of approximately 1 m and a diameter of 90 mm (Fig. 1.14).

The main purpose of the device is to stabilize the passive state due to the shift between the pressure center of the sail and the center of the satellite mass center. The inflatable mast folds up and in the folded configuration occupies no more than 63 mm of height in a cubic meter. The cylinder cover is an aluminum polymer laminate, and the inflation system consists of two small cold gas generators. Only one cold gas generator is needed for deployment and stiffness of the boom, the second is for redundancy. The inflatable rigid mast is designed for a long service lifetime in orbit (>15 years). Because the process of rigid deformation of aluminum polymer laminates does not require chemical reaction or softening solvents, and because cold gas generators have been demonstrated to exhibit gas storage for many years in space, this system is well suited for forming structural components in SDO deorbit missions or other long-duration missions. Other advantages of the system include its simplicity (no moving parts), its fundamentally light weight, and the possibility of creating such ADSs for larger spacecraft.

Multi-module inflatable ADS (Alpatov, 2015, 2017b), (Patent of Ukraine for invention № 109318, 2015; Patent of Ukraine for invention № 113747, 2017; Patent of Ukraine for invention № 109194, 2015) has received a rather in-depth study and scientific and theoretical justification. It has been determined that the creation of such structures allows for an increase in the reliability of inflatable ADSs. Thus, the use of multi-module inflatable aerodynamic elements allows the system to remain operational even in the event of space debris piercing the shell. Also, due to the use of a double shell, this design increases the reliability of the ADS when exposed to atomic oxygen and when electrostatic breakdown is possible.

Thus, it can be concluded that inflatable ADSs have a sufficient level of scientific and practical justification and are quite effective means of ADS removal. However, inflatable ADSs need to equip the spacecraft with additional inflation

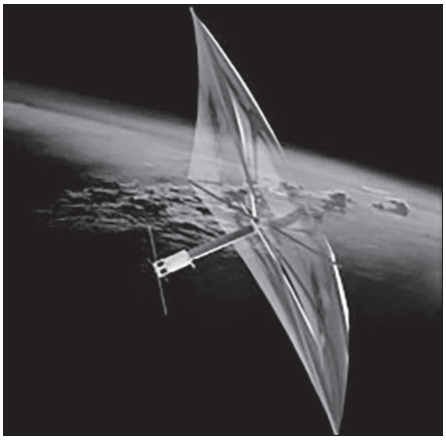

Fig. 1.14. ADS consisting of an inflatable mast and a sail

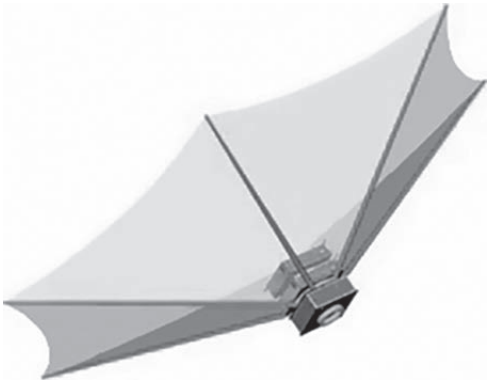

Fig. 1.15. Device for interorbital transfer of spacecraft

systems, and are subject to the impact of space factors, which can change the geometry of the aerodynamic elements and reduce their efficiency. Also, it is rather difficult to equip a space vehicle with an ultra-dense layout of the payload with inflatable anti-aircraft guns.

Aerodynamic sailing flat and frame shunting systems deployed by mechanical devices. Unfolding film structures represent a class of aerodynamic devices, which are made of various types of masts and sheets of thin film materials. In (US patent for the invention № 6550720; Gloyer, 2002) an inflatable combined transport device for the interorbital transfer of spacecraft is presented (Fig. 1.15). This device includes a fluid jet propulsion system and an aerodynamic braking device. The braking aerodynamic device is made in the shape of an umbrella from kapton material, which is covered on both sides with a thin layer of aluminum to increase strength. This device is designed to transfer a spacecraft from geostationary orbit (GSO) to a near-circular LEO by using the force of the aerodynamic resistance of the atmosphere at the perigee of the spacecraft orbit. Being in an elliptical transitional orbit, when the spacecraft reaches a perigee altitude of 155 km, this device deploys and begins to function. As soon as the required amount of kinetic energy is reduced, the device is either disconnected or folded up and stored on board the spacecraft. The development of this device is carried out by the company AeroAstro together with AFRL (Research Laboratory of the US Air Force). The designers of these companies presented several configurations of the device in the form of: balls, torus, umbrellas, etc. The design sample has been made in the form of an umbrella from six segments fixed on inflatable masts. Several ways of deploying the device have been considered: radial extension, radial unwinding, spiral deployment, and sliding folding. The membranes are made of fabric material, which is covered with a polyamide film for reinforcement. This device can also be used to carry out a maneuver to remove spacecraft from orbit after the end of their lifetime.

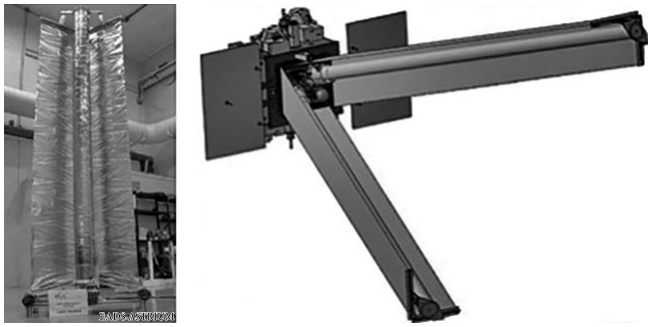

a *b*

Fig. 1.16. Device for deorbiting microsatellites *a* — experimental sample of the ADS; b — the ADS model

In (Patent of the EU for the invention № EP1989112; Dupuy, 2010) a device for satellites deorbiting from orbit is proposed (Fig. 1.16). The device is based on the use of an aerodynamic surface, which has been improved in such a way that the aerobraking device remains compact in the folded state, requires a small amount of energy for deployment — this makes its mass relatively small and gives high reliability, ensuring the possibility of its use at the end of the satellite's service lifetime.

In addition, the aerodynamic surface is designed in such a way that it performs the functions of an orientation system and a system of deorbiting the spacecraft from orbit after the end of its lifetime.

Once the airfoil is deployed, it contains at least one element of the airfoil, forming a three-dimensional structure consisting of at least two panels that pass along intersecting planes and form a dihedral angle.

In (Patent application for the invention No. WO2012092933), a device for the deorbiting of spent spacecraft of the «Cubesat» class from the LEO has been proposed (Fig. 1.17). Structurally, the device is made of at least one aerodynamic element, which during the shell lifetime of the spacecraft is in a folded position on one of the side panels of the spacecraft. The aerodynamic element is made in the form of a round shield. The shield contains a flexible frame, which is made of material with structural shape memory, a canvas of thin-film polymer material, for example, kapton, with a working temperature range of +273...+400 °C is attached to the frame. The thin film web can also be made from a composite material containing an aramid fabric, such as Kevlar. As soon as the spacecraft has finished its lifetime, the device deploys, the cross-sectional area increases, and, due to aerodynamic interaction, the spacecraft begins to gradually deorbit. The advantage of this device is the absence of a device for deployment in its design, and the disadvantages include increased weight, as a result of the use of rigid structures.

In (Maesen, 2007), a device for spacecraft deorbiting is presented, which is made in the form of a four-sided pyramid (Fig. 1.18). The pyramid is made of a central inflatable mast with a length of 40 cm and four transverse inflatable masts with a length of 30 cm. The diameter of the masts is 1 cm, and the thickness of the multilayer material from which they are made is 120 microns (70 microns of fibrous composite material and two layers of Upilex-S material with a thickness of 25 μm).

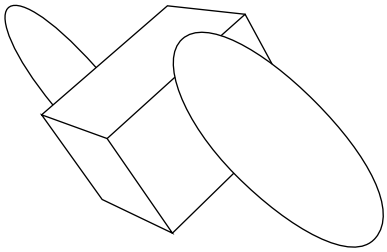

Fig. 1.17. Spacecraft removal device with deployable aerodynamic elements

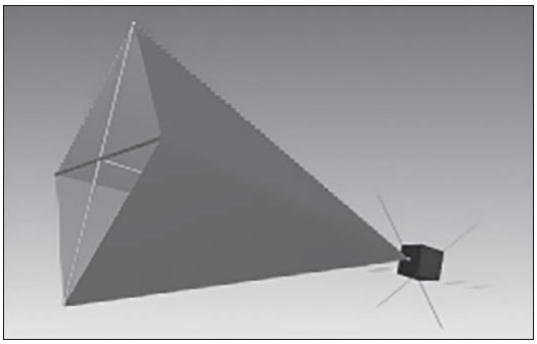

Fig. 1.18. A device for spacecraft deorbiting, which is made in the form of a four-sided pyramid

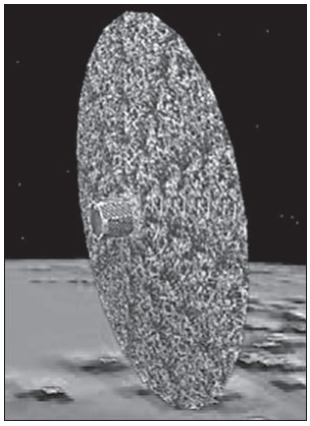

Fig. 1.19. The device for the spacecraft deorbiting in the MUSTANG project

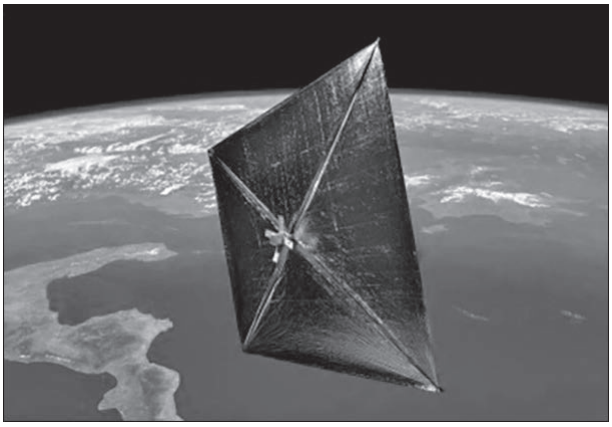

Fig. 1.20. NanoSail-D2 ADS

The thickness of triangular membranes made of Upilex-S material is 25 microns. The mass of the inflation system is 30 g. The mass of the entire system is 94 g. The device in the folded state occupies a volume of ~16 cm^3. The volume occupied by the entire system when folded is 103 cm3.

There is a well-known ADS given in (Roberts, 2002), which is made in the form of a round shield made of thin-film material (Fig. 1.19), for example, made of kapton covered with a thin layer of aluminum. This device has been developed as part of the MUSTANG project.

Another direction of the ADS development is the use of deployable sailing aerodynamic elements. Thus, the task of deploying an atmospheric sail for the purpose deorbiting of low-orbiting rockets has received active development in the last decade. Today, many test launches of spacecraft with sail-based deorbit

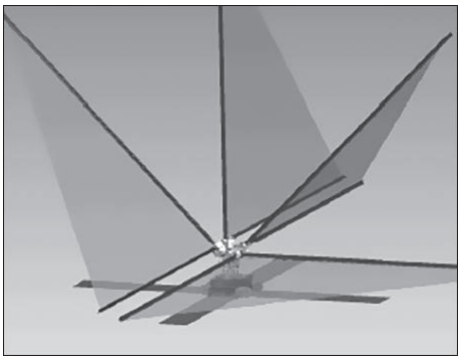

Fig. 1.21. FeatherSail concept

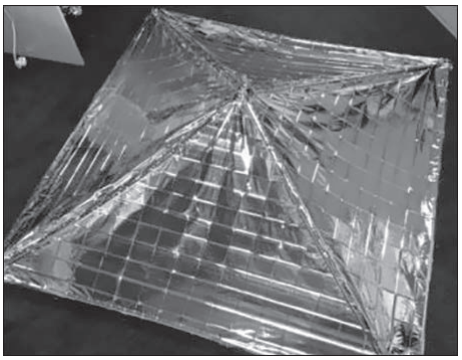

Fig. 1.22. FRODO module of StrathSat-R spacecraft

systems have been carried out. One of these test launches is the NanoSail-D2 spacecraft (Alhorn, 2011) (Fig. 1.20) developed by NASA, which was launched into orbit at the end of 2010. This spacecraft was an exact copy of the main NanoSail-D spacecraft lost during launch on August 3, 2008. The three-unit CubeSat (3U CubeSat) was separated from another small FASTSAT spacecraft on January 19, 2011. The main goal of the NanoSail-D2 mission was to test the mechanism of deployment of the sail itself.

The use of the sail as atmospheric braking to deorbit the spacecraft from orbit was a secondary task. The membrane consisted of four petals, which together formed a square with an area of about 10 m^2. According to the preliminary calculations of the developers, it has been assumed that due to atmospheric braking, the spacecraft would descend from the initial close-to-circular orbit, 650 kilometers high, and burn up in the atmosphere in 70—120 days. However, the angular movement of the sail was uncontrollable and the satellite began to rotate chaotically. The effective area turned out to be much smaller than the nominal one, and it took 240 days to deorbit the spacecraft from orbit (Anderson, 2011). The difference of 2—3 times between the expected and obtained lifetime shows the importance of detailed consideration of the issue of modeling the angular motion of the spacecraft with a sail at the mission design stage.

Based on the technological advances of NanoSail-D, NASA is exploring another advanced concept known as the FeatherSail. A FeatherSail has a sail that is divided into different sections, each of which is equipped with a mechanical drive to change the angle of orientation of these sail sections (Fig. 1.21) (Alhorn, 2010).

Using this design makes it possible to change the direction of the solar pressure flux impact created by a particular sail panel, and hence, the load on the entire surface of the sail. This control method increases the controllability of the satellite solar sail and allows it to generate control torques in all directions using solar radiation pressure. However, given its complexity, this design has not yet been practically implemented. So, this sailing system is only at the concept level, and so far no known mission has been planned using the FeatherSail

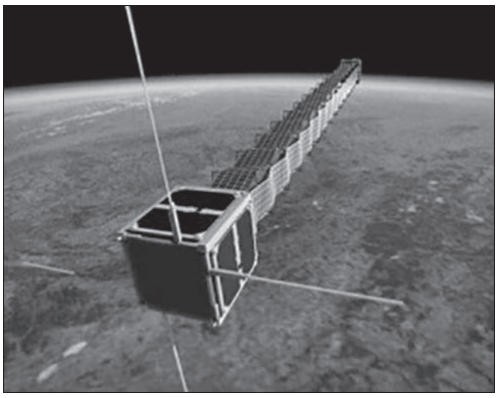

Fig. 1.23. PW-Sat with a tail-shaped sail

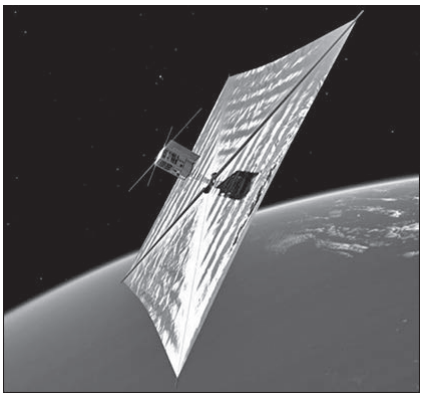

Fig. 1.24. PW-SAT2 spacecraft with an aerodynamic sail deployed in orbit

control concept. After the successful deorbiting of the NanoSail-D spacecraft, many countries began to actively develop ADS projects.

An example of this is the StrathSat-R spacecraft project. Structurally, this spacecraft is made of a set of service systems and payload. The FRODO module (Fig. 1.22) (Sinn, 2012) is used as a payload. The FRODO module is a folded thin-film structure in the form of a square pyramid, consisting of self-inflating masts and sheets of aluminized polymer film. To increase the survivability of the sail, under the influence of SF, the masts are divided into autonomous spherical sections. When deployed in orbit, the sail will have the following dimensions: the height of the pyramid is 0.512 m, the length of the base is 1.772 m, and the surface area is 3.628 m^2. It is assumed that the sail will perform the functions of an aerodynamic and solar sail, which will allow bringing a 1.5 kg spacecraft out of orbit from an altitude of up to 3.000 km.

Another sail tested in practice is the system on the Polish satellite PW-Sat. PW-Sat was launched on February 13, 2012, on the first launch of the Vega launch vehicle, and placed into orbit with a perigee of 300 km and an apogee of 1023 km (Wolanski, 2012). The device is a simple 1U cubesat, and its atmospheric sail is similar to a gravity rod (Fig. 1.23). Instead of a standard sail design, a device resembling a «tail» has been used on the satellite. The advantage of this approach is the simplification of the deployment system since schemes similar to gravity rods have been used for a long time.

However, the device with the configuration shown in Fig. 1.9 has several problems. Thus, the aerodynamic moment tends to orient the satellite with its «tail» along the oncoming flow. In this case, an increase in the effective cross-sectional area will be observed only until the device calms down, and then — in the regime of small fluctuations relative to the equilibrium position — it will become very insignificant. In the case of a greater influence of the gravitational torque on the spacecraft, the orientation of the satellite with its «tail» along the radius vector

is observed, which means that it is perpendicular to the oncoming atmospheric flow and maximizes its effective area. Thus, the required orientation is achieved at high altitudes, where the aerodynamic torque is small. Unfortunately, the force of atmospheric braking will also be small. When entering the denser layers of the atmosphere, for which an atmospheric sail is mainly intended, there is no favorable orientation. So, the mission of the Polish spacecraft was unsuccessful, because the sail was not opened. This is due to the command to open it, sent from Earth, was not accepted by the onboard equipment. Without the sail structure, the process of cubesat deorbiting took more than two and a half years.

In turn, during the PW-SAT2 spacecraft mission, it is planned to develop an aerodynamic sail also made in the shape of a square pyramid (Fig. 1.24), its surface area will be 4 m^2 (PW-SAT2…, 2014).

Another example of nano- and pico-class spacecraft launch systems under development is the sail parachute launch system. Thus, at the beginning of 2017, the NASA space agency demonstrated a new technology that provides the opportunity to return the results of scientific experiments from the International Space Station to the Earth in their entirety.

The technology, named «Exo-Brake» (Fig. 1.25), is a flexible braking device resembling a parachute that deploys from the back of the spacecraft to brake it (Williams, 2017).

The first stage of the mission involved the deorbiting of the nanosatellite using the passive Exo-Brake system. The braking parachute deployed from the nanosatellite increased its aerodynamic drag and also increased its ballistic coefficient. Exo-Brake's first experimental flight was aboard TechEdSat-3p (TES-3p) and was deployed from the ISS in November 2013. TES-3p was a 3U cubesat with an estimated

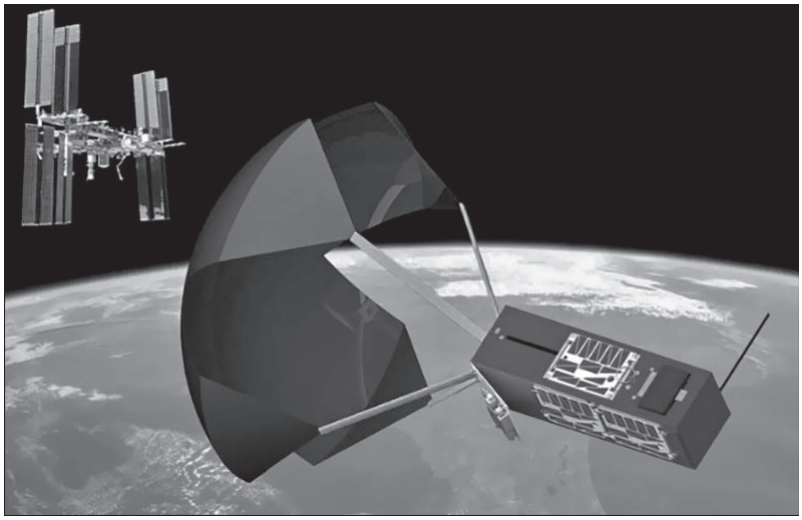

Fig. 1.25. «Exo-Brake» technology for safe removal and return to Earth

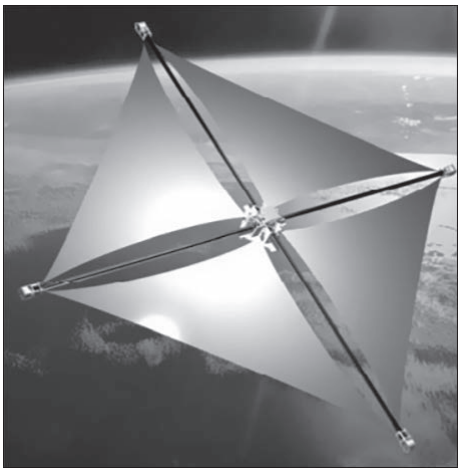

Fig. 1.26. Gossamer 1 sail structure

lifetime of about eight months. Two-line elements collected from USSTRATCOM showed that TES-3p spent about 28 days in deorbit orbit before re-entering Earth's atmosphere. Exo-Brake deployment with a forward cross-section of about one square meter reduced the deorbit time by about seven months.

Another example of the sail systems creation is the project of the European Space Agency called «Gossamer Structures» (Sproewitz, 2017; Visagie, 2015). «Gossamer structures» for solar sails require technology to control reliable deployment. To stop and restart the deployment in case of failures, as well as to prevent the sail from entangling with other elements, appropriate methods of laying the sails are used. Gossamer-1 uses the knowledge gained in previous projects (DLR, Odissee, GEOSAIL), as well as previously developed carbon fiber booms and modern aluminum-coated polyimide foil.

Concerning the deployment and development of mechanisms, it has been recognized that previous strategies had shortcomings related to the control and automation of deployment. Ultimately, these earlier projects failed to accomplish such a mission. Consequently, phased development focused on deployment has been conducted beginning with Gossamer-1.

It is a low-cost technology demonstrator as part of a planned three-stage scalable technology development that covers membranes, booms, photovoltaics and related mechanisms. Scalability means that Gossamer-1 (Fig. 1.26) is a technology demonstrator using technology suitable 5×5 m^2, for assembly of Gossamer-2 with 25×25 m^2 and Gossamer-3 with 50×50 m^2.

A series of presented sailing systems has been developed for a dual purpose. For example, for high-orbit spacecraft, this sail has been proposed as a solar sail, and in low Earth orbit, as a sailing passive deorbit system of the spacecraft from orbit after the end of its lifetime. The Gossamer-1 is based on a cross-boom configuration with four sail segments. At the geometric center of the spacecraft, at the point of the boom intersection, the central spacecraft carries the main bus system of the satellite, including all electronics covering command and data control, the power supply system, as well as the ground communication system. Four side and sail deployment units are mounted on booms, one on each boom. In the folded configuration, they are mechanically locked and electrically connected to the central unit. To deploy, the blocks are unlocked and detached from the central block by moving outwards, thereby simultaneously deploying the jibs and sail segments. During deployment, communication with the central unit is

Fig. 1.27. dragNET MMA sailing ADS

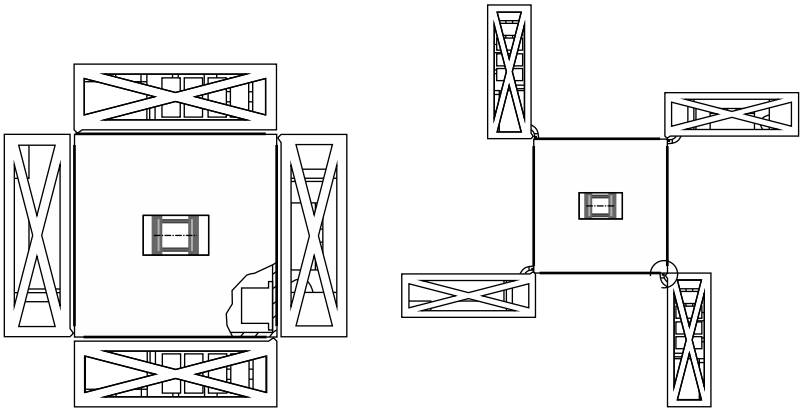

Fig. 1.28. Variant of the spacecraft design transformation

achieved using a wireless onboard communication system, each of which has its own power supply and onboard computer, since there are no wired connections in the booms.

Yes, it is planned to test this sample at an altitude of 600 km as a means of removal. When launched, the Gossamer Deorbit Sail is extremely compact, taking up only 2 kg of space and weighing only 2 kg. According to the calculations, it has been determined that the sail would be enough to deorbit the 700 kg spacecraft from the 600 km orbit in just 1 year.

Another example of the use of sailing inflatable ADS is the dragNET MMA system, which has successfully deorbited the ORS-3 Minotaur I platform from orbit within two years (Fig. 1.27) (MMA Design…, 2013; Stohlman, 2014). The dragNET MMA system consisted of four compactly packed thin membranes that have been produced using one electric drive. Deployment is accomplished by

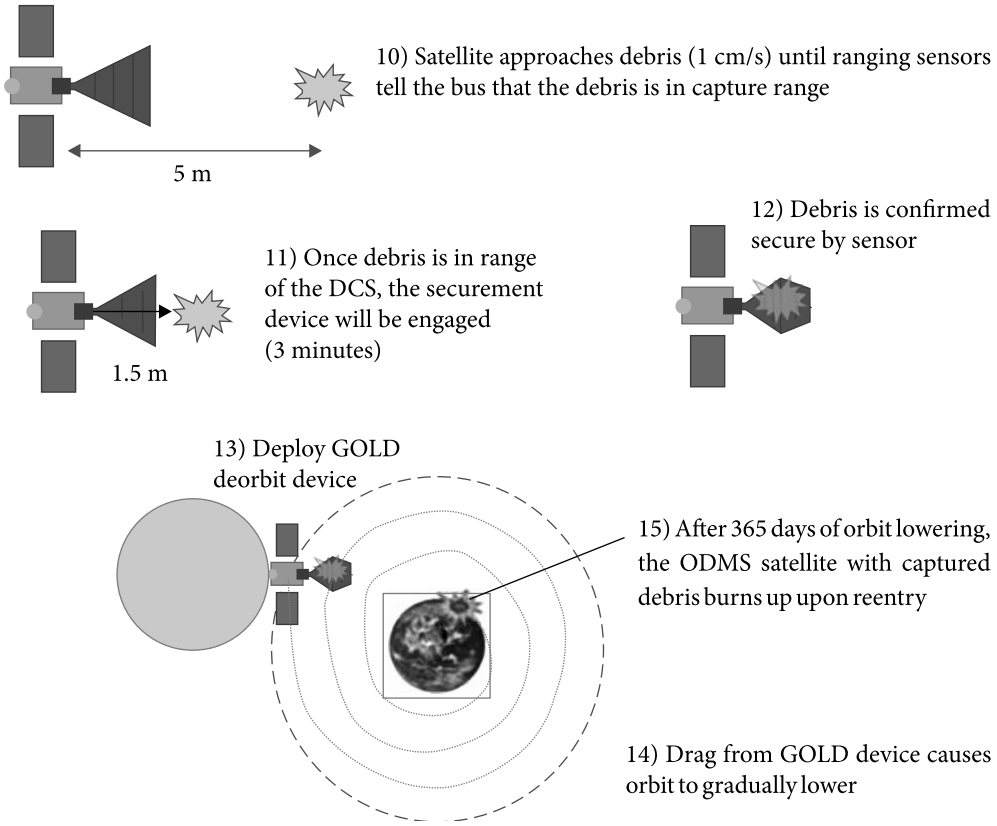

Fig. 1.29. Scheme of deorbiting SDO using an active ADS

spring energy acting through hinged booms, and once tensioned, the membrane forms an aerodynamic shape with high drag.

The dragNET launch system weighs only 2.8 kg and can launch a 180 kg spacecraft from an 850 km high orbit in less than 10 years. Also, the main advantages of this deployment of a sailing ADS should include high-performance, reliable spring-fed deployment and efficient, scalable packaging that allows dragNET integration for any spacecraft design.

Thus, based on the conducted analysis of sailing aerodynamic deorbiting systems that are deployed with the help of mechanical devices, it can be concluded that this direction in the creation of passive deorbit systems is promising and has scientific and practical experimental confirmation of space tests. The calculated data showed that the border of effective application of such systems is at altitudes of up to 700—800 km, where the motion of the spacecraft is significantly impacted by the atmosphere and the deorbit time meets the requirements of 25 years. However, it was noted that the efficiency of the application of flat sail aero-

dynamic elements decreases in the case of non-oriented motion of the spacecraft-ADS system. Hence it has been established that for such systems it is necessary to take into account the need to stabilize the aerodynamic element perpendicular to the dynamic flux vector of the oncoming atmosphere.

Aerodynamic deorbit systems with the use of space object structural elements to reduce the term of their ballistic existence.

There are known methods and spacecraft that use the results of the aerodynamic interaction between the spacecraft and the environment to perform their tasks, including by transforming their design after the end of their lifetime. The transformation is carried out exclusively with the use of special additional devices, which, as a rule, are not necessary for the performance of the main functions of the spacecraft.

In (U.S. Patent for invention No. 6220548), it is proposed to use the transformation of the spacecraft design to expand the functional capabilities of the limited spacecraft volume (Fig. 1.28). The design of the spacecraft is made in the form of deployable modules. Expandable modules can be used as heat protection. The temperature-sensitive equipment is mounted on the inside of the rectangular deployable modules. Equipment and modules are appropriate. As soon as the spacecraft is launched into orbit, the modules are deployed by rotating each module by 90°, thus, the heat-shielding surface is directed into outer space. As a result of the increase in the area of the heat-shielding surface, the maximum allowable power of small, fixed-shaped space vehicles increases. In another design, the heat-shielding structure consists of eight modules, each additional module is deployed by turning it by 90°.

Active aerodynamic deorbit systems. This class of aerodynamic deorbit systems implies the use of these systems to capture SDO and remove them from orbit due to aerodynamic interaction.

An example of this class of systems is the REDCROC project (Zinner, 2011), in which after capturing the SDO with the help of an inflatable device (Fig. 1.29) located on the service spacecraft, a spherical aerodynamic element is deployed, and the SSC-SDO connection begins deorbiting process.

1.3.2. Electrodynamic tether systems, electromagnetic devices and solar sails

The next method of passive deorbiting of SDO is the use of electrodynamic tether and electromagnetic systems. The principle of operation of electrodynamic tether and electromagnetic systems is based on the generation of the electromagnetic field of the spent spacecraft with the help of special electrical devices, such as electromagnetic coils, highly conductive tethers and complex lattice structures. According to Biot—Savard Laplace's law, the electric current that flows through these devices generates an electromagnetic field around the conductive circuits and the entire spacecraft (Caparelli, 2001). This electromagnetic field of the

spacecraft interacts with the dynamic flux of ionospheric plasma and the Earth's magnetic field. As a result of this interaction, a braking force is generated, which transfers the spent spacecraft to lower orbits with subsequent burning in the dense layers of the atmosphere (Kawashima, 2018).

One of the most famous examples of such systems is the Terminator Tether (TT) electromagnetic tether system (Myshchenko, 2017, 2018—2020), (Hoyt, 1998, 1999; Pardini, 2009). The basis of TT operation is based on the law of electromagnetic induction (EMI) and plasma dynamic braking. After deploying a long highly conductive TT in the orbit during spacecraft motion within the Earth's magnetic field (EMF), according to EMI, an electric current is induced in it. According to the law of Bio—Savar Laplace, an electromagnetic field of its own is generated around the cable with an electric current, which, when interacting with the dynamic pressure of charged particles of the ionospheric plasma, creates a braking force.

Theoretical estimations of the lead time when using TT for spacecraft of different orbital groupings have quite optimistic results, which are presented in Table 1.2.

Analyzing these results, it can be concluded that the use of TT as a deorbit system is effective since TT can be used for a large range of altitudes. Also, according to the data in Table 1.2, TTs can deorbit spent spacecraft from orbit quite quickly compared to similar systems.

However, the operation of the TT has some difficulties associated with the stabilization of the relative position of the cable. The proposed TT length of about 5—10 km makes it almost impossible to stabilize during deployment when using modern technologies. In turn, the conducted tests also showed the difficulties associated with the mechanical deployment of the TT, the possibility of over-

Table 1.2. **The time of some spacecraft removal using TT**

Grouping	Altitude at perigee (km)	Inclination (degrees)	Removal time without TT (years)	Average removal speed (km/day)	Removal time with TT
Orbocomm 1	775	45	100	44	11 days
Orbocomm 2	775	70	100	11.6	41 days
LEO One USA	950	50	600	32	18 days
GlobalStar	1390	52	9000	22.3	37 days
Skybridge	1475	55	11000	18.5	46 days
FaiSat	1000	66	800	13.5	45 days
Iridium	780	86.4	100	2.1	7.5 months
M-Star	1350	47	7000	27	28 days
Celestri	1400	48	9000	26	32 days
Teledesic	1350	~85	7000	1.7	17 months

burning due to short circuits and maintaining the relative position of the spacecraft—TT system (Voloshenyuk, 2011). Thus, the TT, regardless of its theoretically calculated effective key indicators, was not implemented for serial use in SDO deorbiting missions.

In turn, (Maslova, 2015) have proposed approaches that allow for partial elimination of the above-mentioned shortcomings of electrodynamic space tether systems. Thus, (Maslova, 2015) shows that if the deployment speed does not exceed 1 m/s, a fairly high reliability of deployment and stabilization of the tether system is ensured and the probability of entanglement is significantly reduced. Also, (Hoyt, 1998, 1999; Pardini, 2009; Maslova, 2015) show a fairly high reliability of the tether system concerning the influence of resonant electrodynamic perturbations during orbital motion.

Another direction of electromagnetic deorbit means is to equip the spacecraft with electromagnetic devices. The principle of operation of electromagnetic devices is similar to electrodynamic space tether system (EDSTS), but unlike EDSTS, they require a constant power source on board the deorbited spacecraft. For example, in (Kawashima, 2018) it has been shown that the time to deorbit a Cubesat-class spacecraft from an altitude of 800 km using an electromagnetic device was about 25 years. It is quite difficult to maintain a power supply in working order for such a long period. Hence, a lead system using permanent magnets (PM) has been proposed, which is a version of electromagnetic devices where permanent magnets are used instead of electromagnets (Shuvalov, 2016, 2018a; Lapkhanov, 2019b). Such a replacement eliminates the drawback associated with the constant use of on-board energy to power the electromagnet. Experimental substantiation of this concept is provided in (Shuvalov, 2016, 2018a, 2018b; Patent of the Ukraine № 125265), where the existence of forces arising from the interaction of permanent magnets with the flow of ionospheric plasma has been proved. Based on this, devices with permanent magnets can be used to deorbit SDOs from LEOs, but require experimental tests in outer space.

As for solar sails, their principle of action is essentially reminiscent of the principle of action of an ADS, but instead of interaction with the oncoming atmospheric flow, the braking effect is used due to the influence of solar pressure (Heaton, 2014; Mori, 2009; Herbeck, 2002; Leipold, 1999). The use of a solar sail is effective at altitudes above 800 km, where the force of solar pressure is greater than the force of aerodynamic resistance. The possibility of using this class of deorbit means, as well as in the ADS, has been confirmed experimentally. One of the successful experiments is the deployment of a 200 square meter solar sail in (Mori, 2009) the Ikaros mission.

The application of SDO deorbiting using a solar sail is usually not used, since this concept has been developed to solve the problem of developing fuel-free propulsion systems to control the orbital motion of spacecraft in high elliptical orbits and interplanetary space. However, the solar sail can significantly expand the limits of the effective use of ADS when developing a hybrid-type system.

1.4. Prerequisites for the creation of hybrid means of space debris objects deorbiting from working orbits

Based on the above complex analysis of known means of ADS deorbiting, their generalized comparative characteristics are proposed, taking into account the main efficiency criteria (Table 1.3). Thus, the main criteria for effective use are proposed to include: the average speed of deorbiting within the limits of the LEO (speed code), the reliability of the deorbit systems and the consumption of fuel and on-board electrical energy. Also, it is proposed to include the presence or absence of experimental confirmation in space and on Earth as the main criterion that can affect the effectiveness of the use of SDO deorbiting systems.

Thus, the ratings are in the range from «1» to «10», where 10» indicates the maximum presence of advantage according to this efficiency criterion, and «1» — its practical absence, the symbol SP indicates the presence of space experiments, and the symbol GR — the conducted ground experiments in laboratory conditions. Thus, the highest indicators are obtained by the ADS systems in combination with a solar sail, EDSTS and devices with permanent magnets. However, it can be concluded that none of the above means of deorbiting objects is universal for use in all missions.

Table 1.3. **Classification of means of space debris objects removal from working orbits**

Means of spacecraft object removal	Removal speed	Reliability	Low fuel consumption	Low on-board energy consumption	Exp. confirmation of possible use in space
Active thruster	8	8	1	1	SP
Active contact	8	1	1	1	n/a
LEOSWEEP	7	4	1	4	GR
ADS	3	8	10	8	SP + GR
EDSTS	10	1	10	7	SP
Plasmodynamic devices with permanent magnets	3	7	10	9	GR
Solar sails (used in combination with ADS)	1	6	10	8	SP + GR
Hybrid (combined) means of ADS removal	A new approach in the creation of systems for the SDO deorbiting from near-Earth orbits, which allows expanding the limits of the application of existing the near-Earth space pollution mitigration means (active ADS, motor-aerodynamic, LEOSWEEP system with an aerodynamic compensator can be included)				

Thus, the problem has arisen to find optimal technical solutions to expand the limits of application of each deorbit system, by creating hybrid (combined) means of deorbit SDO, while using the advantages of each system of clearing the near-Earth space from SDO.

1.5. State of the art of the hybrid space debris deorbiting means development

One of the examples of the creation of hybrid removal is the improvement of the technology of using the space «shepherd with an ion beam» by equipping the SSC with an aerodynamic compensator. Thus, in research works (Alpatov, 2016b; Svorobyn, 2018) the possibility of using an aerodynamic compensator for SSC technology «LEOSWEEP» is considered for compensating the operation of the SSC electrojet propulsion system. It has been found that replacing the electrojet propulsion with an aerodynamic compensator can significantly reduce the onboard energy consumption of the SSC, however, as shown in (Svorobyn, 2018), the weight and complexity of the design do not justify this advantage. At the same time, if for one SSC mission, it is possible to provide for the implementation of several deviations from the orbit of different SDO's, then the use of an aerodynamic compensator may be justified. Thus, this concept requires revisions and a more complete justification.

The next example of the development of hybrid deorbit devices, including aerodynamic modules, is the active-passive propulsion-aerodynamic system presented in (Dron', 2018, 2019a, 2019b; Golubek, 2020a). This system consists of two submodules: the propulsion system installation and the aerodynamic element. The use of the propulsion-aerodynamic system is proposed for the deorbit of SDO from orbits up to 2000 km altitude. The deorbiting is carried out in two stages, where in the first stage the SDO is transferred to an elliptical orbit with a perigee in the altitude range of up to 800 km. At these altitudes, the force of aerodynamic resistance creates a significant impact on the SDO motion. After that, the opening of the aerodynamic element occurs and the spacecraft is passively deorbit with further combustion in the dense layers of the atmosphere.

Also, a fairly promising direction in the development of hybrid deorbit means is the combination of aerodynamic deorbit systems and magnetic actuators. This is explained by the intensive development of aerodynamic flat-sail deorbit systems, class «Gossamer 1», «NanoSail-D2» and PW-Sat. In turn, during the flight tests of «NanoSail-D2» the need has been determined to stabilize and orient the flat sail aerodynamic element perpendicular to the dynamic flow of the oncoming atmosphere.

Thus, during the development of the ACADS (Attitude Control and Aerodynamic Drag Sail) aerodynamic system (Pfisterer, 2011), a hypothesis has been put forward about the possibility of stabilizing a flat aerodynamic element using elec-

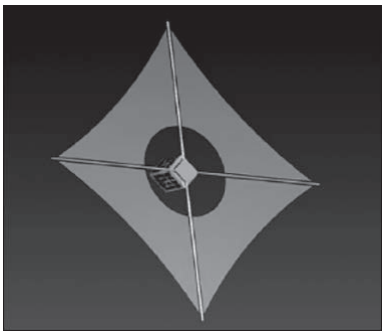

Fig. 1.30. ACADS system

tromagnetic coils. The ACADS sail system has been developed as an experimental payload of the KnightSat II project by the Nanosatellite Program Force research laboratory. Thus, it has been suggested that the use of additional electromagnetic coils in ACADS will allow orientation and stabilization of the aerodynamic flat sail element perpendicular to the dynamic flow of the oncoming atmosphere. When performing such an orientation, the area of the spacecraft's midsection increases significantly, hence the ballistic coefficient and aerodynamic braking force. This system has been tested in the laboratory using sails of size, allowing this deorbit device to be used for SDOs of various sizes. The uniform deployment of ACADS (Fig. 1.30), and the use of magnetic coils for orientation with the oncoming atmospheric flow, can provide stabilization in flight and the potential for future development of missions without the use of fuel. Thus, according to calculations, the use of ACADS made it possible to reduce the time of KnightSat II's existence in an orbit at an altitude of 580 km from 18.5 years to 3 months.

It should be noted that ACADS has a disadvantage, which is the significant complexity of the design. Thus, the location of electromagnets along the perimeter of a flat aerodynamic element can cause difficulties when deploying an ADS. Also, according to the design scheme (Pfisterer, 2011), the arrangement of electromagnetic actuators (coils) in one plane, in comparison with the classical orthogonal arrangement along the main axes of inertia of the spacecraft, imposes restrictions on the controllability of the system. In turn, for the functioning of ACADS, a necessary condition is the operability of the spacecraft orientation and stabilization systems and the spacecraft power system, which is quite difficult after the end of the operational lifetime. To solve this problem, it is necessary to develop less low-cost magnetic actuators and search for algorithms and control methods that allow reducing the cost of on-board electrical energy. However, this has not been done during the development of ACADS. Based on this, the development of ACADS is only hypothetical and theoretical.

Another approach is based on the aeromagnetic combined system usage (Lapkhanov, 2019c; Alpatov, 2020). In this case, the new executive devices with rotated permanent magnets were proposed to stabilize the attitude position of aerodynamic sales. The orientation system in the aeromagnetic combined method using permanent magnets consists of PMs 8, which are attached to the rotary actuators on micro stepper motors 9. In turn, the micro stepper motors 9 with the permanent magnets 8, orthogonal to one another, are mounted on the SC body mounts 10. The PMs are shielded with special screen capsules 3, which, if necessary, are opened and closed in a certain algorithm. Control of the opening and

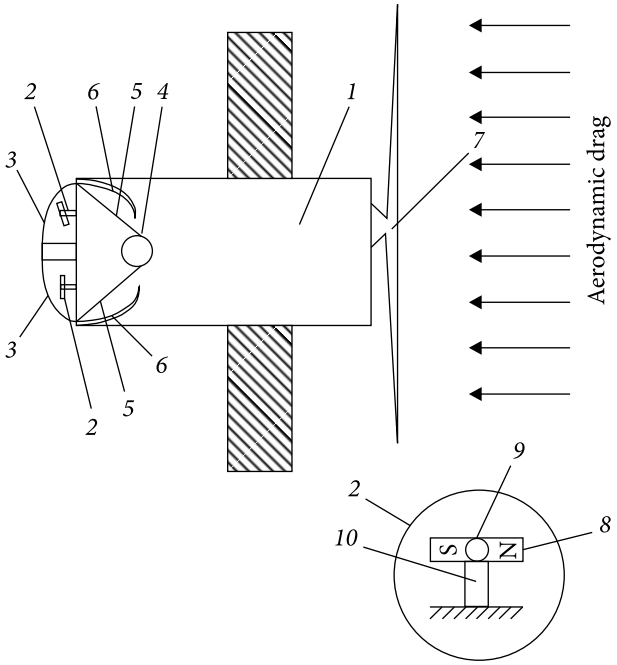

Fig. 1.31. The structural design of the hybrid deorbiting system (HDS): *1* — the deorbited spacecraft; *2* — the biaxial orientation system with permanent magnets; *3* — screen capsules; *4* — the electronic control node of the opening-closing (O-C CN); *5* — transmission mechanisms; *6* — niches for the screen capsules in the closed state; *7* — the aerodynamic sail element; *8* — a permanent magnet; *9* — a micro stepper motor that rotates a permanent magnet; *10* — special attachments of permanent magnets to the body of the spacecraft

closing of the screen capsules is carried out on the electronic control node of the opening-closing (O-C CN) 4 with the help of special transfer mechanisms 5. In the closed state, the shutters of the screen capsules are placed into special niches 6, which are located in the SC body 1 (Fig. 1.31).

The HDS operates according to a special algorithm. Thus, after the expiration of the active operation of the SC 1 and the deployment of the aerodynamic element 7, there is the orientation of the aerodynamic element of the HDS perpendicular to the vector of the dynamic flow of the atmosphere. The orientation is implemented using magnetic controls with rotating permanent magnets 2.

The usage of such executive devices allowed to reduce the onboard electricity consumption by an order of magnitude, which is very important in long-term missions.

The next stage of the development of this idea is based on the combination aeromagnetic deorbit system system (Lapkhanov, 2019c; Alpatov, 2020) with an aerodynamic-propulsion system (Dron', 2018, 2019a, 2019b; Golubek, 2020a) which is described in (Alpatov, 2023a). In turn, in this case, due to the complicity of the system it has been used spacecraft magnetorques instead of devices with permanent magnets.

CHAPTER 2

MATHEMATICAL MODEL FOR STUDYING THE ORBITAL AND ATTITUDE MOTION OF THE SPACECRAFT WITH AERODYNAMIC DEORBIT SYSTEM

2.1. Reference frames and corresponding quaternion relations for analysis of spacecraft position

1) ***Earth central inertial reference frame OXYZ***. It has been accepted the **J2000** reference frame as the standard. The origin of the Reference Frame, point *O*, placed in the center of the Earth, the axis *OZ* is directed along its axis of rotation in the direction of the north pole N, axes *OX, OY* axes of inertia are located in the plane of the Earth's equator so that the axis *OX,* directed to the vernal equinox ♈ (on 1 January 2000), and axis *OY*completed the reference frame to the right (Fig. 2.1).

2) ***WGS-84 Reference frame*** $O_gX_gY_gZ_g$. Non-inertial reference frame. The origin of the reference frame is placed at the center of the Earth, the point O_g. The axis O_gX_g lies in the plane of the equator and is directed towards the intersection of the equator with the Greenwich meridian, axis O_gZ_g coincides with the axis *OZ* of the J2000 reference frame and with the angular velocity vector of the Earth's daily rotation, axis O_gY_g completed the reference frame to the right (Golubek, 2020).

Then it can be determined the matrix of the transition from J2000 to WGS-84, can be written as follows:

$$M_{X_g \leftarrow X} = W \cdot \begin{bmatrix} \cos(GAST) & \sin(GAST) & 0 \\ -\sin(GAST) & \cos(GAST) & 0 \\ 0 & 0 & 1 \end{bmatrix} \cdot M_N \cdot M_P \cdot M_B,$$
$$M_{X \leftarrow X_g} = M^T_{X_g \leftarrow X}, \tag{2.1}$$

where $M_{X_g \leftarrow X}$ is the transition matrix from J2000 to WGS-84; $M_{X \leftarrow X_g}$ is the transition matrix from WGS-84 to J2000; *W* is the polar correction matrix; *GAST* is the Greenwich ap-

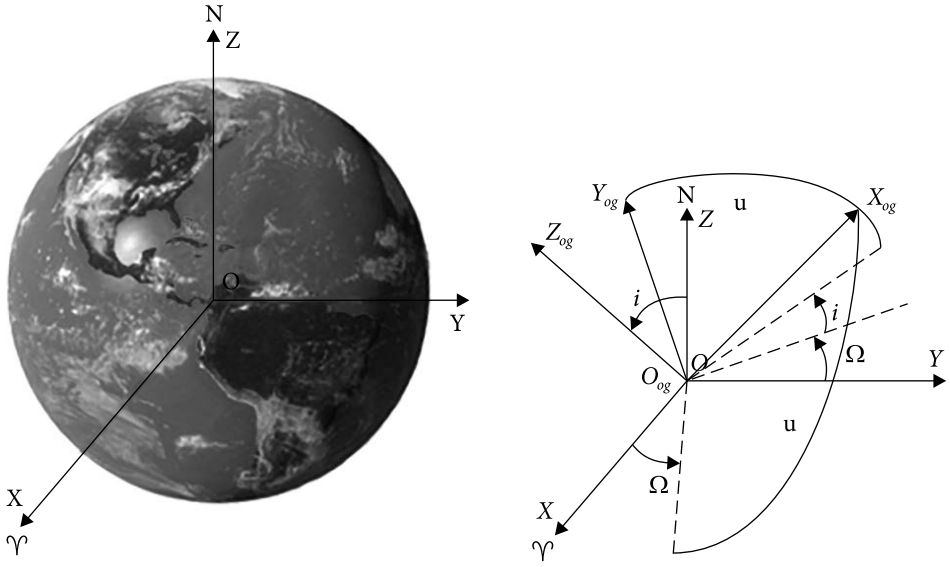

Fig. 2.1. J2000 Reference Frame ϒ is a sign of direction to the vernal equinox without taking into account precession and nutation of the Earth; *N* is the direction to the point of the north pole

Fig. 2.2. OGRF relative to J2000: $O_{og}X_{og}Y_{og}Z_{og}$ is Orbital General Reference Frame (OGRF); *OXYZ* is J2000 reference frame; ϒ is the sign of direction to the vernal equinox without taking into account precession and nutation of the Earth; N is the direction to the point of the north pole; *u* is the argument of latitude; is the orbit inclination; Ω is the RAAN

parent sidereal time; M_B is the bias matrix; M_N is the nutation matrix; M_P is the precession matrix; *t* is the time is calculated from the Julian date.

3) ***Orbital General Reference Frame (OGRF)*** $O_{og}X_{og}Y_{og}Z_{og}$. Non-inertial reference frame. The center O_{og} is at the center of the Earth. The axis $O_{og}X_{og}$ lies in the plane of the orbit and is directed along the radiusvector of the spacecraft motion. The Axis $O_{og}Z_{og}$ is perpendicular to the plane of the orbit of the spacecraft and coincides with the integral vector of the plane. Axis $O_{og}Y_{og}$ completed the reference frame to the right. The transition from J2000 to OGRF is realized by a sequence of rotations to the right ascension of the ascending node (RAAN) angle Ω, inclination *i*, and argument of latitude *u* (Fig. 2.2). The transition matrix from J2000 to OGRF is written as follows:

$$M_{X_g \leftarrow X} = W \cdot \begin{bmatrix} \cos(GAST) & \sin(GAST) & 0 \\ -\sin(GAST) & \cos(GAST) & 0 \\ 0 & 0 & 1 \end{bmatrix} \cdot M_N \cdot M_P \cdot M_B,$$

$$M_{X \leftarrow X_g} = M^T_{X_g \leftarrow X}, \tag{2.2}$$

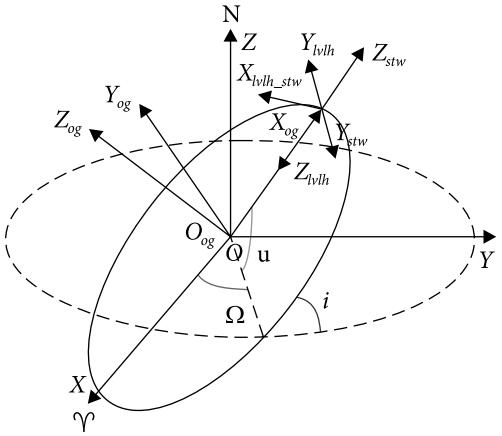

Fig. 2.3. STW, OGRF, LVLH and J2000 Reference Frames: $O_{og}X_{og}Y_{og}Z_{og}$ is OGRF; *OXYZ* is J2000 reference frame; $O_{STW}X_{STW}Y_{STW}Z_{STW}$ the Orbital Associated Upper Reference Frame (STW); $O_{lvlh}X_{lvlh}Y_{lvlh}Z_{lvlh}$ is Local Vertical Local Horizontal Reference Frame (LVLH); ϒ is the sign of direction to the vernal equinox without taking into account precession and nutation of the Earth; N is the direction to the point of the north pole; *u* is the argument of latitude; *i* is the orbit inclination; Ω is the RAAN

where $M_{X_{og}\leftarrow X}$ is the transition matrix from J2000 to OGRF; $M_{X\leftarrow X_{og}}$ is the transition matrix from OGRF to J2000; $O_{og}X_{og}Y_{og}Z_{og}$ is Orbital General Reference Frame (OGRF); *OXYZ* is J2000 reference frame; ϒ is the sign of direction to the vernal equinox without taking into account precession and nutation of the Earth; N is the direction to the point of the north pole; *u* is the argument of latitude; *i* is the orbit inclination; Ω is the RAAN

4) ***Orbital Associated Upper Reference Frame (STW)*** (Fortescue, 2011) $O_{STW}X_{STW}Y_{STW}Z_{STW}$. Non-inertial reference frame. The center O_{STW} is located in the center of the mass (COM) of spacecraft. The axis $O_{STW}Z_{STW}$ is directed along the radiusvector of the spacecraft (***S***-axis), axis $O_{STW}X_{STW}$ lies in the plane of the orbit and is directed in the direction of the spacecraft motion (creates an acute angle with the orbital velocity vector – ***T***-axis), axis $O_{STW}Y_{STW}$ completed the reference frame to the right (***W***-axis) (Fig. 2.3)

The transition from OGRF to STW is implemented using the next sequence of rotations: by the angle 90 deg around the axis $O_{og}Y_{og}$ until the $O_{og}Z_{og}$ axis coincides with $O_{og}X_{og}$ and by the angle 90 deg around a rotated axis $O_{og}Z_{og}$ (Fig. 2.3). The matrix for the transition from OGRF to STW is written in the following order:

$$M_{X_{STW}\leftarrow X_{og}} = \begin{pmatrix} 0 & 1 & 0 \\ 0 & 0 & 1 \\ 1 & 0 & 0 \end{pmatrix}, \quad M_{X_{og}\leftarrow X_{STW}} = M^{T}_{X_{STW}\leftarrow X_{og}}, \tag{2.3}$$

where $M_{X_{STW}\leftarrow X_{og}}$ is the transition matrix from OGRF to STW; $M_{X_{og}\leftarrow X_{STW}}$ is the transition matrix from STW to OGRF;

5) Local vertical local horizontal reference frame (LVLH) $O_{LVLH}X_{LVLH}Y_{LVLH}Z_{LVLH}$. Non-inertial reference frame. The center O_{LVLH} is located in the center of the mass (CM) of the spacecraft. The axis $O_{LVLH}Z_{LVLH}$ is directed to the center of the Earth,

axis $O_{LVLH}X_{LVLH}$ lies in the plane of the orbit, and is directed in the direction of the spacecraft motion (creates an acute angle with the orbital velocity vector), axis $O_{LVLH}Y_{LVLH}$ completes the reference frame to the right (Fig. 2.3). The transition matrix which connecting the STW and LVLH reference frames is written as follows:

$$M_{X_{LVLH}\leftarrow X_{STW}} = \begin{pmatrix} 1 & 0 & 0 \\ 0 & -1 & 0 \\ 0 & 0 & -1 \end{pmatrix},$$
$$M_{X_{STW}\leftarrow X_{LVLH}} = M^{T}_{X_{LVLH}\leftarrow X_{STW}}. \tag{2.4}$$

6) Spacecraft Body Reference Frame (SBRF) $O_{SB}X_{SB}Y_{SB}Z_{SB}$. The center of the SBRF is a point O_{SB}, located in the CM of the spacecraft. The axes of SBRF coincide with the main axes of inertia of spacecraft. The transition from LVLH to SBRF is realized by a sequence of turns to roll φ, pitch θ and yaw Ψ angles. The transition matrix can be written as follows:

$$M_{X_{SB}\leftarrow X_{LVLH}} = \begin{pmatrix} \cos\psi\cos\theta & \begin{bmatrix}\sin\psi\cos\varphi + \\ +\cos\psi\sin\theta\sin\varphi\end{bmatrix} & \begin{bmatrix}\sin\psi\sin\varphi - \\ -\cos\psi\sin\theta\cos\varphi\end{bmatrix} \\ -\sin\psi\cos\theta & \begin{bmatrix}\cos\psi\cos\varphi - \\ -\sin\psi\sin\theta\sin\varphi\end{bmatrix} & \begin{bmatrix}\cos\psi\sin\varphi + \\ +\sin\psi\sin\theta\cos\varphi\end{bmatrix} \\ \sin\theta & -\cos\theta\sin\varphi & \cos\theta\cos\varphi \end{pmatrix},$$
$$M_{X_{LVLH}\leftarrow X_{SB}} = M^{T}_{X_{SB}\leftarrow X_{LVLH}}, \tag{2.5}$$

where $M_{X_{SB}\leftarrow X_{LVLH}}$ is the transition matrix from LVLH to SBRF; $M_{X_{LVLH}\leftarrow X_{SB}}$ is the transition matrix from SB to LVLH.

In turn, roll φ, pitch θ, and yaw Ψ angles can be calculated from the matrix (2.5) as:

$$\psi = -\arctan 2\left(\frac{M_{X_{SB}\leftarrow X_{VLX}21}}{M_{X_{SB}\leftarrow X_{VLX}11}}\right),$$
$$\theta = \arcsin\left(M_{X_{SB}\leftarrow X_{VLX}31}\right), \tag{2.6}$$
$$\varphi = -\arctan 2\left(\frac{M_{X_{SB}\leftarrow X_{VLX}32}}{M_{X_{SB}\leftarrow X_{VLX}33}}\right),$$

where arctan 2 is a special arctangent function that takes into account the value of the quadrant when calculating in different programming languages;

7) Local tangent plane coordinates (LTP) $O_{LTP}X_{LTP}Y_{LTP}Z_{LTP}$. This is an orthogonal, right rectangular, reference system defined with its origin O_{LTP} at an arbitrary point on (or possibly near) the Earth's surface. The vertical axis $O_{LTP}Z_{LTP}$ is then taken to be straight up, opposite the plumb line. The other axes are perpendicular to the vertical axis aligned with local geographic East $O_{LTP}X_{LTP}$ and North $O_{LTP}Y_{LTP}$.

$$M_{X_g \leftarrow X_{LTP}} = \begin{pmatrix} -\sin(L) & -\sin(B_e)\cos(L) & \cos(B_e)\cos(L) \\ \cos(L) & -\sin(B_e)\sin(L) & \cos(B_e)\sin(L) \\ 0 & \cos(B_e) & \sin(B_e) \end{pmatrix},$$
$$M_{X_{LTP} \leftarrow X_g} = M^T_{X_g \leftarrow X_{LTP}}. \tag{2.7}$$

where $M_{X_g \leftarrow X_{LTP}}$ is the transition matrix from LTP to WGS-84; $M_{X_{LTP} \leftarrow X_g}$ is the transition matrix from WGS-84 to LTP, L is the longitude; B_e is the geocentric latitude.

7) Local geodetic coordinates (LGC) $O_{LGC}X_{LGC}Y_{LGC}Z_{LGC}$ This is an orthogonal, right rectangular, reference system defined with its origin O_{LTP} at an arbitrary point on the Earth's surface (without taking into account the terrain, altitude 0 m above sea level. The Earth model is Reference Ellipsoid). $O_{LGC}Z_{LGC}$ is directed orthogonally to the tangent plane to the Earth surface at the arbitrary point. The other axes are perpendicular to the vertical axis aligned with local geodetic East $O_{LGC}X_{LGC}$ and North $O_{LGC}Y_{LGC}$.

$$M_{X_g \leftarrow X_{LTP}} = \begin{pmatrix} -\sin(L) & -\sin(B)\cos(L) & \cos(B_e)\cos(L) \\ \cos(L) & -\sin(B)\sin(L) & \cos(B)\sin(L) \\ 0 & \cos(B) & \sin(B) \end{pmatrix},$$
$$M_{X_{LTP} \leftarrow X_g} = M^T_{X_g \leftarrow X_{LTP}}. \tag{2.8}$$

where $M_{X_g \leftarrow X_{LTP}}$ is the transition matrix from LGC to WGS-84; $M_{X_{LTP} \leftarrow X_g}$ is the transition matrix from WGS-84 to LGC, L is the longitude; B is the geodetic latitude.

Another approach to defining the attitude parameters of spacecraft motion is the use of quaternions (Gordeev, 2016).

According to the matrix (2.5), it can be determined the quaternion of rotation from LVLH to SBRF. According to the rotation matrix (2.5), the first rotation is around $O_{LVLH}X_{LVLH}$ by roll angle φ counterclockwise, the second rotation is performed around the rotated axis $O_{LVLH}Y_{LVLH}$ by pitch angle θ counterclockwise, and the third rotation is made around the rotated axis $O_{LVLH}Z_{LVLH}$ by yaw angle Ψ

counterclockwise. Using the properties of half-exponential quaternions, it can be written the corresponding quaternions for each rotation, as follows:

$$Q_{\varphi} = \begin{pmatrix} \cos\left(\frac{\varphi}{2}\right) \\ \sin\left(\frac{\varphi}{2}\right) \\ 0 \\ 0 \end{pmatrix}, \; Q_{\theta} = \begin{pmatrix} \cos\left(\frac{\theta}{2}\right) \\ 0 \\ \sin\left(\frac{\theta}{2}\right) \\ 0 \end{pmatrix}, \; Q_{\psi} = \begin{pmatrix} \cos\left(\frac{\psi}{2}\right) \\ 0 \\ 0 \\ \sin\left(\frac{\psi}{2}\right) \end{pmatrix}, \tag{2.9}$$

where O_{φ}, O_{θ}, O_{ψ} are roll, pitch, and yaw quaternions, respectively.

The resulting quaternion will be written as follows:

$$Q = Q_{\varphi} \circ Q_{\theta} \circ Q_{\psi} = \begin{pmatrix} Q_0 \\ Q_X \\ Q_Y \\ Q_Z \end{pmatrix} = \begin{pmatrix} \cos\left(\frac{\varphi}{2}\right)\cos\left(\frac{\theta}{2}\right)\cos\left(\frac{\psi}{2}\right) - \sin\left(\frac{\varphi}{2}\right)\sin\left(\frac{\theta}{2}\right)\sin\left(\frac{\psi}{2}\right) \\ \sin\left(\frac{\varphi}{2}\right)\cos\left(\frac{\theta}{2}\right)\cos\left(\frac{\psi}{2}\right) + \cos\left(\frac{\varphi}{2}\right)\sin\left(\frac{\theta}{2}\right)\sin\left(\frac{\psi}{2}\right) \\ \cos\left(\frac{\varphi}{2}\right)\sin\left(\frac{\theta}{2}\right)\cos\left(\frac{\psi}{2}\right) - \sin\left(\frac{\varphi}{2}\right)\cos\left(\frac{\theta}{2}\right)\sin\left(\frac{\psi}{2}\right) \\ \cos\left(\frac{\varphi}{2}\right)\cos\left(\frac{\theta}{2}\right)\sin\left(\frac{\psi}{2}\right) + \sin\left(\frac{\varphi}{2}\right)\sin\left(\frac{\theta}{2}\right)\cos\left(\frac{\psi}{2}\right) \end{pmatrix} \tag{2.10}$$

where ∘ is the symbol of the quaternion multiplication operation; O_0 — scalar part of quaternion; O_X, O_Y, O_Z is the vector part of the quaternion.

Taking into account that this quaternion is normalized, using the properties of quaternions (Gordeev, 2016), the transition matrix from LVLH to SBRF will be written as follows (Gordeev, 2016):

$$M_{X_{SBRF} \leftarrow X_{LVLH}} = \begin{pmatrix} Q_0^2 + Q_X^2 - Q_Y^2 - Q_Z^2 & 2\cdot\left(Q_X Q_Y + Q_0 Q_Z\right) & 2\cdot\left(Q_X Q_Z - Q_0 Q_Y\right) \\ 2\cdot\left(Q_X Q_Y - Q_0 Q_Z\right) & Q_0^2 + Q_Y^2 - Q_X^2 - Q_Z^2 & 2\cdot\left(Q_Y Q_Z + Q_0 Q_X\right) \\ 2\cdot\left(Q_X Q_Z + Q_0 Q_Y\right) & 2\cdot\left(Q_Y Q_Z - Q_0 Q_X\right) & Q_0^2 + Q_Z^2 - Q_X^2 - Q_Y^2 \end{pmatrix}. \tag{2.11}$$

Then, taking into account (2.9), formulas (2.6) will be written in the following form:

$$\psi = -\arctan 2\left(\frac{2\cdot\left(Q_X Q_Y - Q_0 Q_Z\right)}{Q_0^2 + Q_X^2 - Q_Y^2 - Q_Z^2}\right),$$

$$\theta = \arcsin\left(2\cdot\left(Q_X Q_Z + Q_0 Q_Y\right)\right), \tag{2.12}$$

$$\varphi = -\arctan 2\left(\frac{2\cdot\left(Q_Y Q_Z - Q_0 Q_X\right)}{Q_0^2 + Q_Z^2 - Q_X^2 - Q_Y^2}\right).$$

For the algorithm of the transition from J2000 to OGRF (2.2), the quaternion will be written in the following form:

$$L = L_\Omega \circ L_i \circ L_u = \begin{pmatrix} \cos\left(\frac{\Omega}{2}\right) \\ 0 \\ 0 \\ \sin\left(\frac{\Omega}{2}\right) \end{pmatrix} \circ \begin{pmatrix} \cos\left(\frac{i}{2}\right) \\ 0 \\ \sin\left(\frac{i}{2}\right) \\ 0 \end{pmatrix} \circ \begin{pmatrix} \cos\left(\frac{u}{2}\right) \\ 0 \\ 0 \\ \sin\left(\frac{u}{2}\right) \end{pmatrix} = \begin{pmatrix} \cos\left(\frac{i}{2}\right)\cos\left(\frac{\Omega+u}{2}\right) \\ \sin\left(\frac{i}{2}\right)\cos\left(\frac{\Omega-u}{2}\right) \\ \sin\left(\frac{i}{2}\right)\sin\left(\frac{\Omega-u}{2}\right) \\ \cos\left(\frac{i}{2}\right)\sin\left(\frac{\Omega+u}{2}\right) \end{pmatrix}, \tag{2.13}$$

where L is the quaternion of transition from J2000 to OGRF.

In turn, the quaternion of the transition from OGRF to STW reference frame can be written in the following form:

$$\Lambda = \Lambda_{90^o} \circ \Lambda_{90^o} = \begin{pmatrix} \frac{\sqrt{2}}{2} \\ 0 \\ \frac{\sqrt{2}}{2} \\ 0 \end{pmatrix} \circ \begin{pmatrix} \frac{\sqrt{2}}{2} \\ 0 \\ 0 \\ \frac{\sqrt{2}}{2} \end{pmatrix} = \begin{pmatrix} \frac{1}{2} \\ \frac{1}{2} \\ \frac{1}{2} \\ \frac{1}{2} \end{pmatrix}, \tag{2.14}$$

where Λ is the quaternion of the transition from OGRF to STW reference frame.

According to (2.4), the quaternion connecting STW and LVLH is written as follows:

$$\Lambda_{BH} = \begin{pmatrix} 0 \\ 1 \\ 0 \\ 0 \end{pmatrix}.$$

2.2. Mathematical model of spacecraft orbital motion

To avoid singularities, it is advisable to use systems of differential equations with Laplace elements (Fortescue, 2011). The use of these components makes it possible to avoid the degeneracy of solutions when analyzing the motion of spacecraft in near-circular orbits. The components of the Laplace vector are written as follows:

$$q = e\cos\omega,\ k = e\sin\omega. \tag{2.16}$$

Taking this into account, the system of differential equations is written as follows (Fortescue, 2011):

$$\left.\begin{aligned}
\frac{d\Omega}{dt} &= \frac{r_{SC}}{\sqrt{\mu\cdot p}}\cdot\frac{\sin u}{\sin i}\cdot W \\
\frac{di}{dt} &= \frac{r_{SC}}{\sqrt{\mu\cdot p}}\cdot\cos u\cdot W \\
\frac{dp}{dt} &= 2r_{SC}\cdot\sqrt{\frac{p}{\mu}}\cdot T \\
\frac{dq}{dt} &= \sqrt{\frac{p}{\mu}}\left[\sin u\cdot S+\left(\left(1+\frac{r_{SC}}{p}\right)\cos u+\frac{r_{SC}}{p}q\right)T+\right. \\
&\quad \left.+\frac{r_{SC}}{p}k\sin u\cdot\cot i\cdot W\right] \\
\frac{dk}{dt} &= \sqrt{\frac{p}{\mu}}\left[-\cos u\cdot S+\left(\left(1+\frac{r_{SC}}{p}\right)\sin u+\frac{r_{SC}}{p}k\right)T-\right. \\
&\quad \left.-\frac{r_{SC}}{p}q\sin u\cdot\cot i\cdot W\right] \\
\frac{du}{dt} &= \frac{\sqrt{\mu p}}{r_{SC}^2}\left(1-\frac{r_{SC}^3}{\mu p}\cot i\cdot\sin u\cdot W\right)
\end{aligned}\right\}, \tag{2.17}$$

where $r_{SC}=\dfrac{p}{1+q\cos u+k\sin u}$ is the module of spacecraft radius-vector (distantance from the Earth center to spacecraft); $\omega=\arctan\left(\dfrac{k}{q}\right)$, a is the orbit semi-

major axis; e is the eccentricity of the orbit; Ω is the RAAN of the orbit; ω is the argument of perigee; μ is the gravity constant, $\mu = 3.986 \cdot 10^5$ km^3/s^2; p is the focal parameter of the orbit, $p = a(1-e^2)$; i is the orbit inclination; u is the orbit argument of latitude; ϑ is the orbit truth anomaly; t is the time of spacecraft motion; *S, T, W* are projections of the disturbing radial, transversal, and normal accelerations on the axis of the STW reference frame.

The system of differential equations (2.17) can be used quite well for orbits that are close to circular and do not lie close to the equatorial plane. The system has no peculiarities in polar orbits and is quite effective for Earth Remote Sensing satellites motion analysis. Its effectiveness is explained by a small number of substitutions and necessary calculations.

However, the universal system of differential equations, which does not have peculiarities in close to circular, polar, and equatorial orbits, has a more complex form and is written as follows (Fortescue, 2011):

$$\left.\begin{aligned}
\frac{dh}{dt} &= \frac{h^2}{\xi}\cdot T \\
\frac{de_x}{dt} &= h\cdot\left[S\cdot\sin F + T\cdot\left[\left(\xi+1\right)\cdot\cos F + e_x\right] - W\cdot e_y\frac{\eta}{\xi}\right] \\
\frac{de_y}{dt} &= h\cdot\left[-S\cdot\cos F + T\cdot\left[\left(\xi+1\right)\cdot\sin F + e_y\right] + W\cdot e_x\frac{\eta}{\xi}\right] \\
\frac{di_x}{dt} &= \frac{h\cdot\tilde{\varphi}}{2\xi}W\cdot\cos F \\
\frac{di_y}{dt} &= \frac{h\cdot\tilde{\varphi}}{2\xi}W\cdot\sin F \\
\frac{dF}{dt} &= \frac{\xi^2}{h^3\mu} + W\cdot h\cdot\eta
\end{aligned}\right\}, \qquad (2.18)$$

where

$$e_x = e\cdot\cos\left(\omega+\Omega\right);\ e_y = e\cdot\sin\left(\omega+\Omega\right);\ i_x = \mathrm{tg}\left(\frac{i}{2}\right)\cdot\cos\Omega;$$

$$i_y = \mathrm{tg}\left(\frac{i}{2}\right)\cdot\sin\Omega;\quad h = \sqrt{\frac{p}{\mu}};\quad \xi = 1 + e_x\cos F + e_y\sin F;$$

$$\eta = i_x\sin F - i_y\cos F;\ \tilde{\varphi} = 1 + i_x^2 + i_y^2;\ F = \omega + \Omega + \vartheta.$$

Thus, the usage of this system of differential equations (2.18) makes it possible to avoid all the abovementioned limitations of the analysis of the spacecraft's orbital motion.

2.3. Disturbance model in the analysis of the translational motion of the spacecraft

To analyze the Earth's remote sensing satellite motion, it is advisable to take into account the following perturbations:

1) gravitational perturbations associated with the non-spherical form of the Earth (S_G, T_G, W_G);
2) aerodynamic perturbations of the atmosphere (S_A, T_A, W_A);
3) sunlight pressure perturbations (S_S, T_S, W_S);
4) gravitational perturbations of the Sun (S_{Sn}, T_{Sn}, W_{Sn});
5) Lunar gravitational perturbations (S_L, T_L, W_L);

2.3.1. Gravitational perturbations associated with the Earth's non-sphericity

The main gravitational impact on the spacecraft motion is caused by a perturbation of the deviation of the Earth's gravitational field from the central one. The expansion of the perturbation function in terms of spherical functions is written as follows (National geospatial-intelligence…, 2008):

$$W\left(r_{SC},\phi,\lambda\right)=\frac{\mu}{r_{SC}}\sum_{l=2}^{l_{\max}}\left(\frac{R_{Earth}}{r_{SC}}\right)^{l}\sum_{m=0}^{l}P_{lm}(\sin\phi)\left(C_{lm}^{W}\cos m\lambda+S_{lm}^{W}\sin m\lambda\right), \quad (2.19)$$

where R_{Earth} is the average value of the Earth's radius, 6371 km λ is the geocentric longitude; ϕ is the geocentric latitude; m, l are spherical harmonics degrees; P_{lm} are normalized Legendre functions; C_{lm}^{W}, S_{lm}^{W} are normalized Stokes coefficients.

Thus, r_{SC}, λ, ϕ constitutes a spherical coordinate system that has the following relationship with the cartesian coordinates in WGS-84:

$$\begin{aligned} X_g &= r_{SC}\cos\phi\cos\lambda,\\ Y_g &= r_{SC}\cos\phi\sin\lambda, \quad (2.20)\\ Z_g &= r_{SC}\sin\phi. \end{aligned}$$

In turn, the projections of the acceleration of the gravitational perturbations on the radius vector (r_{SC}), geocentric longitude (λ), and geocentric latitude (ϕ) taking into account the calculation methods (Zbrutskii, 2011) can be written as follows:

$$F_{r_{SC}}=\frac{1}{N_1}\frac{\partial W\left(r_{SC},\phi,\lambda\right)}{\partial r_{SC}}=$$

$$=-\frac{\mu}{r_{SC}^{2}}\sum_{l=2}^{l_{\max}}(l+1)\left(\frac{R_{Earth}}{r_{SC}}\right)^{l}\sum_{m=0}^{l}P_{lm}(\sin\phi)\left(C_{lm}^{W}\cos m\lambda+S_{lm}^{W}\sin m\lambda\right), \quad (2.21)$$

$$F_\lambda = \frac{1}{N_2}\frac{\partial W\left(r_{SC},\phi,\lambda\right)}{\partial\lambda} =$$

$$= \frac{\mu}{r_{SC}^2\cos\phi}\sum_{l=2}^{l_{\max}}\left(\frac{R_{Earth}}{r_{SC}}\right)^l\sum_{m=0}^{l}P_{lm}(\sin\phi)m\left(-C_{lm}^W\sin m\lambda + S_{lm}^W\cos m\lambda\right),$$

$$F_\phi = \frac{1}{N_3}\frac{\partial W\left(r_{SC},\phi,\lambda\right)}{\partial\phi} =$$

$$= \frac{\mu\cos\phi}{r_{SC}^2}\sum_{l=2}^{l_{\max}}\left(\frac{R_{Earth}}{r_{SC}}\right)^l\sum_{m=0}^{l}\frac{\partial P_{lm}(\sin\phi)}{\partial\phi}\left(C_{lm}^W\cos m\lambda + S_{lm}^W\sin m\lambda\right),$$

where $F_{r_{SC}}$, F_λ, F_ϕ are projections of the gravitational perturbations along the radiusvector, geocentric longitude, and latitude; N_1, N_2, N_3 are Lamé coefficients.

For S_G, T_G, W_G perturbative acceleration calculation the next algorithm is needed:

1) Formation of STW vector $\boldsymbol{STW_G} = \begin{bmatrix} T_G & W_G & S_G \end{bmatrix}^T$;

2) Calculation projections of gravitational perturbations on WGS-84 reference frame axes $\boldsymbol{G_{J2000}} = \begin{bmatrix} G_{J2000.x} & G_{J2000.y} & G_{J2000.z} \end{bmatrix}^T$:

$$\boldsymbol{G_{wgs}} = M_{X_g \leftarrow X_{LTP}} \cdot \begin{bmatrix} F_\lambda \\ F_\phi \\ F_{r_{SC}} \end{bmatrix}. \tag{2.22}$$

3) Calculation projections of gravitational perturbations on J2000 reference frame axes $\boldsymbol{G_{J2000}} = \begin{bmatrix} G_{J2000.x} & G_{J2000.y} & G_{J2000.z} \end{bmatrix}^T$:

$$\boldsymbol{G_{J2000}} = M_{X \leftarrow X_g} \cdot \boldsymbol{G_{wgs}}. \tag{2.23}$$

4) Calculation projections of gravitational perturbations on OGRF reference frame axes $\boldsymbol{G_{OGRF}} = \begin{bmatrix} G_{OGRF.x} & G_{OGRF.y} & G_{OGRF.z} \end{bmatrix}^T$:

$$\boldsymbol{G_{OGRF}} = M_{X_o \leftarrow X} \cdot \boldsymbol{G_{J2000}}. \tag{2.24}$$

5) Calculation projections of gravitational perturbations on STW reference frame axes $\boldsymbol{STW_G}$:

$$\boldsymbol{STW_G} = M_{X_{STW} \leftarrow X_{og}} \cdot \boldsymbol{G_{OGRF}}. \tag{2.25}$$

2.3.2. Aerodynamic perturbative accelerations

The aerodynamic perturbative acceleration is proposed to calculate on the base of the methodology which is described in (Fortescue, 2011). The S_A, T_A, W_A are

calculated as follows:

$$S_A = -\frac{1}{2}\rho V \delta \left(\frac{\mu}{pF}\right)^{\frac{1}{2}} \cdot e \cdot \sin \vartheta, \tag{2.26}$$

$$T_A = -\frac{1}{2}\rho V \delta \left(\frac{\mu}{pF}\right)^{\frac{1}{2}} \cdot \left(1 + e \cdot \cos \vartheta + r_{SC} \cdot \alpha_{atm} \cdot \left(\frac{p}{\mu}\right)^{\frac{1}{2}} \cos i\right), \tag{2.27}$$

$$W_A = -\frac{1}{2}\rho V \delta \frac{r_{SC} \cdot \alpha_{atm}}{\sqrt{F}} \cdot \sin i \cdot \cos u, \tag{2.28}$$

where δ is ballistic coefficient, $\delta = \frac{C_x S_{mid}}{2m_{SC}}$, C_x in this case, is taken equal to C_x = = 2.1...2.2 at altitudes from 400 km;

$$F = \left(1 - \frac{r_{per} \cdot \alpha_{atm}}{V_{per}} \cos i\right)^2, \tag{2.29}$$

where α_{atm} is the angular velocity of atmosphere flux rotation, take α_{atm} equal to the Earth's angular velocity around its axis, $\alpha_{atm} = 7.292115 \cdot 10^{-5}$ rad/s; ρ is the atmosphere density; V is the module of spacecraft velocity; r_{per} is the radius vector of the spacecraft at the perigee of the orbit; V_{per} is the velocity of the spacecraft at the perigee of the orbit; S_{mid} is the projection of the spacecraft area to the plane which is orthogonal to the vector of atmospheric dynamic flux; m_{SC} is the spacecraft mass;

Different atmospheric models can be used to calculate the density. The most well-known are JB2006 (Bowman, 2008), NRLMSISE-00 (Picone, 2002), and CIRA-2012 (COSPAR International…, 2012).

2.3.3. Solar pressure perturbations

It is known that the interaction between light radiation and a body that reflects (absorbs) light can lead to pressure on the body. The strength of the light pressure depends on the radiation power and is equal to under normal light incidence on the body (Fortescue, 2011):

$$F_{SP} = \nu \cdot p_{SL} \cdot C_R \frac{S_{sol}}{m_{SC}} \left(\frac{a}{r}\right)^2, \tag{2.30}$$

where ν is the function of the eclipse, $\nu = 1$, if solar part of the orbit, and $\nu = 0$, if eclipse part of the orbit; P_{SL} is the pressure of sunlight, within 1 astronomical unit ($149.6 \cdot 10^6$ km), $P_{SL} = 4.56 \cdot 10^{-6}$ N/m^2, C_R is the light reflection coefficient;

S_{sol} is the reflecting surface area; a is the distance from the Sun to the Earth; r is the distance from the spacecraft to the Sun.

The perturbative acceleration projections S_S, T_S, W_S that affect the movement of the spacecraft under the impact of the sunlight pressure force are determined by the following expressions:

$$S_S = F_{SP}\left(\begin{array}{c} -\cos^2\frac{i}{2}\cos^2\frac{\varepsilon}{2}\cos(\lambda_S-\omega-\vartheta-\Omega)-\sin^2\frac{i}{2}\sin^2\frac{\varepsilon}{2}\times \\ \times\cos(\lambda_S-\omega-\vartheta+\Omega)-\frac{1}{2}\sin i\sin\varepsilon\times \\ \times\left(\cos\left(\lambda_S-\omega-\vartheta\right)-\cos\left(-\lambda_S-\omega-\vartheta\right)\right)-\sin^2\frac{i}{2}\cos^2\frac{\varepsilon}{2}\times \\ \times\cos\left(-\lambda_S-\omega-\vartheta+\Omega\right)-\cos^2\frac{i}{2}\cos^2\frac{\varepsilon}{2}\cos(-\lambda_S-\omega-\vartheta-\Omega) \end{array}\right), \quad (2.31)$$

$$T_S = F_{SP}\left(\begin{array}{c} -\cos^2\frac{i}{2}\cos^2\frac{\varepsilon}{2}\sin(\lambda_S-\omega-\vartheta-\Omega)-\sin^2\frac{i}{2}\sin^2\frac{\varepsilon}{2}\times \\ \times\sin(\lambda_S-\omega-\vartheta+\Omega)-\frac{1}{2}\sin i\sin\varepsilon\times \\ \times\left(\sin\left(\lambda_S-\omega-\vartheta\right)-\sin\left(-\lambda_S-\omega-\vartheta\right)\right)-\sin^2\frac{i}{2}\cos^2\frac{\varepsilon}{2}\times \\ \times\sin\left(-\lambda_S-\omega-\vartheta+\Omega\right)-\cos^2\frac{i}{2}\cos^2\frac{\varepsilon}{2}\sin(-\lambda_S-\omega-\vartheta-\Omega) \end{array}\right), \quad (2.32)$$

$$W_S = F_{SP}\left(\begin{array}{c} \sin i\cos^2\frac{\varepsilon}{2}\sin\left(\lambda_S-\Omega\right)-\sin i\sin^2\frac{\varepsilon}{2}\sin\left(\lambda_S+\Omega\right)- \\ -\cos i\sin\varepsilon\sin\lambda_S \end{array}\right), \quad (2.33)$$

where ε is the ecliptic inclination; λ_s is the ecliptic longitude of the Sun.

2.3.4. Sun and Lunar gravitational perturbative accelerations

Sun and Lunar gravitational perturbations are calculated using the next algorithm (Zbrutskii, 2011):

1) Using approaches of astronomical calculations it can be determined the positions of the Moon and Sun in J2000 cartesian coordinates $\boldsymbol{R}_{\boldsymbol{Lun}} = \left[X_L \;\; Y_L \;\; Z_L\right]^T$; $\boldsymbol{R}_{\boldsymbol{Sun}} = \left[X_{Sn} \;\; Y_{Sn} \;\; Z_{Sn}\right]^T$.

2) Using transition matrixes (1.1—1.4) or quaternions (1.11—1.13) calculate cartesian coordinates of spacecraft in J2000 $\boldsymbol{R_{SC}} = \begin{bmatrix} X_{SC} & Y_{SC} & Z_{SC} \end{bmatrix}^T$. For example, it can be calculated as follows:

$$\begin{bmatrix} X_{SC} \\ Y_{SC} \\ Z_{SC} \end{bmatrix} = \begin{pmatrix} \begin{pmatrix} \cos\Omega\cos u - \\ -\sin\Omega\sin u\cos i \end{pmatrix} & \begin{pmatrix} \sin\Omega\cos u + \\ +\cos\Omega\sin u\cos i \end{pmatrix} & \sin i\sin u \\ \begin{pmatrix} -\cos\Omega\sin u - \\ -\sin\Omega\cos u\cos i \end{pmatrix} & \begin{pmatrix} -\sin\Omega\sin u + \\ +\cos\Omega\cos u\cos i \end{pmatrix} & \sin i\cos u \\ \sin\Omega\sin i & -\cos\Omega\sin i & \cos i \end{pmatrix}^T \begin{bmatrix} r_{SC} \\ 0 \\ 0 \end{bmatrix}.$$

3) Calculate the distances from the Moon to the Earth center R_{Lun}, and from the Sun to the Earth center R_{Sun}:

$$\begin{aligned} R_{Lun} &= \sqrt{X_{Lun}^2 + Y_{Lun}^2 + Z_{Lun}^2}, \\ R_{Sun} &= \sqrt{X_{Sun}^2 + Y_{Sun}^2 + Z_{Sun}^2}. \end{aligned} \tag{2.34}$$

4) Calculate the distances from spacecraft to the Moon and Sun :

$$\begin{aligned} R_{SC\ \ Lun} &= \sqrt{\left(X_{Lun} - X_{SC}\right)^2 + \left(Y_{Lun} - Y_{SC}\right)^2 + \left(Z_{Lun} - Z_{SC}\right)^2} \\ R_{SC\ \ Sun} &= \sqrt{\left(X_{Sun} - X_{SC}\right)^2 + \left(Y_{Sun} - Y_{SC}\right)^2 + \left(Z_{Sun} - Z_{SC}\right)^2} \end{aligned} \tag{2.35}$$

5) Calculate the projections of perturbative gravitational accelerations on the J20000 reference frame.

A) Vector of Lunar perturbative accelerations projections on J2000 Reference Frame axes $\boldsymbol{W_{Lun}} = \begin{bmatrix} W_{L.X} & W_{L.Y} & W_{L.Z} \end{bmatrix}^T$:

$$\begin{aligned} W_{L.X} &= \frac{\mu_{Lun}\cdot\left(X_{Lun} - X_{SC}\right)}{R_{SC-Lun}^3} - \frac{\mu_{Lun}X_{Lun}}{R_{Lun}^3}, \\ W_{L.Y} &= \frac{\mu_{Lun}\cdot\left(Y_{Lun} - Y_{SC}\right)}{R_{SC-Lun}^3} - \frac{\mu_{Lun}Y_{Lun}}{R_{Lun}^3}, \\ W_{L.Z} &= \frac{\mu_{Lun}\cdot\left(Z_{Lun} - Z_{SC}\right)}{R_{SC-Lun}^3} - \frac{\mu_{Lun}Z_{Lun}}{R_{Lun}^3}, \end{aligned} \tag{2.36}$$

where μ_{Lun} is the Lunar gravitational constant.

B) Vector of Sun perturbative accelerations projections on J2000 Reference Frame axes $\boldsymbol{W_{Sun}} = \begin{bmatrix} W_{S.X} & W_{S.Y} & W_{S.Z} \end{bmatrix}^T$:

$$W_{S.X} = \frac{\mu_{Sun} \cdot \left(X_{Sun} - X_{SC} \right)}{R_{SC-Sun}^3} - \frac{\mu_{Sun} X_{Sun}}{R_{Sun}^3},$$

$$W_{S.Y} = \frac{\mu_{Sun} \cdot \left(Y_{Sun} - Y_{SC} \right)}{R_{SC-Sun}^3} - \frac{\mu_{Sun} Y_{Sun}}{R_{Sun}^3}, \tag{2.37}$$

$$W_{S.Z} = \frac{\mu_{Sun} \cdot \left(Z_{Sun} - Z_{SC} \right)}{R_{SC-Sun}^3} - \frac{\mu_{Sun} Z_{Sun}}{R_{Sun}^3}.$$

where μ_{Sun} is the Sun's gravitational constant.

6) Using matrixes (1.2)—(1.3) calculate the S_{Sn}, T_{Sn}, W_{Sn} and S_L, T_L, W_L from W_{Sun} and W_{Lun} vectors respectively.

2.4. Mathematical model of spacecraft attitude motion

The mathematical model of spacecraft motion with a payload around the center of mass is described by the dynamic Euler equations:

$$J \frac{d\omega}{dt} + \omega \times \left(J\omega \right) = \mathrm{M}^{\mathrm{cont.}} + \mathrm{M}^{\mathrm{pert.}}, \tag{2.38}$$

where $J = \begin{bmatrix} J_{xx} & J_{xy} & J_{xz} \\ J_{yx} & J_{yy} & J_{yz} \\ J_{zx} & J_{zy} & J_{zz} \end{bmatrix}$ is the inertia tensor of the spacecraft is calculated in the Body Reference Frame; $\omega = \begin{bmatrix} \omega_x & \omega_y & \omega_z \end{bmatrix}^{\mathrm{T}}$ is the angular velocity vector of the spacecraft rotation measured in BRF (rotation BRF relative J2000 in BRF coordinates); $\mathrm{M}^{\mathrm{cont.}} = \begin{bmatrix} M_x^{cont.} & M_y^{cont.} & M_z^{cont.} \end{bmatrix}^{\mathrm{T}}$ is the vector of the control torques in BRF; $\mathrm{M}^{\mathrm{pert.}} = \begin{bmatrix} M_x^{pert.} & M_y^{pert.} & M_z^{pert.} \end{bmatrix}^{\mathrm{T}}$ is the vector of the total torque of perturbations acting on the spacecraft in BRF.

The models take into account gravitational, aerodynamic, and magnetic perturbative torques, as well as the solar pressure perturbative torque. In turn, the control torque can be the torques generated by Reaction Wheels (RW), jet actuators of angular motion, or magnetorquers.

In turn, to analyze the kinematic parameters of the spacecraft attitude motion, it is advisable to use the equation in Rodrigues—Hamilton parameters,

which is written as follows (Alpatov, 2019b):

$$\begin{bmatrix} \frac{dQ_0}{dt} \\ \frac{dQ_X}{dt} \\ \frac{dQ_Y}{dt} \\ \frac{dQ_Z}{dt} \end{bmatrix} = 0,5 \cdot \begin{bmatrix} 0 & -\omega_x & -\omega_y & -\omega_z \\ \omega_x & 0 & \omega_z & -\omega_y \\ \omega_y & -\omega_z & 0 & \omega_x \\ \omega_z & \omega_y & -\omega_x & 0 \end{bmatrix} \begin{bmatrix} Q_0 \\ Q_X \\ Q_Y \\ Q_Z \end{bmatrix}, \tag{2.39}$$

where Q_0, Q_1, Q_2, Q_3 are the components of the quaternion of rotation from LVLH to BRF in BRF coordinates.

2.4.1. Perturbative torques

The gravitational torque is calculated as follows:

$$\mathrm{M}^{\mathrm{grav.}} = 3 \cdot \frac{\mu}{r_{SC^3}} \cdot \overline{k} \times j \cdot \overline{k}\,, \tag{2.40}$$

where $\overline{k}$ a unit vector directed along the radius vector connecting the center of the Earth with the center of mass of the satellite; r_{SC} is a module of spacecraft radius-vector; J is the inertia tensor of the spacecraft is calculated in the BRF.

The vector of the aerodynamic torque acting on the spacecraft can be written as follows (Markley, 2014):

$$\mathrm{M}^{\mathrm{aero}} = \sum_{i=1}^{n} (r_i^A \times f_a^i), \tag{2.41}$$

where r_i^A is the vector directed from the center of mass of the spacecraft to the i-th panel center of aerodynamic pressure; f_a is the aerodynamic braking force acting on the i-th plate.

The vector of the solar pressure torque acting on the spacecraft can be determined using a similar aerodynamic torque approach:

$$\mathrm{M}^{\mathrm{solar}} = \sum_{i=1}^{n} (r_i^S \times f_s^i)\,, \tag{2.42}$$

where r_i^S is the vector from the spacecraft's center of mass to the center of pressure of the SRP on the i-th plate; f_S is the solar pressure force acting on the i-th plate.

The magnetic perturbative torque vector is defined as follows:

$$\mathrm{M}_m^{per.} = \overline{\mathrm{p}}_m \times B_{EMF}\,, \tag{2.43}$$

where $\overline{p}_m$ is the vector of the residual magnetic dipole moment of the spacecraft generated as a result of the operation of the electromagnetic systems of all electrical equipment; B_{EMF} is the vector of Earth's magnetic field (EMF) induction in SBF coordinates.

In general, when it is necessary to accurately determine the values of the Earth's magnetic field vector in the polar geographic coordinate system, the WMM2023 (State of the Geomagnetic…, 2023) or (Chulliat, 2020) is used, the potential expansion of which is written as follows:

$$V\left(r_{SC},\phi_1,\lambda\right)=R_{Earth}\sum_{n=1}^{N}\left(\frac{R_{Earth}}{r_{SC}}\right)^{n+1}\sum_{m=0}^{n}\left(g_n^m\left(t\right)\cdot\cos m\lambda+h_n^m\left(t\right)\sin m\lambda\right)P_{nm}(\cos\phi_1),\tag{2.44}$$

where $R_{Зем}$ = 6371 km is the averaged Earth radius; r_{SC} is the spacecraft radius-vector module; λ is the longitude; $\phi_1 = 90° - \phi$ is addition to geocentric latitude (co-latitude) g_n, h_n are the time-dependent Schmidt coefficients determined according to Table (Chulliat, 2020); P_{nm} are the quasi-normalized Legendre functions.

In turn, the projections of the EMF vector on the r_{SC}, λ, ϕ_1 axes are written as follows:

$$B_{\phi_1}=-\frac{1}{r_{SC}}\frac{\partial V\left(r_{SC},\phi_1,\lambda\right)}{\partial\phi_1}=$$

$$=-\sum_{n=1}^{N}\left(\frac{R_{Earth}}{r_{SC}}\right)^{n+2}\sum_{m=0}^{n}\left(g_n^m\left(t\right)\cdot\cos m\lambda+h_n^m\left(t\right)\sin m\lambda\right)\frac{\partial P_{nm}(\cos\phi_1)}{\partial\phi_1},$$

$$B_{\lambda}=-\frac{1}{r_{SC}\sin(\phi_1)}\frac{\partial V\left(r_{SC},\phi_1,\lambda\right)}{\partial\lambda}=$$

$$=\sum_{n=1}^{N}\left(\frac{R_{Earth}}{r_{SC}}\right)^{n+2}\sum_{m=0}^{n}m\left(g_n^m\left(t\right)\cdot\sin m\lambda-h_n^m\left(t\right)\cos m\lambda\right)\frac{P_{nm}(\cos\phi_1)}{\sin\phi_1},$$

$$B_{r_{SC}}=-\frac{\partial V\left(r_{SC},\phi_1,\lambda\right)}{\partial r_{SC}}=$$

$$=\sum_{n=1}^{N}(n+1)\left(\frac{R_{Earth}}{r_{SC}}\right)^{n+2}\sum_{m=0}^{n}\left(g_n^m\left(t\right)\cdot\cos m\lambda+h_n^m\left(t\right)\sin m\lambda\right)P_{nm}(\cos\phi_1),\tag{2.45}$$

where $B_{\phi 1}$, B_{λ}, B_{rSC} are projections on r_{SC}, λ, ϕ_1.

The conversion of the magnetic induction vector to other coordinate systems is carried out by the same method as the conversion of the gravitational potential.

CHAPTER 3

MODELS TO CHOOSE DESIGN PARAMETERS OF AERODYNAMIC DEORBITING SYSTEMS

3.1. Classification of aerodynamic deorbit systems

It is expedient to subordinate the development of general models of technical systems to a set of rules that will streamline the process of creating models and improve the quality of modeling. One of the main such rules is the use of classification of systems as a basis for building a model of a technical system. The availability of classification of technical systems makes it possible to determine the type of structure of a complex technical system, which allows the system to be decomposed according to a typical structure.

The most complete definition of the concept of classification is given in (Kondakov, 1975): «Classification (lat. Classis — category, group; facio — to do) — the division of objects of any kind into interconnected classes according to the most significant features characteristic of objects of a given kind[1] and which distinguishes them from objects of other kinds». Each class occupies a certain permanent place in the obtained system — classifier and is divided into subclasses.

When classifying any artificial information, the starting point in the distribution of concepts is the uncontroversial establishment of types. In this case, the specific concept is the aerodynamic deorbit system. Structurally, the aerodynamic system consists of an aerodynamic element (AE), inflation, deployment, and storage subsystems on board the spacecraft. In the figure shown in Fig. 3.1 classification (Palii, 2017), all signs mainly refer to the shape, formation, and various modifications of the AE, which directly interacts with the oncoming flow of rarefied atmosphere.

[1] A kind is a logical characteristic of a class of objects, which includes other classes of objects that are types of a given kind — a concept broader in scope than that compared to it (Kondakov, 1975).

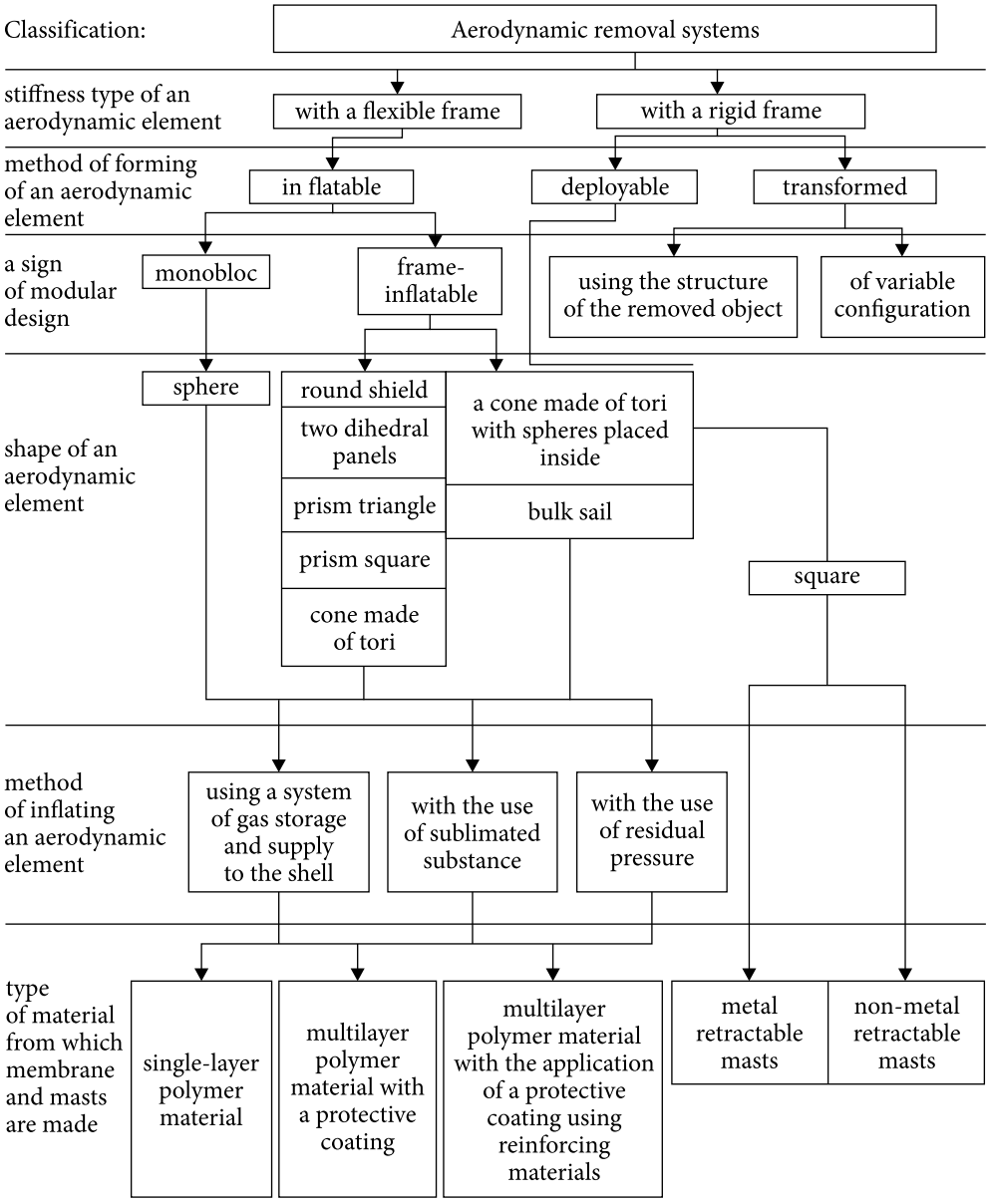

Fig. 3.1. Classifier of aerodynamic deorbit systems

Aerodynamic deorbit systems can be divided into classes according to the degree of rigidity of the aerodynamic element: ADS with a flexible frame; and ADS with a rigid frame. All inflatable ADSs with a flexible frame are included, and ADSs with a rigid frame are ADSs, the AE frame of which is made of metal or composite material. Each of the presented classes can be divided into subclasses according to the most characteristic features of ADS.

According to the method of forming, aerodynamic deorbit systems are divided into subclasses: inflatable, deployable, and transformed. Inflatable ADSs can be classified according to the modularity of the AE design into groups: monoblock, and frame-inflatable. Also, on this basis, transformed ADS can be classified using the transformation of the design elements of the removed object, the variable configuration. The subgroup of monoblock ADS includes systems with spherical AE.

Modular ADSs in the form of AE, in turn, are divided into groups: round shield; two dihedral panels; pyramide triangle; pyramide square; a cone composed of tori; a torus with spheres placed inside; bulk sail.

Deployable ADSs are divided into subgroups according to the shape of AE. An example of such a subgroup is AE in the form of a square sail. Also, inflatable ADSs are divided into subgroups based on the method of AE inflation: due to the use of the gas storage and supply system to the inflatable element of the AE; due to the use of a sublimating substance; due to the use of residual pressure.

Depending on the type of masts used to form AEs, deployable systems are divided into subclasses: using metal masts to form AEs; with the use of non-metal masts for the formation of AE.

Depending on the type of material from which the AE membrane is made, systems of this type are divided into the following subgroups: a membrane made of a single-layer polymer material; a membrane made of multilayer polymer material with a protective coating; a membrane made of multilayer polymer material with a protective coating using reinforcing materials.

According to the degree of complexity of the elements of the system, three of its levels will be considered:

systems level; level of subsystems; and element level.

Depending on the class, the ADS contains the following subsystems: the aerodynamic element (AE); the inflation system (IS); the deployment system (DS); the storage system (SS) on board the SC.

In general, the ADS consists of the following modules: AE, IS, DS, and SS. Thus, the ADS mass m_{ACB} will be determined by the expression:

$$m_{ACY} = m_{A\Theta} + m_{CH} + m_{CP} + m_{CX}, \tag{3.3}$$

where $m_{A\Theta}$ is the mass of AE; m_{CH} — mass of IS; m_{CP} — mass of DS; m_{CX} — mass of SS.

The aerodynamic element is a part of the aerodynamic deorbit system, which directly interacts with the flow of the oncoming rarefied atmosphere, therefore, it has requirements for the reliability of functioning under the influence of space factors (space vacuum, solar radiation, atomic oxygen, SD). The IS is made in the form of a gas storage and supply system to the inflatable element of the AE. Deployment system ADS consists of a combination of coils on which retractable masts are wound, pressure rollers, and electric drives. The SS is a container with a lid that opens before the ADS is activated.

3.2. Determination of the aerodynamic deorbiting system parameters functioning

As you know, the structure and functioning are the most important properties of the system. The functioning of the system is determined by the structure. According to (Kondakov, 1975): «structure (lat. structura — structure, connection) is a strong, relatively stable connection (relationship) and interaction of elements, parties, parts of an object, phenomenon, process as a whole.» An ordered set of elements that make up a technical system is grouped by systems of lower levels of complexity. The hierarchical structure of the ADS and the composition of the corresponding project parameters are shown in Fig. 3.2 (Wang, 2023).

In Fig. 3.2 is shown: I, II, III — levels of systems, subsystems, and elements, respectively; t_L is the term of the orbital existence of a space object; S_M is the cross-section area of the aerodynamic element; m_{ACB} is the ADS mass; m_{AE} is the mass of the aerodynamic element; $S_{ПНЕ}$ is the total surface area of inflatable elements; $S_{ПЕР}$ is the cross-section area of deployable elements; V_{MHE} is the volume of inflatable elements; V_{MEP} is the volume of deployable elements; m_{HE} is the mass of inflatable elements; m_{EP} is the mass of deployable elements; V_{CP} is the volume of deployment system; m_{CP} is the mass of deployment system; $m_Г$ is the mass of gas for inflation; $m_{СГЗР}$ is the mass of gas storage and supply system to the shell; m_{CH} is the mass of inflation system; R_E is the volume coefficient of deorbited mass under the action of atomic oxygen in near-Earth space; δ_{MEP} is the material thickness of deployable elements; ρ_{MEP} is the material density of deployable elements; a_{EP} is the width of a deployable element; l_{EP} is the length of a deployable element;

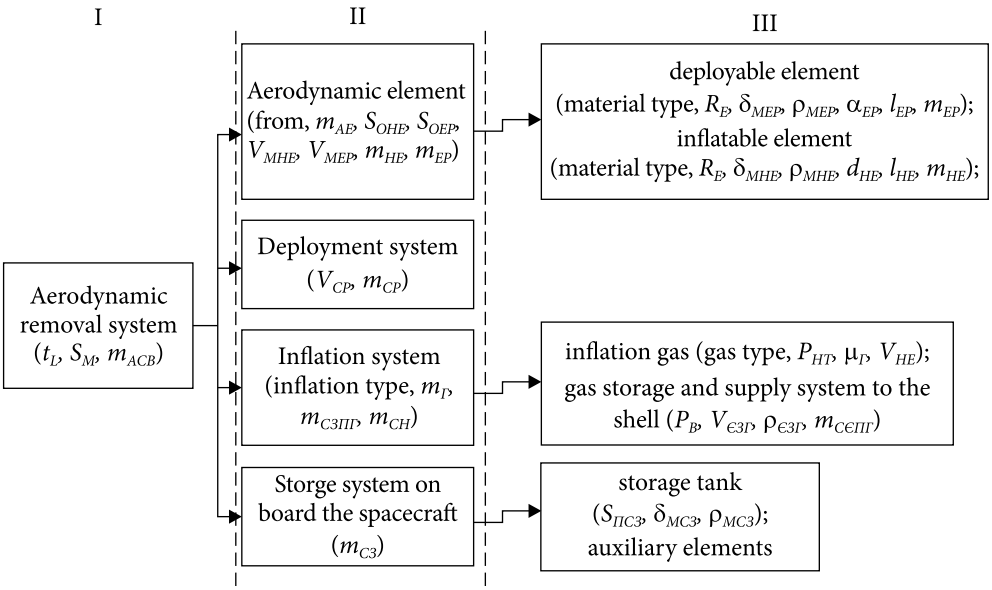

Fig. 3.2. Hierarchical structure of ADS

δ_{MHE} is the material thickness of inflatable elements; ρ_{MHE} is the material density of inflatable elements; d_{HE} is the diameter of an inflatable element; l_{HE} is the length of an inflatable element; P_{HT} is the excess pressure in an inflatable element; μ_{Γ} is the molecular mass of gas for inflation; V_{HE} is the volume of inflatable elements; P_B is the internal pressure in the gas storage due to inflation; $V_{\epsilon 3\Gamma}$ is the volume of the gas storage tank; $\rho_{\epsilon 3\Gamma}$ is the density of the gas storage tank material; $S_{\Pi 3\Gamma}$ is the surface area of the storage system; δ_{MC3} is the material thickness of the storage system; ρ_{MC3} is the density of the material of the storage system.

The design parameters indicated by the given classifier of aerodynamic deorbit systems and the corresponding description of the structure of the deorbit system are calculated using appropriate mathematical models. The following initial data are used to calculate the parameters of the deorbit system: the lifetime, the mass of the deorbited space object and its cross-sectional area, and the cross-sectional area of the aerodynamic element. The latter is calculated according to the following model (Klinkrad, 2006):

$$S_M = \frac{2m_{KA}\sqrt{\frac{a}{\mu}}\cdot X(e,z)}{t_L 3\rho_{pe}C_X} + S_{MKO}, \tag{3.2}$$

$$X(e,z) = \frac{3\cdot e\cdot \exp(z)}{4I_0(z)+8eI_1(z)}\left\{1+\frac{7e}{6}+\frac{5e^2}{16}+\frac{1}{2z}\left(1+\frac{11e}{12}+\frac{3}{4z}+\frac{3}{4z^2}\right)\right\}, \tag{3.3}$$

where C_X is the coefficient of aerodynamic resistance; ρ_{pe} is the density of the atmosphere at the perigee of the orbit; $I_k(z)$ — Bessel functions of order k = 0 and 1 and argument $z = ae/H_{\rho,pe}$; e —orbital eccentricity; μ — gravitational parameter of the Earth; m_{KA} — spacecraft mass; a — the semi-major axis of the orbit; $H_{\rho,pe}$ — the height of the dense atmosphere.

The selection of initial data for the calculation of the parameters of the ADS under the conditions of the movement of the removing object along the appropriate orbit is carried out using the appropriate nomograms, which are given in Chapter 5, and calculated according to the methodology outlined in Chapter 3.

3.3. Aerodynamic element parameters

In general, the mass of the aerodynamic element is determined using the expressions:

$$m_{A\Theta} = m_{H\Theta} + m_{P\Theta}, \tag{3.4}$$

$$m_{H\Theta} = V_{MH\Theta}\cdot \rho_{MH\Theta}, \tag{3.5}$$

$$m_{P\Theta} = V_{MP\Theta}\cdot \rho_{MP\Theta}\, m_{P\Theta} = V_{MP\Theta}\cdot \rho_{MP\Theta}, \tag{3.6}$$

$$V_{MH\Theta} = S_{\Pi H\Theta}\cdot \delta_{MH\Theta}, \tag{3.7}$$

$$V_{MP\Theta} = S_{\Pi P\Theta}\cdot \delta_{MPE}\, V_{MP\Theta} = S_{\Pi P\Theta}\cdot \delta_{MP\Theta}, \tag{3.8}$$

where $m_{AЭ}$ is a mass of AE; $m_{НЭ}$ is the mass of inflatable elements; $m_{РЭ}$ is the mass of deployable elements; $V_{МНЭ}$ is the material volume of inflatable elements; $\rho_{МНЭ}$ is the material density of inflatable elements; $V_{МРЭ}$ is the material volume of deployable elements; $\rho_{МРЭ}$ is the material density of deployable elements; $S_{ПНЭ}$ is the surface area of inflatable elements; $\delta_{МНЭ}$ is the material thickness of inflatable element; $S_{ПРЭ}$ is the surface area of deployable elements; $\delta_{МРЭ}$ is the material thickness of deployable elements.

These parameters are calculated according to the following algorithm and corresponding mathematical models.

The analysis of the ADS design schemes, the descriptions of which are given in Chapter 1, showed that polymer film materials are used for the manufacture of aerodynamic elements, the characteristics of which are given in Table 3.1.

The design value of the material thickness of inflatable and deployable elements is determined by the formula (Wang, 2023):

$$\delta_{MHE} = \delta_{MPE} = \delta_0 + \left(\delta_C + \delta_A\right) \cdot \left(1 + \underline{\delta}\right), \tag{3.9}$$

where δ_0 is the minimum thickness of the film material at which the shell maintains its integrity under the influence of internal pressure, since the internal pressure in the ADS shell is several times of magnitude higher than the external pressure of the Earth's atmosphere, the deforming moments can be neglected, thus the minimum thickness of the film material is calculated using known expressions from the theory of momentless shells; δ_C is the thickness of the material that will be removed from the shell due to the influence of space vacuum (sublimation); δ_A is the thickness of the material that will be removed from the shell due to the influence of atomic oxygen; δ_{MHE} is the estimated material thickness of inflatable elements; δ_{MPE} is the calculated material thickness of deployable elements; $\underline{\delta}$ is

Table 3.1. **Characteristics of polymer film materials**

Material	Volumetric coefficient of mass loss R_e, cm³/atom	Density ρ, kg/m³	Modulus of elasticity $\sigma_{пр}$, Pa
Mylar	$3.01 \cdot 10^{-24}$ (McCarthy, 2010)	1390 (Mylar…, 2017)	$3.38 \cdot 10^{9}$ (Mylar…, 2017)
Upilex-S	$9.22 \cdot 10^{-25}$ (McCarthy, 2010)	1470 (Upilex…)	$9.1 \cdot 10^{10}$ (Upilex…)
Kapton-H	$3 \cdot 10^{-24}$ (McCarthy, 2010)	1420 (DuPont™ Kapton)	$2.76 \cdot 10^{10}$ (DuPont™ Kapton)
PTFE	$1.42 \cdot 10^{-25}$ (McCarthy, 2010)	2150 (McCarthy, 2010)	$1.75 \cdot 10^{10}$ (Overview of…)
Kapton-Al_2O_3	$2.5 \cdot 10^{-26}$ (Space…, 1996)	1390 (DuPont™ Kapton)	$3.38 \cdot 10^{9}$ (DuPont™ Kapton)
Kapton-FN	$5 \cdot 10^{-26}$ (Space…, 1996)	1530 (DuPont™ Kapton FN)	$2.48 \cdot 10^{10}$ (DuPont™ Kapton FN)

the calculation error, which is determined using the expression:

$$\underline{\delta} = \delta_{BK} + \delta_{F10.7} + \delta_{AK}, \tag{3.10}$$

δ_{BK} is the error to determine the ballistic coefficient, according to (Patent of the Russian Federation for the invention No. 2463223), (Nazarenko, 2013), we take 600—1000 km for the entire range of orbital altitudes; $\delta_{F10.7}$ is the error to forecast the solar activity index, according to (Vitinsky, 1973), (State Standard 25645.302-83), we take 600—1000 km for the entire range of orbital altitudes; δ_{AK} is the error to determine the concentration of atomic oxygen, according to (Montenbruck, 2005), (State Standard R 25645.166-2004), we take 600—750 km for the range of orbital altitudes, 750—1000 km for the range of orbital altitudes.

Thus, the coefficient of error to determine the material thickness of inflatable and deployable elements for the range of orbital altitudes of 600—750 km will be equal to $\delta_{AK} = 0.02$, and for the range of orbital altitudes of 750—1000 km will be equal to $\delta_{AK} = 0.25$. For a spherical film element, the minimum thickness of the film material δ_0 will be defined as (Pisarenko, 1988):

$$\delta_0 = \frac{P_{HT} r_C}{2\sigma}, \tag{3.11}$$

where P_{HT} is the excess pressure in the shell of the inflatable element of the ADS; r_C is the radius of the spherical inflatable element; σ is the tensile strength of the material, according to (Handbook…, 1987).

For a cylindrical film element, the minimum thickness of the film material will be determined as [(Pisarenko, 1988):

$$\delta_0 = \frac{P_{HT} r_{Ц}}{\sigma}, \tag{3.12}$$

where $r_{Ц}$ is the radius of the cylindrical inflatable element.

For a toroidal film element, the minimum thickness of the film material will be determined (Pisarenko, 1988):

$$\delta_0 = \frac{P_{HT} r_{CT} \left(2r_T - r_{CT}\right)}{2\sigma\left(r_T - r_{CT}\right)}, \tag{3.13}$$

where r_{CT} is the cross-sectional radius of the toroidal inflatable element; r_T is the radius of the toroidal inflatable element.

The impact of the space vacuum on the polymer material leads to its loss, primarily due to its sublimation. The rate of change in the thickness of the polymer material under the influence of sublimation is determined by the expression (Evaporation effects…, 1961):

$$\delta_C = \int_{t_0}^{t} S_{П} \frac{p_{THГ}}{\rho_{ПМ}} \sqrt{\frac{\mu_{ПМ}}{2\pi N_A k \ T_{ППМ}}}\, dt, \tag{3.14}$$

where $S_{П}$ is the surface area of the ADS; $p_{ТНГ}$ is the saturated gas pressure of the sublimated material is determined by the formula (Evaporation effects…, 1961):

$$p_{ТНГ} = 0.0007181 \cdot e^{\left(A - \frac{B}{T_{ППМ_i}}\right)}, \quad (3.15)$$

where A, B are the coefficients, taken according to (Jensen, 1956) to be equal to $A = 3$, $B = 3000$; $\rho_{ПМ}$ is the density of sublimated film material; $\mu_{ПМ}$ is the molecular mass of the film material; N_A is the Avogadro's number, $N_A = 6.022 \cdot 10^{23}$ mol^{-1}; $k_Б$ is the Boltzmann constant, $k_Б = 1.38 \cdot 10^{-23}$ J/K; $T_{ППМ_i}$ — temperature of the film material surface, which is calculated according to the formulas (Fortescue, 2011) in the shady and sunny parts of the orbit:

$$T_{ППМ_0} = \sqrt[4]{\frac{S_Ç J_Ç}{S_П \sigma} + \frac{S_A J_A}{S_П}\left(\frac{\alpha}{\varepsilon}\right)}, \quad (3.16)$$

where S_3 is the projection area of the spacecraft onto the plane perpendicular to the direction of the Earth's radiation, for unoriented flight, we take it equal to the area of the middle cross-section S_M; J_3 is the intensity of the Earth's radiation; α is the material absorption coefficient, for example, for polyimide (Fortescue, 2011); ε is the emissivity of the material, for example, for polyimide (Fortescue, 2011); $S_П$ is the surface area of the spacecraft; σ is the Stefan Boltzmann constant, $\sigma = 5.67 \cdot 10^{-8}$ W $\cdot$ m^{-2} $\cdot$ K^{-4}; S_A is the projection area of the spacecraft on the plane perpendicular to the direction of the radiation of the Sun reflected from the Earth; J_A is the intensity of the radiation of the Sun reflected from the Earth;

$$T_{ПППМ_1} = \sqrt[4]{\frac{S_Ç J_Ç}{S_П \sigma} + \frac{\left(S_A J_A + S_C J_C\right)}{S_П}\left(\frac{\alpha}{\varepsilon}\right)}, \quad (3.17)$$

S_C is the projection area of the spacecraft on the plane perpendicular to the direction of the Sun's radiation; J_C is the intensity of the Sun's radiation.

As is known (Shuvalov, 2014), the environment around the space vehicle during its movement at altitudes of up to ≈800 km is aggressive towards polymer films and coatings of the space vehicle. In near-Earth orbits, the factors that determine the change in the chemical, thermo-optical, and mechanical properties of polymers are high-speed atomic oxygen flows. The change in film thickness under the influence of atomic oxygen is determined by the formula (Shuvalov, 2014):

$$\delta_{AK} = \int_{t_0}^{t} R_E \cdot \Phi_{AK} dt, \quad (3.18)$$

where R_E is the volumetric coefficient of film mass loss, which is determined by the formula (Jenkins, 2001):

$$R_E = 10^{-30} \cdot \left(9.5 - 8.3 \cdot e^{0.15(1-\gamma)}\right), \quad (3.19)$$

where γ is the erosion coefficient; Φ_{AK} is the atomic oxygen flow found from the expression (Space environmental…, 1995):

$$\Phi_{AK} = \rho_{O_i} \cdot V_{KA_i}, \tag{3.20}$$

where ρ_{O_i} is the atomic oxygen concentration at the orbit altitude h_i; V_{KA_i} is the spacecraft velocity at the orbit altitude h_i, for a circular orbit is determined using the expression:

$$V_{KA_i} = \sqrt{\frac{\mu}{r_i}}, \tag{3.21}$$

where r_i is the radius vector of the spacecraft; h_i is the altitude of the spacecraft orbit.

For the ADS class using the transformation of the structural elements of space objects, the AE parameters are not calculated, since it is assumed that the functions of the AE will be performed by the transformed structural elements of the space objects.

3.3.1. Monoblock systems parameters

Structurally, monoblock ADSs consist of AE, IS, and SS. In this work, a sphere is chosen as a typical AE of a system of this class.

The «Sphere» ADS configuration consists of a spherical AE. So, the AE parameters of this configuration are:

- diameter of AE $d_{C\Phi}$;
- volume of AE $V_{C\Phi}$;
- mass of AE $m_{A\Theta}$.

The diameter of the sphere can be expressed in terms of the area of the median cross-section S_M, which for unoriented flight is equal to (Wang, 2023):

$$S_M = \frac{S_{\Pi}}{4}, \tag{3.22}$$

$$S_{\Pi} = 3.141593 d_{C\Phi}^2, \tag{3.23}$$

$$d_{C\Phi} = 1.13\sqrt{S_M}, \tag{3.24}$$

where S_{Π} is the surface area of the sphere.

The volume of the sphere is determined from the ratio:

$$V_{C\Phi} \approx 0.5236 d_{C\Phi}^3 = 0.755\sqrt{S_M^3}. \tag{3.25}$$

The mass of AE is determined using the formulas

$$m_{AE} = 4 S_M \delta_{MHE} \rho_{MHE}, \tag{3.26}$$

where $\rho_{MH\Theta}$ is the material density of inflatable elements; $\delta_{MH\Theta}$ is the material thickness of an inflatable element.

3.3.2. Frame-inflatable systems parameters

Frame-inflatable ADSs structurally consist of a combination of inflatable elements (for example, inflatable masts) and a membrane made of thin-film elastic material.

The following configurations of frame-inflatable ADSs are considered in the work:

«Round Shield»;
«Two dihedral panels»;
«Pyramide Triangle»;
«Pyramide Square»;
«A cone made of tori»;
«A cone made of tori with spheres placed inside»;
«Bulk sail».

The configuration of the «Round shield» ADS consists of 4 inflatable elements (3 inflatable masts and a torus shell) and one deployable element (a flat round shield).

The AE parameters of this configuration are: shield diameter of AE $d_{Щ}$; and volume of inflatable elements V_{HE} mass of AE.

The starting data to calculate the mass of the ADS in the form of a flat round shield are: the area of the median cross-section S_M of the ADS; length of the inflatable masts l_{HM}, which is equal to the diameter of the round shield $d_{Щ}$; diameter of the inflatable masts d_{HM} depends on the length of the inflatable mast l_{HM} and is defined as $d_{HM} = 0.035\ l_{HM}$.

The mass of AE m_{AE} in the form of a flat round shield is determined by the ratios (Wang, 2023):

$$m_{AE} = m_{HE} + m_{PE}, \tag{3.27}$$

$$m_{HE} = V_{MHE}\rho_{MHE}, \tag{3.28}$$

$$m_{PE} = V_{MPE}\rho_{MPE}, \tag{3.29}$$

$$V_{MHE} = S_{ПHE}\delta_{MHE}, \tag{3.30}$$

$$S_{ПHE} = 3S_{HC} + S_T = 0.693d^2, \tag{3.31}$$

where S_{HC} is the surface area of the inflatable sling;

$$S_{HC} \approx 0.112d^2_{Щ}, \tag{3.32}$$

S_T is the surface area of the torus shell to which the circular shield is attached;

$$S_T \approx 0.357d^2_{Щ}, \tag{3.33}$$

$d_{Щ}$ — diameter of the flat round shield;

$$d_{Щ} \approx 1.329\sqrt{S_M}, \tag{3.34}$$

$$V_{MPE} = S_{ПPE}\delta_{MPE}, \tag{3.35}$$

$$S_{ППЕ} = S_{Щ}, \tag{3.36}$$

$S_{Щ}$ — area of the round shield;

$$S_{Щ} \approx 1.571 d^2_{Щ}. \tag{3.37}$$

The volume of inflatable elements is calculated as follows:

$$V_{НЕ} = V_{Т} + V_{НС} \approx 0.01\sqrt{S^3_{М}} \tag{3.38}$$

where $V_{Т}$ is the volume of the torus shell; $V_{НС}$ is the volume of the inflatable sling.

The «Two dihedral panels» ADS configuration consists of 2 inflatable elements (2 inflatable mastribs) and 2 deployable elements (4 faces).

The AE parameters of this configuration are: length of the inflatable mast $l_{НМ}$, by which the length $l_{ДП}$ is determined; diameter of the inflatable mast $d_{НМ}$, it has been accepted $d_{НМ} = 0.035\ l_{ДП}$; width $a_{ДП}$ of the polymer material web of each dihedral panel, while $l_{ДП} = l_{НМ}$ and $a_{ДП} = 0.12\ l_{ДП}$; mass of AE .

The mass of AE m_{AE} in the form of two dihedral panels is determined by the ratios (Wang, 2023):

$$m_{AE} = m_{HE} + m_{PE}, \tag{3.39}$$

$$m_{HE} = V_{MHE}\rho_{MHE}, \tag{3.40}$$

$$m_{PE} = V_{MPE}\rho_{MPE}, \tag{3.41}$$

$$V_{MHE} = S_{ПHE}\delta_{MHE}, \tag{3.42}$$

$$S_{ПHE} = 2S_{НМ}, \tag{3.43}$$

where $S_{НМ}$ is the surface area of the inflatable mast

$$S_{НМ} \approx 0.17\ l^2_{ДП}, \tag{3.44}$$

$l_{ДП}$ — length of the dihedral panel

$$l_{ДП} \approx 1.768\sqrt{S_{М}}, \tag{3.45}$$

$$V_{MPE} = S_{ПPE}\delta_{MPE}, \tag{3.46}$$

$$S_{ПPE} = S_{ТП}, \tag{3.47}$$

$S_{ТП}$ — area of the fabric

$$S_{ТП} \approx 0.48\ l^2_{ДП}. \tag{3.48}$$

The volume of inflatable elements $V_{НЕ}$ is calculated using the following formulas:

$$V_{HE} = 2V_{НМ} \approx 0.011\sqrt{S^3_{М}}, \tag{3.49}$$

where $V_{НМ}$ is the volume of the inflatable mast.

The ADS configuration «Pyramide Triangle» consists of 6 inflatable elements (3 inflatable masts-ribs of the pyramid and 3 inflatable masts-sides of the base of the pyramid) and 3 deployable elements (3 faces of the pyramid).

The initial data to calculate the mass of the AE in the form of a three-sided pyramid are: the diameter of inflatable masts d_{HM} depends on the length of the inflatable mast l_{HM} and is defined as $d_{HM} = 0.035\, l_{HM}$; flat angle A at the top of the pyramid is 60°; area of the median cross-section S_M of the ADS. The AE parameters of this configuration are: the length of the base of the pyramid a_O; and the mass of AE m_{AE}.

The mass of AE in the form of a three-sided pyramid is determined by the relations (Wang, 2023):

$$m_{AE} = m_{HE} + m_{PE}, \tag{3.50}$$

$$m_{HE} = V_{MHE}\rho_{MHE}, \tag{3.51}$$

$$m_{PE} = V_{MPE}\rho_{MPE}, \tag{3.52}$$

$$V_{MHE} = S_{\Pi HE}\delta_{MHE}, \tag{3.53}$$

$$V_{MPE} = S_{\Pi PE}\delta_{MPE}, \tag{3.54}$$

$$S_{\Pi HE} = S_{HM} = 6\left(2 \cdot \pi \cdot 0.0175 a_O^2\right) \approx 0.66 a_O^2, \tag{3.55}$$

where a_O is the length of the base side of the triangular pyramid; S_{HM} is the surface area of inflatable masts;

$$S_{\Pi PE} = S_\Gamma = \frac{p_2 A_2}{2} \approx 1.305 a^2, \tag{3.56}$$

S_Γ is the area of the faces of the pyramid; p_2 is the perimeter of the base of the pyramid

$$p_2 = 3a_O, \tag{3.57}$$

A_2 is the length of the apophemum (height of the face) of the pyramid

$$A_2 = \sqrt{a_f^2 - \frac{a_f^2}{4}} \approx 0.87 a_f^2 \cdot \tag{3.58}$$

Let's express the length of the base of the pyramid in terms of the area of the median cross-section of the ADS (Wang, 2023):

$$S_M = \frac{S_\Pi}{4}, \tag{3.59}$$

$$S_\Pi = S_{\Pi HE} + S_{\Pi PE} = 1.965 a^2, \tag{3.60}$$

$$a_O \approx 1.427\sqrt{S_M}. \tag{3.61}$$

The volume of inflatable elements V_{HE} is calculated using the following formulas:

$$V_{HE} = 6V_{HM} \approx 0.017\sqrt{S_M^3}, \tag{3.62}$$

where V_{HM} the volume of the inflatable mast.

The configuration of the ADS «Pyramide square» consists of 8 inflatable elements (4 inflatable masts-ribs of the pyramid and 4 inflatable masts-sides of the base of the pyramid) and 4 deployable elements (4 faces of the pyramid).

The initial data to calculate the mass of the ARS in the form of a four-sided pyramid are: diameter of inflatable masts d_{HM} depends on the length of the inflatable mast and is defined as $d_{HM} = 0.035 l_{HM}$; flat angle A at the top of the pyramid is 60°; area of the median cross-section of the ARS S_M. The AE parameters of this configuration are: length of the base of the pyramid a_O; mass of AE.

The mass of AE in the form of a triangular pyramide is determined by the relations (Wang, 2023):

$$m_{AE} = m_{HE} + m_{PE}, \tag{3.63}$$

$$m_{HE} = V_{MHE}\rho_{MHE}, \tag{3.64}$$

$$m_{PE} = V_{MPE}\rho_{MPE}, \tag{3.65}$$

$$V_{MHE} = S_{\Pi HE}\delta_{MHE}, \tag{3.66}$$

$$V_{MPE} = S_{\Pi PE}\delta_{MPE}, \tag{3.67}$$

$$S_{\Pi HE} = S_{HM} = 8\left(2 \cdot \pi \cdot 0.0175 a_O^2\right) \approx 0.88 a_O^2, \tag{3.68}$$

where a_O is the length of the side of the base of the triangular pyramid; S_{HM} is the area of inflatable masts;

$$S_{\Pi PE} = S_\Gamma = \frac{p_2 A_2}{2} \approx 1.74 a_O^2, \tag{3.69}$$

S_Γ is the area of the faces of the pyramid; p_2 is the perimeter of the base of the pyramid

$$p_2 = 4a_O, \tag{3.70}$$

A_2 is the length of the apophemum (height of the face) of the pyramid

$$A_2 = \sqrt{a_f^2 - \frac{a_f^2}{4}} \approx 0.87 a_f^2 \cdot \tag{3.71}$$

Let's express the length of the base of the pyramid in terms of the area of the median cross-section of the ARS:

$$S_M = \frac{S_\Pi}{4}, \tag{3.72}$$

$$S_\Pi = S_{\Pi HE} + S_{\Pi PE} = 1.965 a_O^2, \tag{3.73}$$

$$a_O \approx 1.235\sqrt{S_M}. \tag{3.74}$$

The volume of inflatable elements V_{HE} is calculated using the followiing formulas:

$$V_{HE} = 6V_{HM} \approx 0.015\sqrt{S_M^3}\,, \tag{3.75}$$

where V_{HM} is the volume of an inflatable mast.

ADS «Cone made of tori» is made in the form of a conical shell made of tori shells. The number of tori is selected based on the conditions to ensure the required area of the median cross-section. The ADS parameters of this configuration will be: diameter of the 1st torus d_{T_1}; diameter of the nth torus d_{T_n}; the mass of AE m_{AE}. The mass of AE in the form of a conical shell composed of toric shells is determined by the following relations (Wang, 2023):

$$m_{AE} = m_{HE}\,, \tag{3.76}$$

$$m_{HE} = V_{MHE}\rho_{MHE}\,, \tag{3.77}$$

$$V_{MHE} = S_{\Pi HE}\delta_{MHE}\,, \tag{3.78}$$

$$S_{\Pi HE} = S_{\Pi TO} + S_{\Pi HC}\,, \tag{3.79}$$

where$S_{\Pi TO}$ is the surface area of the torus shells

$$S_{\Pi TO} = \sum_{n=1}^{i} S_{\Pi TO_n}\,, \tag{3.80}$$

n is the torus shell number; i is the number of torus shells in AE;

$$S_{\Pi TO_1} = 19.74 d_{KA}\,, \tag{3.81}$$

d_{KA} is the diameter of the removed spacecraft;

$$S_{\Pi TO_n} = 9.87 d_{T_n} d_{KO}\,, \tag{3.82}$$

d_{T_n} is the diameter of the nth torus shell;

$$d_{T_n} = d_{T_{n-1}} + 0.74 d_{KA}\,, \tag{3.83}$$

$S_{\Pi HC}$ is the surface area of inflatable slings

$$S_{\Pi HC} \approx 9.425 d_{HC} l_{HC}\,, \tag{3.84}$$

d_{HC} is the diameter of the inflatable slings, we accept $d_{HC} = 0.1\ d_{KA}$; l_{HC} is the length of the removed spacecraft, we accept $l_{HC} = 0.5\ d_{KA}$.

ADS «Cone made of tori, with spherical shells placed inside» are made in the form of a conical shell, made of toric shells, inside which spherical shells are placed. The number of tori is also selected based on the conditions for ensuring the required cross-section area. The ADS parameters of this configuration will be: diameter of the 1st torus d_{T_1}; diameter of the nth torus d_{T_n}; the diameter of the spherical shell placed inside the torus $d_{C\Phi}$; the number of torus shells n; the number of spherical shells m; the mass of AE m_{AE}. The mass of an aerodynamic element in the form of a cone made of tori, with spherical shells placed inside is determined by the following ratios:

$$m_{AE} = m_{HE}, \tag{3.85}$$

$$m_{HE} = V_{MHE}\rho_{MHE}, \tag{3.86}$$

$$V_{MHE} = S_{ПHE}\delta_{MHE}, \tag{3.87}$$

$$S_{ПHE} = S_{ПТО} + S_{ПНС} + S_{ПС}, \tag{3.88}$$

where $S_{ПТО}$ is the surface area of the torus shells, which is determined using ratios (3.80 — 3.83); $S_{ПНС}$ is the surface area of inflatable slings is defined using an expression (3.84); $S_{ПС}$ is the surface area of the spherical shells, which are placed inside the toric shells, is determined as follows:

$$S_{ПС} = \sum_{n=1}^{i} \left(m_n \pi d_{СФ} \right), \tag{3.89}$$

where n is the amount of torus shells; i is the number of torus shells; $d_{СФ}$ is the diameter of the spherical shell is defined as follows:

$$d_{СФ} = \sqrt{\frac{4S_M - \pi d_{KA}}{12\pi}} \tag{3.90}$$

S_M is the ADS cross-sectional area; d_{KA} is the diameter of a deorbiting space object, for a cylindrical shape, we will apply that in the diameter of its base, for the shape of a cube and a parallelepiped, it will be added that in the diameter of the circle described above; m_n is the number of spherical shells of the nth torus shell is calculated using the scheme shown in Fig. 3.3 and the following ratios (Patent of Ukraine for invention № 109194, 2015):

$$m_n = \frac{\pi(d_{n_{зов}} + d_n)}{d_{n_{зов}} - d_n} \tag{3.91}$$

$d_{n_{зов}}$ is the outer diameter of the nth torus shell is determined as follows:

$$d_{n_{зов}} = d_n + d_{СФ} \tag{3.92}$$

d_n is the diameter of the nth torus; $d_{n_{вн}}$ is the inner diameter of the nth torus shell is calculated using the expression:

$$d_{n_{вн}} = d_n - d_{СФ} \tag{3.93}$$

ADS «Bulk sail» structurally consists of 3 round membranes, which are placed orthogonally to each other, to which are attached toric shells, inside which spherical shells are placed. To increase the rigidity of the structure, inflatable masts are orthogonally attached to the diameter of the shield, which also contains spherical shells inside. Let us assume that the cross-sectional diameter of the torus shell d_{TO} coincides with the cross-sectional diameter of the inflatable mast $d_{НЩ}$ and is defined as $d_{TO} = d_{НЩ} = 0.035d_M$, where d_M is the diameter of the membrane of

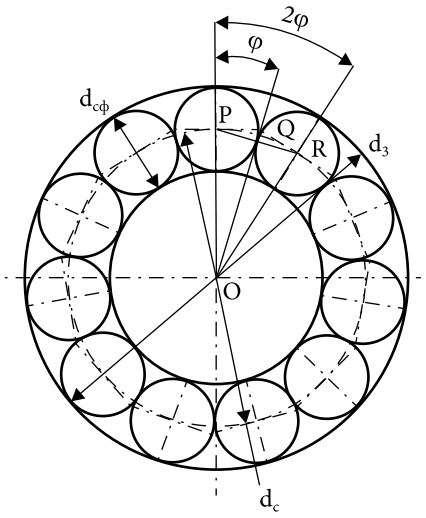

Fig. 3.3. Structural diagram for calculating the number of spherical shells: d_C — cross-sectional diameter of the torus; $d_{C\Phi}$ — diameter of the spherical shell, which is placed in the torus shell; $d_з$ — diameter of the torus; φ — angle of placement of spherical shells in the torus shell

the round shield. The AE parameters of this ADS configuration are the following list: the diameter of the membrane of the round shield d_M; and the mass of the aerodynamic element m_{AE}.

The mass of the aerodynamic element m_{AE} is determined using the expressions:

$$m_{AE} = m_{HE} + m_{PE}, \tag{3.94}$$

where m_{HE} is the mass of inflatable elements; m_{PE} is the mass of deployable elements. The mass of inflatable elements is defined as:

$$m_{HE} = m_{НЩ} + m_{TO}, \tag{3.95}$$

$$m_{НЩ} = 3S_{ПНЩ} \cdot \delta_{МНЩ} \cdot \rho_{МНЩ} + n_{СФНЩ} S_{ПСНЩ} \cdot \delta_{МСНЩ} \cdot \rho_{МСНЩ},$$

$$S_{ПНЩ} = 0{,}11 d^2_M \tag{3.96}$$

$$n_{СФНЩ} = 3\frac{d_M}{0.035 d_M} \approx 87, \tag{3.97}$$

$$S_{ПСНЩ} = 0{,}00385 d^2_M, \tag{3.98}$$

$$m_{TO} = 3S_{ПТО} \cdot \delta_{МТО} \cdot \rho_{МТО} + n_{СФТО} S_{ПСТО} \cdot \delta_{МСТО} \cdot \rho_{МСТО}, \tag{3.99}$$

$$S_{ПТО} = 0{,}03575 d^2_M, \tag{3.100}$$

$$n_{СФТО} = 3\frac{\pi\left(d_M + 0.035 d_M\right)}{0.035 d_M} \approx 279, \tag{3.101}$$

$$S_{СПТО} = 0{,}00385 d^2_{НЩ}, \tag{3.102}$$

where m_{HE} is the mass of inflatable elements; $m_{НЩ}$ is the mass of inflatable masts; m_{TO} is the mass of toric shells; $S_{ПНЩ}$ is the surface area of the inflatable mast; $\delta_{МНЩ}$ is the thickness of the material of the inflatable mast; $\rho_{МНЩ}$ is the density of the material of the inflatable mast; $n_{СНЩ}$ is the number of spherical shells placed in inflatable masts; $S_{ПСНЩ}$ is the surface area of the spherical shell, which is placed in the inflatable mast; $\delta_{МСНЩ}$ is the thickness of the material of the spherical shell, which is placed in the inflatable mast; $\rho_{МСНЩ}$ is the density of the material of the spherical shell, which is placed in the inflatable mast; $S_{ПТО}$ is the surface area of

the torus shell; $\delta_{МНЩ}$ is the thickness of the material of the torus shell; $\rho_{МНЩ}$ is the density of the material of the torus shell; $n_{СТО}$ is the number of spherical shells that are placed in toric shells; $S_{ПСТО}$ is the surface area of the spherical shell, which is placed in the torus shell; $\delta_{МСТО}$ is the thickness of the material of the spherical shell, which is placed in the torus shell; $\rho_{МСТО}$ is the density of the material of the spherical shell, which is placed in the torus shell.

Also, in its composition, the aerodynamic element has the following 3 round membranes. The mass of the deployable elements$m_{РЕ}$ is determined as follows:

$$m_{МРЕ} = 3S_{ПМ} \cdot \delta_{ММ} \cdot \rho_{ММ} \tag{3.103}$$

$$S_{ПМ} = 0{,}7854 d_{М}^{2} \tag{3.104}$$

where $S_{ПМ}$ is the membrane surface area; $\delta_{ММ}$ is the thickness of the membrane material; $\rho_{ММ}$ is the density of the membrane material.

It is assumed that the deorbiting space object with the help of this system, will move around the orbit in a non-orientational way. For non-orientational orbital motion, it was expressed the area of the medial cross-section $S_{М}$ of the aerodynamic element of the ADS using the following expression:

$$S_{М} = \frac{S_{ПАЕ}}{4} = 1.5287 d^{2}, \tag{3.105}$$

where $S_{ПАЕ}$ is the total surface area of the aerodynamic element.

Next, we will express the diameter of the membrane in terms of the area of the average cross-section of the aerodynamic element of the ADS:

$$d_{М} = 0.81\sqrt{S_{М}} \ . \tag{3.106}$$

The design value of the material thickness of inflatable and deployable elements is determined according to the algorithm given in subsection 3.2.3. The assessment of the impact of space debris fragments on the ADS is performed using the algorithm given in subsection 3.2.4.

3.3.3. Parameters of deployable systems

Deployable ADSs are made in the form of square sails. The sail consists of 4 retractable masts and a fabric canvas. The AE parameters of ADS this configuration: length of the base of the sail $a_{П}$; mass of AE $m_{АЕ}$.

The mass of AE is determined using ratios

$$m_{АЕ} = m_{РЕ} + m_{ВЕ}, \tag{3.107}$$

where is the mass of deployable elements

$$m_{РЕ} = V_{МРЕ} + \rho_{МРЕ}, \tag{3.108}$$

V_{MPE} is the material volume of deployable elements; ρ_{MPE} is the material density of deployable elements;

$$V_{MPE} = S_{ПРЕ} \cdot \delta_{MPE} V_{MPЭ} = S_{ПРЭ} \cdot \delta_{MPЭ}, \quad (3.109)$$

$S_{ПРЕ}$ is the surface area of deployable elements

$$S_{ПРЕ} = a^2_{П} \quad (3.110)$$

$a_{П}$ is the length of the base of the AE sail

$$a_{П} = 2\sqrt{S_M}\ , \quad (3.111)$$

m_{BE} is the mass of retractable elements

$$m_{BE} = \bar{m}_{BE} \cdot l_{BE}\,, \quad (3.112)$$

$\bar{m}_{BE}$ is the linear density (mass per unit length) of retractable elements, we take $\bar{m}_{BE} = 0.025$ kg/m ; l_{BE} is the length of retractable elements

$$l_{BE} = 2.83\sqrt{S_M}\ . \quad (3.113)$$

3.2.4. Parameters of the aerodynamic element of the transformed aerodynamic deorbit systems

When using the method of transforming the structure of a space object into an aerodynamic system, the mass of the system will be determined by the mass of the deployment system

$$m_{ACB} = m_{CP}. \quad (3.114)$$

To calculate the limits of applicability of this method, the area of the median cross-section, in this case, will be determined by the overall characteristics of the spacecraft:

$$S_M = \frac{S_{БПКО} + S_{ПКО}}{4}, \quad (3.115)$$

where $S_{БПКО}$ is the area of the side panels of the spacecraft; $S_{ПКО}$ is the total surface area of the spacecraft.

For the option of the spacecraft layout in the form of a square pyramide, the area of the side panels will be determined:

$$S_{БПКО} = 4a^2, \quad (3.116)$$

where a is the length of the face of the side panel.

For the option of the spacecraft layout in the form of a rectangular pyramide, the area of the side panels will be determined:

$$S_{БПКО} = 4ab, \quad (3.117)$$

where b is the width of the face of the side panel.

3.4. Deployment system parameters

The deployment system of deployable aerodynamic systems consists of two components: a deployable mast deployment system in which the four twisted masts are stored and deployed, and an airfoil storage spindle around which the four quadrants of film material are wound. The deployment system of deployable masts consists of coils, pressure rollers, and an electric drive. Thus, the mass of the deployment system is determined using the following expressions:

$$m_{СР} = m_К + m_{НВ} + m_Ш + m_{ЕП}, \tag{3.118}$$

where $m_К$ is the mass of coils on which deployable masts are wound; $m_{НВ}$ is the mass of pressure rollers; $m_Ш$ is the mass of the spindle on which the aerodynamic element is wound; $m_{ЕП}$ is the mass of the electric drive that starts the deployment mechanism. We assume that deployable aerodynamic systems have similar deployment mechanisms.

3.5. Inflation system parameters

Inflation of the ADS can be carried out in several ways:

a) with the help of a gas storage and supply system to the shell;

b) using residual pressure;

c) with the help of sublimation of a powder substance.

When using the first method, the mass of the inflation system is determined by the sum of the gas mass $m_Г$ and the mass of the gas storage and supply system to the shell $m_{СЗПГ}$:

$$m_{СН} = m_Г + m_{СЗПГ}. \tag{3.119}$$

When using the second and third methods, the mass of the inflation system will be determined by the gas mass $m_Г$ or the mass of the powder substance $m_{ПР}$, respectively:

$$m_{СН} = m_Г = m_{ПР}. \tag{3.120}$$

The gas mass $m_Г$ required to ensure the excess pressure $p_{НТ}$ of the inflatable element with a volume $V_{НЕ}$ is determined from the Clapeyron—Mendeleev equation (Yavorsky, 2006):

$$p_{НТ}V_{НЕ} = \frac{m_Г}{\mu_Г} R_0' T_{атм}, \tag{3.121}$$

$$m_Г = \frac{p_{НТ}V_{НЕ}\mu_Г}{R_0 T_{атм}}, \tag{3.122}$$

where $\mu_Г$ is the molecular mass of the gas; R_0 is the universal gas constant, $R_0 = 8.31 \frac{\text{J}}{\text{Mol}\cdot\text{K}}$; $p_{НТ}$ is the excess pressure in the shell.

When choosing a gas for inflation, it is necessary to take into account the peculiarity of the neutrality of the gas to the material of the shell of the aerodynamic element of the system. For space inflatable systems with a forced inflation method, inert gases can be used, which are used in rocket engine supercharging systems, the molar masses of which are given in Table 3.2.

The successful use of powder substances for supercharging space inflatable systems was demonstrated on the Echo spacecraft (The Echo-I…, 1964). Substances whose characteristics are listed in Table 3.3 can be used as sublimating substances.

When choosing a substance for inflation, it is necessary to take into account several nuances: it should correspond to the requirements for pressure and temperature; the melting temperature must be higher than any temperature expected while the ADS is packed inside the container to prevent liquid flow that could unbalance the spacecraft payload; the lowest molecular weight should be chosen to minimize weight requirements; it must be non-toxic for safe use.

The mass of the powder substance $m_{ПР}$ is calculated according to the formula:

$$m_{ПР} = \frac{p_{НТ} V_{НЕ} \mu_{ПР}}{R_0 T_{атм}}, \tag{3.123}$$

where $\mu_{ПР}$ is the molecular mass of the powder substance.

Table 3.2. **Molar masses of inert gases for inflation**

Gas	Helium	Neon	Argon	Xenon
Molar mass, mol/kg	4.003	20.179	39.948	131.29

Table 3.3. **Characteristics of sublimable substances for inflation**

Substance	Molecular weight	Density, kg/m³	Melting point, K	Boiling point, K	Sublimation parameters	
					Heat of sublimation, $\frac{\text{J}}{\text{kg}\cdot\text{K}}$	Vapor pressure, $\log p = A' - \frac{B'}{T}$
d-Camphor	152.23	1000	451.5	477	$5.073 \cdot 10^8$	$26.571 - \frac{6090}{T}$
Naphthalene	128.16	1145	353.22	490.9	$6.739 \cdot 10^8$	$31.948 - \frac{8326}{T}$
Benzoic acid	122.12	1265.9	394.7	602.22	$6.848 \cdot 10^8$	$29.595 - \frac{8223}{T}$
Anthracene	178,22	1250	490	627	$10.339 \cdot 10^8$	$36.530 - \frac{12436}{T}$
Anthraguinone	208,2	1419	559	652	$12.307 \cdot 10^8$	$40.145 - \frac{15206}{T}$

With the forced inflation method, the shell is inflated by supplying gas from the gas storage tank. The mass of the gas storage and supply system is determined using the expressions:

$$m_{СЗПГ} = m_{ЕЗГ} + m_{СПГ} + m_Г m_{СХПГ} = m_{ЕХГ} + m_{СПГ} + m_Г, \qquad (3.124)$$

where $m_{ЕЗГ}$ is the mass of the gas storage container; $m_{СПГ}$ is the mass of the gas supply system to the shell, according to (Thunnissen, 1991), for a single-component gas, it has been accepted $m_{СПГ}$ = 0.01...0.2 kg.

The assessment of the effect of FSD on ADS is carried out using the algorithm (Skorik, 2013), (Paliy, 2015):

- determination of the minimum size of the FSD d_{min} capable of penetrating the shell thickness δ;
- calculation of the collision frequency N of the ADS shell with the FSD;
- assessment of pressure losses in the ADS shell.

To determine the minimum size d_{min} of the FSD capable of penetrating a shell with a thickness δ, the ballistic equation (Alpatov, 2012) is solved:

$$d_{\min} = \left(0.106022 \cdot t \cdot H_B^{1/4} \cdot \sqrt{\rho_t / \rho_p} \cdot (c/V)^{2/3}\right)^{0.947368}, \qquad (3.125)$$

where d_{min} is the FSD diameter; H_B is the Brinell hardness of the target material; ρ_t, ρ_p are the densities of FSD and film materials; is the sound velocity in FSD material, for aluminum c = 5.1 km/s; is the FSD velocity (average velocity is $V \approx 10$ km/s).

Based on the found value, the frequency of collisions of the ADS shell with the FSD is calculated (Skorik, 2013):

$$N = S_П \cdot Q(d_i); \qquad (3.126)$$

$$d_{min} \le d_i \le d_{max} \qquad (3.127)$$

where $S_П$ is the surface area of the inflatable elements of the ADS; is the average flow of FSD with a diameter at a given flight altitude, calculated using the MASTER-2009 space debris environment model (Meteoroid and space…, 2010); d_{min}, d_{max} are the minimum and maximum size of FSD in MASTER-2009.

After that, an assessment is held of pressure losses inside the ADS shell due to the effect of FSD during t_L. Based on the values d_i and the calculated flow $Q(d_i)$ for the ADS with the surface area $S_П$ of the inflatable elements, the area of the formed holes S_0 in the shell is calculated over time t_L.

$$S_0 = \int_{T_0}^{t_L} \sum_{i=1}^{n} \frac{\pi d_i^2}{4} \cdot N(d_i)\, dt, \qquad (3.128)$$

where d_1 is the minimum size, $d_1 = d_{min}$; d_n is the maximum size of FSD, the flow of which is calculated using MASTER-2009; $N(d_i)$ is the frequency of collisions of the diameter FSD with the shell, which is determined from the expression (Skorik, 2013):

$$N(d_i) = Q(d_i) \cdot S_П, \qquad (3.129)$$

where is the surface area of the ADS shell.

The amount of gas that can flow out of the opening with the area of the inflatable element of the ADS is obtained by the formula (Koshmarov, 1977):

$$\Delta_3 = \int_{t_0}^{t_L} \frac{1}{\sqrt{2\pi R}} \left(\frac{p_1}{\sqrt{T_1}} - \frac{p_2}{\sqrt{T_2}} \right) S_O dt \,, \tag{3.130}$$

where p_1, p_2, is the gas pressure in the shell and exosphere, respectively; T_1, T_2 are the temperatures of gas in the shell and exosphere, respectively; R — universal gas constant, $R = 8.3144621 \frac{\text{m}^2 \cdot \text{kg}}{\text{s}^2 \cdot \text{K} \cdot \text{Mol}}$

To determine the weight of the ADS inflation system of various configurations, Table 3.4 shows the main dependencies.

Table 3.4 shows: m_{CH} is the mass of the inflation system; ρ_A is the atmospheric density; V is the orbital velocity of the SO; S_M is the cross-sectional area; μ_A is the molecular weight of the gas for inflation; R_0 is the universal gas constant; T_A is the atmospheric temperature; $m_{C3\Pi\Pi}$ is the weight of the gas storage and supply system to the inflatable element of the system; V_{TO_n} is the volume of the n-th torus, is determined by the following expression:

$$V_{TO_n} = 2,467 d_{T_n} d_{KO}^2 \,. \tag{3.131}$$

d_{T_n} is the diameter of the n-th torus; d_{KO} is the diameter of the deorbit space object; V_{HE_n} is the volume of the n-th inflatable element, in this case, it is the volume of the spherical shell and is determined by the expression:

$$V_{HE_n} = 0.5236 d_{C\Phi}^2 \,. \tag{3.132}$$

ν is the total number of spherical shells, which is determined by the following ratio:

$$\nu = n_{CH\Pi} + n_{CTO} \tag{3.133}$$

$$m_{C3\Pi\Gamma} = m_{Б} + m_{\Gamma\Pi} \tag{3.134}$$

$$m_{Б} = S^{Б}_{\Pi} . \delta^{Б}_{M} . \rho^{Б}_{M} \tag{3.135}$$

$$m_{\Gamma\Pi} = m_{PT} + m_{ДТ} + m_{3A} \tag{3.136}$$

$m_{C3\Pi\Gamma}$ is the mass of the gas storage and supply system for inflation; $m_{\Gamma\Pi}$ is the mass of the gas supply system for inflation; m_{PT} is the mass of the inflation pressure regulator; $m_{ДТ}$ is the mass of pressure sensors; m_{3A} is the mass of the valves; p_{HT} is the overpressure in the inflatable elements of the AE; V_{HE} is the volume of AE inflatable elements; μ_I is the molecular weight of the gas for inflation; $m_{Б}$ is the mass of the gas storage cylinder; $\delta^{Б}_{M}$ is the thickness of the gas cylinder material; $\rho^{Б}_{M}$ is the density of the material from which the gas cylinder is made.

Table 3.4. **Relationships for determining the mass of the inflation system of aerodynamic systems of various configurations**

ADS configuration	The mass of the inflation system
«Sphere»	$m_{CH} = \frac{\left(\frac{\rho_A V^2}{2}\right)\left(0{,}755\sqrt{S_M^3}\right)\mu_\Gamma}{R_0 T_A} + m_{C3\Pi\Gamma}$
«Round shield»	$m_{CH} = \frac{\left(\frac{\rho_A V^2}{2}\right)\left(0{,}01\sqrt{S_M^3}\right)\mu_\Gamma}{R_0 T_A} + m_{C3\Pi\Gamma}$
«Dihedral panels»	$m_{CH} = \frac{\left(\frac{\rho_A V^2}{2}\right)\left(0{,}011\sqrt{S_M^3}\right)\mu_\Gamma}{R_0 T_A} + m_{C3\Pi\Gamma}$
«Pyramide Triangle»	$m_{CH} = \frac{\left(\frac{\rho_A V^2}{2}\right)\left(0{,}017\sqrt{S_M^3}\right)\mu_\Gamma}{R_0 T_A} + m_{C3\Pi\Gamma}$
«Pyramide Square»	$m_{CH} = \frac{\left(\frac{\rho_A V^2}{2}\right)\left(0{,}015\sqrt{S_M^3}\right)\mu_\Gamma}{R_0 T_A} + m_{C3\Pi\Gamma}$
«A cone made of tori»	$m_{CH} = \frac{\left(\frac{\rho_A V^2}{2}\right)\left(\sum_{n=1}^{k} V_{TO_n}\right)\mu_\Gamma}{R_0 T_A} + m_{C3\Pi\Gamma}$
«A cone made of tori with spheres placed inside»	$m_{CH} = \left(\sum_{n=1}^{k} m_{CH} = \frac{\left(\frac{\rho_A V^2}{2}\right) V_{C_n}\mu_\Gamma}{R_0 T_A}\right) + m_{C3\Pi\Gamma}$
«Bulk sail»	$m_{CH} = \left(\sum_{n=1}^{v} \frac{\left(\frac{\rho_A V^2}{2}\right) V_{HE_n}\mu_\Gamma}{R_0 T_A}\right) + m_{C3\Pi\Gamma}$

We assume that the gas cylinder has several configurations: sphere, torus, and cylinder. The working pressure in the cylinder is orders of magnitude higher than the ambient pressure, and the thickness of the cylinder material is calculated according to the momentumless theory. Formulas for calculating material thick-

Table 3.5. **Material thickness of gas cylinder in different configurations**

Gas cylinder shape	Cylinder material thickness, m	Surface area of the cylinder, m^2
Cylinder	$\delta^{Б}_{M} = \frac{p_{PT} d_{Б}}{2\delta}$	$S_{П}^{Б} = 1.57 d_{Б}^{2} + 3.142 d_{Б} l_{Б}$
Torus	$\delta^{Б}_{M} = \frac{p_{PT} d_{Б} (d_{T} - d_{Б})}{2\delta\ (d_{T} - d_{Б})}$	$S_{П}^{Б} = 9.87 d_{T} d_{П}^{Б}$
Sphere	$\delta^{Б}_{M} = \frac{p_{PT} d_{Б}}{4\delta}$	$S_{П}^{Б} = 3.142 d_{Б}^{2}$

Table 3.6. **Characteristics of structural materials of rocket and space technology**

Material	Density ρ, kg/m^3	Modulus of elasticity $\sigma_{пр}$, Pa
Metals		
Aluminum alloys		
AlMg-6 (Shalin, 1996)	2640	$7.1 \cdot 10^9$
1420 (Shalin, 1996)	2470	$7.5 \cdot 10^9$
1460 (Shalin, 1996)	2600	$8 \cdot 10^9$
2090 (Shalin, 1996)	2590	$7.6 \cdot 10^9$
8090 (Shalin, 1996)	2560	$7.7 \cdot 10^9$
Titanium alloys		
Ti–6Al–4V (Ti 6Al 4V…)	4430	$1.14 \cdot 10^{11}$
Ti-5Al-2Sn-2Zr-4Mo-4Cr (Titanium Ti-5…)	4650	$1.15 \cdot 10^{11}$
Ti–10V–2Fe–3Al (Titanium Ti-10…)	4650	$1.1 \cdot 10^{11}$
Ti–5.5Al–3.5Sn–3Zr–1Nb (Titanium IMI…)	4540	$1.25 \cdot 10^{11}$
Composite materials		
Honeycomb structures with aluminum filling (Gaydachuk, 2012)	37	$1.1 \cdot 10^{11}$
Carbon fiber plastics (Banichuk, 1997)	1500	$1.8 \cdot 10^{11}$
Fiberglass plastics (Banichuk, 1997)	2100	$5.7 \cdot 10^{10}$

ness $\delta^{Б}_{M}$ and surface area $S^{Б}_{П}$ of gas cylinders of different configurations are shown in Table 3.5 (Pisarenko, 1988).

The formulas in Table 3.5 indicate: $d_{Б}$ is the diameter of the cylinder; $p_{РТ}$ is the working pressure in the cylinder; σ is the tensile strength of the cylinder material; $d_{Т}$ is the torus diameter; $l_{Б}$ is the length of the cylinder; $d^{Б}_{П}$ is the cross-sectional diameter of the torus cylinder.

The practice of designing gas cylinders for launch vehicle propulsion systems shows that aluminum and titanium alloys (Sutton, 2010) are used for their manufacture, the characteristics of which are given in Table 3.6.

3.6. Storage system parameters

The following requirements are imposed on the materials used to manufacture the ADS storage system: material resistance to space factors; resistance to dynamic loads at the stage of launching a space object into orbit and resistance to temperature deformation of the material. Material selection and assessment of the possibility of its use at the initial stages of design is based on the analysis of some basic material characteristics, such as parameters characterizing strength and stiffness properties, and mass characteristics. A variety

Table 3.7. **Dependencies for determining the weight of the ADS storage system of different configurations**

ADS configuration	Weight of the storage system
«Sphere»	$m_{СЗ} = 6\left(\sqrt[3]{4S_M\delta_{МНЕ} + V_{ЗПГ}}\right)^2 \cdot \delta_{МСЗ} \cdot \rho_{МСЗ}$
«Round shield»	$m_{СЗ} = 6\left(\sqrt[3]{1,224S_M\delta_{МНЕ} + 1,388S_M\delta_{МРЕ} + V_{ЗПГ}}\right)^2 \cdot \delta_{МСЗ} \cdot \rho_{МСЗ}$
«Dihedral panels»	$m_{СЗ} = 6\left(\sqrt[3]{1,06S_M\delta_{МНЕ} + 1,5S_M\delta_{МРЕ} + V_{ЗПГ}}\right)^2 \cdot \delta_{МСЗ} \cdot \rho_{МСЗ}$
«Pyramide Triangle»	$m_{СЗ} = 6\left(\sqrt[3]{1,344S_M\delta_{МНЕ} + 2,657S_M\delta_{МРЕ} + V_{ЗПГ}}\right)^2 \cdot \delta_{МСЗ} \cdot \rho_{МСЗ}$
«Pyramide Square»	$m_{СЗ} = 6\left(\sqrt[3]{1,342S_M\delta_{МНЕ} + 2,654S_M\delta_{МРЕ} + V_{ЗПГ}}\right)^2 \cdot \delta_{МСЗ} \cdot \rho_{МСЗ}$
«A cone made of tori»	$m_{СЗ} = 6\left(\sqrt[3]{(S_{ППТО} + S_{ППНМ})\delta_{МНЕ} + V_{ЗПГ}}\right)^2 \cdot \delta_{МСЗ} \cdot \rho_{МСЗ}$
«A cone made of tori with spheres placed inside»	$m_{СЗ} = 6\left(\sqrt[3]{(S_{ППТО} + S_{ППНМ} + S_{ППС} \cdot k)\delta_{МНЕ} + V_{ЗПГ}}\right)^2 \cdot \delta_{МСЗ} \cdot \rho_{МСЗ}$
«Bulk sail»	$m_{СЗ} = 6\left(\sqrt[3]{(S_{ППТО} + S_{ППНМ} + S_{ППС} \cdot \nu)\delta_{МНЕ} + V_{ЗПГ}}\right)^2 \cdot \delta_{МСЗ} \cdot \rho_{МСЗ}$

of metal alloys, polymeric, and composite materials are used in the design of space technology elements. Table 3.6 shows some characteristics of the main structural materials.

To determine the mass of the storage system, we will assume that it is made in the form of a cube. The parameters of the storage system are determined by the volume of the aerodynamic element in the folded state and the volume of the material of the supercharging system. In general, the mass of the storage system is calculated using the following relationship:

$$m_{C3} = 6\left(\sqrt[3]{V_{MHE} + V_{MPE} + V_{3ПГ}}\right)^2 \cdot \delta_{MC3} \cdot \rho_{MC3}, \qquad (3.137)$$

where V_{MHE} is the volume of material of inflatable elements; V_{MPE} is the material volume of deployable elements; $V_{3ПГ}$ is the volume of the gas storage and supply system to the inflatable element; is the thickness of the storage system material; is the density of the storage system material. We assume that at the initial design stage of the ADS, the material thickness of its onboard storage system is the same as the material thickness of the structure of the space object being deployed. Table 3.7 shows the main dependencies for determining the mass of the ADS storage system of various configurations.

CHAPTER 4

DESIGN SCHEMES OF AERODYNAMIC SYSTEMS FOR DEORBITING SPACE OBJECTS

Space objects subject to deorbit after the end of their active lifetime are spacecraft and upper stages of launch vehicles. In this section, design schemes of aerodynamic systems for the deorbiting of the following classes of space objects are proposed: space objects of the «nano», «micro» and «large» class. The space object nano class is characterized by a mass range [1—10 kg], the micro class — [150—600 kg], and the large class [>1000 kg].

Space objects of the «nano» class are mainly used for demonstration missions to test new elements of space technology. The term of orbital lifetime of these objects for the range of orbital altitudes of 600—700 km can reach 150—200 years. In this section, it is proposed to use the principle of transformation of the structure of the apparatus into an aerodynamic system of deorbiting a spacecraft of this class.

Spacecraft of the «micro» class are used in remote sensing of the Earth's surface. As a rule, they are placed in orbits with an altitude range of [600—800 km], where the period of orbital existence for these devices can reach more than 500 years. To ensure the recommended period of their orbital existence, original design schemes of aerodynamic deorbit systems are proposed.

Also, in this section, schemes of aerodynamic systems for the deorbit of «large» class spacecraft are considered, namely, the upper stages of launch vehicles and modular large-sized structures (using the example of orbital stations). A feature of the deorbit of the upper stages of the launch vehicles is that even in the case of the presence of the necessary amount of fuel to perform the descent maneuver from orbit, there is a probability of failure to perform the reorientation in the event of a failure of the control system. To ensure the recommended period of orbital existence, these objects are proposed to be equipped with ADS. Several schemes for the implementation

of ADS at objects of this class are given. As for the problem of deorbiting large-sized modular structures, the weight of which is tens, and in some cases, hundreds of tons, for these purposes, a specialized transport vehicle is launched into orbit, which docks with the object and with the help of its on-board propulsion system, a detour maneuver is performed from orbit. To save costs for the deorbit of objects of this class, it is proposed to divide the object into modules equipped with aerodynamic deorbiting systems before deorbiting.

4.1. Schematic of the aerodynamic deorbiting systems of space objects of the «nano» class

At the moment, the space object cubesat platform, which belongs to the «nano» class and consists of one cube-shaped module, or their combination, is widely used to perform simple space missions. This configuration covers classes by mass of space objects from «nano» to «micro». There is a need to reduce the ballistic life

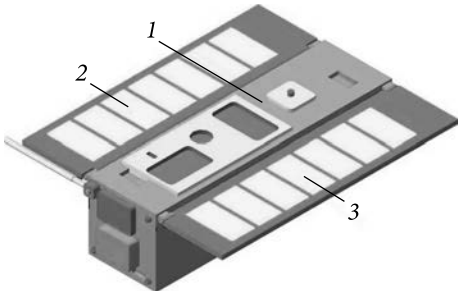

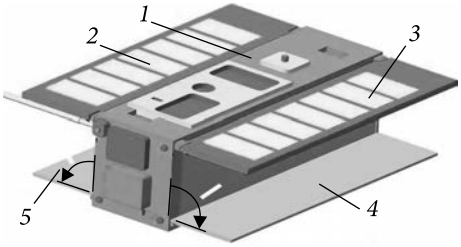

Fig. 4.1. The space object is made based on the CubeSat platform in a regular mode of operation: *1* — space object; *2, 3* — solar panels

Fig. 4.2. The space object made based on the CubeSat platform in deorbit mode, with protective panels retracted: *1* — space object; *2, 3* — solar panels; *4, 5* — deployable elements of the structure

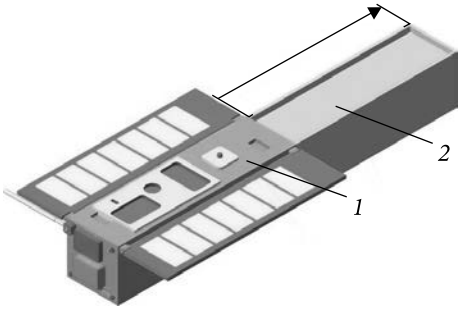

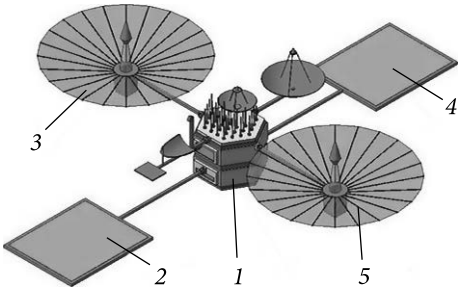

Fig. 4.3. A space object of the «nano» class in the mode of deorbiting, with the structure shifted along the longitudinal axis: *1* — space object; *2* — the body of the space object is shifted along the longitudinal axis

Fig. 4.4. Space object in regular operation mode: *1* — space object; *2* — solar panel; *3* — antenna; *4* — solar panel; *5* — antenna

of space objects made based on the CubeSat platform, after the end of their active lifetime. To solve the problem of deorbiting a «nano» space object from orbit, a design scheme of the separation system is proposed, based on the transformation of the space object design into an ADS. With the help of the proposed method, it is possible to reduce the period of ballistic existence of these space objects. So, for example, a space object *1* (Fig. 4.1) (Patent of Ukraine for the invention No. 113747), made in the form of a prism from a set of cubic-shaped modules, functions in orbit in normal mode with deployed solar panels *2, 3.* As soon as the term of active lifetime of space object 6 ends, it will go to the mode of non-orientational flight, to reduce the period of its ballistic existence, structural elements *4* and *5* of space object *1*, which are not used in the normal mode of its operation, are tilted by 90° in the direction indicated in Fig. 4.2 by arrows. In this way, the cross-sectional area of the space object increases and, as a result, the period of its ballistic existence decreases. If the reduction of the ballistic lifetime due to the rejection of structural elements *4* and *5* is not enough, to reduce it, it is proposed to make the body *2* of the space object 1 slide and move it in the direction indicated in Fig. 4.3 with an arrow.

It should be noted that the approach to increase the ballistic coefficient of a space vehicle based on the use of its standard structural elements can be applied to second-class space vehicles as well if the calculations confirm this possibility and there are no technological problems with the final transformation of the space vehicle at the end of its regular operation.

4.2. Scheme of the aerodynamic deorbiting system of space objects of the «micro» class

In the ADS, based on the transformation of the design of the space object, to increase the area of the median cross-section, the regular structural elements of the corresponding object are used (Patent of Ukraine for the invention No. 113747, 2017), (Alpatov, 2015), also to increase the area of the median section, additional modules can be used, which are transformed into a rigid AE. Structurally, systems of this class consist of an aerodynamic element and a deployment system.

To increase the cross-sectional area and aerodynamic drag coefficient of the spacecraft, standard elements of its design (solar panels, space antennas, protective screens, etc.) are used.

At the end of the active lifetime of the spacecraft, these elements are set from their regular position (Fig. 4.4) to the one that provides the maximum coefficient of aerodynamic drag and the cross-section area (Fig. 4.5), as a result of which the ballistic lifetime of the spacecraft is reduced.

As an example, let's consider the transformation of the «Sich» type spacecraft design (Fig. 4.6) into ADS.

Two variants of the space object structure transformation have been considered: dropping protective screens (Fig. 4.7); displacement of the body along the

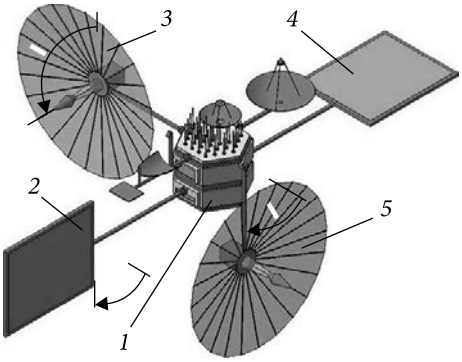

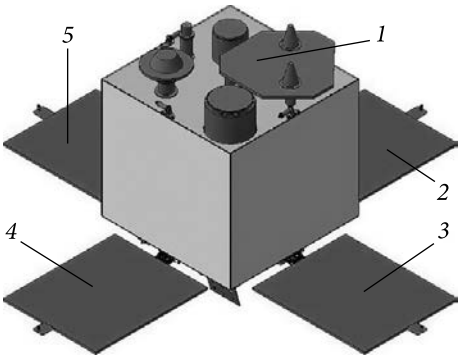

Fig. 4.5. Space object in the deorbiting mode: *1* — space object; *2* — solar panel; *3* — antenna; *4* — solar panel; *5* — antenna

Fig. 4.6. Space object of the «micro» class in regular mode of operation: *1* — spacecraft; *2—5* — solar panels

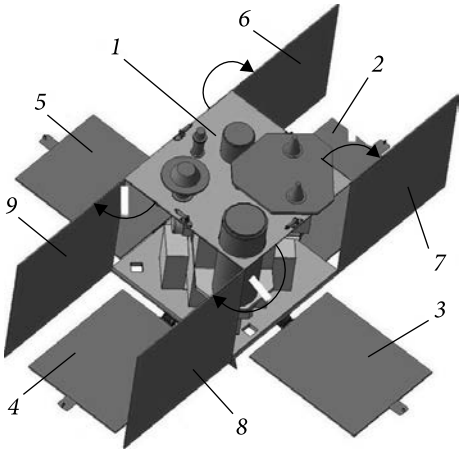

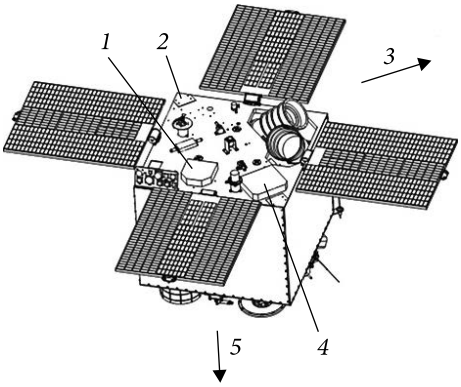

Fig. 4.7. Micro class space object in the deorbiting mode with protective panels retracted: *1* — spacecraft; *2—5* — solar panels; *6—9* — protective screens

Fig. 4.8. Area for ADS placement on the «micro» space object plate: *1* — zone of ADS placement; *2* — base plate; *3* — flight direction; *4* — zone of ADS placement; *5* — the direction to the Earth

longitudinal axis. For a typical structural scheme of «micro» class objects, the placement of the ADS should be implemented on the base plate of the space object. A phenomenological analysis of the options to choose the zones of the ADS placement on the slab leads to the option shown in Fig. 4.8.

The container body, where the ADS is placed has a box shape. It is advisable to produce it from thin-sheet aluminum material with a protective coating. This also applies to the container lid. To choose a material, you need to create a list of re-

quirements for these structural elements. The main ones are the requirements for materials that must be in outer space for a long time. The accumulated experience of using materials for the conditions of open space allows us to form a certain list of such materials, Table. 3.6. The container serves as a storage system for aerodynamic elements (deployed sails and deployment mechanisms) until the end of the period of active operation of the spacecraft.

The design scheme of the ADS includes the following elements: a rigid frame, which can be in the state of packaging and the working non-deployed state, the canvas of the sail element, which is made of a film resistant to the influence of space factors, a deployment system, a device for checking the container.

The rigid frame consists of spring masts, which are made of a set of conical springs. The spring masts are connected with plates to make the structure more rigid. The material from which the springs are made has the same requirements as the materials of the container body, which are listed in Table 3.6. The canvas of the sailing element is made in the form of two cylinders connected by a strip of polymer film material. During long-term operation in orbits higher than 600 km due to the influence of atomic oxygen, polymer materials degrade, which leads to a decrease in their thickness. Sufficient experience in orbital experimental research has been accumulated, which allows materials with the least sensitivity to the influence of atomic oxygen to be absorbed.

During operation, after opening the lid of container *2* with the help of a pyro lock and spring mechanisms, the aerodynamic sail elements are deployed with the help of special electric drives *3* (Fig. 4.9) (Alpatov, 2022a).

A typical sail drive (Fig. 4.10) is designed to control the configuration of the device from commands coming from the space object. It consists of a bracket *1*, a direct current

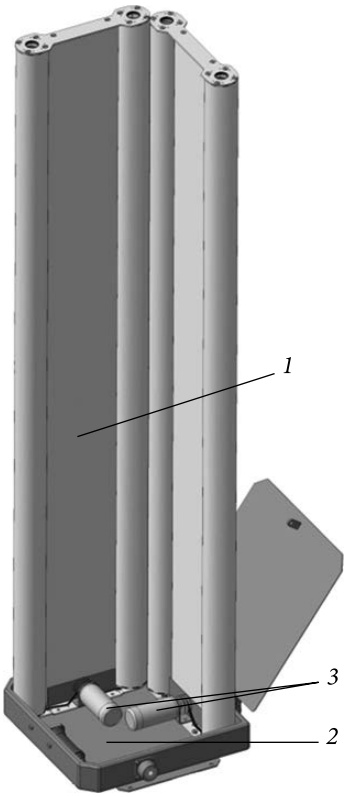

Fig. 4.9. Aerodynamic sail element in the deployed state: *1* — aerodynamic sailing element; *2* — container for storage on board the spacecraft; *8* — drives for deploying the aerodynamic sail element

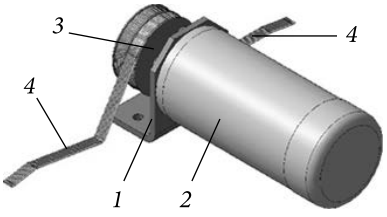

Fig. 4.10. Sail drive for deploying an aerodynamic sail element: *1* — bracket; *2* — electric motor; *3* — coil; *4* — traction

Fig. 4.11. Sail frame: *1* — spring mast; *2* — drive

electric motor *2*, a coil *3*, and two rods *4*. The motor, rotating in one direction or another, unwinds or winds the rods on the coil. The tractions pass through the rods and are fixed in the upper plate of the frame of the sailing element. Under the action of conical springs, the plate of the frame rises with the canvas of the sail up when the tension of the rods is weakened or falls when the tension of the rods is increased, overcoming the resistance of the springs.

Placing the sails in the container is carried out with the help of appropriate technological equipment. The ADS to remove the «micro» class spacecraft from orbit functions as follows. The device in the closed position of the container is installed on the spacecraft. The electrical connector of the device is connected to the power system of the spacecraft. The frame of the sail (Fig. 4.11) is made of two elastic masts installed between the base of the frame and the upper plate. The canvas of the sail is fixed under the support discs of the masts. The canvas of the sail is placed at the bottom in casing 4 at the base of the frame, and at the top is fixed with a bar on the plate of the frame. The drive rods that pass through the mast discs provide additional stability and protect the sailcloth from getting under the mast discs and springs.

The ADS of this type functions as follows. At the command from the spacecraft, voltage is applied to the system's pyro lock. The pyro cartridge and the rod of the pyro lock are activated, thus the tab of the container lid is released. The lid opens under the action of the spring mechanism of the container. Inside the container, two sail mechanisms are installed at an angle to each other in a compressed position. The spring of the masts of the sails squeezes the upper plates of the frames of the sails with the canvases of the sails fixed on them, which occupy the working position.

At the command from the spacecraft, voltage is applied to the motors of the sail mechanisms to rotate the motor in the direction of unwinding the rods from the drive coil. Traction tension weakens. The springs of the sail masts squeeze the top plate of the sail frame with the sail cloth attached to it. In this way, the sails deployed on the spacecraft body are brought to their working state (Fig. 4.12) (Alpatov, 2022a).

The use of this deorbiting device makes it possible to reduce the period of orbital existence in case of non-orientational movement of the removed object. The use of spring masts makes it possible to reduce the sensitivity of the aerodynamic element to the impact of damaging fragments of space debris. It should be noted that such a sailing system can be effective as long as the space object rotates relative to the oncoming flow.

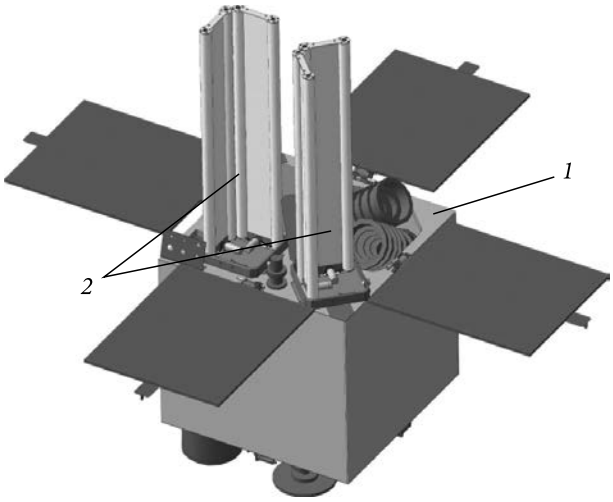

Fig. 4.12. Aerodynamic sail elements in the deployed state on board the «micro» class spacecraft: *1* — spacecraft of the «micro» class; *2* — aerodynamic sail elements

Therefore, it is necessary to carry out appropriate calculations of the dynamics of such a system to calculate the time interval during which the system will stop rotating and will be stabilized relative to the velocity vector of the mass center.

4.3. Diagrams of the aerodynamic systems of deorbiting space objects of the «large» class

The design scheme of the ADS is based on the use of a combined design, which consists of a shell filled with toroidal elements to increase the reliability of the system against its damage by particles of space debris. Such a system can be used to deorbit the last stages of the LV (Patent of Ukraine for invention № 109194, 2015), (Alpatov, 2017b) (Fig. 4.13). or other designs that have a large mass and a small ballistic coefficient. The design of the ADS has the form of a conical thin-walled film shell (CFS), which consists of inflatable annular toroidal shells that touch each other and the inner surface of the CFS. The ADS is connected to the LV stage using special multi-layer slings. The parameters of the slings (length, cross-section, material, their number, and structure) are calculated under the conditions of ensuring the appropriate reliability indicators and restrictions on their mass and volume. To increase the reliability of the system against damage by small fragments of debris, spherical thin-walled film shells are placed in the inner cavities of the inflatable ring torus shells, which touch each other and the inner surface of the CFS.

ADS functions as follows. If it is necessary to deorbit the LV stage of the ADS, the cross-sectional area of the LV stage increases sharply, as a result of which the aerodynamic resistance of the stage increases, and it begins to be gradually withdrawn from the orbit into the dense layers of the atmosphere. It should be noted that autonomous spherical shells are located in the CFS, which take a

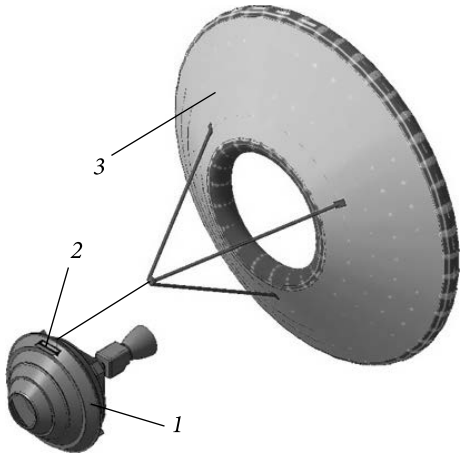

Fig. 4.13. The stage of a launch vehicle with an aerodynamic deorbiting system: *1* — launch vehicle stage; *2* — container for storing the aerodynamic deorbiting system; 3 conical thin-walled film shell

spherical shape in orbit due to residual pressure. Violation of the integrity of a separate shell does not lead to the failure of a separate CFS, which would happen when using a CFS, the cavities of which are not divided into separate autonomous sections. This ensures a significant increase in the period of active existence of the ADS because the failure of part of the total number of spherical shells does not lead to a change in the overall configuration and dimensions of the ADS, that is, it does not affect the efficiency of its operation. However, the size of the damaged part is subject to appropriate estimates.

Thus, the proposed ADS is designed to ensure the reduction of the last stage of the launch vehicle from the Earth orbit with the simplicity of the design and high reliability of the ADS implementation under the conditions of the appropriate calculation and optimization of the parameters of such a system.

However, such a scheme has a drawback — with the non-orientational movement of a space object that is being eliminated, the maximum cross-sectional area is reached only at angles of attack of 0^o and 180^o, and at angles of attack of 90^o and 270^o, the cross-sectional area of the cross-section is almost halved, and as a result, the force of the aerodynamic braking. Thus, it is advisable to use this device during tentative deorbiting. To solve the problem of increasing the area of the median cross-section during non-orientational movement, a unified design scheme of an aerodynamic element that does not require its orientation is proposed (Fig. 4.14) (Alpatov, 2022b).

The aerodynamic element 2 of the device (Fig. 4.14) is made in the form of three orthogonal planes to obtain the maximum aerodynamic resistance at any of its positions. It consists of a frame, twelve canvases, and a connecting flange. The transition from the stowed position inside the container to the operating position in Earth orbit occurs due to the excess pressure inside the shell of the frame concerning the environment.

The frame of the aerodynamic element (Fig. 4.15) is hermetically made of high-strength light polymer material in the form of three internal torus shells *1*, interconnected by inflatable masts *2*. Spherical shells 3 are placed inside the torus shells and inflatable masts to increase their reliability due to the action of fragments of space debris.

The canvas of the aerodynamic element is made of high-strength, light polymer material in the form of a sail. It serves to create additional aerodynamic re-

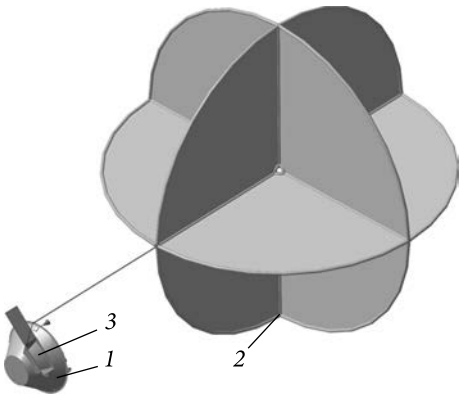

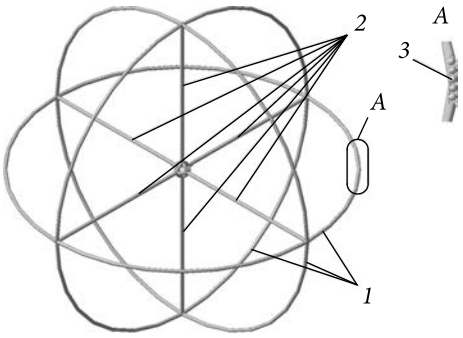

Fig. 4.14. Aerodynamic deorbiting system in operating position: *1* — space object that is being deorbited; *2* — aerodynamic element; *3* — storage and deployment system container

Fig. 4.15. The frame of an aerodynamic element: *1* — torus shells; *2* — inflatable masts; *3* — spherical shells

sistance to the space object. The connecting flange of the aerodynamic element is made of high-strength polymer material with ball support under the traction for connection with the mast of the device bracket. The thrust of the device connects the aerodynamic element with the space object. It consists of a cable and two ball supports at the ends of the cable, made of high-strength polymer material.

The device works as follows. On the outer surface of the space object, a container of the deorbiting device is fixed, in the inner cavity of which an aerodynamic element is placed in a deployed form. The lid of the container is closed by the latches of the lock lever and fixed by the pyro check of its drive. At the specified time, a command is sent from the space object to trigger the drive pyro check of the container lid closing mechanism. The pyro check releases the drive rod of the lid lock, which moves in the drive housing under the action of a compression spring. The rod, which is connected by an earring to the arm of the lid lock lever, turns its latches around the axis of the shaft and releases the container lid, which is spring-loaded in its axes. The lid of the container opens, releasing the exit zone of the aerodynamic element. The arm of the mast, turning around its axis, is set in the working position. The shells of the aerodynamic element, coming out of the container, are inflated under the action of the remaining air in their internal cavity to the working state. The aerodynamic element is held on the space object by the thrust of the device.

To deorbit modular large-sized space objects (MLSO) from LEOs, it is assumed that the structure is formed in such a way that it disintegrates into separate modules at the end of the term of active existence (Fig. 4.16—4.18) (Patent of Ukraine for the invention No. 107880, 2015), (Palii, 2014). Each structural module of the MLSO is pre-equipped with deployed self-contained ADSs in the form of inflatable shells associated with them.

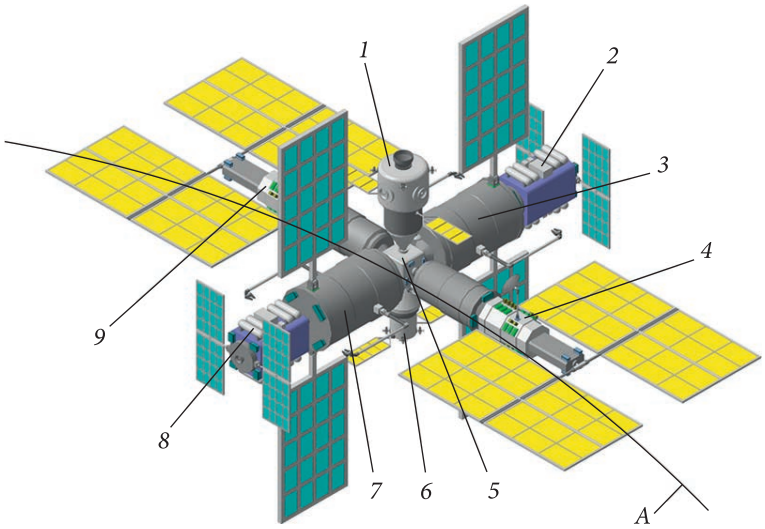

Fig. 4.16. Basic configuration of a modular large space object: *1—9* — structural modules of MLSO; A is the orbit of the MLSO

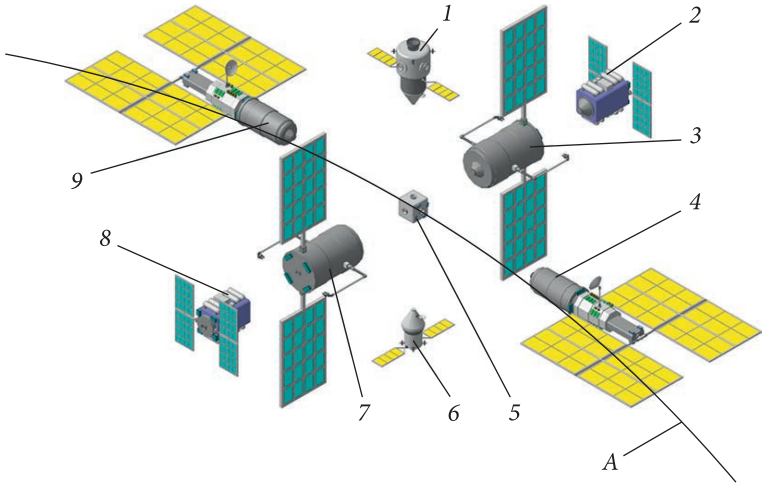

Fig. 4.17. Orbit separation of separated MLSO modules at a distance acceptable for the deployment of the aerodynamic system: *1—9* — structural modules of MLSO; A is the orbit of the MLSO

The design scheme of the complex space object's deorbiting system consists of the design schemes of the deorbiting systems of each of the identified structural modules into which the basic system is divided. In this way, the elements of the deorbiting system are designed by the mass and design characteristics of each module. Thus, the drainage system as a whole consists of a set of its corresponding elements, which can be developed autonomously according to the appropriate methods of designing ADS.

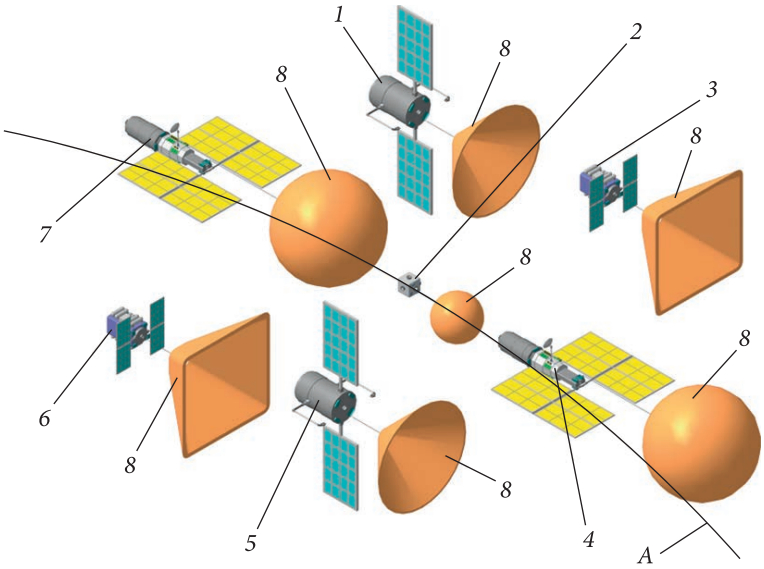

Fig. 4.18. Modules of MLSO with implemented ADS: *1—7* — structural modules of MLSO; *8* — ADS; A is the orbit of the MLSO

Such a system functions as follows. If it is necessary to deorbit the MLSO (Fig. 4.16) from low Earth orbit A, it is pre-divided into separate modules (Fig. 4.17). After modules 1 — 7 have separated in orbit to a distance acceptable for the deployment of the ADS, they are deployed (Fig. 4.18). The cross-sectional area increases, as a result of which the force of aerodynamic resistance increases, and the modules begin to be gradually withdrawn from orbit into the dense layers of the atmosphere.

If it is necessary to deorbit a separate module of the MLSO, it is separated from the base space object, and after moving away in orbit to a distance acceptable for the deployment of the ADS, it is deployed and the module is deorbited.

CHAPTER 5

METHODS TO ANALYZE THE INFLUENCE OF THE PARAMETERS OF THE AERODYNAMIC SYSTEM FOR DEORBITING SPACE OBJECTS ON ITS EFFICIENCY

5.1. The method to determine the parameters of the aerodynamic system

To determine the parameters of the aerodynamic deorbiting systems for space technology objects, methods have been developed based on the synthesis of the modular structure of the system, the decomposition of partial models of interconnected subsystems based on their physical, mathematical and combined models (Skorik, 2013), (Paliy, 2015). The scheme of the methods is shown in Fig. 5.1. The method is based on the iterative method of calculating the mass-dimensional characteristics of the ADS based on the solution of partial design tasks and includes:

- a model of the geometry and masses of the ADS;
- a mathematical model of the disturbed orbital motion of the space object with the ADS, which is being deorbited;
- a model for taking into account the influence of space factors on the functioning of the ADS;
- an algorithm to select the type of ADS;
- an algorithm to choose rational design parameters of the ADS from the set of solutions obtained according to the chosen criterion, taking into account the limitations on the time of the ADS's active existence;
- verification of solutions to the design problem by performing verification calculations.

In the first stage, the calculation of the area of the median cross-section of the ADS and the analysis of the influence of space vacuum (sublimation) and atomic oxygen on the material of the shell of the aerodynamic element are carried out. As a result, the parameters of the aerodynamic element are determined to ensure the given period of orbital existence.

In the second stage, the probability of the breakdown of the inflatable elements of the aerodynamic element is estimated,

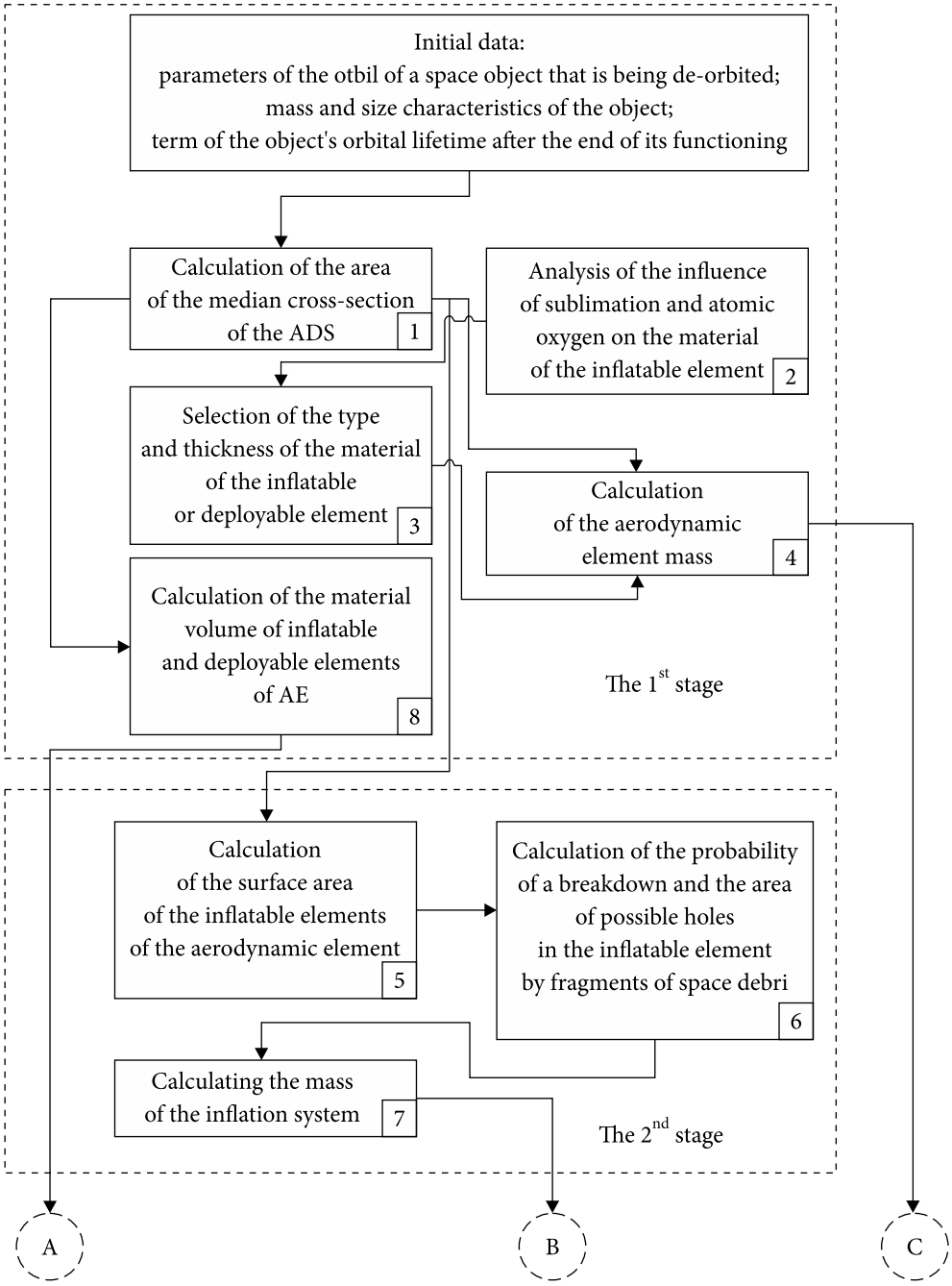

Fig. 5.1. Scheme of the design method of aerodynamic deorbiting systems (see also page 98)

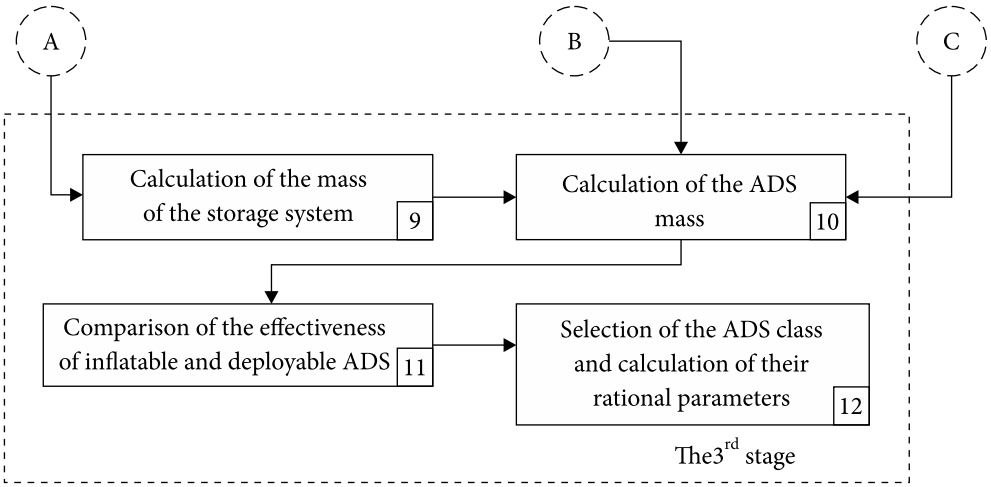

Fig. 5.1. The end

and the area of the probable holes in the inflatable element is calculated. As a result, the parameters of the inflation system are determined.

In the third stage, the parameters of the storage system and the parameters of the ADS as a whole are calculated. Assessments of the effectiveness of the ADS and comparison of inflatable, deployable, and transformed ADSs are carried out and the class of the aerodynamic system is selected to ensure the given period of orbital existence.

The calculation of the above parameters is performed according to the mathematical models and algorithms in sections *2* and *3*.

5.2. Calculation of aerodynamic element parameters

Calculation of the parameters of the aerodynamic element of the deorbiting system is performed based on the analysis of the influence of space factors on the aerodynamic element, in particular, on the type and thickness of the shell material to ensure the reliable functioning of the ADS during the given period of orbital existence. For these purposes, it is necessary to perform many calculations, namely, to construct appropriate nomograms for common ranges of working parts and mass-dimensional characteristics of the space object. Calculation of nomograms is performed according to the following algorithm:

1) calculate the area of the median cross-section of the space object with the ADS;

2) determine the surface area of the inflatable ADS elements;

3) determine the surface area of the deployable ADS elements;

4. evaluate the effect of space vacuum (sublimation) and atomic oxygen on the shell material;

5) determine the thickness of the material of the aerodynamic element of the ADS.

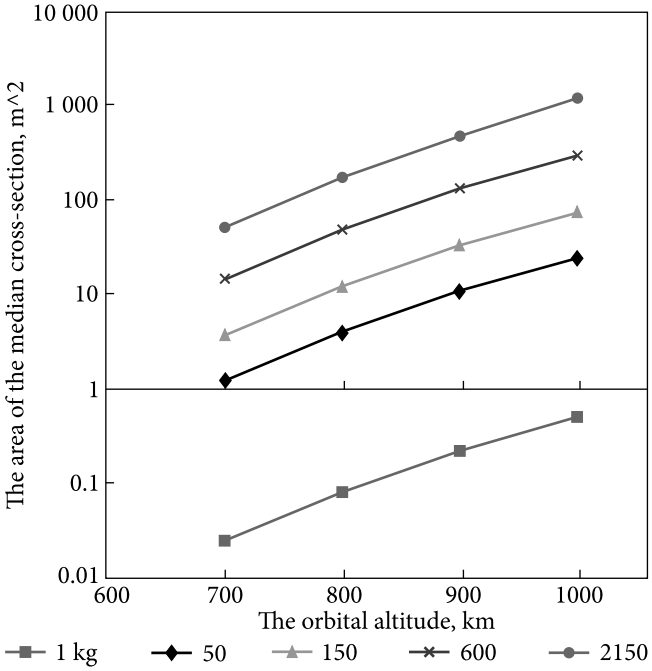

Fig. 5.2. Dependence of the ADS cross-section area on the orbital altitude of the space object that is being deorbited

The area of the median cross-section of the ADS is calculated using analytical dependencies (3.1), and (3.2). At the same time, the following set of output data of the deorbited space object is used:

- range of orbit altitudes, km: 700—1000;
- mass range of ADS, kg: 1—2150;
- the range of the space object cross-section area, m^2: 0.015—22;
- the term of orbital existence is 25 years.

The results of the calculations are shown in Fig. 5.2.

The following algorithm is used to assess the influence of space factors. The entire altitude range of the space objects, which are being deorbited, from the initial altitude to the boundary of the dense layers of the atmosphere (≈200 km), is represented by the altitude of the orbits by a layer-by-layer structure with a step of 50 km. At the initial stage, the change rate in the material thickness under the influence of space vacuum and atomic oxygen is calculated and taken as constant during the time during which the space object from the ADS will decrease to the altitude of the next layer. Based on the solution of the system of equations of orbital motion (2.1), the time during which the space object from the ADS will decrease to the orbital altitude of the next calculation layer is determined. Having determined the time interval during which the space object from the ADS will leave the range of altitudes of the current layer and the change rate in the material thickness on this layer, we will calculate the change in the mate-

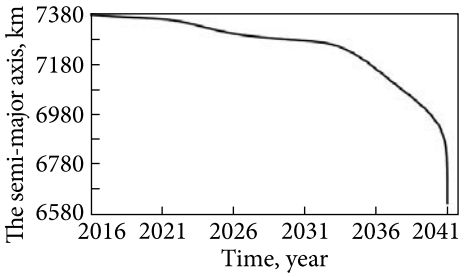

Fig. 5.3. Dependence of the semi-major axis of the space object orbit on time

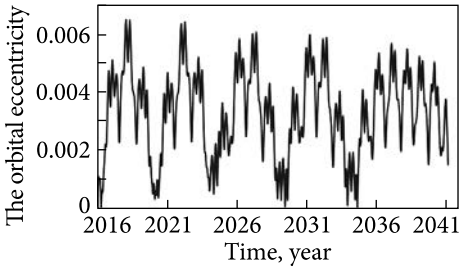

Fig. 5.4. Dependence of the eccentricity of the space object orbit on time

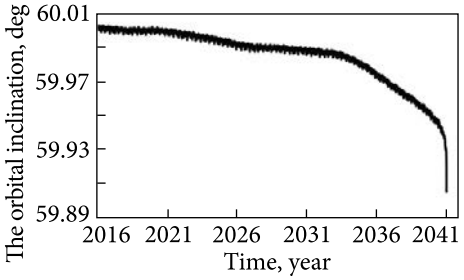

Fig. 5.5. Dependence of the inclination of the space object orbit on time

rial thickness using mathematical ratios (3.9)—(3.21). Upon reaching the space object range of the orbital altitudes of the next layer, the change rate of the material thickness is recalculated and assumed to be constant within the limits of the current layer. The procedure is repeated until the space object reaches the altitude of the boundaries of the dense layers of the atmosphere, the cycle is stopped, the changes in material thickness are summed up, and thus the nominal material thickness necessary for the reliable functioning of the ADS during the entire period of orbital existence is determined. To determine the design thickness, the value dispersion coefficient of the volume coefficient of mass loss and the sublimation rate are used. The value of this coefficient lies in the range of 1.22—1.45. The design value is determined by multiplying the nominal value of the shell thickness by this factor. Its lower value is used for the range of orbital altitudes (700—750) km, the upper value is used for the range of orbital altitudes (750—1000) km.

The system of equations (2.1) describing the orbital motion of the space object with the ADS is solved by the Adams-Bashforth method of the 4th order, with an integration step of 1 day.

We will consider the use of the above algorithm on the example of deorbiting a 2150 kg LV upper stage. In this case, a set of initial data is used: the orbital altitude is 1000 km; the beginning of the deorbiting time on 01/01/2016; orbital eccentricity 0.000072; orbit inclination 60°; a right ascent of the ascending node of the orbit 60°; the perigee argument of the orbit is 80° the area of the median crossing of the ADS is 1385 m^2 the term of orbital lifetime is 25 years.

The results of solving the system of equations (2.1) are shown in Fig, 5.3—5.7.

To use the obtained results in the model of taking into account the influence of space factors, we will convert the change in the major semi-axis of the orbit into the change in the altitude of the apogee and perigee of the orbit (Fig. 5.8).

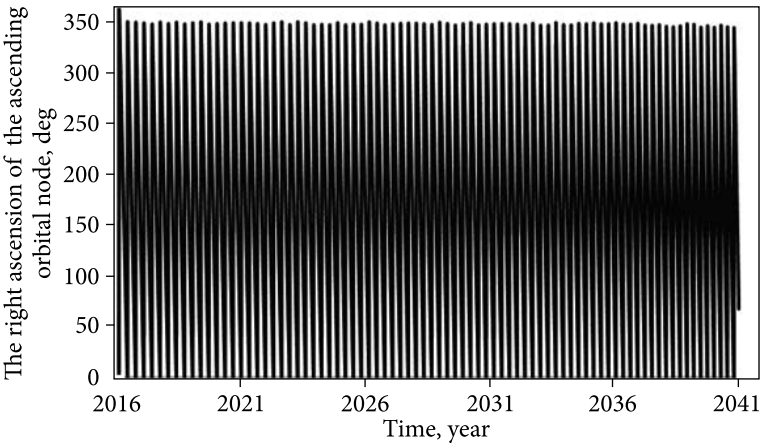

Fig. 5.6. Dependence of the right ascent of the ascending node of the space object orbit on time

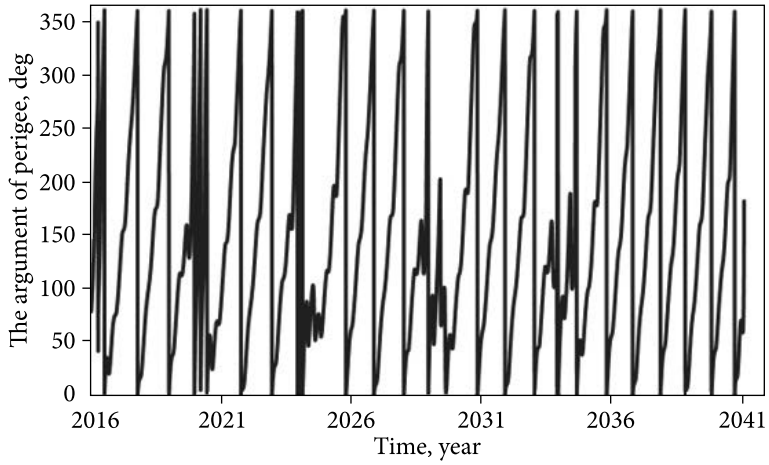

Fig. 5.7. Dependence of the perigee argument of the space object orbit on time

From the graphs shown in Fig. 5.8, it can be seen that at an altitude of ≈450 km, the eccentricity of the orbit goes to zero and the orbit becomes circular.

Next, the altitude range of the space object orbit (in this case, 1000—200 km) is divided into layers of 50 km each. The results of the breakdown are shown in Fig. 5.9.

The graph is shown in Fig. 5.9, points show the moments of the start of a new iteration (reaching the altitude of the next layer). The obtained values are used to evaluate the influence of outer space factors (space vacuum, atomic oxygen, and SF).

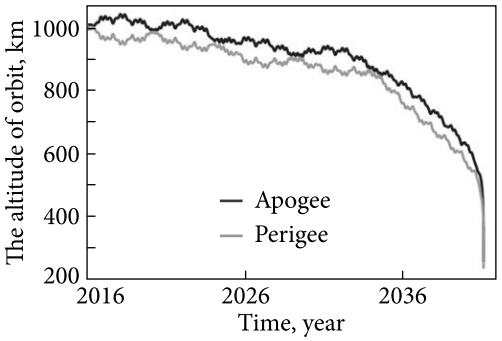

Fig. 5.8. Dependence of the altitude of the apogee and perigee of the orbit on time

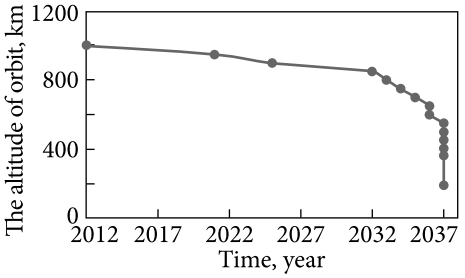

Fig. 5.9. Dependence of the perigee altitude of the orbit on time

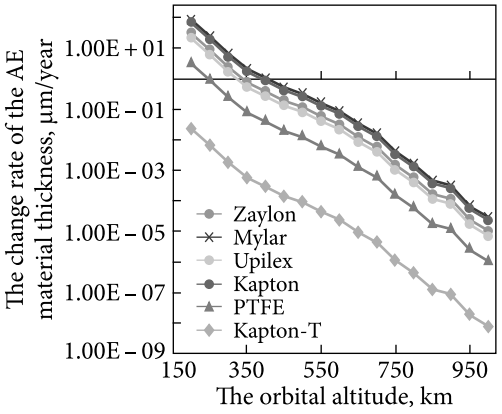

Fig. 5.10. Dependence of the change rate of the AE material thickness on the orbital altitude of the space object that is being deorbited

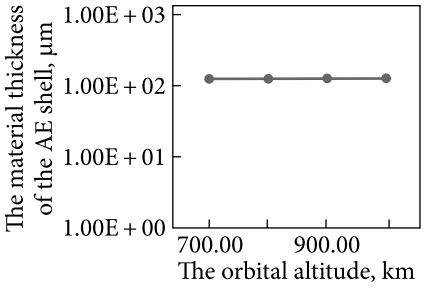

Fig. 5.11. Dependence of the material thickness of the AE shell on the initial orbital altitude of the space object that is being deorbited

To determine the material thickness, the change rate of the material thickness is determined, then the thickness of the AE material is determined to ensure the reliable functioning of the ADS during the given period of orbital existence. The following raw data are additionally used:

• type of AE material: «Zaylon»; «Mylar»; «Upilex»; «Kapton»; «PTFE»; «Kapton-T»;

• volume coefficient of mass loss: $1.36 \cdot 10^{-24}$ cm^3/atom; $3.7 \cdot 10^{-24}$ cm^3/atom ; $9.22 \cdot 10^{-25}$ cm^3/atom; $3 \cdot 10^{-24}$ cm^3/atom; $1.42 \cdot 10^{-25}$ cm^3/atom; $1.10 \cdot 10^{-25}$ cm^3/atom.

The results of calculating the change rate in material thickness under the influence of space vacuum and atomic oxygen are shown in Fig. 5.10.

In Fig. 5.10 it is shown: PTFE — polytetrafluoroethylene; Kapton-T — kapton covered with a layer of Teflon to increase resistance against the influence of atomic oxygen.

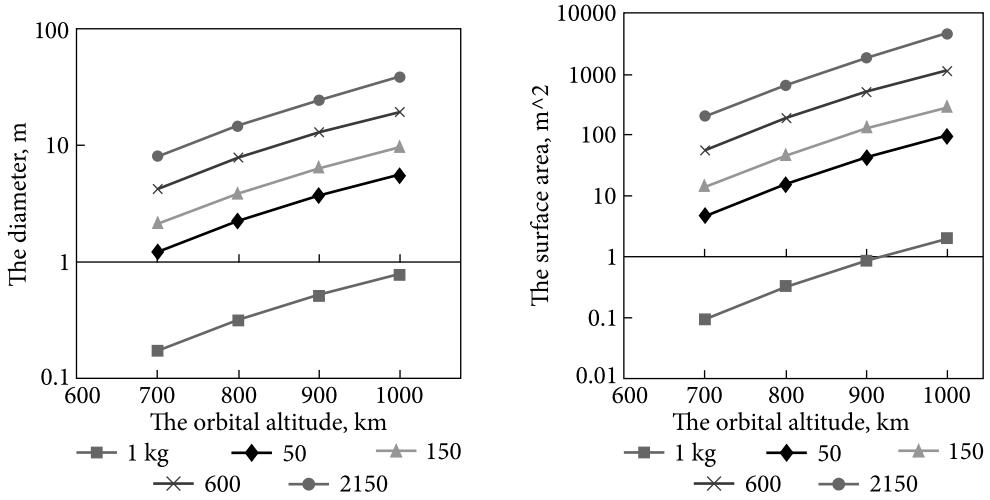

Fig. 5.12. Dependence of the diameter of the aerodynamic element of the «Sphere» ADS configuration on the altitude of the space object orbit

Fig. 5.13. Dependence of the surface area of the inflatable element of the «Sphere» ADS configuration on the altitude of the space object orbit

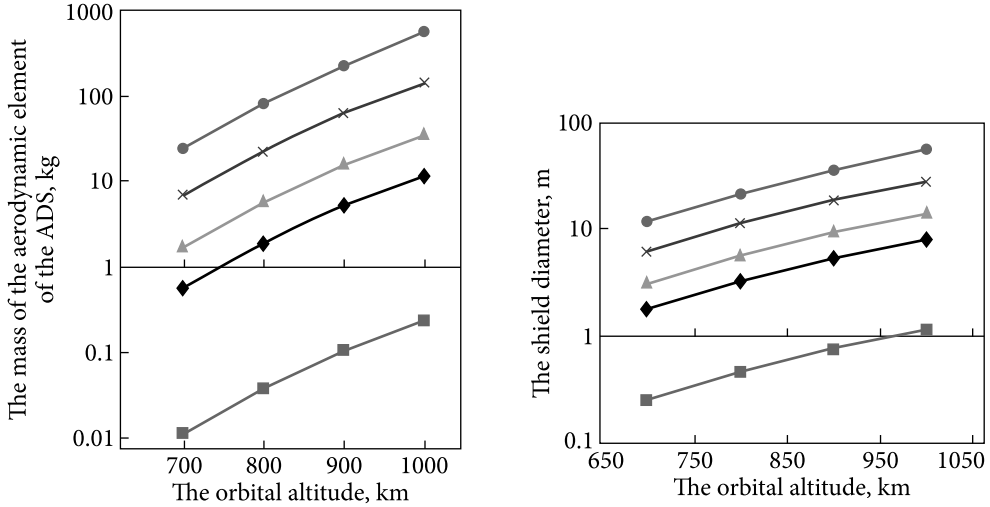

Fig. 5.14. Dependence of the mass of the aerodynamic element of the «Sphere» ADS configuration on the altitude of the space object orbit. Legend of the Figures — see Fig. 5.13

Fig. 5.15. Dependence of the shield diameter of the aerodynamic element of the «Round shield» ADS configuration on the altitude of the space object orbit. Legend of the Figures — see Fig. 5.13

As a result of the analysis of the results shown in Fig. 5.10, it can be concluded that the Kapton-T material is significantly superior to its analogs. That's why it has been chosen for AE of the inflatable ADS. For the Kapton-T mate-

rial, the thickness at which the ADS will function during the given period of orbital existence is calculated. The results of the thickness calculation are shown in Fig. 5.11.

Fig. 5.11 shows that the material thickness of the AE shell depends slightly on the initial orbital altitude of the space object that is being deorbited. The weak dependence can be explained by a significant decrease in the concentration of atomic oxygen at altitudes (700—1000) km, at which ADSs with the deorbited space object move for ≈97% of the entire period of their orbital existence (Fig. 5.8). Based on this, we set the maximum value of the material thickness of the AE, equal to 130 μm, which we will use for all the initial altitude of the space object which is being deorbited.

5.2.1. Selection of parameters of the aerodynamic element of monoblock systems

For the initial data given above, using mathematical expressions (3.22)—(3.26), calculations are made of the diameter of the aerodynamic element of the «Sphere» ADS, the surface area of the inflatable element, and the mass of the aerodynamic element, the results of which are shown in Fig. 5.12—5.14.

5.2.2. Selection of parameters of the aerodynamic element of frame-inflatable systems

The AE of the inflatable ADS consists of inflatable elements (inflatable masts) and deployable elements (thin film membrane). To determine the general characteristics of the AE, it is necessary to know the area of the median cross-section of the ADS, taking into account the given term of the orbital existence of the space object being deorbited.

The following configurations of frame-inflatable ADSs have been considered: «Round Shield»; «Two dihedral panels»; «Pyramide-triangle»; «Pyramide-square»; «A cone made of tori»; «A cone composed of tori with spherical shells placed inside»; «Bulk sail».

For the initial data given above, using mathematical expressions (3.27)—(3.38), calculations are made of the diameter of the aerodynamic element of the «Round Shield», the surface area of the inflatable elements, the area of the deployable surface of the element and the AE mass, the results of which are shown in Fig. 5.15—5.18.

For the initial data given above, using mathematical expressions (3.39) —(3.49), the diameter of the aerodynamic element of the «Two Dihedral Panels» ADS, the surface area of the inflatable elements, the surface area of the deployable elements and the mass of the aerodynamic element are calculated, the results of which are shown in Fig. 5.19—5.22.

For the initial data given above, using mathematical expressions (3.50—3.62), the diameter of the aerodynamic element of the «Pyramide-triangle» ADS, the surface area of the inflatable elements, the surface area of the deployable ele-

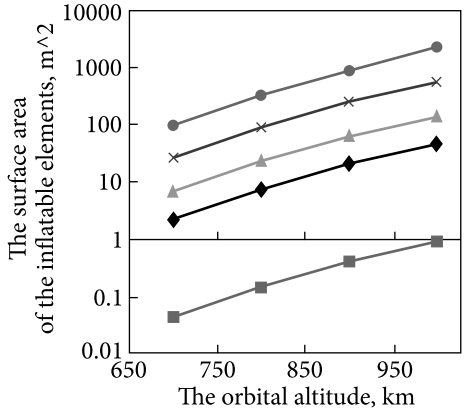

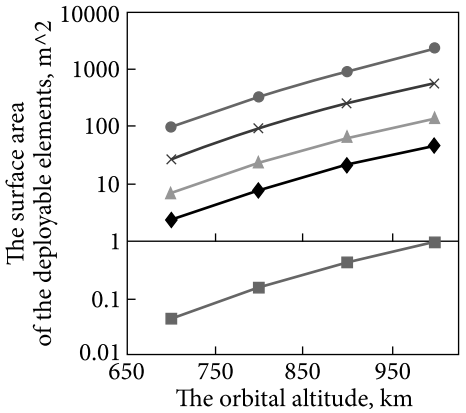

Fig. 5.16. Dependence of the surface area of the inflatable elements of the aerodynamic element of the «Round Shield» ADS configuration on the altitude of the space object orbit. Legend of the Figures — see Fig. 5.13

Fig. 5.17. Dependence of the surface area of the deployable elements of the aerodynamic element of the «Round shield» ADS configuration on the altitude of the space object orbit. Legend of the Figures — see Fig. 5.13

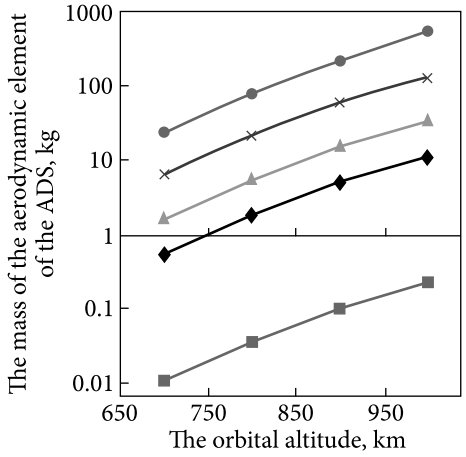

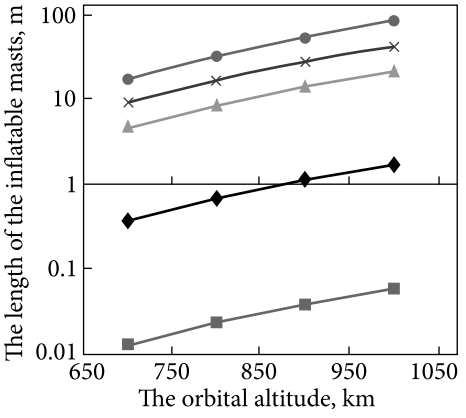

Fig. 5.18. Dependence of the mass of the aerodynamic element of the «Round shield» ADS configuration on the altitude of the space object orbit Legend of the Figures — see Fig. 5.13

Fig. 5.19. Dependence of the length of the inflatable masts of the «Two dihedral panels» ADS configuration on the altitude of the space object orbit. Legend of the Figures — see Fig. 5.13

ments and the mass of the aerodynamic element are calculated, the results of which are shown in Fig. 5.23—5.26.

For the initial data given above, using mathematical expressions (3.63)—(3.75), the diameter of the aerodynamic element of the «Pyramide-square» ADS, the surface area of the inflatable elements, the surface area of the deployable elements and the mass of the aerodynamic element are calculated, the results of which are shown in Fig. 5.27—5.30.

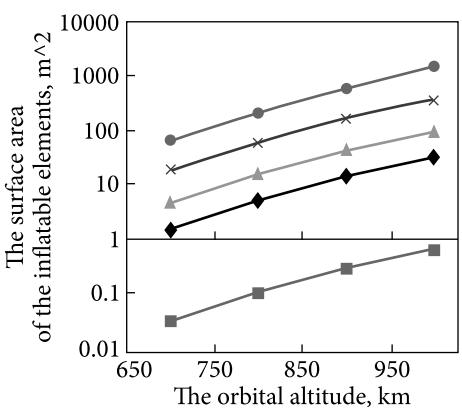

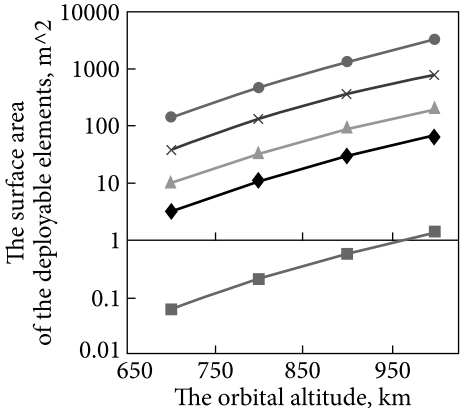

Fig. 5.20. Dependence of the surface area of the inflatable elements of the aerodynamic element of the «Two dihedral panels» ADS configuration on the altitude of the space object orbit. Legend of the Figures — see Fig. 5.13

Fig. 5.21. Dependence of the surface area of the deployable elements of the aerodynamic element of the «Two dihedral panels» ADS configuration on the altitude of the space object orbit. Legend of the Figures — see Fig. 5.13

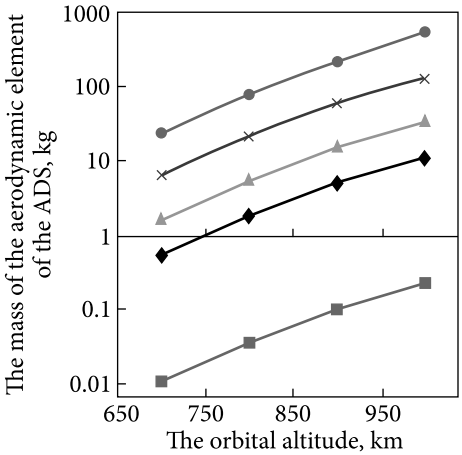

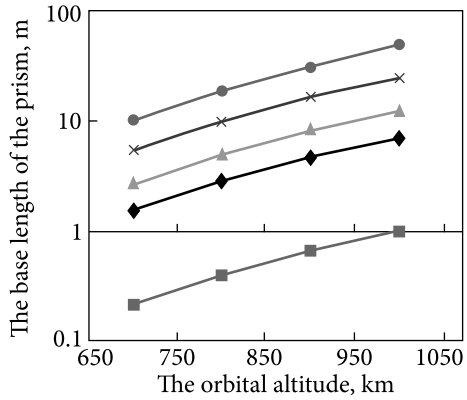

Fig. 5.22. Dependence of the mass of the aerodynamic element of the «Two dihedral panels» ADS configuration on the altitude of the space object orbit. Legend of the Figures — see Fig. 5.13

Fig. 5.23. Dependence of the base length of the prism of the «Prism-square» ADS configuration on the altitude of the space object orbit. Legend of the Figures — see Fig. 5.13

For the initial data given above, using mathematical expressions (3.76)—(3.84), calculations are made of the cross-section diameter of the torus shell of the aerodynamic element of the «Cone made of tori» ADS, the surface area of the inflatable elements and the mass of the aerodynamic element, the results of which are shown in Fig. 5.31—5.33.

For the initial data given above with the help of mathematical expressions (3.85)—(3.93), calculations are made of the diameter of the cross-section of

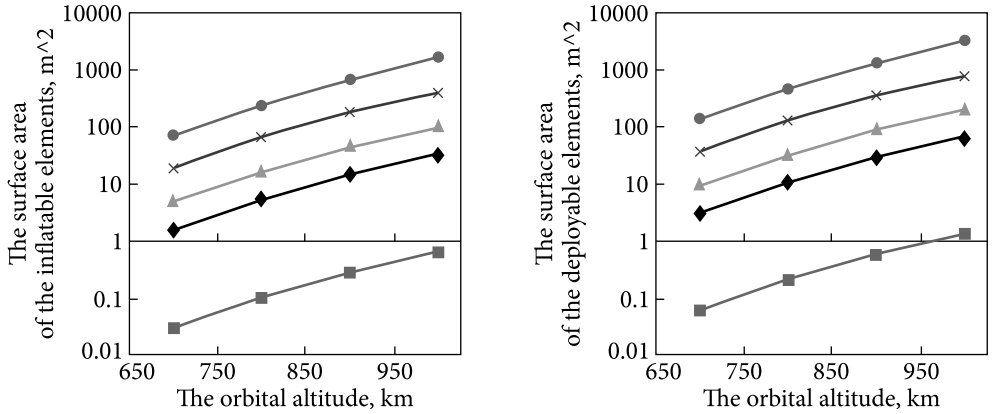

Fig. 5.24. Dependence of the surface area of the inflatable elements of the aerodynamic element of the «Pyramide-square» ADS configuration on the altitude of the space object orbit. Legend of the Figures — see Fig. 5.13

Fig. 5.25. Dependence of the surface area before the deployment of the elements of the aerodynamic element of the «Prism-square» ADS configuration on the altitude of the space object orbit. Legend of the Figures — see Fig. 5.13

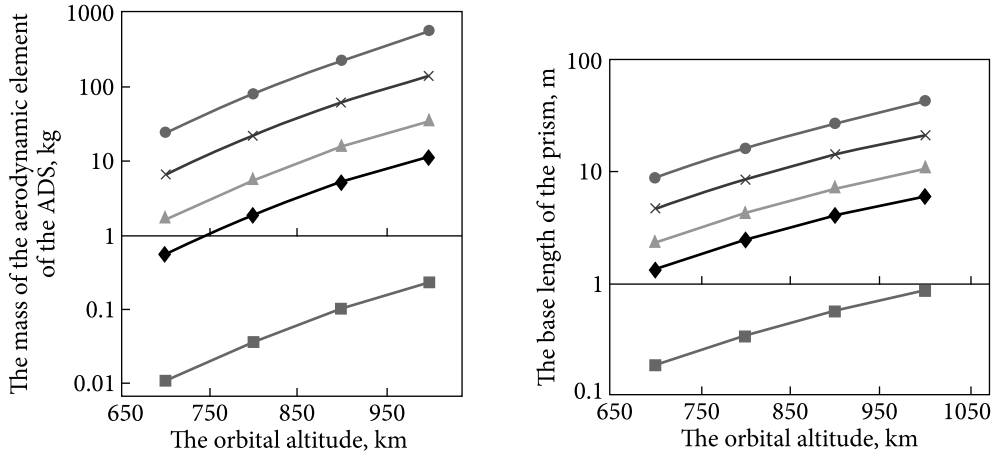

Fig. 5.26. Dependence of the mass of the aerodynamic element of the «Prism-square» ADS configuration on the altitude of the space object orbit. Legend of the Figures — see Fig. 5.13

Fig. 5.27. Dependence of the base length of the prism of the «Prism-square» ADS configuration on the altitude of the space object orbit. Legend of the Figures — see Fig. 5.13

the torus shell of the aerodynamic element of the «Cone composed of tori with spherical shells placed inside» ADS, the surface area of the inflatable elements and the mass of the aerodynamic element, the results of which shown in Fig. 5.34—5.37.

For the initial data given above, using mathematical expressions (3.94)—(3.106), calculations are made of the diameter of the cross-section of the torus shell of the aerodynamic element of the «Bulk sail» ADS, the diameter of the

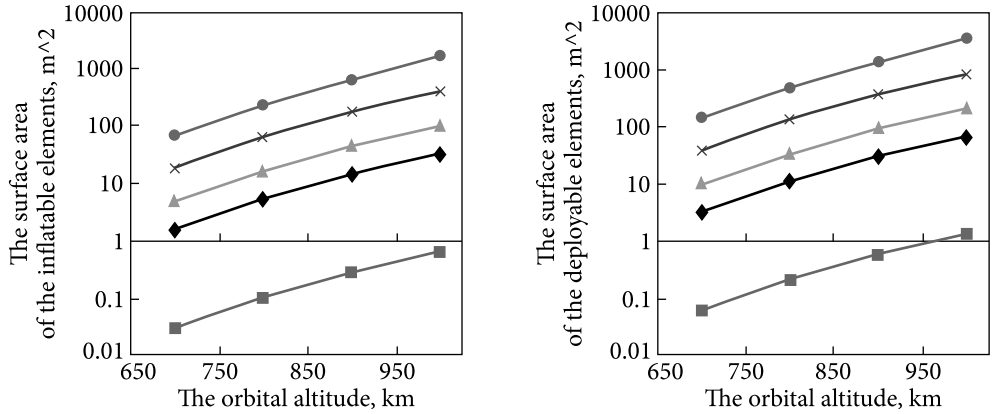

Fig. 5.28. Dependence of the surface area of the inflatable elements of the aerodynamic element of the «Pyramide-square» ADS configuration on the altitude of the space object orbit. Legend of the Figures — see Fig. 5.13

Fig. 5.29. Dependence of the surface area before the deployment of the elements of the aerodynamic element of the «Pyramide-square» ADS configuration on the altitude of the space object orbit. Legend of the Figures — see Fig. 5.13

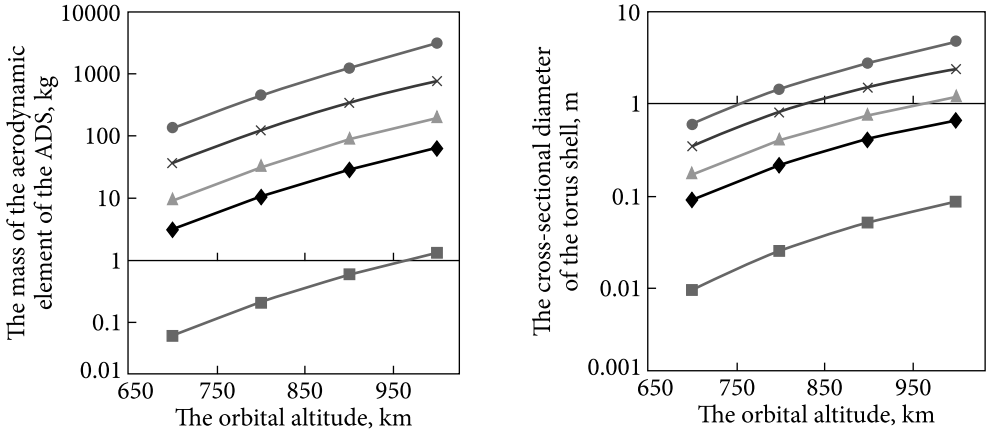

Fig. 5.30. Dependence of the mass of the aerodynamic element of the «Pyramide-square» ADS configuration on the altitude of the space object orbit. Legend of the Figures — see Fig. 5.13

Fig. 5.31. Dependence of the cross-sectional diameter of the torus shell of the «Cone made of tori» ADS configuration on the altitude of the space object orbit. Legend of the Figures — see Fig. 5.13

membrane; cross-sectional diameter of the torus shell; surface area of the aerodynamic element and its mass, the results of which are shown in Figs. 5.38—5.41.

5.2.3. Selection of the parameters of the aerodynamic element of deployable aerodynamic deorbiting systems

For the initial data given above, mathematical expressions (3.107)—(3.113) are used to calculate the length of the side of the square and the surface area

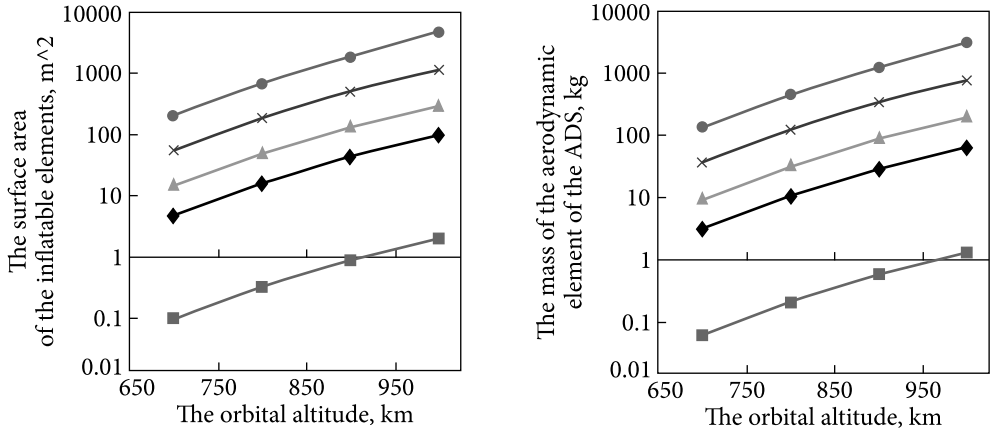

Fig. 5.32. Dependence of the surface area of the inflatable elements of the AE configuration of the «Cone composed of tori» ADS on the altitude of the space object orbit. Legend of the Figures — see Fig. 5.13

Fig. 5.33. Dependence of the AE mass of the «Cone made of tori» ADS configuration on the altitude of the space object orbit. Legend of the Figures — see Fig. 5.13

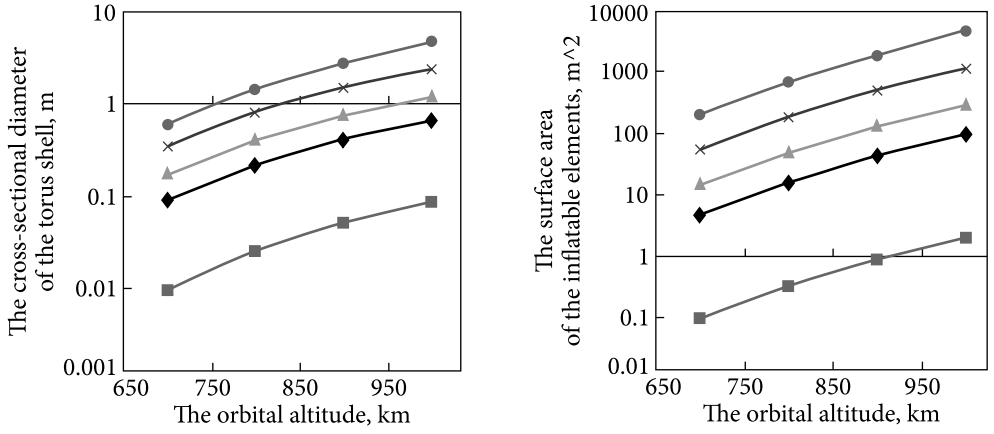

Fig. 5.34. Dependence of the diameter of the cross-section of the torus shell of the «A cone made of tori with spherical shells placed inside» ADS configuration on the altitude of the space object orbit. Legend of the Figures — see Fig. 5.13

Fig. 5.35. Dependence of the surface area of the inflatable elements of the AE of the «A cone made of tori, with the ones placed inside» ADS configuration on the altitude of the space object orbit. Legend of the Figures — see Fig. 5.13

of the deployable elements and the mass of AE, the results of which are shown in Fig. 5.42, 5.43.

When the array of AE mass-dimensional characteristics of inflatable and deployable ADSs is formed, it is possible to proceed to the next stage of ADS design: the selection of the inflation system parameters.

5.3. Selection of the inflation system parameters

The ADS inflation system must ensure its reliable functioning during the entire period of the orbital existence of the space object. To achieve this, it is necessary to evaluate the impact of the SF on the inflatable elements of the ADS AE of various configurations, calculate the period of active existence of the system, and

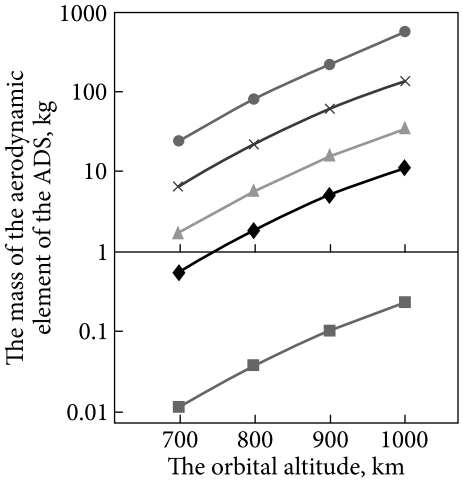

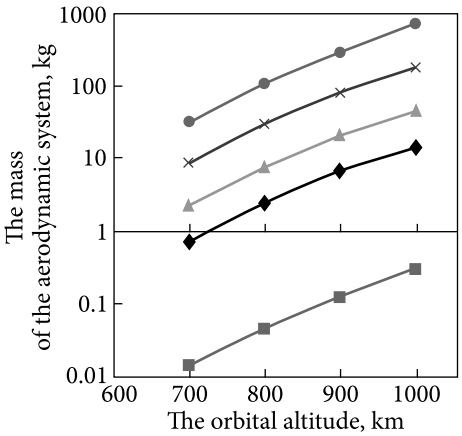

Fig. 5.36. Dependence of the mass of the aerodynamic element of the «Cone made of tori, with the ones placed inside» ADS configuration on the altitude of the space object orbit. Legend of the Figures — see Fig. 5.13

Fig. 5.37. Dependence of the mass of the «Cone composed of tori, with tori placed inside» ADS configuration on the altitude of the space object orbit. Legend of the Figures — see Fig. 5.13

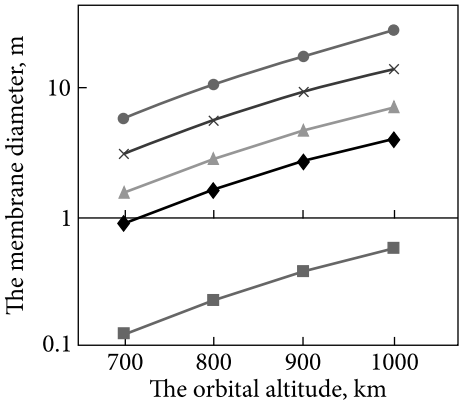

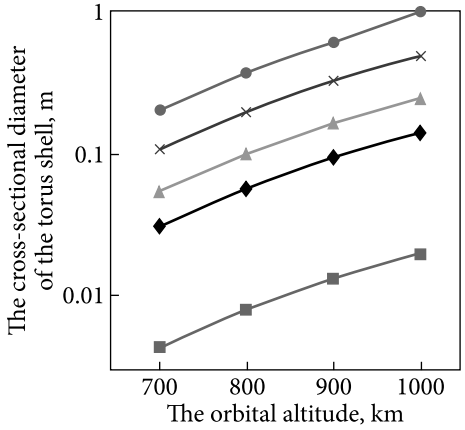

Fig. 5.38. Dependence of the membrane diameter of the «Bulk sail» ADS on the altitude of the space object orbit. Legend of the Figures — see Fig. 5.13

Fig. 5.39. Dependence of the cross-section diameter of the torus shell of the «Bulk Sail» ADS on the altitude of the space object orbit. Legend of the Figures — see Fig. 5.13

select the parameters of the inflation system to ensure the reliable functioning of the system throughout the entire period of orbital lifetime.

The term of active lifetime is calculated according to the following algorithm: calculation of the minimum size of the SF capable of piercing the inflatable element of the AE of the given thickness; calculation of the flow of space debris fragments; determination of the increase rate in the area of the holes in the inflatable

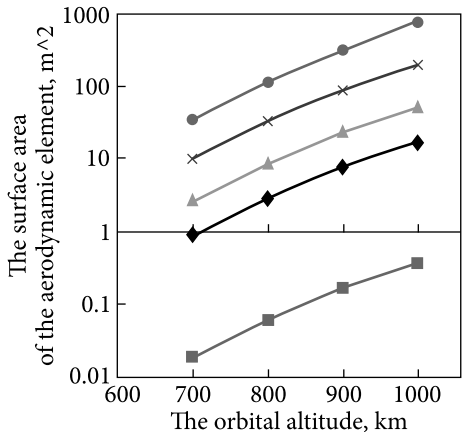

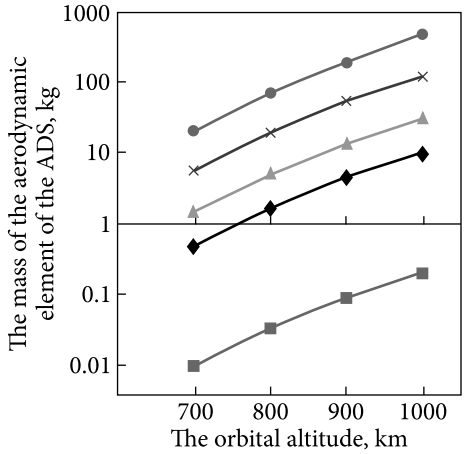

Fig. 5.40. Dependence of the surface area of the aerodynamic element of the «Bulk sail» ADS configuration on the altitude of the space object orbit. Legend of the Figures — see Fig. 5.13

Fig. 5.41. Dependence of the mass of the aerodynamic element of the «Bulk sail» ADS configuration on the altitude of the space object orbit. Legend of the Figures — see Fig. 5.13

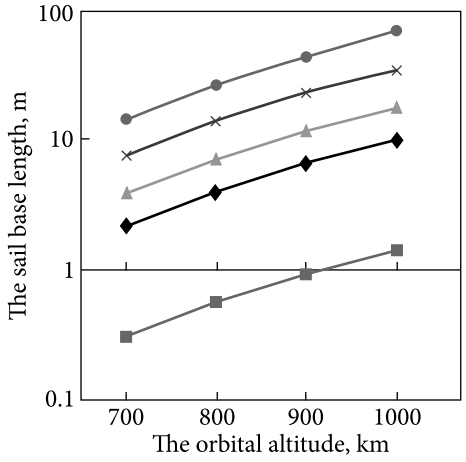

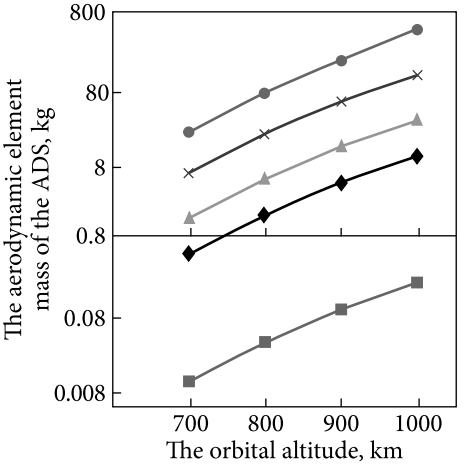

Fig. 5.42. Dependence of the sail base length of deployable ADSs on the altitude of the space object orbit. Legend of the Figures — see Fig. 5.13

Fig. 5.43. Dependence of the AE mass of the deployable ADS on the altitude of the space object orbit. Legend of the Figures — see Fig. 5.13

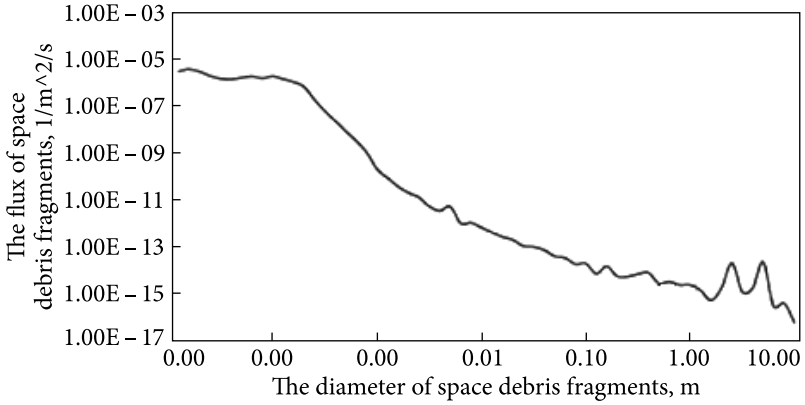

Fig. 5.44. Dependence of the SD flux on the cross-sectional diameter of the fragment.

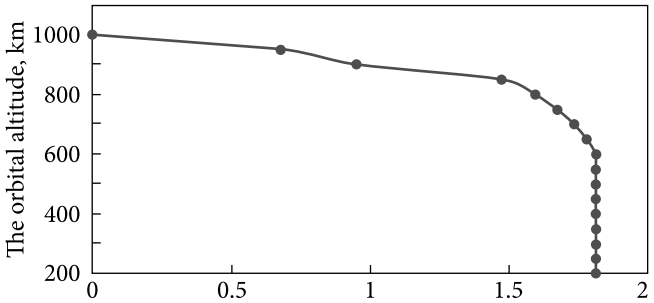

Fig. 5.45. Dependence of the area of the holes in the inflatable element on the altitude of the space object orbit.

element for a given period of orbital lifetime; calculation of gas flow parameters; calculation of the period of the ADS's active lifetime.

The calculation of the SD flux (Fig. 5.44) has been performed for the following initial data: subclass ADS — monoblock spherical; the initial altitude of the orbit is 1000 km; sphere diameter — 34 m; the term of orbital lifetime is 25 years.

The calculated SF flow and the time for which the space object will decrease to the altitude of each layer (according to the algorithm for taking into account the influence of space factors) allow us to calculate the area of the formed holes in the inflatable element (Fig. 5.45). The area of the holes formed in the inflatable elements makes it possible to determine the FSD parameters to ensure the reliable functioning of the ADS. The FSD parameters are the excess pressure in the inflatable element (Fig. 5.46) and the gas mass for inflating the inflatable element (Fig. 5.47).

The movement of gas from the inflatable element under the influence of SD is determined by the following parameters:

$$N_1 = \frac{p_1}{\sqrt{T_1}}, \tag{5.1}$$

$$N_2 = \frac{p_2}{\sqrt{T_2}}, \tag{5.2}$$

where p_1 is the excess pressure inside the inflatable element of the ADS; p_2— atmospheric pressure; T_1— gas temperature inside the inflatable element; T_2 — atmospheric temperature.

Gas from the inflatable element will stop flowing under the condition when $N_1 = N_2$ (Fig. 5.48), at this moment it is considered that the ADS has ceased to exist. From the graph in Fig. 5.48 it can be seen that the ADS will stop functioning after ≈ 21 days.

Next, the parameters of the inflation system are determined to ensure the reliable functioning of the ADS during the given period of orbital lifetime of the

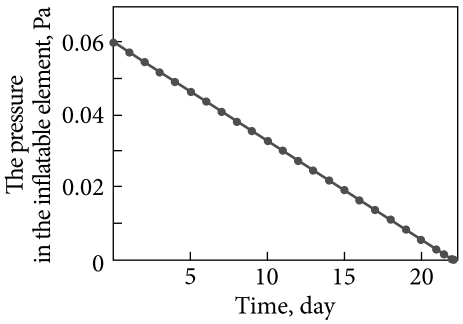

Fig. 5.46. Time dependence of the pressure in the inflatable element

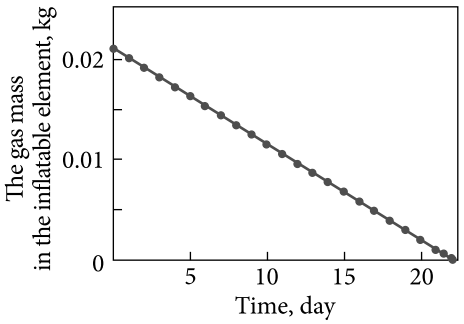

Fig. 5.47. Time dependence of the gas mass in the inflatable element

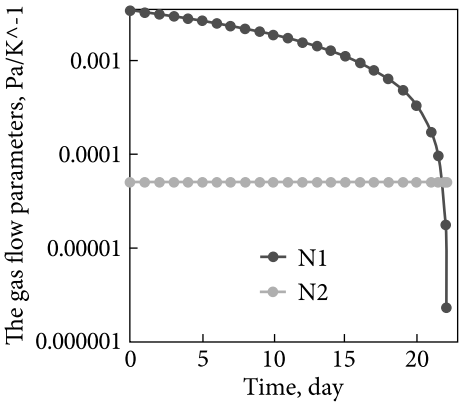

Fig. 5.48. Time dependence of gas flow parameters from an inflatable element

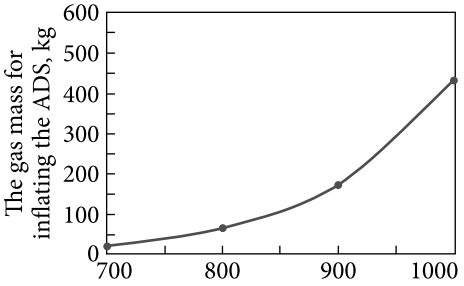

Fig. 5.49. Dependence of the gas mass for inflating the ADS on the altitude of the initial orbit of the space object

space object with ADS. As an example, consider the mass of the inflation system of a spherical ADS for de-orbiting at an altitude of: 700 km; 800 km; 900 km; or 1000 km, the mass of the space object is 2150 kg, the period of orbital lifetime is 25 years. The results are shown in Fig. 5.49.

Mathematical expressions (3.119—3.140) and Tables 3.4, and 3.5 are used to determine the parameters of the ADS inflation system of various configurations.

5.4. Assessment of the limits of the effective applicability of aerodynamic deorbiting systems

At the final stage of design, an assessment of the effectiveness of ADS of various types and configurations is carried out. For this purpose, the parameters of the ADS are determined, taking into account the masses of the storage system, the inflation system, and the deployment system, and the limits of their effective use are determined. At this stage, the analysis of the ADS form is carried out. The configuration of the ADS must satisfy the restrictions imposed on the ADS, while the system must have a minimum mass m_{ACB}. In this case, the following restrictions are imposed on the ADS configuration:

- the term of active lifetime of ADS t_A should be greater than or equal to the term of orbital lifetime of the space object with ADS;
- the mass of the ADS m_{ACY} should not exceed the specified value. The statistical value is 5% of the mass of the space object m_{KO}.

The mathematical formulation of the selection of the ADS parameters at this stage consists of minimizing the mass of the ADS, taking into account the restrictions imposed on its design. At the same time, the ratio expressing the criterion to choose a rational ADS is valid:

$$m_{ACB} = f\left(m_{AE}, m_{C3}, m_{CH}, m_{CP}\right) \rightarrow \min \begin{vmatrix} k_2 \le 0{,}05 \\ t_A \le t_L \end{vmatrix}, \tag{5.3}$$

where m_{AE} is the mass of the aerodynamic element; m_{C3} — the mass of the storage system; m_{CH} — the mass of the inflation system; m_{CP} — the mass of the deployment system; m_{KO} — the mass of the space object; k_2 — the specific mass of the ADS is determined using the following expression:

$$k_2 = \frac{m_{ACB}}{m_{KO}}, \tag{5.4}$$

t_A — the term of active lifetime of ADS; t_L— the term of the orbital existence of the ADS.

At this stage, the mass of the ADS of various configurations is also calculated. Once the masses are determined, the efficiency of different configurations is compared. First, different modifications of inflatable ADSs are compared. One of the

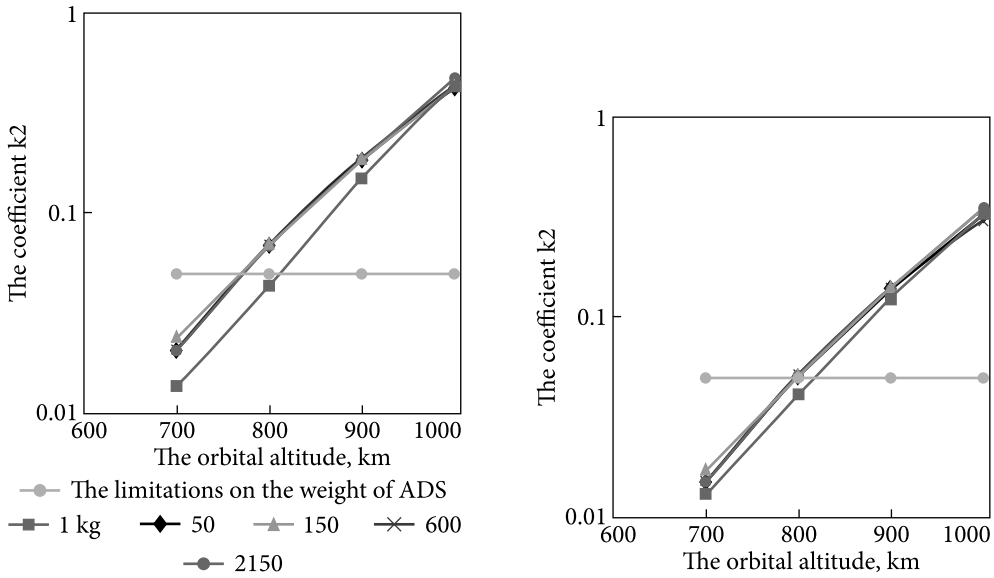

Fig. 5.50. Dependence of the specific mass of inflatable ADSs of the «Sphere» configuration on the altitude of the orbit, for the deorbiting of space objects of different mass

Fig. 5.51. Dependence of the specific mass of inflatable ADSs of the «Round shield» configuration on the altitude of the orbit, for the deorbiting of space objects of different mass. Legend of the Figures — see Fig. 5.50

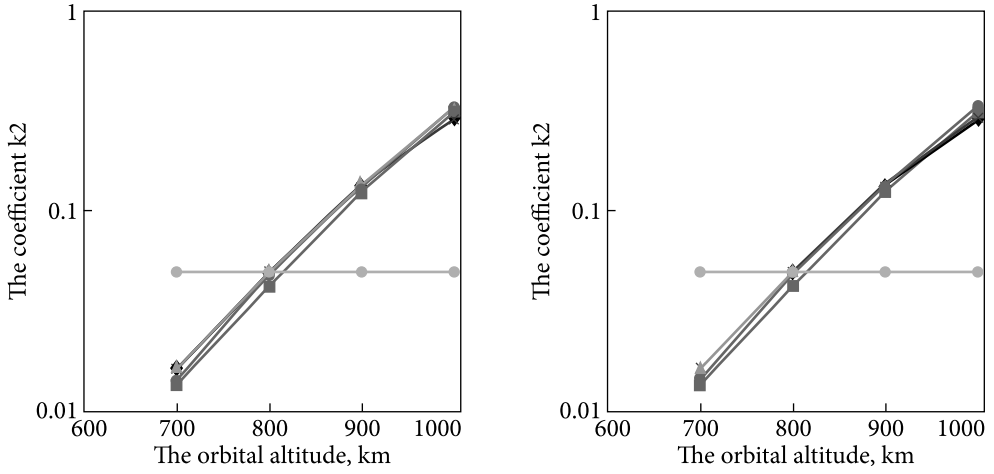

Fig. 5.52. Dependence of the specific mass of inflatable ADSs of the «Two dihedral panels» configuration on the altitude of the orbit, for the deorbiting of space objects of different mass. Legend of the Figures — see Fig. 5.50

Fig. 5.53. Dependence of the specific mass of inflatable ADSs of the «Triangle Pyramide» configuration on the altitude of the orbit, for the deorbiting of space objects of different mass. Legend of the Figures — see Fig. 5.50

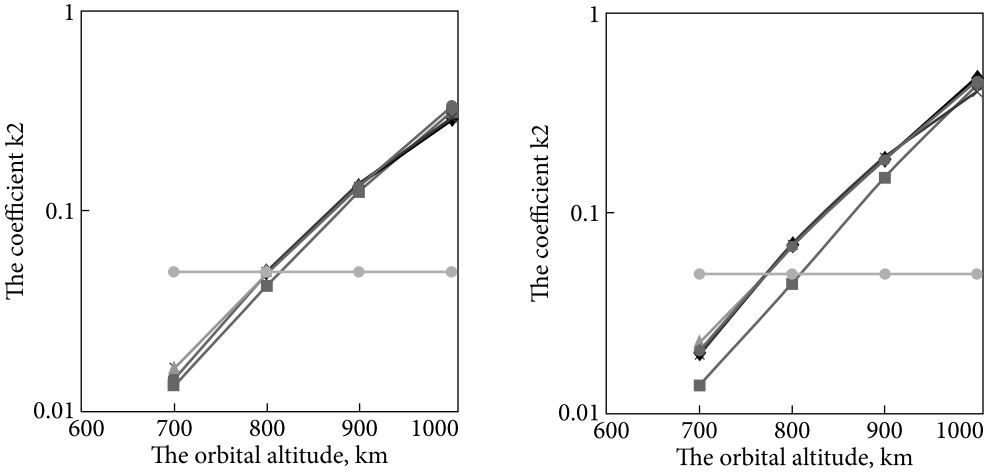

Fig. 5.54. Dependence of the specific mass of inflatable ADSs of the «Pyramide square» configuration on the altitude of the orbit, for the deorbiting of space objects of different mass. Legend of the Figures — see Fig. 5.50

Fig. 5.55. Dependence of the specific mass of inflatable ADSs of the «Cone made of tori» configuration on the altitude of the orbit, for the deorbiting of space objects of different mass. Legend of the Figures — see Fig. 5.50

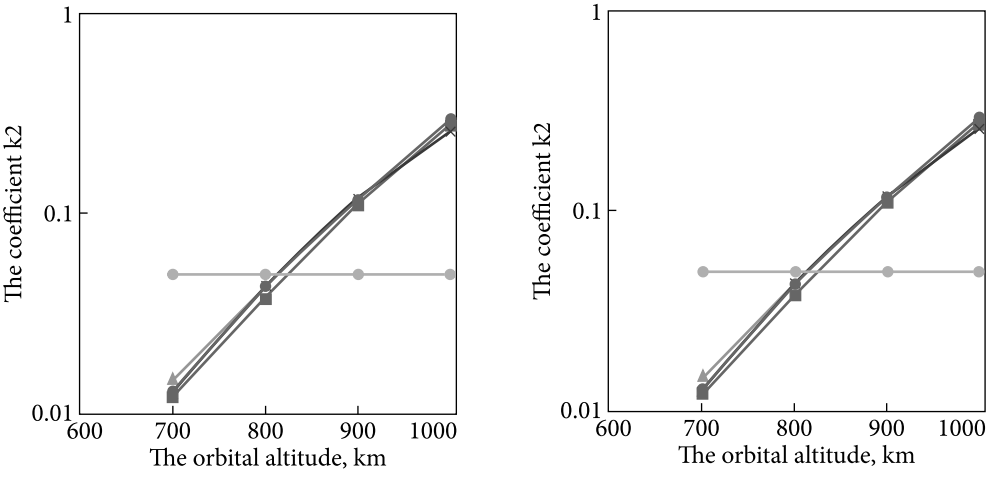

Fig. 5.56. Dependence of the specific mass of inflatable ADSs of the «Cone made of tori with spheres placed inside» configuration on the altitude of the orbit, to deorbit space objects of different mass. Legend of the Figures — see Fig. 5.50

Fig. 5.57. Dependence of the specific mass of inflatable ADSs of the «Bulk sail» configuration on the altitude of the orbit, to deorbit space objects of different mass. Legend of the Figures — see Fig. 5.50

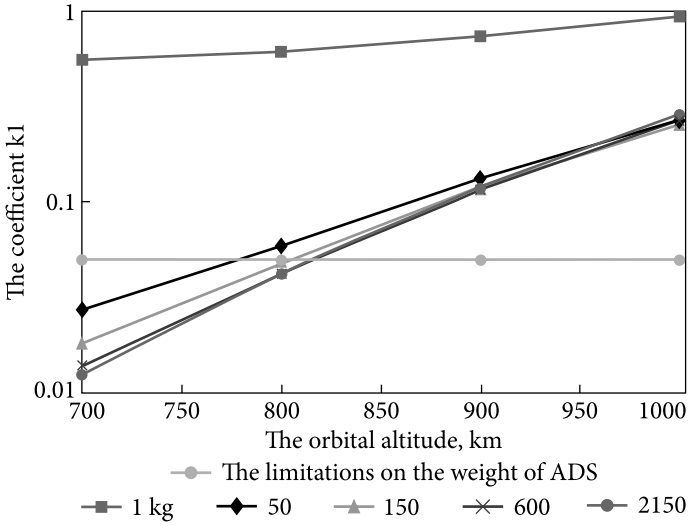

Fig. 5.58. Dependence of the specific mass of deployable ADSs on the altitude of the orbit

most widely used systems are the systems classified as deployable. Therefore, the most effective inflatable system is compared with the deployable ADS, and the limits of the effective applicability of various types of inflatable systems are determined. The initial data to evaluate the effectiveness of inflatable ADSs are the following ranges of relevant data: the mass of the space object: 1; 50; 150; 600; 2150 kg; the altitude of orbit: 700; 800; 900; 1000 km; orbital eccentricity 0.000075; the area of the median cross-section of the space object: 0.015; 0.3; 0.62; 2.16; 12 m^2; the term of orbital lifetime of the space object is 25 years; configurations of inflatable ADSs: «Sphere», «Round shield», «Two dihedral panels», «Pyramide triangle», «Pyramide square», «Cone made of tori», «Cone made of tori with spheres placed inside», «Bulk sail»; configurations of deployable ADSs: square sail.

For the specified initial data, the parameters have been selected and the specific mass (coefficient) of the inflatable ADS has been calculated, which will ensure reliable functioning during the given period of orbital existence. The results are shown in Fig. 5.50—5.57.

Analysis of the results shown in Fig. 5.41—5.48, shows that the most effective from the point of view of the minimum mass is the «Bulk Sail» ADS configuration and it is advisable to use it in orbits up to ≈850 km high.

The calculation of the specific mass of deployable ADSs to ensure reliable functioning during the given period of orbital lifetime is carried out using mathematical expressions (3.169)—(3.175). The calculation results are shown in Fig. 5.58.

From the graphs shown in Fig. 5.49, it can be seen that it is advisable to use deployable ADS at altitudes of up to 800 km. It has also been determined that systems of this class are impractical to use on small cubesat-type spacecraft, this is explained by the fact that the deployment system of the deployable ADS has certain dimensions and mass, which are about 30% of the volume of the space object and about 50% of its mass.

5.5. Determination of the limit of effective application of the unified aerodynamic deorbiting system

5.5.1. Computer modeling of the orbital motion of the upper stage of a launch vehicle with a unified aerodynamic deorbiting system

We will consider the features of the application of a unified aerodynamic element for input from the final orbit of a typical booster unit of a launch vehicle. A close analog of such a carrier is the «Cyclone-1M» launch vehicle. For the final calculations, we will use the values of the parameters of the upper stage, which are close to the values of the parameters of this rocket that have been published (Dimensions of the payload…). The size of the transition ring, on which it is planned to place the container for storage and deployment of the aerodynamic de-orbiting system, is approximately less than one meter in diameter, the height is approximately 0.2 m, and the mass is about 300 kg.

The mathematical model (2.1)—(2.69) is used for computer modeling of the orbital movement of the upper stage of a launch vehicle with a modernized aerodynamic deorbiting system, based on which a corresponding application program has been developed to calculate the time of deorbiting of various dislocations.

Table 5.1. **Time of orbital lifetime of the upper stage of the launch vehicle**

Mass of the stage, kg	Area of the median of the stage, m^2	Time of orbital existence of the upper stage of the launch vehicle, years (orbital eccentricity — 0.0001, inclination 81 degrees)						
300	2.2557	Altitude values at perigee, km	500	600	700	800	900	1000
		Time of orbital lifetime, years	2.9	13.83	55.68	189.182	545.84	1272.98

Table 5.2. **The deorbiting time of the upper stage of the launch vehicle when using the «Sphere» ADS type with a diameter of 4 m**

Mass of the stage, kg	Median area of the stage, m^2	The de-orbiting time of the upper stage of the launch vehicle when using the «Sphere» ADS type with a diameter of 4 m, (eccentricity of orbits — 0.0001, inclination 81 degrees)						
300	2.2557	Altitude values at perigee, km	500	600	700	800	900	1000
		Deorbiting time, years	0.37	1.8	7.6	26.936	78.58	189.855

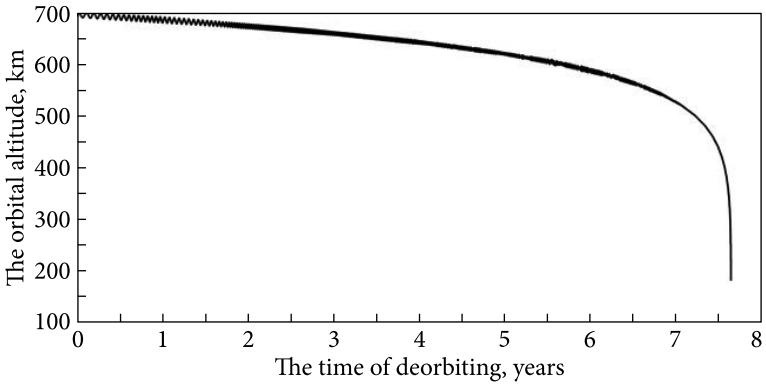

Fig. 5.59. The deorbiting time of the upper stage of the launch vehicle when using the «Sphere» ADS type with a diameter of 4 m

Table 5.3. **The deorbiting time of the upper stage of the launch vehicle when using the «Cone» ADS type with a base diameter of 4 m and a height of 2 m time**

Mass of the stage, kg	Median area of the stage, m^2	The deorbiting time of the upper stage of the launch vehicle when using the «Cone» ADS type with a diameter of 4 m and a height of 2 m (orbital eccentricity — 0.0001, inclination 81 degrees)						
300	2.2557	Altitude values at perigee, km	500	600	700	800	900	1000
		Deorbiting time, years	0.55	2.772	12.05	43.512	131.91	309.3936

The parameters and average time of orbital lifetime of the upper stage of the launch vehicle in near-circular orbits of different altitudes are given in Table 5.1.

Based on the obtained results, it can be seen that the need to reduce the period of orbital lifetime for the upper stage of the launch vehicle, taking into account the limitation of 25 years, occurs from an altitude of about 626 km in close to circular orbits. In turn, in cases where there is a possibility of creating a danger for functioning orbital groups, the need for evacuation may also be from altitudes of less than 650 km. Taking this into account, we will conduct a study of the orbital motion of the upper stage of the launch vehicle when using inflatable aerodynamic systems of various configurations. Thus, with the average values of solar activity and the NRLMSISE-00 atmosphere model (Picone, 2002), the time for the deorbit of the upper stage of a launch vehicle from an altitude of 700 km in a polar close-to-circular orbit (e = 0.0001) when using an aerodynamic inflatable system of the «Sphere» type with a diameter of 4 m is approximately 7.6 years (Fig. 5.59).

The deorbiting time of another dislocation when using the «Sphere» ADS type with a diameter of 4 m is given in Table 5.2.

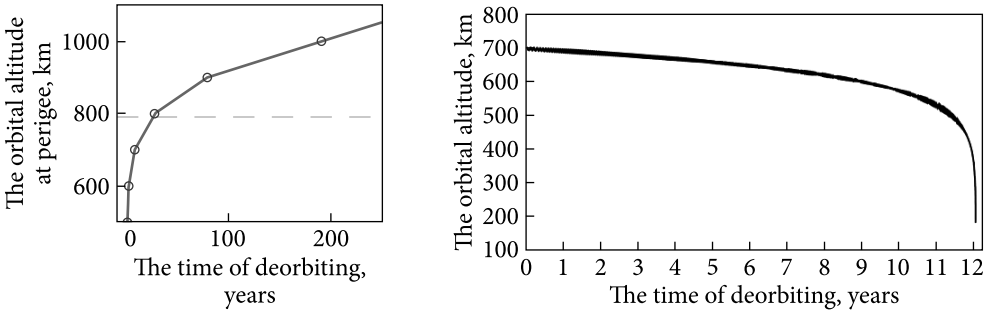

Fig. 5.60. Linear interpolation of the obtained data on the deorbiting time of the upper stage of the launch vehicle when using the «Sphere» ADS type with a diameter of 4 m

Fig. 5.61. The deorbiting time of the upper stage of the launch vehicle when using the «Cone» ADS type with a base diameter of 4 m and a height of 2 m

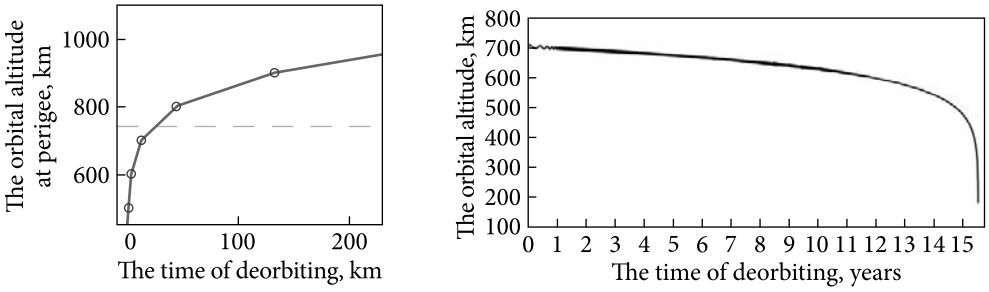

Fig. 5.62. Linear interpolation of the obtained data on the deorbiting time of the upper stage of the launch vehicle when using the «Cone» ADS type with a diameter of 4 m and a height of 2 m

Fig. 5.63. The deorbiting time of the upper stage of the launch vehicle when using the «Flat disk» ADS type with a diameter of 4 m

We will interpolate the obtained results. We apply data alignment using linear interpolation (Fig. 5.60). Based on the obtained data, it has been established that the limit of effective use of the «Sphere» ADS type with a diameter of 4 m is an altitude of 790 km.

The dashed line indicates the altitude corresponding to the deorbiting time of 25 years.

In turn, when using the «Cone» ADS type with a base diameter of 4 m and a height of 2 m, the time to deorbit the upper stage of the launch vehicle from a perigee altitude of 700 km to a perigee altitude of 180 km close to a circular orbit (eccentricity of the orbit — 0.0001) is 12.5 years (Fig. 5.61). The increase in the deorbiting time from the given orbit of the «Cone» ADS type compared to the «Sphere» ADS type is explained by the fact that the area of the full surface of the sphere is larger than the area of the cone, which is significant for calculating the average value of the area of the median in the case of non-oriented movement.

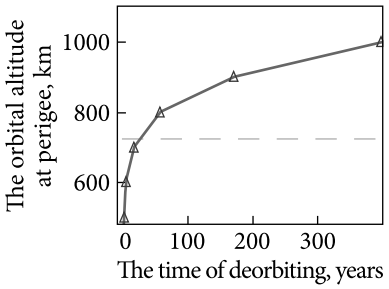

Fig. 5.64. Linear interpolation of the received data on the deorbiting time of the upper stage of the launch vehicle when using the «Flat Sail» ADS type with a diameter of 4 m

In turn, the «Cone» ADS types have a smaller volume compared to the «Sphere», which can affect the mass of the entire ADS during further development and installation on the upper stage of the launch vehicle.

The deorbiting time from close to polar orbits of another dislocation in terms of altitudes when using the «Cone» ADS type with a base diameter of 4 m and a height of 2 m is given in Table 5.3.

The interpolation of the results is shown in Fig. 5.62.

The dashed line indicates the altitude corresponding to the deorbiting time of 25 years.

Based on the obtained results, it has been determined that the limit of effective use of the «Cone» ADS type with these parameters is an altitude of 741 km for orbits with an eccentricity of 0.0001.

Based on the research, it has been established that the smallest mass of aerodynamic elements (without taking into account the deployment and storage system) has flat aerodynamic sail deorbiting systems (Anderson, 2011), (Alhorn, 2010), (Stohlman, 2014). Taking this into account, it is proposed to conduct a study of the deorbiting time of the upper stage of the launch vehicle when using a «Flat disk» ADS with a diameter of 4 m. Thus, the deorbiting time from a perigee altitude of 700 km to a perigee altitude of 180 km close to a circular orbit (eccentricity of the orbit — 0.0001) is approximately 15.5 years (Fig. 5.63).

Comparing the obtained results with the results of deorbit when using the «Sphere» (Fig. 5.54) and the «Cone» (Fig. 5.55) ADS types, it can be concluded that in the case of using the «Flat Disk» ADS type, the deorbiting time is the longest. This is explained by the fact that flat sailing elements significantly lose their effectiveness with non-oriented deorbit (Klinkrad, 2006).

Table 5.4. **The deorbiting time of the upper stage of the launch vehicle when using the «Flat Sail» ADS type with a diameter of 4 m**

Mass of the stage, kg	Median area of the stage, m^2	The de-orbiting time of the upper stage of the launch vehicle when using the «Flat Sail» ADS type with a diameter of 4 m (orbital eccentricity — 0.0001, inclination 81 degrees)						
300	2.2557	Altitude values at perigee, km	500	600	700	800	900	1000
		Deorbiting time, years	0.7	3.35	15.5	55.78	169.11	396.65

The deorbiting time from close to polar orbits of another dislocation in terms of altitudes when using the «Flat Sail» ADS type with a diameter of 4 m is given in Table 5.4.

We will perform a linear interpolation (Fig. 5.64) of the results given in Table 5.4.

The dashed line indicates the altitude corresponding to the deorbiting time of 25 years. The results of the interpolation have shown that the limit of effective use of the «Flat Disk» ADS is the altitude at the perigee of 723.6 km (which corresponds to the deorbiting time of 25 years).

5.5.2. Justification of the choice of structural type and design parameters of the modernized aerodynamic deorbiting system

Based on the analysis of the deorbiting time of the upper stage of the launch vehicle when using different types of ADS, the following conclusions can be drawn:

• The largest limits of effective application in terms of the maximum deorbiting altitude belong to the «Sphere» ADS type. This is explained by the design features of such ADSs, which provide the possibility of ensuring the maximum area of the median at different orientations to the vector of the dynamic flow of the atmosphere. In turn, ADSs of this structural type have a significantly greater mass than ADSs of other types, which is explained by the significant overall characteristics of the aerodynamic element, and the need to be equipped with a powerful inflation system and a storage system. Also, with a monolithic layout (without the use of cellular structures), the ADSs of this type are significantly exposed to the influence of outer space (OSD penetration, atomic oxygen exposure, electrostatic breakdown), which significantly reduces their reliability and performance in long-term missions.

• The lowest deorbiting altitude of the upper stage of the launch vehicle belongs to the «Flat Sail» ADS type with the same diameter as the «Sphere» ADS type. This is explained by the presence of a large difference in the area of the median of the aerodynamic element at different orientation angles to the vector of the dynamic flow of the oncoming atmosphere. Thus, with non-oriented movement, the average value of the median area is significantly smaller than that of the «Sphere» ADS type. In turn, the mass of the aerodynamic element is the smallest, which is explained by its overall characteristics. However, ADSs, which have flat aerodynamically unstable aerodynamic elements of the sail type, as a rule, require the equipment of the space object to be deorbited with a mechanical deployment system. Taking into account certain design features of such mechanical deployment systems, their impact on the total mass of the ADS can also be significant and cause additional difficulties in equipping different types of OSD.

• «Cone» ADS types are in the middle in terms of application efficiency between the «Sphere» and «Flat Sail» ADS types, when the diameter of the base is equal to the diameter of the sphere and disc. However, the ADSs of the «Cone»

type (monolithic layout) also require an inflation system and are exposed to the effects of space debris.

In turn, the use of cellular structures for the aerodynamic elements of the «Sphere» and «Cone» ADS can significantly increase the mass of the system itself, and hence reduce the limits of application for certain classes of OSD. Thus, the question arose of finding the optimal combination of design features of the above-mentioned types of ADS, which would ensure the maximum area of the median depending on the orientation angles with the minimum mass of the aerodynamic element of the ADS.

To solve this problem, a new approach to the design of the ADS has been put forward, which consists of the development of the ADS of the «Bulk Sail» type (see Chapter 4). This approach makes it possible to ensure the necessary parameters of the ADS by combining the design advantages of inflatable volumetric ADS and flat aerodynamically unstable sailing elements.

The work proposes to combine the design features of the «Sphere» and «Flat Sail» ADSs by creating a three-sided «Bulk sail» consisting of three orthogonal inflatable disks. This approach makes it possible to significantly reduce the mass of the aerodynamic element in comparison with the «Sphere» type design while ensuring the maximum area of the median depending on the different orientation angles to the vector of the dynamic flow of the oncoming atmosphere.

As a first approximation, the diameter of each orthogonal disk is proposed to be 4 m, which corresponds to the limit of effective use of the «Sphere» ADS to deorbit the upper stage of the launch vehicle from an altitude of 790—800 km at average solar activity.

5.5.3. General mass and dimensional characteristics of the modernized aerodynamic deorbiting system of the upper stage of the launch vehicle

The general mass and dimensional characteristics of the space debris object and the aerodynamic deorbiting system can be summarized in Table 5.5.

The maximum allowable mass of the ADS has been calculated taking into account the limitation — the mass of the ADS is equal to 5% of the mass of the deorbited OSD.

5.5.4. Determining the limit of effective application of the modernized aerodynamic deorbiting system of the upper stage of the launch vehicle in close to circular low Earth orbits

It is known that today one of the greatest interests of modern cosmonautics is the creation of orbital groups. Taking into account the current trends in the creation of orbital groups of satellite Internet in low Earth orbits, the launch vehicle

«Cyclone-1M» can be used precisely for these tasks. Thus, SpaceX plans to launch up to 42,000 Starlink satellites weighing up to 300 kg into low Earth orbits at altitudes ranging from 550 km to 1,500 km with inclinations of 53.2°, 70°, and 97.6°. Taking this into account, the use of a modernized ADS to deorbit the upper stages of launch vehicles of the class from a given range of orbits may be appropriate.

So, let's consider the calculations of the deorbiting time of the upper stage of the launch vehicle from close to circular low Earth orbits (e = 0.0005) of different altitudes with inclinations of 53.2, 70, and 97.6°, the results of which are shown in Table 5.6.

Based on the obtained results, it can be seen that the use of the modernized «Bulk sail» ADS type with the specified parameters meets the requirements for a deorbiting time of 25 years in the altitude range from 700 to 800 km. For an accurate determination, we will perform a linear interpolation of the obtained results (Fig. 5.65).

The dashed line indicates the altitude corresponding to the deorbiting time of 25 years

It has been determined that the limit of effective use is 771.9 km at perigee. We will consider orbits with inclinations of 70° (Table 5.7).

The interpolation of the obtained results of Table 5.7 is shown in Fig. 5.66.

The dashed line indicates the altitude corresponding to the deorbiting time of 25 years

The limit of effective application at an inclination of 70° is an altitude of 780.25 km at perigee. We will consider an inclination of 97.6° (Table 5.8).

The interpolation of the obtained results of Table 6.8 is shown in Fig. 5.67.

The dashed line indicates the altitude corresponding to the deorbiting time of 25 years.

Thus, based on the study results of the limits of the effective application of the modernized aerodynamic de-orbiting system of the «Bulk sail» type, it can be concluded that the maximum altitude of the deorbit of the upper stage of the launch

Table 5.5. **Characteristics of the spacecraft for the study**

Mass of the object of space debris (type — the upper stage of the launch vehicle), m_{KA}, kg	300
Cross-section area of objects of space debris S_M, m^2	2.2557
The maximum cross-section area of the aerodynamic element of the «Bulk sail» ADS type, S_{AE}, m^2	12.566 (for a maximum deorbiting altitude of 800 km) 4.448 (for a maximum deorbiting altitude of 700 km)
The maximum possible mass of the «Bulk sail» ADS type, m_{ACB}, kg	15

Table 5.6. **The deorbiting time of the upper stage of the launch vehicle with the modernized ADS with a diameter of the aerodynamic element of the «Bulk sail» of 4 m, a range of orbits with inclinations of 53.2°**

Mass of the stage, kg	Cross-section area of the stage, m^2	The deorbiting time of the upper stage of the launch vehicle when using a modernized ADS of the «Bulk Sail» type with a diameter of the main discs of 4 m, (eccentricity of the orbits — 0.0005, inclination of 53.2 degrees)						
300	2.2557	Altitude values at perigee, km	500	600	700	800	900	1000
		Deorbiting time, years	0.43	2.1	8.835	31.32	97.372	220.761

Table 5.7. **The deorbiting time of the upper stage of the launch vehicle with the modernized ADS with a diameter of the aerodynamic element of the «Bulk sail» of 4 m, a range of orbits with inclinations of 70°**

Mass of the stage, kg	Cross-section area of the stage, m^2	The deorbiting time of the upper stage of the launch vehicle when using the modernized ADS of the «Bulk Sail» type with a diameter of the main discs of 4 m, (eccentricity of the orbits — 0.0005, inclination of 53.2 degrees)						
300	2.2557	Altitude values at perigee, km	500	600	700	800	900	1000
		Deorbiting time, years	0.4	1.96	8.26	29.12	90.55	205.308

Table 5.8. **The deorbiting time of the upper stage of the launch vehicle with the modernized ADS with a diameter of the aerodynamic element of the «Bulk sail» of 4 m, a range of orbits with inclinations of 97.6°**

Mass of the stage, kg	Cross-section area of the stage, m^2	The deorbiting time of the upper stage of the launch vehicle when using the modernized ADS of the «Bulk Sail» type with a diameter of the main discs of 4 m, (eccentricity of orbits — 0.0005, inclination of 97.6 degrees)						
300	2.2557	Altitude values at perigee, km	500	600	700	800	900	1000
		Deorbiting time, years	0.385	1.89	7.992	28.159	87.56	198.53

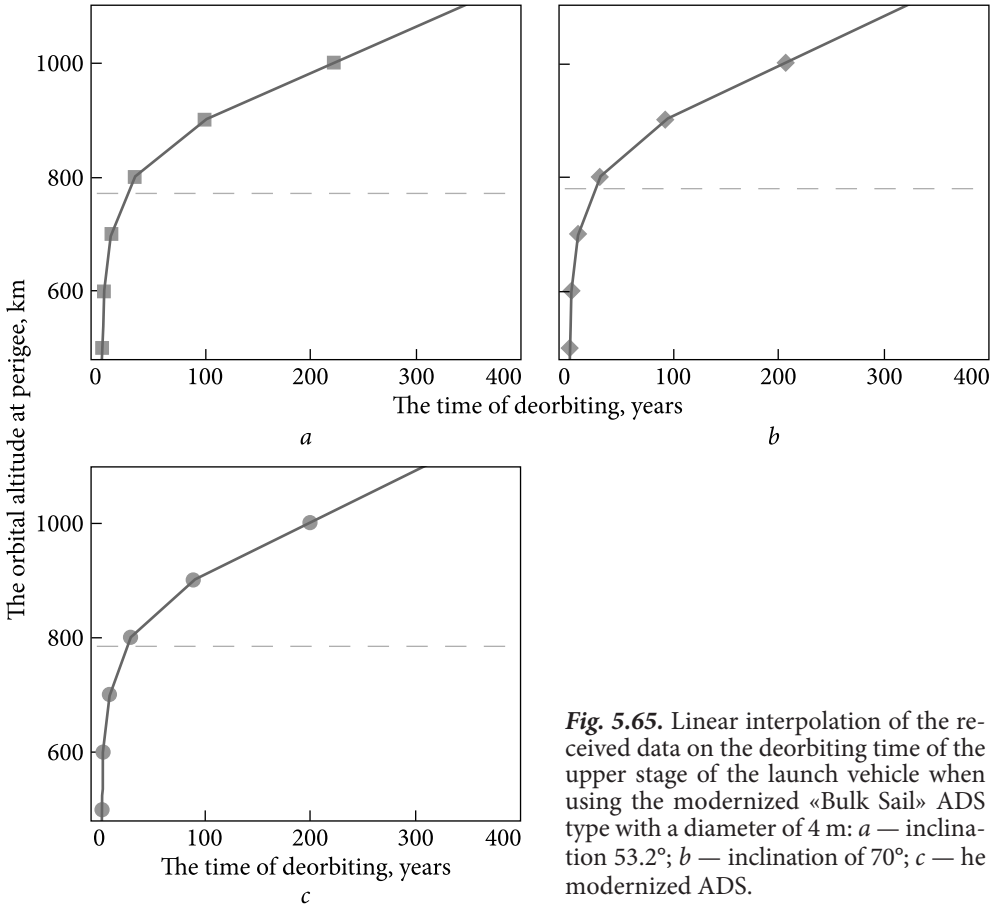

Fig. 5.65. Linear interpolation of the received data on the deorbiting time of the upper stage of the launch vehicle when using the modernized «Bulk Sail» ADS type with a diameter of 4 m: *a* — inclination 53.2°; *b* — inclination of 70°; *c* — he modernized ADS.

vehicle is 784.336 km in a close-to-circular orbit with an eccentricity of 0.0005 and an inclination 97.6°. On other close-to-circular orbits with inclinations of 53.2° and 70°, the maximum deorbiting altitudes were 771.9 and 780.25 km, respectively. The decrease in the maximum deorbiting altitude when the orbital inclination approaches the equator is explained by the uneven distribution of the gravitational potential and the average density of the atmosphere. The results of the calculations of the maximum deorbiting altitudes of the upper stage of the launch vehicle, which correspond to the time of existence in the orbit of 25 years, have been obtained with a diameter of the aerodynamic elements of the «Bulk sail» of 4 m (the average value of the cross-section area has been 12.566). In turn, when setting a maximum deorbiting altitude of 700 km on orbits with such an eccentricity, the diameter of the flat disks of the «Bulk sail» can be reduced to 2.38 m (with the average value of the cross-section area equal to 4.448).

5.5.5. Determining the limit of effective application of the modernized aerodynamic deorbiting system of the upper stage of the launch vehicle in low Earth elliptical orbits

Low-Earth elliptical orbits include orbits whose apogee altitude does not exceed 2,000 km. It should be noted that in such orbits, the effectiveness of the ADS application will be significantly lower since the influence of aerodynamic disturbances will be significantly reduced in the section of the trajectory located in the vicinity of the apogee. The probability of finding the upper stage of the launch vehicle in the orbits of such a dislocation is low. However, in the event of certain abnormal situations associated with a deviation from the given trajectory, it is quite possible for the upper stage to enter such orbits.

Thus, we will consider the deorbit of the upper stage of the launch vehicle with the help of the modernized ADS from small elliptical orbits ($0.005<e<0.05$) of different dislocations. Orbit parameters and launch time calculations for the upper stage of the launch vehicle are given in Table 5.9.

Based on the conducted analysis of the deorbiting of the upper stage of the launch vehicle when using the modernized ADS from low-elliptical orbits of various dislocations, it can be concluded that at the above-mentioned altitudes (altitudes at perigee 500—600 km and at apogee 850—1400 km) the time of orbital existence meets the requirements of the Interagency Committee by space debris (for 90% of the analyzed orbits, the lifetime is less than 25 years, for 10% it does not significantly exceed). Let's calculate the statistical indicators of the values in Table 5.9 and list them in Table 5.10.

Based on the obtained calculations of the statistical indicators of the deorbit (Table 5.10) of the upper stage of the launch vehicle with the use of the modernized aerodynamic deorbiting system, it can be concluded that in small elliptical orbits with an average eccentricity of 0.446, an apogee altitude of 1241.667 km and a perigee of 580 km, the lifetime of the upper stage is less than 25 years. In turn, the limits of effective application depend on the ellipticity of the orbit and the altitude values at perigee and apogee.

5.5.6. Calculation of the parameters of the modernized aerodynamic deorbiting system

Parameters of the orbit of the upper stage of the launch vehicle: the altitude of the orbit is 700; 800 km; eccentricity 0.0005; orbit inclination 86°; term of orbital existence ≤25 years.

For the initial data, the parameters of the modernized aerodynamic de-orbiting system have been calculated using formulas (4.3—4.15). The results of the calculations are given in the Table. 5.11—5.13. Mass of inflation system, kg: orbital altitude 700 km — 0.53; 800 km — 1.5.

Table 5.9. **The deorbiting time of the upper stage of the launch vehicle from low-elliptical orbits of various dislocations**

Altitude at apogee, km	Altitude at perigee, km	Eccentricity	Inclination, degrees	The deorbiting time of the upper stage of the launch vehicle when using the modernized ADS with a disk diameter of 4 m, years
600	950	0.021	80	13.07
600	950	0.021	60	11.88
650	950	0.02089	80	22.21
600	1100	0.03458	60	21.99
650	1050	0.0276	30	28.12
500	1300	0.0549	80	11.44
500	1300	0.0549	45	10.43
550	1300	0.0513	80	20.4
550	1300	0.0513	45	19.06
550	1300	0.0513	20	17.46
500	1400	0.061	80	13.54
500	1400	0.061	20	11.26
700	850	0.01	80	21.93
700	850	0.01	50	21.7
700	850	0.01	10	19.16
550	1400	0.057	80	24.37
550	1400	0.057	30	21.77
550	1400	0.057	45	22.76
600	1150	0.0379	80	25.34
600	1150	0.0379	60	24.71
600	1150	0.0379	30	22.97
600	1150	0.0379	10	21.51
500	1500	0.0677	80	15.89
500	1500	0.0677	60	14.96
500	1500	0.0677	20	13.09
500	1800	0.0863	80	23
500	1800	0.0863	60	21.95
500	1800	0.0863	20	19.13
750	850	0.0069	80	30.87
750	850	0.0069	10	27.23

5.5.7. Conclusions to subsection 5.5

1. The study of the orbital period of existence of the upper stage of the launch vehicle has been carried out. It has been determined that from altitudes of 626 km close to circular orbits, the orbital lifetime period of the upper stage of the launch vehicle exceeds 25 years.

2. The study of the orbital motion of the upper stage of a launch vehicle with aerodynamic deorbiting systems of the constructive type «Sphere», «Cone» and «Flat Sail» has been carried out. Based on calculations of the deorbiting time of the upper stage of the launch vehicle from close to circular polar orbits, it has been established that the limits of the maximum effective application limits in terms of deorbiting altitude belong to aerodynamic deorbiting systems of the «Sphere» type (altitude 790 km, with a sphere diameter of 4 m). In turn, flat aerodynamically unstable sailing systems of the «Flat Sail» type have the smallest mass of the aerodynamic element. However, with non-oriented movement in the «Flat disk» type aerodynamic deorbiting systems, the average value of the median area is much smaller, and hence the maximum deorbiting altitude, which satisfies the term of 25 years (altitude 723.6 km).

3. Taking into account the advantages and disadvantages of the use of the «Sphere», «Cone» and «Flat disk» aerodynamic deorbiting systems, the justifica-

Table 5.10. **Statistical indicators of the deorbiting time of the upper stage of the launch vehicle from low-elliptical orbits**

Parameter	Mathematical Expectation	Average absolute deviation	Dispersion	Average square deviation	Max. value	Min. value
Eccentricity	0.0446	0.020298	0.000581	0.0241	0.0069	0.0863
Altitude at perigee, km	580	65.33	6310.345	79.43768	750	500
Altitude at apogee, km	1241.667	235.55	82428.16	287.103	1800	850
Deorbiting time, years	19.773	4.445	29.33	5.416	30.87	10.43

Table 5.11. **Parameters of the new aerodynamic element**

Cross-section area, S_M, m	Membrane diameter, d_M, m	Surface area of inflatable masts, $S_{ПНЩ}$, m^2	Surface area of toric shells, $S_{ПТО}$, m^2	Surface area of the spherical shell, $S_{ПСФ}$, m^2	Number of spherical shells, pcs.	Membrane surface area, $S_{ПМ}$, m^2
4.448	1.7	0.32	1.04	0.01	366	2.29
12,. 66	2.8	0.91	2.94	0.03	366	6.47

tion of the choice of the structural type and design parameters of the modernized aerodynamic deorbiting system has been made. A new type of design of aerodynamic deorbiting systems has been developed «Bulk sail».

5.6. Determining the limits of application of the deorbiting system based on the transformation of a space object into an aerodynamic system

To determine the limits of the application of the proposed method, we will calculate the term of orbital existence of space objects of different masses. In the extreme case, consider the layout of the space object in the form of a square prism. Space object parameters: mass: 1; 50; 150; 600 kg; the length of the flat of the side surface: 0.1; 0.45; 0.65; 1.2 m; type of orbit — circular; altitude of orbit: 600; 700; 800; 900; 1000 km.

First, the area of the median cross-section of the space object is determined by taking into account the opened side panels according to the formula:

$$S_M = \frac{S_{БПКО} + S_{ПКО}}{4}, \tag{5.5}$$

where $S_{БПКО}$ is the area of the side panels of the space object; $S_{ПКО}$ is the surface area of the space object.

Table 5.12. **Mass of the aerodynamic element**

Material type	Material thickness, *m*	Material density, kg/m^3	Mass of AE, kg, for orbital altitudes of	
			700 km	800 km
Kapton	$7.5327 \cdot 10^{-5}$	1420	1.61	4.56
Teflon	$1.96054 \cdot 10^{-5}$	2150	0.636	1.8
Mylar	$6.14072 \cdot 10^{-5}$	1390	1.29	3.64
Kunar	$2.63174 \cdot 10^{-5}$	1770	0.730	1.98
Zaylon	$2.7745 \cdot 10^{-5}$	1560	0.653	1.84

Table 5.13. **Mass of the storage system**

Material type	Material thickness, *m*	Material density, kg/m^3	Mass of SS, kg
Aluminum alloy AMg6	$1 \cdot 10^{-3}$	2760	2.4
Titanium alloy	$3 \cdot 10^{-4}$	4500	1.2366
Cellular three-layer structure, A5T-2,5-40P	$1 \cdot 10^{-2}$	68	0.623

Next, the term of the orbital lifetime of the space object is determined according to the relations (Klinkrad, 2006):

$$t_L = \frac{2}{3\rho_{pe} B \sqrt{\mu}} \cdot X(e,z), \tag{5.6}$$

$$X(e,z) = \frac{3 \cdot e \cdot \exp(z)}{4I_0(z) + 8eI_1(z)} \left\{ 1 + \frac{7e}{6} + \frac{5e^2}{16} + \frac{1}{2z} \cdot \left(1 + \frac{11e}{12} + \frac{3}{4z} + \frac{3}{4z^2} \right) + O\left(e^3, \frac{1}{4z} \right) \right\} \tag{5.7}$$

where B is the ballistic parameter of the space object, $B = C_X S_M / m_{KA}$; ρ_{pe} — the atmosphere density at the orbit perigee; $I_O(z)$ — Bessel function, order k = 0 and 1, and argument; e — orbital eccentricity;μ — gravity table; C_X — coefficient of aerodynamic resistance, we accept; C_M— area of the median cross-section; m_{KA}— mass of the spacecraft; a — major semi-axis of the orbit; Hρ, ρ_{pe}— altitude of the dense layers of the atmosphere at the orbit perigee.

The results of calculating the term of the orbital existence of the space object, taking into account the opened side panels, are shown in Fig. 5.66.

The principle of transformation of the structures of the space object, which is being deorbited, has been used on the Sich-2-1 spacecraft.

Parameters of the «Sich-2-1» spacecraft: mass of the spacecraft is 180 kg; the altitude of the orbit is 600 km; slope of 60°; estimated ballistic lifetime of 75 years.

To deorbit the «Sich 2-1» spacecraft using the proposed method, it is proposed to use turning mechanisms with a spring drive developed by the Yuzhnoye State Design Office.

Characteristics of turning mechanisms: the maximum turning angle is 180°; the mass is 0.34 kg.

We will analyze the version of the transformation of the «Sich-2-1» spacecraft structure, where the panels of the protective screen are folded back to increase the area of the median section. To fold the panels of protective screens, it is necessary to use 4 turning mechanisms, the mass of which will be 1.36 kg. The area of the median cross-section as a result of the rotation of the panels will be 8.7 m^2, which will allow, in turn, to reduce the period of ballistic existence to 33.1 years, in contrast to the calculated 75 years. Thus, to fulfill the requirement to reduce the lifetime of the spacecraft to the directive period of five years, appropriate design changes are required.

5.7. Selection of parameters of the aerodynamic deorbiting system of modular large space objects

The Mir orbital station (Fig. 5.67) has been chosen as a typical modular large-scale space object, which operated in a circular orbit 379 km high and consisted of 7 cylindrical modules, the characteristics of which are given in Table 5.14.

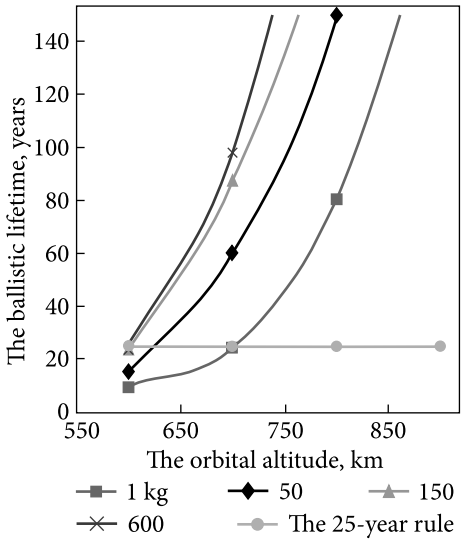

Fig. 5.67. «Mir» Orbital Station

Fig. 5.66. Dependence of the term of the orbital existence of a space object, taking into account the opened side panels, on the orbital altitude

The analysis of design solutions for the Mir station (Nock, 2010) has shown the possibility of using an ADS for its de-orbiting at an altitude of ≈250—380 km with a mass of 140 tons. The ADS is spherical with a diameter of 182 m, which is made of polymer material kapton with a thickness of 9 microns. Technical characteristics of the material kapton (DuPont™ Kapton): maximum working temperature +300 °C, density 1.42 kg/m^3, modulus of elasticity 231 MPa. The mass of such an ADS would be ≈893 kg. The use of such a system for the deorbiting of the MLSO is practically impossible since its manufacture and deployment in outer space is problematic because its dimensions and mass are much larger than the acceptable sizes of known thin-walled film space objects manufactured and used in space (for example, Echo-1 and Echo-2 satellites (Jenkins, 2001)), the launch and deployment of which demonstrated the successful use of inflatable thin-film devices in space.

The effect of SF on the shell at an altitude of 379 km is very small, so it can be neglected. However, the size of the spherical shell of the ADS proposed in (Nock, 2010) is unreasonable, because it is known that at the time of the launch of the Echo spacecraft (Jenkins, 2001), the largest shell that could be manufactured under ground conditions, put into orbit and successfully deployed, was 36 m in diameter. More than half a century has passed since the launch of the «Echo» spacecraft, all this time the technologies for the manufacture of space inflatable systems have been improved and, as a result of the development of the technology for the manufacture of space inflatable systems, the creation of an airship 90 m long and 30 m wide, which will function at an altitude of ≈20 km (Liao, 2009).

Table 5.14. **Characteristics of the modules of the Mir orbital station**

Module name	Mass, *t*	Module cross-section area, m^2	Module name	Mass, *t*	The area of the median cross-section of the module, m^2
Base unit	20.90	49.56	«Spectrum» module	19.34	53.10
«Quantum» module	11.05	25.67	Docking compartment	3.90	10.02
«Quantum-2» module	19.50	49.80	«Nature» module	19.34	43.80
«Crystal» module	19.50	48.09			

Table 5.15. **The ADS parameters of each module of the Mir orbital station (Palii, 2014)**

Module name	Diameter of the ADS shell d_i, *m*	Shell thickness, 10^{-6} *m*	Internal pressure of the ADS, Pa	Shell mass, kg	Gas mass required to inflate the ADS,	Mass of the ADS, m_i, kg
Base unit	34	6	0.08	126.47	0.176	126.65
«Quantum» module	25	6	0.08	66.90	0.068	66.98
«Quantum-2» module	33	6	0.08	118.01	0.158	118,17
«Crystal» module	33	6	0.08	118.01	0.158	118.17
«Spectrum» module	33	6	0.08	116.59	0.155	116.75
Docking compartment	15	6	0.08	24.10	0.015	24.12
«Nature» module	33	6	0.08	117.30	0.157	117.36

Currently, the maximum diameter of the shell d_{max} is considered to be 90 m (Liao, 2009), and the minimum mass of the ADS for the de-orbiting of the MLSO from the LEO is 893 kg (Nock, 2010). In this regard, to check the technical feasibility of using the ADS, we will determine the diameter of the ADS shell of each module d_i, if $d_i \le d_{max}$, we can conclude the possibility of using this ADS. To evaluate the effectiveness of using the method proposed in (Patent of Ukraine for

the invention No. 107880, 2015), let's calculate the mass of the ADS of all modules Σm_i, if , we can draw a conclusion about the effectiveness of using this ADS from the point of view of the minimum spent mass.

The parameter d_i can be obtained based on the median cross-sectional area of the shell of each module Σm_i using geometric ratios.

To determine Σm_i, it is necessary to calculate the ADS parameters for each module: shell thickness; internal shell pressure; a volume of the shell in the deployed state; volume of the gas required to inflate the shell.

To calculate the ADS parameters of each module, the method of selecting the ADS parameters developed by the author has been used. Input data for calculation: characteristics of the modules of the «Mir» station; altitude of the orbit of the «Mir» station — 379 km; deorbiting time t_L = 3 days; shell material — polyimide PM-A, density 1420 kg/m^3; gas to inflate the shell — air; mass of the ADS is calculated based on the amount of polymer substance and the gas to inflate the shell.

To analyze the possibility of using the proposed method based on the initial data of Table 5.15, with the help of the method to select the ADS parameters (Skorik, 2013), (Paliy, 2015), the parameters of the ADS have been calculated for each module of the MLSO. Table 5.15 shows the results of the calculation of the ADS parameters for the modules of the Mir station.

For the calculated mass of the ADS for each module listed in Table 5.15, the parameter Σm_i=688.2 kg is determined. Thus, for the output data of the corresponding Mir orbital station, the maximum diameter of the ADS shell of the corresponding module is which is less than , therefore, it is possible to use the proposed form of the ADS to de-orbit MLSO from the LEO. The mass of the ADS of all modules Σm_i=688.2 kg is smaller than m_{min}, so the use of the ADS in this case is effective. In addition, the proposed approach gives an additional advantage in saving mass for the considered case, which amounted to 204.8 kg.

CHAPTER 6

SPECIALIZED INFLATABLE AERODYNAMIC SYSTEMS

6.1. Inflatable modules of the space industrial platform

Mankind is facing the need to solve the problems of global warming and shortage of Earth's resources. One of the constituent ways of solving these problems is the step-by-step industrialization of space, which results in the transfer of high-energy production to space. Space industrial platforms are the technological basis for the transfer of certain types of industrial production (Alpatov, 2013b). Of particular interest is the production of unique materials and substances with characteristics that can be achieved in weightlessness and vacuum conditions. In some cases, exposure to harsh radioactive radiation may also be necessary. Thus, a whole direction in the field of space technology development has emerged, related to the design of specialized space platforms, oriented to ensure the production of unique materials and products requiring open space conditions.

At the initial stage of development of a new spacecraft, developers usually have a limited set of initial data. For example, when developing a space industrial platform (SIP), the following initial data are available: the composition of the main and auxiliary modules; parameters of technological processes implemented on the platform (vacuum and microgravity levels, power capacity of equipment, etc.); composition of technological equipment for production on the industrial platform (Palii, 2021), (Palii, 2022a). The development of design methods requires the formation of a certain set of criteria for the classification of technological processes in outer space, corresponding to the classifier for the need to classify these processes when the latter are implemented on a space-industrial platform (Palii, 2022a). The analysis of technological processes implemented in outer space makes it possible to form a set of their parameters that must be provided on the space industrial platform. The use

of the classifier makes it possible to quickly analyze the functional diagrams of various technological processes that can be implemented in near space to formulate requirements for the methodological development of appropriate design technologies for both basic industrial platforms and specialized ones.

In general, the industrial platform is equipped with main and auxiliary modules (Palii, 2023a). The main modules include: a hull with a supporting structure, a control module, an energy complex, a thermal management module, an orientation and stabilization module, an onboard transport system, an industrial module, receiving and shipping docks, and a finished product storage module. The industrial module houses the basic equipment for the implementation of technological processes. The set of auxiliary modules is determined by the type of production. In general, the auxiliary modules are characterized by the following list: raw material storage module, raw material primary processing module, raw material supply module to process equipment, module for storing and supplying auxiliary substances (water, gas, solution) to process equipment, auxiliary substance preparation module, heat removal module from equipment to the platform's thermal control system, gas removal module from equipment to the platform's ventilation and gas removal system.

The industrial platform has many features, namely (Palii, 2023b): significant weight and dimensions of the structure; modular construction principle; maintainability; use of standardized structural elements, such as unified electrical connectors, attachment points and fixing elements for equipment, etc; availability of specialized docks that include systems for guidance, docking, and fixing the service spacecraft; availability of the necessary interface for servicing by service space systems.

The design scheme of the SIP significantly depends on the requirements of the technological processes implemented on it: The formation of the SIP design depends largely on several criteria arising from the functional features of the platform. These are the following criteria (Palii, 2023b): modularity of the structure, type of shell frame, method of shell formation, type of sealing, availability, and needs of a special gas environment, availability of special process compartments, type of orientation and stabilization, type of power system, type of thermal control, availability of microclimate, type of preliminary preparation of raw materials and its components. Using these criteria, a classification of the functional features of the SIP shell is proposed, the structure of which is shown in Fig. 6.1 (Palii, 2023b).

The monoblock configuration of SIP is characterized by the placement of all components of the platform to ensure the technological process under one shell. Its design is determined by a certain set of parameters: weight $m_{об}$, dimensional characteristics (length $l_{об}$, width (diameter) $d_{об}$, and height $h_{об}$), thickness of the shell material $\delta_{об}$, and material density $\rho_{об}$. Unlike a monoblock configuration, a modular configuration consists of a set of modules, so the mass of the platform will be determined as $\sum_{i=1}^{n} m_{об}$, where i — platform module number, n — number of platform modules.

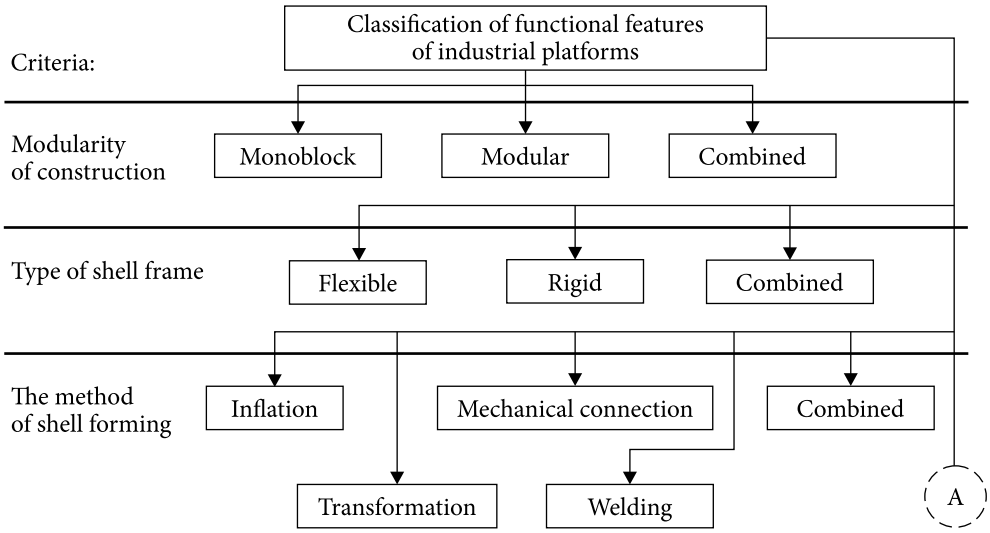

Fig. 6.1. Structure of classification of functional features of SIP (see also p. 138)

The flexible frame is made of inflatable polymer or composite material and has the following characteristics: weight $m_{ГК}$, length $l_{ГК}$, diameter $d_{ГК}$, thickness $\delta_{ГК}$, material density $\rho_{ГК}$, weight of the inflation system $m_{СН}^{ГК}$, internal pressure $p_{вн}^{ГК}$, and gas mass for inflation $m_{Г}^{ГК}$. The rigid frame has the following characteristics: weight $m_{ЖК}$, length $l_{ЖК}$, cross-section area $S_{П}^{ЖК}$, thickness $\delta_{ЖК}$, and material density $\rho_{ЖК}$.

The formation of inflatable SIPs is carried out by inflating and the set of their parameters is expanded by the parameters of the supercharging system, namely: the mass of the system for storing and supplying gas to the shell $m_{ПГ}$, weight of the pressure control system $m_{СКТ}$, internal pressure of the inflatable platform $p_{вн}^{НП}$. The transformation of the SIP is ensured by the use of specialized units with the following characteristics: energy power $P_{П}^{АТ}$, weight $m_{АТ}$, and volume $V_{АТ}$. Assembled SIPs are characterized by the use of additional elements of connection and fixation of modules (EC), which have the following characteristics: number of elements $n_{Е3}$, element weight $m_{Е3}$, surface area of the element $S_{П}^{Е3}$, material thickness $\delta_{Е3}$, and material density $\rho_{Е3}$.

When using hermetic SIP modules, sealing is ensured with the help of specialized assembly equipment. The parameters of the supercharging system of sealed systems are similar to those of inflatable systems. In this case, the module body is made of high-strength materials that can withstand the specified internal pressure.

If the technological process requires the use of additional gases, the SIP is equipped with auxiliary equipment with appropriate systems for storing and supplying these gases to the technological equipment. This equipment has the following characteristics: gas type, and gas parameters (weight $m_{Г}^{ДО}$, gas pressure $P_{вн}^{ДО}$).

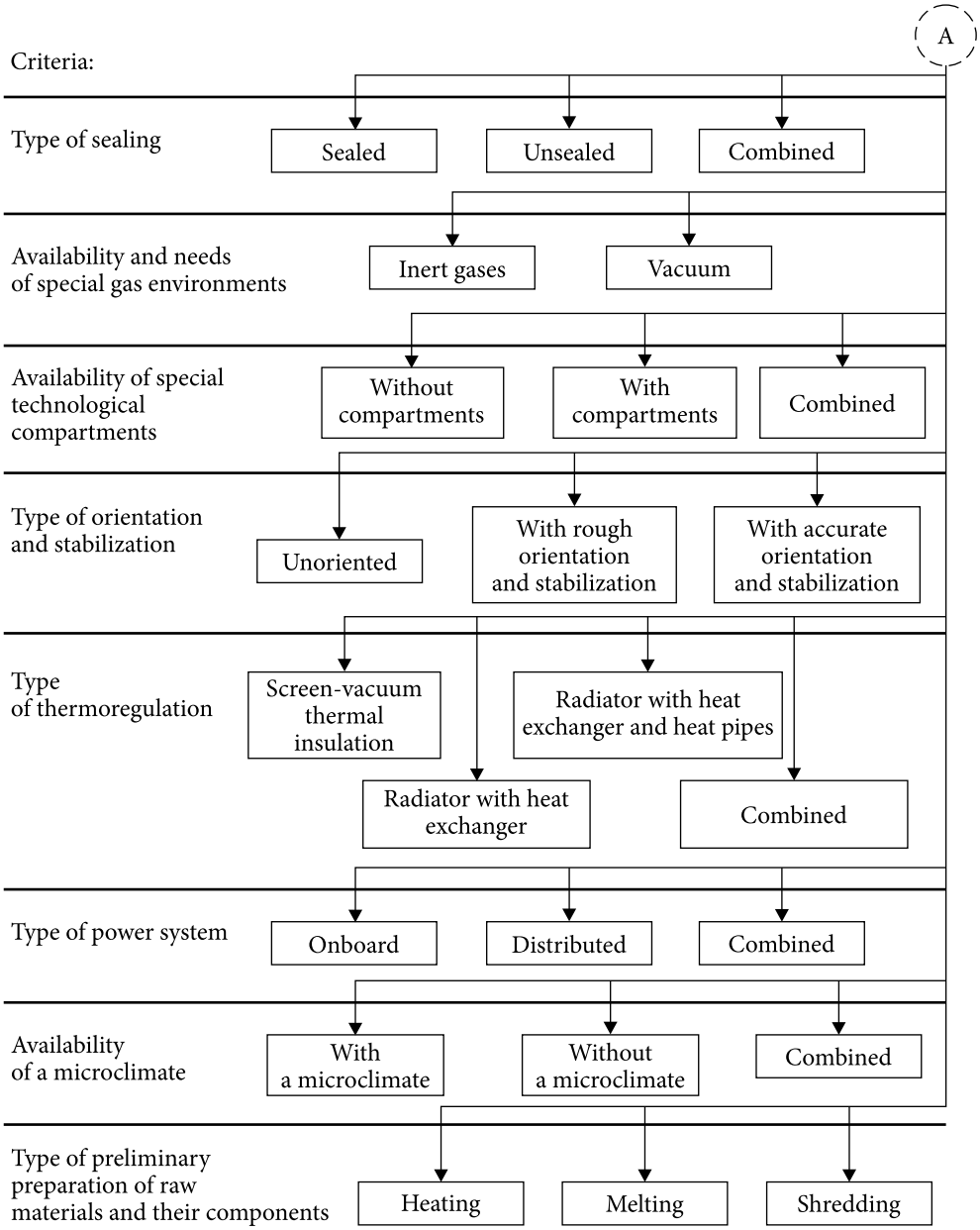

Fig. 6.1. The end

When forming platform modules with compartments, they will have additional characteristics (the shape of the compartment, which depends on the shape of the module, the cross-sectional area of the compartment $S_{П}^{B}$, compartment length l_B, total surface area of the transition zone of the compartment $S_{ПВ}^{B}$, char-

acteristics of auxiliary equipment: dimensions of the frame for mounting valves (length l_p, width (diameter) d_p, height h_p), frame weight m_p, material thickness δ_p, material density ρ_p, dimensions of the valve (length l_{3A}, width (diameter) d_{3A}, height h_{3A}), weight of the valve m_{3A}, material thickness δ_{3A}, material density ρ_{3A}.

When forming modules of a platform with thermal management, they will have additional devices with appropriate design characteristics. Thus, when using a passive thermal management system, the module is equipped with screen-vacuum thermal insulation with the following characteristics: thermal insulation weight m_{TI}, surface area S_{Π}^{TI}, material thickness δ_{TI}, material density ρ_{TI}, material absorption coefficient and α_{TI}, material emissivity coefficient ε_{TI}. When using an active thermal control system with a radiator and a heat exchanger, the set of module parameters is expanded by the following parameters: weight of the thermal control system m_{3TP}, radiator weight m_P^{3TP}, heat exchanger weight m_T^{3TP}, thermal conductivity coefficient of the radiator material k_p^{3TP} and the heat exchanger k_{TO}^{3TP}, dimensions of the radiator (length l_p^{3TP}, width (diameter) d_p^{3TP}, height h_p^{3TP}) and heat exchanger (length l_{TO}^{3TP}, width (diameter) d_{TO}^{3TP}, height h_{TO}^{3TP}), thickness of the radiator material δ_{TO}^{3TP} and heat exchanger δ_P^{3TP}, density of the radiator material ρ_p^{3TP} and heat exchanger ρ_{TO}^{3TP}. When using a thermal control system with heat pipes, in addition to the radiator and heat exchanger, pipes filled with refrigerant are used. Thus, the set of SIP parameters is expanded by the following list: mass of heat pipes m_{TT}^{3TP}, refrigerant mass m_X^{3TP}, number of heat pipes n_{TT}^{3TP}, dimensional characteristics of pipes: (length l_{TT}^{3TP} and diameter d_{TT}^{3TP}), internal pressure in the pipes $p_{вн}^{TT}$, refrigerant flow rate v_X^{TT}, weight of equipment for refrigerant circulation $m_{OЦX}$, the power of this equipment $P_{OЦX}$.

An industrial platform with a microclimate is equipped with special equipment to ensure it. This includes, in addition to sealing equipment, ventilation, and gas removal systems. In this case, the set of SIP parameters is expanded by an additional set: the weight of the ventilation and gas removal system $m_{ВГВ}$, internal temperature of the module $T_{вн}$, and humidity $\varphi_{вн}$.

The implementation of energy-intensive technological processes requires significant reserves of electricity on board the spacecraft. In general, the platform is equipped with an onboard power system that ensures the functioning of the main onboard systems (control, orientation and stabilization, thermal control, propulsion systems, etc.). When the capacity of the onboard power system becomes insufficient, the platform is equipped with a power system. A distributed system can be used, which contains a grouping of power spacecraft moving in higher orbits that are compatible with the spacecraft. The main function of energy spacecraft is to accumulate energy on board, convert it into an ultra-high frequency energy beam, and radiate it using an onboard antenna device in the direction of the spacecraft receiver. At the receiver spacecraft, the microwave energy beam is converted into electrical energy, accumulated and, if necessary, further converted back into a microwave beam and transmitted to the SIP. The antenna device, which is located on the industrial platform, receives the microwave beam,

and then, with the help of auxiliary microwave systems, the energy is converted into electrical energy and the onboard electrical energy storage devices (batteries, supercapacitors, etc.) are charged. The capacity of electric energy storage devices is determined by the capacity of the energy-intensive technological process. The set of parameters of the SIP is expanded by the following list: the area of the on-board solar panels of the SIP $S_{СБ}^{КІП}$, power of onboard solar panels $P_{СБ}^{КІП}$, capacity of on-board electric power storage devices of the SIP $Q_{ПЗЕ}^{КІП}$, the aperture area of the on-board antenna device of the SIP $A_r^{КІП}$, weight of the device for converting microwave energy into electricity $m_{НЕ}^{КІП}$, aperture area of the power spacecraft transmitter (SCT) $A_t^{ЕКА}$, area of onboard solar panels of the SCT $S_{СБ}^{ЕКА}$, power of onboard solar panels of the SCT $P_{СБ}^{ЕКА}$, mass of the device for converting electrical energy into microwave energy of the SCT $m_{ЕН}^{ЕКА}$, capacity of onboard electric power storage devices of the SIP $Q_{ПЗЕ}^{ЕК}$, aperture area of the power spacecraft-receiver (SCR) $A_r^{ПКА}$, area of the onboard solar panels of the SCR $S_{СБ}^{ПКА}$, capacity of the onboard solar panels of the SCR $P_{СБ}^{ПКА}$, weight of the device for converting microwave energy into electrical energy of the SCR $m_{НЕ}^{ПКА}$, mass of the device for converting electrical energy into microwave energy of the SCR $m_{ЕН}^{ПКА}$, capacity of on-board electric power storage devices of the SCR $Q_{ПЗЕ}^{ПКА}$.

In the implementation of technological processes that require preliminary processing of raw materials (heating, melting, grinding), the SIP is equipped with appropriate equipment that has the following characteristics: weight of the heating equipment $m_{ОН}$, for melting $m_{ОР}$ and for shredding raw materials $m_{ОП}$, power of raw material pretreatment equipment $P_{ОПО}$.

When designing space systems, the following areas of optimization of the design characteristics of the mass and dimensions of the spacecraft and its modules are distinguished (Palii, 2023b): reducing the weight of the platform and its modules; reducing the size of the platform by optimizing its layout.

It is also possible to combine the above areas when optimizing the SIP parameters.

When choosing the first direction, it is necessary to decompose the industrial platform to the level of structural elements of its modules. Each vector of parameters of the *i*-th module of the platform for the implementation of the *j*-th technological process (TP) on it can be represented as (Palii, 2023b):

$$\begin{aligned} P_1^1 &= \left[h_1, h_2, h_3, \ldots h_n\right], \\ P_2^1 &= \left[h_1, h_2, h_3, \ldots h_k\right], \\ P_1^2 &= \left[h_1, h_2, h_3, \ldots h_l\right], \\ P_j^i &= \left[h_1, h_2, h_3, \ldots h_j\right], \end{aligned} \tag{6.1}$$

where P_j^i — is a vector of parameters of the i-th platform module depending on the j-th type of TP; n,k,l,j — is the number of parameters of the i-th platform module depending on the j-th type of TP.

In turn, the weight of the SIP depends on the parameters of each module and the technological process. This dependence can be described as follows (Palii, 2023b):

$$M_{KIII} = \begin{vmatrix} m_1^1\left(P_1^1\right), m_2^1\left(P_2^1\right) \ldots m_j^1\left(P_j^1\right) \\ m_1^2\left(P_1^2\right), m_2^2\left(P_2^2\right) \ldots m_j^2\left(P_j^2\right) \\ \ldots\ldots\ldots\ldots\ldots\ldots\ldots\ldots\ldots\ldots \\ m_1^i\left(P_1^i\right), m_2^i\left(P_2^i\right) \ldots m_j^i\left(P_j^i\right) \end{vmatrix}, \tag{6.2}$$

where M_{KIII} — is the vector-matrix of the dependence of the masses of the i-th modules on the vector of parameters of the j-th TP; $m_j^i\left(P_j^i\right)$ — is the dependence of the mass of the i-th platform module on the vector of parameters of the j-th TP.

The mass of the SIP at different module configurations, depending on the j-th TP, can be represented as (Palii, 2023b):

$$\begin{aligned} M_1 &= \sum_{i=1}^{n} m_1^i, \\ M_2 &= \sum_{i=1}^{n} m_2^i, \\ M_3 &= \sum_{i=1}^{n} m_3^i, \\ &\vdots \\ M_j &= \sum_{i=1}^{n} m_j^i, \end{aligned} \tag{6.3}$$

where M_j — is the mass of the SIP configuration for the realization of the j-th TP.

If the main parameter of the SIP is its total mass, then the problem of optimizing the mass of the SIP will be in the form (Palii, 2023b):

$$\begin{aligned} M_1^{opt} &= arg\,min\left[M_1 \right], \\ M_2^{opt} &= arg\,min\left[M_2 \right], \\ M_3^{opt} &= arg\,min\left[M_3 \right], \\ &\vdots \\ M_j^{opt} &= arg\,min\left[M_j \right], \end{aligned} \tag{6.4}$$

where M_j^{opt} — is the optimal weight of the SIP configuration for the realization of the j-th TP.

The stages of optimization are as follows: analysis of technological processes implemented on the SIP; formation of clusters of design parameters that need to be optimized; construction of a matrix of correspondence of parameters of SIP modules to the parameters of technological processes; determination of optimal vectors of parameters of platform modules (Palii, 2023b).

6.1.2. State of the art of inflatable space systems development

Today, due to the high level of development of composite materials, space inflatable systems have become quite popular in the development of complex orbital modules, modules on the ISS, and spacecraft deorbitalization systems at the end of active service lifetime. One example of the development of such orbital modules is the inflatable space stations designed by NASA (Pedley, 2001), (Atwell, 2000), (Kennedy, 2016). Thus, from 1992 to 2000. NASA proposes to create a residential inflatable module TransHab in orbit (Fig. 6.2).

The design feature of the TransHab module was the integration of a rigid frame and an inflatable shell into a single structure. The base of the module consisted of a soft fabric transformable shell with built-in micrometeorite and radiation protection. The layout diagram of the multilayer material of the Transhab inflatable manned module (Fig. 6.3) (Pedley, 2001) shows that the inflatable shell consists of multiple layers that perform different functions, specifically an outer coating for protection against atomic oxygen, deployment system elements, multilayer insulation, a protective layer against FCM effects, a containment layer, duplicate shell layers, and an inner thin layer. The multilayer material for isolation (MLI) consists of 42 layers, the characteristics of which are summarized in Table 6.1 (Pedley, 2001). From the outside to the inside of the cabin, this package contained 20 layers of MLI consisting of 18 inner silver metalized Mylar® layers placed inside two outer gold metalized Mylar® layers, 9 layers of NextelTM ceramic fabric, 7 layers of Kevlar® polyaramid liquid crystal polymer (LCP) fabric, 2 layers of Vectran® aromatic polyester LCP film, 3 layers of Cadpak® HD200 duplicate layers, and 1 layer of Nomex® fabric, 27 polyaramid LCP.

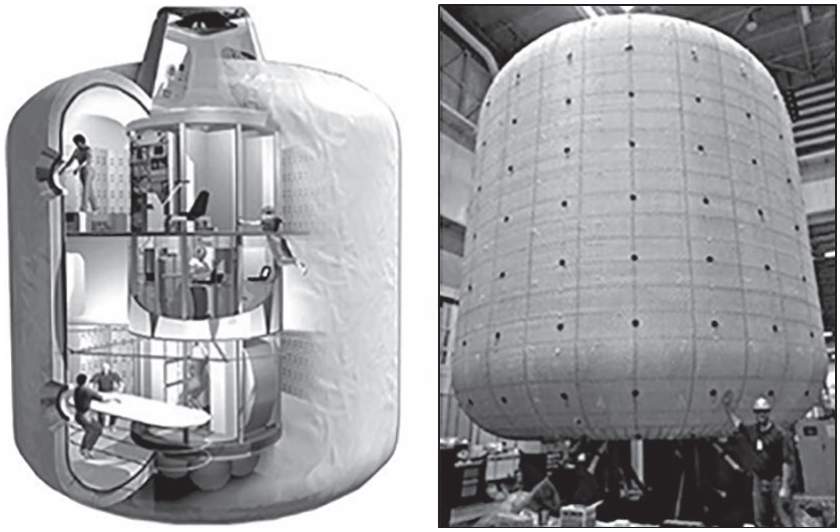

Fig. 6.2. Design of the proposed TransHab deployable housing module

Table 6.1. **Characteristics of multilayer material (Pedley, 2001)**

Material	Number of layers	Function
Mylar® with metallized gold coating	2	Multilayer thermal insulation
Mylar® with metallized silver coating	18	" " " " " "
Ceramic fabric Nextel	9	Inflatable MMOD barrier
Fabric Kevlar®	7	" " " " " "
Film Vectran®	2	Inflatable restraint layer
Fabric Cadpak® HD200	3	Inflatable bladder
Fabric Nomex®	1	Inflatable inner scuff liner

A flexible multi-impact (FMI) FCM protection shield consists of three or more stacked layers of ballistic fabrics such as Nextel™ and Kevlar®. Each «stack» of materials may contain multiple layers of fabric. Nextel™ is typically used for the outer «bumper» layers of the FMI. Ideally, these layers serve to consistently break down the SD particles into smaller particles. Kevlar is typically used as the final layer of the FMI to trap particles and remaining intact fragments.

The FSD shield was hypersonic impact tested by irradiating the material with small particles at velocities comparable to space flight velocities to simulate the effects of cosmic radiation and small pieces of space debris.

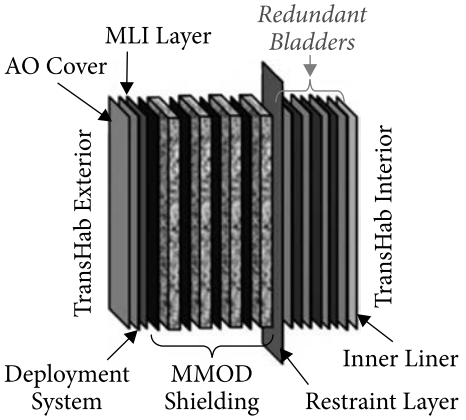

Fig. 6.3. Multilayer material structure of the Transhab inflatable manned module. MMOD — micrometeoroid and orbital debris

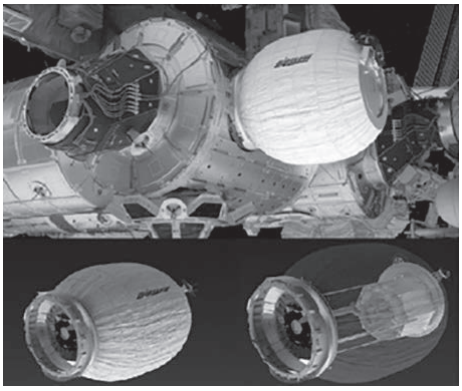

Fig. 6.4. BEAM Inflatable Space Habitat Deployable Module on the ISS

A comparison of the original unirradiated material and Kevlar® material irradiated with 700 rad 1 GeV protons showed significantly more perforation damage in the second (middle) and third (last) layers of the irradiated material compared to the original material, more detailed test data are given in (Atwell, 2000).

In the course of the NASA project, a large amount of design research and experimental work was carried out, including the creation of full-size mockups of the module shell, strength, and thermal-vacuum tests, as well as tests for resistance to micrometeorite breakdown.

Since 2000, the work was continued by Bigelow Aerospace, which, based on the developments of the TransHab project, began development work on the creation of experimental prototypes and full-size space modules for various purposes. Thus, on April, 16, 2016, NASA together with Bigelow Aerospace transported a deployable inflatable living module BEAM (Fig. 6.4) in a SpaceX Dragon container to the ISS (Saletta, 2016), (Mathewson, 2017).

After a year-long test of the deployed module on the ISS, the BEAM module has shown good results, namely:

• sensors installed inside BEAM showed that the soft inflatable structure can withstand collisions with space debris and micrometeorites, as expected.

• after real-time measurements of radiation levels inside the BEAM habitat by two active radiation monitors, the data showed that galactic space radiation doses inside the BEAM were comparable to galactic space radiation doses compared to other areas of the space station.

The successful test of the BEAM habitation module on the ISS set the vector for the development of inflatable habitable orbital modules.

An equally famous example of space inflatable habitable modules development is the joint project of NASA and the US National Space Grant Foundation (NSGF) to develop X-Hab type ground-based inflatable habitable modules for

Fig. 6.5. The architecture of the X-Hab inflatable ground module

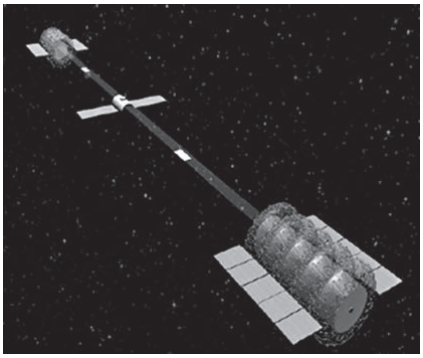

Fig. 6.6. External view of the symmetrical version of the orbital station

missions to the Moon and Mars. One of the most important, in terms of functionality, elements of X-Hab modules is the main support frame (Di Capua, 2011). The framework consists of tubular beams connected by manifolds (Fig. 6.5). The beams are designed to create a triangular cage. The triangular design also provides better resistance to lateral loads by allowing lateral loads to be distributed over multiple force projections.

The proposed X-Hab module has an internal pressure maintenance system, power supply system, ventilation system, and automatic control system, making it autonomous in case of failure of other lunar or Martian base systems.

The rapid development of space-inflatable habitable module concepts has spurred the development of orbital inflatable stations and compounds. One such example is considered in the context of creating an orbital station for servicing interorbital cargo flow, which is based on the proposed use of inflatable manned space modules of the BEAM type (Fig. 6.6) (Sobolev, 2017).

When creating such a design of an orbital station, the key value is the possibility of increasing the working and living volumes of the module while maintaining its mass allowed for launching by the existing carrier in a single launch using deploying a large-sized inflatable structure on its frame. This technology is a logical continuation of the experiment on the deployment of the inflatable BEAM habitation module, which makes it possible to create a single-module orbital station with sufficient working volume, using a single launch into orbit.

The above data indicate that inflatable structures for long-term use in space conditions are currently successfully passing the stage of flight testing and can be applied to form a combined design of space industrial platform modules. For example, a module for storing finished products can be formed by an inflatable module, while an industrial module can be formed by a frame-inflatable module, the frame of which is rigid. Mounting plates are attached to the skeleton, on which the attachment points for technological equipment and interfaces for its connection are located.

6.1.3. Aspects of a conceptual design of inflatable systems of space industrial platform

Inflatable modules are designed in such a way as to provide inside them a given microclimate, namely a certain humidity, temperature, and pressure. As is known (Space Environmental…, 1995), space objects traveling in low-Earth orbits are affected by the following space factors: ultraviolet radiation from the Sun, cosmic electromagnetic radiation, vacuum, atomic oxygen, and small fragments of space debris. By analogy with the inflatable modules of orbital stations, the shell of the inflatable instrumentation module is formed multilayer, with the upper and part of the inner layers performing the function of screen-vacuum thermal insulation, and the subsequent layers — protection from damage by small fragments of space debris and, if necessary, protection from harsh cosmic radiation.

The body with a load-bearing structure (LBS) consists of a rigid, inflatable, or combined frame and mounting plates attached to it. Onboard or process equipment is attached to the plates. The weight of the shell with supporting structures m_{OHK} in this case is described by the following expression (Palii, 2023a):

$$m_{OHK} = \sum_{i=1}^{n}\left(m_{O_i} + m_{ЖHK_i}^{(H)} + m_{MП_i}\right),$$

$$m_{O_i} = S_{ПЛ}^{O_i} \cdot \delta_M^{O_i} \cdot \rho_M^{O_i}, \tag{6.5}$$

$$m_{HK_i}^{Ж} = S_{ПЛ}^{HK_i} \cdot l_M^{HK_i} \cdot \rho_M^{HK_i}, \tag{6.6}$$

$$m_{HK_i}^{H} = S_{ПЛ}^{HK_i} \cdot \delta_M^{HK_i} \cdot \rho_M^{HK_i} + m_{CH}^{HK_i}, \tag{6.7}$$

$$m_{MП_i} = S_{ПЛ}^{MП_i} \cdot \delta_M^{MП_i} \cdot \rho_M^{MП_i}, \tag{6.8}$$

where m_{O_i} — is the mass of the shell of the i-th SIP module; $m_{HK_i}^{Ж}$ — is the mass of the rigid LBS of the i-th SIP module ; $m_{HK_i}^{H}$ — is the mass of the inflatable LBS of the i-th SIP module; $m_{MПi}$— is the mass of the mounting plate of the i-th SIP module; is the surface area of the shell of the i-th SIP module; $\delta_M^{O_i}$ — is the thickness of the shell material of the i-th SIP module, which is determined as follows:

$$\delta_M^{O_i} = f\left(t_O, k_1, k_2, k_3, k_4, k_5\right) \tag{6.9}$$

t_O — the active operating time of the inflatable module; k_1 — coefficient that takes into account the impact of ultraviolet radiation of the Sun on the shell material; k_2— coefficient taking into account the effect of space electromagnetic radiation on the shell material; k_3 — coefficient, taking into account the effect of vacuum on the shell material; k_4 — coefficient, taking into account the influence of atomic oxygen on the shell material; k_5 — coefficient taking into account the impact of

small space debris fragments on the shell material; $\rho_M^{O_i}$ — is the density of the material of the shell of the i-th SIP module; $S_{\Pi}^{HK_i}$ — is the cross-sectional area of the LBS profile of the i-th SIP module; $l_M^{HK_i}$ — is the total length of the LBS edges of the i-th SIP module; $\rho_M^{HK_i}$ — is the density of the LBS material of the i-th SIP module; $S_{\Pi}^{M\Pi_i}$ – is the surface area of the mounting plates of the i-th SIP module; $\delta_M^{M\Pi_i}$ — is the material thickness of the mounting plates of the i-th SIP module; $\rho_{M_M}^{M\Pi_i}$ — is the material density of the mounting plates of the i-th SIP module; $m_{CH}^{HK_i}$ — is the mass of the supercharging system of the LBS of the i-th module of the SIP, which is described by the following expressions (Palii, 2023a):

$$m_{CH}^{HK_i} = m_{\Gamma} + m_{3\Pi\Gamma} + m_{CKH}, \tag{6.10}$$

$$m_{\Gamma} = \frac{p_{HT} V_{HE} \mu_{\Gamma}}{R_0 T_{вн!}}, \tag{6.11}$$

$$m_{3\Pi\Gamma} = m_{Б} + m_{\Gamma\Pi}, \tag{6.12}$$

$$m_{Б} = S_{\Pi}^{Б} \cdot \delta_M^{Б} \cdot \rho_M^{Б}, \tag{6.13}$$

$$m_{CKH} = m_{PT} + m_{Д\,T} + m_{3A}, \tag{6.14}$$

where m_{Γ} — the mass of gas for inflation of the LBS elements; $m_{3\Pi\Gamma}$ — the weight of the gas storage and supply system for inflation; m_{CKH} — the weight of the inflation control system; p_{HT} — overpressure in LBS inflatable elements; V_{HE} — the volume of inflatable elements of the LBS; μ_{Γ} — molecular weight of the gas for inflation; $m_{Б}$— the weight of the gas storage cylinder; $\delta_M^{Б}$ — thickness of the gas cylinder material; p_{PT} — working pressure in the gas cylinder; $d_{Б}$ — cylinder diameter.

A gas cylinder can have several configurations: sphere, torus, and cylinder. The working pressure in the cylinder is orders of magnitude higher than the ambient pressure and the calculation of the thickness of the cylinder material is performed according to the momentless theory. Formulas for calculating the material thickness of a gas cylinder of various configurations are given in Table 6.2 (Palii, 2023a).

Table 6.2. **Material thickness of gas cylinder for various configurations**

The shape of the gas cylinder	Cylinder material thickness
Cylinder	$\delta_M^B = \frac{p_{PT} d_B}{2\sigma}$
Tor	$\delta_M^B = \frac{p_{PT} d_B \left(d_T - d_B\right)}{2\sigma\left(d_T - d_B\right)}$.
Sphere	$\delta_M^B = \frac{p_{PT} d_B}{4\sigma}$

The formulas in Table 6.2 indicate: p_{PT} — working pressure in the gas cylinder; $d_{Б}$ — cylinder diameter; p_{PT} — working pressure in the cylinder; σ — tensile strength of the cylinder material; d_T— torus diameter.

Table 6.3. **The surface area of the shell of SIP modules of different shapes**

Shell shape	Shell surface area	Shell shape	Shell surface area
Cylinder	$S_{\Pi}^{O_i} = 1{,}5708 d_O^2 + 3{,}141593 d_O l_O$	Hexagonal rectangular parallelepiped	$S_{\Pi}^{O_i} = 1{,}299 d_O^2 + 3 d_O l_O$
Square prism	$S_{\Pi}^{O_i} = 3 \cdot d_O^2$	Octahedral rectangular parallelepiped	$S_{\Pi}^{O_i} = 1{,}4143 d_O^2 + 3{,}062 d_O l_O$
Square rectangular parallelepiped	$S_{\Pi}^{O_i} = d_O^2 + 2 \cdot d_O \cdot l_O$	Sphere	$S_{\Pi}^{O_i} = \pi d_O^2$

Table 6.4. **The cross-sectional area of the ribs of the LBS of various shapes**

The ribs shape	Cross-sectional area	The ribs shape	Cross-sectional area
L-shaped	$S_{\Pi}^{HK_i} = 2 a_{\Pi} \delta_{\Pi}$	T-profile	$S_{\Pi}^{HK_i} = 0{,}5 a_{\Pi} \delta_{\Pi} - \delta_{\Pi}^2$
Channel	$S_{\Pi}^{HK_i} = 3 a_{\Pi} \delta_{\Pi} - 2\delta_{\Pi}^2$	Double-T-profile	$S_{\Pi}^{HK_i} = 1{,}5 a_{\Pi} \delta_{\Pi} - \delta_{\Pi}^2$

Table 6.5. **The total length of the ribs of the LBS of the SIP modules shell of various shapes**

Shell shape	The total length of the ribs of the LBS
Cylinder	$l_M^{HK_i} = 5{,}657 d_O + 4 l_O$
Square prism	$l_M^{HK_i} = 8{,}484 d_O$
Square rectangular parallelepiped	$l_M^{HK_i} = 5{,}657 d_O + 4 l_O$
Hexagonal rectangular parallelepiped	$l_M^{HK_i} = 6{,}536 d_O + 4 l_O$
Octahedral rectangular parallelepiped	$l_M^{HK_i} = 6{,}12 d_O + 4 l_O$
Sphere	$l_M^{HK_i} = 6{,}924 d_P$

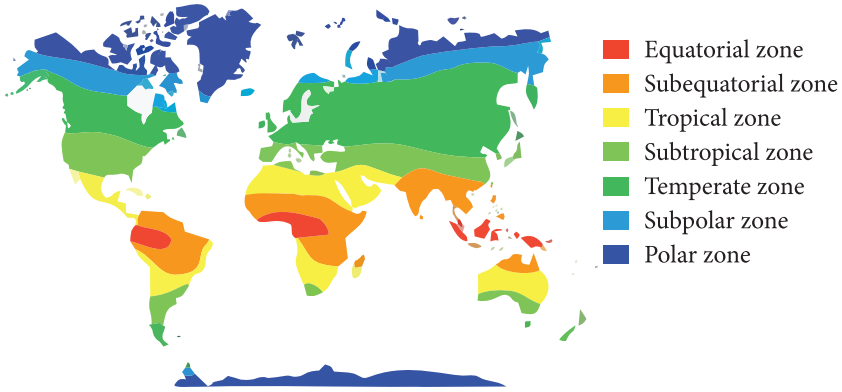

Fig. 6.7. Geographical climate zones

The following set of shapes of the SIP module shell is proposed: cylinder; square prism; square rectangular parallelepiped; hexagonal rectangular parallelepiped; octagonal rectangular parallelepiped; and sphere.

The formulas for calculating the surface area of the shell of SIP modules of various shapes are given in Table 6.3 (Palii, 2023a).

The formulas in Table 6.3 indicate: d_O — diameter of the shell of the SIP module; l_O — is the length of the SIP module shell.

At the initial stage of design, the calculation of the supporting structure is performed for a structure represented in the form of sets of force elements — ribs, which are inscribed in the corresponding shapes: parallelepiped or cube. The ribs of the supporting structure are represented by standard metal shapes that can have the following shapes: L-shaped profile, channel, T-profile, and double-T-profile. The formulas for calculating the cross-sectional area of the ribs and their total length are given in Table 6.4 (Palii, 2023a), and the formulas for calculating the total length of the LBS ribs are given in Table 6.5 (Palii, 2023a).

The formulas in Table 6.4 indicate: $a_П$ — the length of the rib base; $\delta_П$ — the thickness of the profile material.

6.2. Aerodynamic systems for creating orbital solar radiation screens

The problem and general approaches to the creation of aerodynamic solar screens are described in the paper (Alpatov, 2023b). This problem, on the one hand, is connected with the hypothesis of global warming, on the other, aerodynamic solar radiation screens are needed for the countries whose territories are located in «non-convenient» climate zones. These non-convenient» zones, for example, can be equatorial, subequatorial, or tropical with a high percent of deserts (Saudi Arabia, UAE, Amman, Izrael, Jordan, etc.), polar and subpolar zones of such countries as the USA, Canada, Finland, etc. (Fig. 6.7).

Thus, these climate condition in some periods of the year can impact negatively on some parts of the national economies of these countries such as agriculture, tourism, international trade, food production, etc.

Taking into account the problem of the creation of climate-control means can be devoted to two subproblems:

1) creation of global means of Earth protection from solar radiation in the frame of decreasing global warming process (in the frame of global warming concept);

2) creation of regional and local means for time-periodic climate change in determined territory of the Earth.

6.2.1. An overview of the most popular concepts of Earth's global climate control

So, in the frames of global warming theory, some concepts of Earth protection from the solar radiation impact were developed. One of these concepts is based on the Earth's orbit change (Zubrin, 2014; Theresa, 2021). The one of most well-noted scientists of the last decades Robert Zubrin estimated that to increase Earth's distance from the Sun by 5% it is needed the acceleration of $3.8 \cdot 10^{-14}$ m/s^2 (Zubrin, 2014). Taking into account the value of Earth's mass, R. Zubrin calculated that to achieve this acceleration it would be needed the force (thrust) of about 227 billion new tons. In turn, further, it was determined, that thruster to generate the force of such value needs a lot of energy (about $4.7 \cdot 10^{35}$ *J*) (Theresa, 2021).

Considering these aspects into account, there is no possibility and technology to realize this idea today. That's why it can be only a long-term perspective for mankind.

The next approach to Earth protection from increasing the intensity of solar radiation is based on stratospheric aerosol geoengineering (Davidson, 2012; Bingaman, 2020; Kravitz, 2015; Smith, 2022). So, the aerosol injection in the stratosphere using tethered balloons was described in the paper (Davidson, 2012). The authors carried out a deep analysis of the means of delivering aerosols to altitudes up to 20 km in this paper. The usage of naval artillery, different types of missiles, railguns, coilguns, aircrafts, rigid towers, single-use balloons, retrievable balloons, and tethered balloons were compared in the paper. So, using several criteria of comparison (time at altitude, minimum development time, environmental impact, and social impact) it was justified the advantage of the tether balloons creation relative to others means. However, the influence of aerosols on the ecology of the atmosphere has not been carried out. In turn, the new design of using «Sail aircraft» for aerosol delivery was proposed in the paper (Bingaman, 2020). Using the previous experience of creating airplanes with the high altitude of flight (RB-57F and U-2S) it was developed a new airplane that can carry about 13600 kg of aerosol. The planned flight altitude where the aerosol injection is started in this case is 20 km. It was determined that the approximate cost of the mission using «Sail aircraft» would be between $1.1 and $1.5B, (USD FY2020). In turn, taking

into account the instability of the oil market, fuel prices can increase which will lead to significantly increasing in mission costs. Also, the airplane is an additional source of atmospheric pollution which can make its use unattractive from an environmental point of view.

Taking into account the difficulties of aerosol impact on the stratosphere's chemical properties the authors of the paper (Kravitz, 2015) talked about the necessity of a significant number of experiments. These experiments are needed for clarifying or confirming /rejecting of present simulation results of geoengineering research. Also, the scenarios of stratospheric aerosol injection deployment which were being analyzed by researchers in the article (Smith, 2022), showed a great cost (cost-per-deployed-tone of aerosol is 2400$ at an altitude of 20 km) of decreasing the averaged temperature of the Earth by 2 $^{\circ}$C. In turn, it was determined that if this technology is used only for subpolar and polar regions it can allow to reduce costs by 3 times. However, decreasing the temperature by 2 $^{\circ}$C can't significantly help the planet. This can only partially slow down the process of melting glaciers in the Arctic and Antarctica, which, in turn, will reduce the pace of the rise of the world's oceans.

Thus, considering the information from the overview related the stratospheric aerosol geoengineering technologies it can be concluded (Davidson, 2012; Bingaman, 2020; Kravitz, 2015; Smith, 2022):

1) the technology has a significant theoretical background;

2) experiments are being carried out in this area, and a significant part of them are planned;

3) today there is no clear understanding of which means of aerosol delivery are most advantageous to use, the answer is controversial;

4) the full degree of the presented aerosols impact on the ecology of the atmosphere (including air, precipitation, etc.) in the long term is not determined;

5) the technology doesn't operative control of Sun rays protection: there is no possibility of operative shading and after that lighting (if there is a necessity) of the territory;

6) the system has a significant inertia.

Thus, given the properties of these systems, they can be used for tasks of decreasing the global warming process and are difficult be use for regional climate-control with time-periodic shades.

The next concept of Earth climate control is based on the marine cloud brightening (Wood…) — (Diamond, 2019). It is the international collaboration of atmospheric scientists and other experts to advance the understanding of cloud responses to aerosol particles (Wood…). The theoretical background of this concept is based on ship track studies and their impact on cloud radiative properties. This study allowed us to determine the aerosol–cloud radiative interactions and their influence on Earth's albedo (Possner, 2018), (Diamond, 2019). It is assumed that the creation of such clouds will enable a better reflection of the sun's rays and reduce the rate of global warming. However, this concept requires the presence of

significant water resources, the delivery of which to certain regions of the Earth can be difficult.

The name of the next concept is «Sunshade» (Kosugi, 2010; Sánchez, 2015; Fuglesang, 2021). It is based on the usage of special space shading technologies to reduce the impact of solar radiation on the Earth. So, the adventures of perspectives of space sunshade creation are described in the paper (Kosugi, 2010). The author substantiated the need for such systems creation in the context of geoengineering climate control tools development. The economic justification of this concept has been analyzed, but the technical implementation wasn't described. The technology for implementing the «sunshade» system, which is based on the deployment of a large circular disk near the Sun-Earth Lagrangian equilibrium point L1, is presented in (Sánchez, 2015). The paper emphasizes the advantage of the location of the disk around the L1 point from the point of view of ensuring the balance of the forces acting on this disk. So, the position is determined by the condition of compensation of the solar pressure and Earth's gravity forces by the gravitational force of the Sun. It was determined that to reduce the radiation intensity by 1.7%, the radius of the «sunshade» disk should be 915 km. In turn, it was calculated that using the disc with a radius of 1434 km can nullify the impact of greenhouse gas emissions worldwide (Sánchez, 2015). However, creating and launching a disc with such mass-dimensional parameters at point L1 is quite a difficult task and requires a lot of energy.

Later research works in this scientific area show the need to create a constellation of «sunshade» spacecraft (Fuglesang, 2021). It was estimated that for reducing the amount of sunlight for the Earth by 1 %, a solar "shield" with an area of $3.79 \cdot 10^{12}$ m^2 would be needed (Fuglesang, 2021). Considering the proposed area of 9000 m^2 for one sail, it was calculated that from $4.2 \cdot 10^8$ to $1.5 \cdot 10^9$ space sail vehicles located in the vicinity of the point L1 would be required to achieve the necessary area of the solar «shield». With the existing modern technologies for launching satellites into orbits, this will require from 330000 to 830000 launches. A rather significant range of these estimates is explained by the use of different types of sail configurations, especially the difference in the Q parameter (sail efficiency factor) (Fuglesang, 2021). It is planned that the launches will be carried out in orbits close to equatorial, with an altitude of 2000 km. After that, the sailing spacecraft, using the thrust of the solar radiation pressure have to perform orbit transition to the last destination near the vicinity of the L1 point. According to estimates, the orbital transition time in this case will take 1096 days (Fuglesang, 2021).

However, taking into account the given general models of the functioning of «sunshades» systems (Kosugi, 2010; Sánchez, 2015; Fuglesang, 2021), a complete mathematical model of such systems functioning was not presented. Also, these mathematical models given in works (Biktimirov, 2022; Alpatov, 2016c) describe only a special case of peculiarities of «sunshade» modules operation near point L1. In turn, the full range of possible orbits for «sunshade» modules location hasn't been analyzed and described.

In turn, the analysis of the previous researches (Alpatov, 2023b; Zubrin, 2014; Theresa, 2021; Davidson, 2012; Bingaman, 2020; Kravitz, 2015; Smith, 2022; Wood…; Possner, 2018; Diamond, 2019; Kosugi, 2010; Sánchez, 2015; Fuglesang, 2021) show the actuality of global climate-control systems creation. One of the perspective directions of such system creation is based on the development of «sunshade» space-based systems (Diamond, 2019; Kosugi, 2010; Sánchez, 2015; Fuglesang, 2021). In turn, the estimates of the source consumption which is required for creation such system make this concept doubtful from the point of practical realization both at present time and in near future. However, with the development of a new concept of space industrialization (Palii, 2021), (Palii, 2022a), the cost of creating such systems can be reduced by using on-orbit producing technology. This economic effect can be explained by the absence of need for multiple launches into orbits of «sun-shade» modules which requires a lot of costs. On the other hand, the use only «sunshade» technologies for reducing solar rays impact to the Earth doesn't solve the problem of global climate control completely. This can be explained by the presence of both global warming and cooling processes, which can periodically replace each other.

Taking this into account, it is advisable to include both «sunshade» and lighting (illuminative) modules of the Earth's surface as the one of the modules in the space-based global climate control system. In turn, the lighting (illuminative) technologies has a great scientific background since project «Znamya» until modern formation flight satellites including «writing sunlight» technologies (Ivanov, 2019), (Biktimirov, 2022).

6.2.2. Peculiarities of aerodynamic shading system creation

The one of the ways of «sunshade» system creation can be implemented on the base of aerodynamic systems development. Analyzing previous researches of the development of «sunshade» systems (Kosugi, 2010; Sánchez, 2015; Fuglesang, 2021) it can be seen, that only one type of sail geometry and principle of launch were proposed in the frames of this concept (one or a lot of flat sails elements which are launched from Earth). However, it can be other approaches of «sunshade» module types creation. The use of such approaches and the development of new types of aerodynamic shading systems (ASS) can significantly increase their efficiency. Thus, the new structure of ASS is proposed by authors, including approaches of ASS modules in-space producing using industrial platform concept (Palii, 2021), (Palii, 2022a). It is assumed that the production of ASS in space can expand the possibilities for creating new types of such systems, the production of which was previously not available (or difficult available) on Earth conditions. Taking this hypothesis into account it can be determined next structural modules of ASS:

1) Space-based industrial platform for ASS modules production;
2) «Sunshade» modules for reducing solar rays impact;
3) Service spacecraft for ASS transportation and deployment.

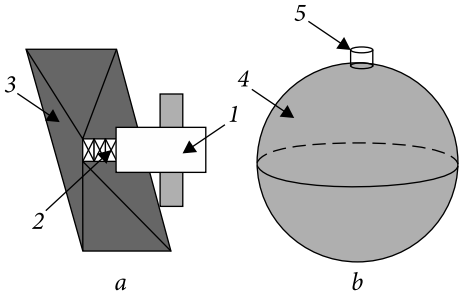

Fig. 6.8. The main types of «Sunshade» modules of space-based climate-control systems: *1* — Service spacecraft of ASS; *2* — Mast element of the sail; *3* — Flat sails «Sunshade» element; *4* — Volume passive «Sunshade» element; *5* — Compression valve for pressurization

Considering this new approach, it is assumed that service spacecraft will execute a delivering function for ASS modules from the space industrial platform to target orbits. The delivering process will include two phases — orbital transition from space industrial platform orbit to target orbit and deploying of «sun-shade»/ illuminative orbital groups on the target orbit. Taking it into account, there are two general types of «sunshade» and illuminative modules of ASS that can be distinguished (Fig. 6.8). These types are flat sail active module (Fig. 6.8, *a*) and volume inflatable passive module (Fig. 6.8, *b*).

So, the first type of «sunshade» module which is based on the use of flat sail elements requires attitude and angular control. It can be explained by the necessity of providing angular stabilization of flat sail elements to the directive vector of solar radiation flux. The goal of such orientation and stabilization support is providing a maximal «sunshade» area in the case of shading.

However, using separate spacecraft with sail elements requires a lot of launches of such satellites (Fuglesang, 2021) or a great number of their on-orbit producing in the case of the creation of on-orbit industrial plants (Palii, 2021), (Palii, 2022a). Taking this into account there is a task of determining the optimal ratio of service spacecraft number to the sail area. One of the directions in this task solving is based on the determination of the required number of service spacecrafts that are needed for providing stable motion of the super-large sail (Fig. 6.9).

Considering the construction presented in Fig. 6.3 it can be seen that the control system of sail attitude motion will be distributed. Taking into account the control algorithm more rational to synthase using mobile control methods (Alpatov, 2016c) and sliding control approaches (Gao, 2021). Thus, it can be an additional direction in the development of these control methods, which can be interesting for both theoretical and applied engineering aspects of science.

The second type of «sunshade» modules is based on the use of passive inflatable volume space structures that don't require providing stability and control. So, the main task, in this case, is to determine and develop the most optimal body geometry of illuminative modules that allow providing sun rays reflection to the Earth's surface during non-oriented free motion. In turn, for «sunshade» mod-

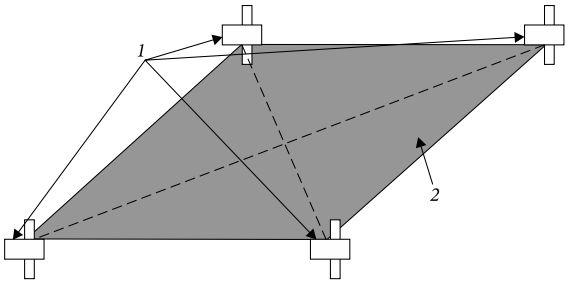

Fig. 6.9. Special Sun orientation of «sunshade» modules: *1* — Number of service spacecraft which provide super-sail controllable and stabile flight; *2* — Super-sail shading element

ules the most optimal body geometry can be sphere, spheroid, and ellipsoid. The advantage of using passive modules is the absence of onboard energy consumption and propulsion. However, in this case, many other problems arise that need to be solved to ensure the normal functioning of such systems. Among these tasks are the following:

• determination of the orbits for passive «sunshade» modules location which will satisfy the requirements of Earth shading;

• development of the special service spacecraft which provides delivery and deployment of the ASS passive modules groups on selected orbits;

• providing deorbiting of the ASS passive modules groups after the finish of the mission in the case of their location on LEO or transporting to disposal orbits with further utilization in the case of location higher than region LEO.

In turn, to solve these problems, the development of ballistic and navigation support (BNS) will be required. Structurally BNS model can be divided into the next parts:

1) Orbit estimator — the structural part of the BNS mathematical model that is needed for the space-based shading and lighting system (SBSLS) modules orbital motion analysis including relative motion of SBSLS modules formation flying.

2) Attitude motion estimator — the structural part of the BNS mathematical model that is needed for the analysis of the SBSLS modules motion around their centers of mass (COM).

3) Attitude orbital control system (AOCS) — the structural part of the BNS mathematical model that is needed for the determination and synthesis of control laws of SBSLS attitude motion.

4) Optical estimator — the structural part of the BNS mathematical model that is needed for the determination of illuminating or shading sail/volume element areas.

5) Geodetic estimator — the structural part of the BNS mathematical model that is needed for determining the current position of the illuminating or «sunshade» module position concerning the Earth's territories and geodetic parameters of lighting and shading areas on the Earth's surface.

Taking into account the proposed structural components of the BNS it will be useful to use reference frames that were fully described in works (Palii, 2022b), (Fortescue, 2011), (Golubek, 2020b), and (Bloise, 2010). These reference frames are: the J2000 reference frame, WGS-84, Orbital general reference frame (OGRF), Local vertical local horizontal (LVLH) (Bloise, 2010) reference frame, STW reference frame (Fortescue, 2011), Body reference frame (BRF) which is connected with i-th SBSLS module (Palii, 2022b). Using these reference frames, it is advisable to represent the structure of the mathematical model as a sequence of algo-

Table 6.6. **Structure of ballistic and navigational support**

Structural part	Reference frames	General mathematical description
Orbit estimator Attitude motion estimator	J2000, WGS-84, OGRF, STW LVLH BRF	Models (2.1—2. 45) in chapter 2
Relative motion estimator	J2000, WGS-84, OGRF, STW	$\mathbf{r_{sh}} = \begin{bmatrix} X_{sh} \\ Y_{sh} \\ Z_{sh} \end{bmatrix} = \begin{pmatrix} \begin{pmatrix} cos\Omega cos\omega - \\ -sin\Omega sin\omega cosi \end{pmatrix} & \begin{pmatrix} sin\Omega cos\omega + \\ +cos\Omega sin\omega cosi \end{pmatrix} & sinisin\omega \\ \begin{pmatrix} -cos\Omega sin\omega - \\ -sin\Omega cos\omega cosi \end{pmatrix} & \begin{pmatrix} -sin\Omega sin\omega + \\ +cos\Omega cos\omega cosi \end{pmatrix} & sinicos\omega \\ sin\Omega sini & -cos\Omega sini & cosi \end{pmatrix}^{\mathrm{T}} \begin{bmatrix} r_{sh}\, cos(u-\omega) \\ r_{sh}\, sin(u-\omega) \\ 0 \end{bmatrix},$ $\mathbf{V_{sh}} = \begin{bmatrix} V_{x.sh} \\ V_{y.sh} \\ V_{z.sh} \end{bmatrix} = \begin{pmatrix} \begin{pmatrix} cos\Omega cosu - \\ -sin\Omega sinucosi \end{pmatrix} & \begin{pmatrix} sin\Omega cosu + \\ +cos\Omega sinucosi \end{pmatrix} & sinisinu \\ \begin{pmatrix} -cos\Omega sinu - \\ -sin\Omega cosucosi \end{pmatrix} & \begin{pmatrix} -sin\Omega sinu + \\ +cos\Omega cosucosi \end{pmatrix} & sinicosu \\ sin\Omega sini & -cos\Omega sini & cosi \end{pmatrix}^{T} \begin{bmatrix} V_{pr.sh} \\ V_{pr.sh} \\ 0 \end{bmatrix},$ $\mathbf{DR}_{kj} = \begin{bmatrix} X_{sh.k} - X_{sc.j} & Y_{sh.k} - Y_{sc.j} & Z_{sh.k} - Z_{sh.j} \end{bmatrix}^{\mathrm{T}},$ $\mathbf{DV}_{kj} = \begin{bmatrix} V_{x.sh.k} - V_{x.sc.j} & V_{y.sh.k} - V_{y.sc.j} & V_{z.sh.k} - V_{z.sh.j} \end{bmatrix}^{\mathrm{T}},$
Relative motion estimator		$\mathrm{D}V_{kj} = \begin{bmatrix} V_{x.sh.k} - V_{x.sc.j} & V_{y.sh.k} - V_{y.sc.j} & V_{z.sh.k} - V_{z.sh.j} \end{bmatrix}^{\mathrm{T}},$ $dV_{kj} = \sqrt{\left(V_{x.sh.k} - V_{x.sc.j}\right)^2 + \left(V_{y.sh.k} - V_{y.sc.j}\right)^2 + \left(V_{z.sh.k} - V_{z.sh.j}\right)^2}$

The end of the Table

Structural part	Reference frames	General mathematical description
Optical estimator	J2000, WGS-84, OGRF, STW LVLH BRF	$$l_{sh} = R\frac{d_{sh}}{d}\sqrt{\frac{\Delta S}{S}},$$ $$R_{sun} = \left[\cos L \;\; \sin L\cos\varepsilon \;\; \sin L\sin\varepsilon\right]^{\mathrm{T}},$$ $$\beta = arcsin\left(\frac{R_E}{r_{sh}}\right),$$ $$\begin{cases} if\ \arccos\left(-R_{sun}\times r_{sh}\right)\le\beta \;\; eclipse\ part\ of\ orbit \\ if\ \arccos\left(-R_{sun}\times r_{sh}\right)>\beta \;\; solar\ part\ of\ orbit \end{cases}.$$ Estimation of shading position $$ORT^{wgs}_{sun\to sc} = \left[r^{wgs}_{sun\to sh.x} \;\; r^{wgs}_{sun\to sh.y} \;\; r^{wgs}_{sun\to sh.z}\right]^{\mathrm{T}},$$ $$Tar\_line = \begin{cases} R^{wgs}_{sh.x} + r^{wgs}_{sun\to sh.x}\lambda, \\ R^{wgs}_{sh.y} + r^{wgs}_{sun\to sh.y}\lambda, \\ R^{wgs}_{sh.z} + r^{wgs}_{sun\to sh.z}\lambda, \end{cases}$$ Intersection with Earth ellipsoid by solving equation for [35]: $$X_{el} = R^{wgs}_{sh.x} + r^{wgs}_{sun\to sh.x}\lambda,\;\; Y_{el} = R^{wgs}_{sh.y} + r^{wgs}_{sun\to sh.y}\lambda,$$ $$Z_{el} = R^{wgs}_{sh.z} + r^{wgs}_{sun\to sh.z}\lambda,\;\; \frac{X^2_{el}}{a^2_{el}} + \frac{Y^2_{el}}{a^2_{el}} + \frac{Z^2_{el}}{b^2_{el}} = 1$$
Geodetic estimator	WGS-84	Using iterative algorithm (Zbrutskii, 2011) for determination geodetic latitude, longitude and altitude of illumi-native and shading modules

rithmic blocks with logical and mathematical connections. Considering this, it is very convenient to use table form with the order of blocks (Table 6.6).

The formulas in Table 6.6 denoted: $r_{sh} = [X_{sh}\, Y_{sh}\, Z_{sh}]^{\mathrm{T}}$ is the radius vector of current «sunshade» i-th module position in J2000 reference frame; $V_{sh} = [V_{x.sh}\, V_{y.sh}\; V_{z.sh}]^{\mathrm{T}}$ is the velocity vector of current «sunshade» i-th module position in J2000 reference frame; $DR_{kj} = [X_{sh.k} - X_{sc.j};\; Y_{sh.k} - Y_{sc.j};\; Z_{sh.k} - Y_{sc.j}]^{\mathrm{T}}$ is the relative position vector of «sunshade» k-th module relative to j-th module in «sunshade»/illuminative orbital group; $V_{pr.x} = \sqrt{\frac{\mu}{p}}\cdot e\cdot sin(u-\omega)$; $V_{pr.y} = \sqrt{\frac{\mu}{p}}\cdot\left(1+e\cdot cos(u-\omega)\right)$; u is the argument of orbit latitude;

Ω is the RAAN; ω is the argument of perigee; e is the eccentricity of the orbit; p is the focal parameter of the orbit; μ is the Earth gravitational constant; $DV_{kj} = [V_{x.sh.k} - V_{x.sc.j};\ V_{y.sh.k} - V_{y.sc.j};\ V_{z.sh.k} - V_{z.sc.j}]^{\mathrm{T}}$ is the velocity vector of current «sunshade»/illuminative i-th module position in J2000 reference frame; l_{sh} is the characteristic size of i-th «sunshade» module; d_{sh} is the distance from i-th «sunshade» module to Earth surface (current altitude of the orbit); d is the distance from i-th «sunshade» module to Earth surface (current altitude of the orbit); R is the Sun radius; $S = 1367$ W/m^2 is the intensity of solar energy flux; ΔS is the amount by which the solar energy flux intensity is reduced due to shading by i-th «sunshade» module; R_{sun} is the direction unit vector from Earth to Sun in J2000 reference frame; L is the Sun's ecliptic longitude; ε is obliquity of the ecliptic; β is the angle that defines the entry and exit positions of eclipse/solar parts of the orbit; R_E is the Earth average radius; $\mathbf{ORT}^{wgs}_{sun\to sc} = \left[r^{wgs}_{sun\to sh.x} \quad r^{wgs}_{sun\to sh.y} \quad r^{wgs}_{sun\to sh.z} \right]^{\mathrm{T}}$ is the unit vector of the direction from Sun to the i-th «sunshade» module and it's components in WGS-84 reference frame; $R^{wgs}_{sh.x}$, $R^{wgs}_{sh.y}$, $R^{wgs}_{sh.z}$ are the coordinates of the i-th «sunshade» module current position in WGS-84 reference frame; *Tar_line* is the target line from Sun to the i-th «sunshade» module; λ is the non-dimensionless parameter.

6.2.3. Determination of further research tasks using the developed SBSLS ballistic and navigational mathematical model structure

The next step of the ASS study will be connected with a conceptual design of «sunshade» and illuminative modules (Blanchard, 2014). It is stage corresponds to phase A (Conceptual phase) and B (Phase of satellite components requirements determination of the development process phases for different spacecraft (Eickhoff, 2009). Using the developed ASS ballistic and navigation support structure it can be started two phases of software development for the study «sunshade»/illuminative modules orbiting: «algorithm in the loop» (Eickhoff, 2009) and «software in the loop» (Eickhoff, 2009). During these phases, it will be necessary to develop software that can allow to simulate the ASS module's flight more closely to real orbiting in space. After that, it is arising many pre-project tasks which are connected with the ASS module orbit selection. Among these tasks are the following:

1) determination of the «sunshade» modules target orbits;
2) determination of several «sunshade» modules in each target orbit;
3) determination of the transition orbits for service spacecraft;
4) determination deorbiting process of «sunshade» modules at the end of the lifetime.

During solving the first and second tasks of ASS modules orbit selection it should be taken into account the «sunshade» or illuminative orbital group efficiency. This efficiency can be determined as a relation of the number of current activated ASS modules to the total number of ASS modules on selected orbit (Fig. 6.10).

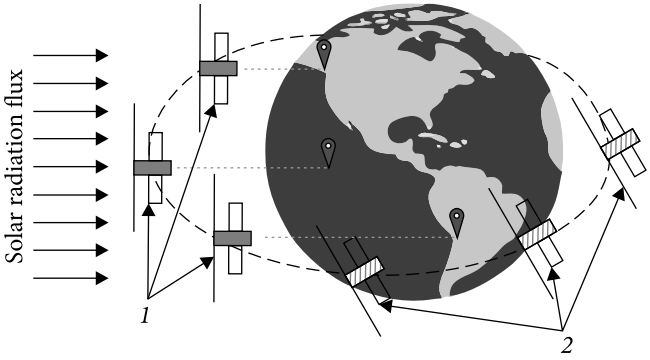

Fig. 6.10. SBSLS orbital group efficiency: *1* — activated ASS modules; *2* — inactivated ASS modules

So, the activated ASS modules will be referred to as modules that can perform «sunshade» tasks at the current time. For example, ASS will be modules that are located in a solar part of the orbit and reduce solar radiation flux intensity above the Earth's surface (Fig. 6.10). The determination of the currently active / inactive status of such ASS module can be estimated by solving intersection equation in «optical estimator» (Table 6.6) with further analysis of geodetic anchoring using «geodetic estimator» (Fig. 6.10). In turn, using «orbit estimator» there is a task of ASS modules activating/inactivating periodicity determination and some activated ASS modules in each time. Thus, it is possible to determine the effectiveness of any ASS constellation at the current time in a certain orbit.

The third task which is connected with orbit transition determination for service spacecraft includes the next subtasks:

- determination of attitude controllability of service spacecraft in each work mode using «attitude motion estimator»;
- gains selection for attitude motion controller of attitude orbital control system;
- calculation of orbit transition maneuver for service spacecraft using «orbital estimator»;
- determination of program attitude spacecraft orientation in the process of passive «sunshade» modules separation.

Also, in addition to the above, the tasks of AOCS development may arise when controlling active «sunshade» modules. In this case, AOCS should provide the necessary stabilization of the flat sail in Sun tracking mode during the shading mission.

The fourth task which is related to the deorbiting process analysis should be solved in satisfaction with the requirements of satellite lifetime restriction (Alpatov, 2019b). Thus, solving this list of problems will allow us to select the design parameters of the ASS system at the conceptual stages of designing.

REFERENCES

(Alhorn, 2010) Alhorn D. C. Feathersail — the next generation of nano-class sail vehicle. July 20, 2010. URL: https://ntrs.nasa.gov/archive/nasa/ casi.ntrs.nasa.gov/20100035087.pdf (access date 30.04.2020).

(Alhorn, 2011) Alhorn D. C., Casas J. P., Agasid E. F., Adams C. L., Laue G., & Kitts C., et al. The Smal.Satellite That Could!. *Proceedings of the 25th Annual AIAA/USU Conference on Smal.Satellites*. Logan, 2011. URL: https://ntrs.nasa.gov/archive/nasa/casi.ntrs.nasa.gov/ 20110015650.pdf (access date 30.04.2020).

(Alpatov, 2012) Alpatov A. P., Bass V. P., Baulin S. A., Brazinsky V. I., Gusynin V. P., Daniev Yu. F., Zasukha S. A. Man-made near-Earth space debris population (in Russian). Dnepropetrovsk: Porogi, 2012. 378 p.

(Alpatov, 2013a) Alpatov A. P., Belonozhko P. A., Belonozhko P. P., Hryhoriyev S. V., Tarasov S. V., Fokov A. A. Modeling of the dynamics of space manipulators on a movable base (in Russian). *Robotics and technical cybernetics*. 2013. No. 1. P. 61—65.

(Alpatov, 2013b) Alpatov A. P., Horbulin V. P. Space platforms for orbital industrial complexes: problems and perspectives (in Russian). *The Bulletin of the NAS of Ukraine*. 2013. No. 12. P. 26—38.

(Alpatov, 2015) Alpatov A. P., Palii O. S., Skorik O. D. Aerodynamic systems for space objects deorbiting (in Russian). *Technical mechanics*. 2015. No. 4. P. 126—138.

(Alpatov, 2016a) Alpatov A., Cichocki F., Fokov A., Khoroshylov S., Merino M., Zakrzhevskii A. Determination of the force transmitted by an ion thruster plasma plume to an orbital object. *Acta Astronautica*. 2016. №119. C. 241—251.

(Alpatov, 2016b) Alpatov A. P., Svorobin D. S., Skoryk O. D. System of contactless removal of space debris objects from near-Earth orbits with an aerodynamic compensator (in Ukrainian). *Technical mechanics*. 2016. No. 3. P. 51—56.

(Alpatov, 2016c) Alpatov A. P. Spacecraft dynamics (in Russian). PH "Naukova Dymka". 2016. 488 p.

(Alpatov, 2017a) Alpatov A. P., Goldstein Yu. M. Bal.stic analysis of the distribution of the orbits of spacecraft of various functional purposes (in Russian). *Technical mechanics*. 2017. No. 2. P. 33—40.

(Alpatov, 2017b) Alpatov A. P., Palii O. S., Skorik O. D. Development of the design scheme and selection of design parameters of the aerodynamic system for de-orbiting booster stages of launch vehicles (in Ukrainian). *Science and innovation*. 2017. Vol. 13. No. 4. P. 33—45.

(Alpatov, 2018) Alpatov A. P. Space debris: aspects of the problem (in Russian). *Technical mechanics*. 2018. No. 1. P. 30—47.

(Alpatov, 2019a) Alpatov A. P., Goldstein Yu. M. Selection of orbits for disposal of space debris (in Russian). *Technical mechanics*. 2019. No. 2. P. 5—15.

(Alpatov, 2019b) Alpatov A. P., Khoroshylov S. V., Maslova A. I. Contactless de-orbiting of space debris by the ion beam. Dynamics and control. Kyiv: Akademperiodyka, 2019. 170 p.

(Alpatov, 2020) Alpatov A., Khoroshylov S., Lapkhanov E. Synthesizing an algorithm to control the angular motion of spacecraft equipped with an aeromagnetic deorbiting system. *Eastern-European Journal of Enterprise Technologies*. 2020. Vol. 1. Iss. 5(103). P. 37—46. URL: https://doi.org/10.15587/1729-4061.2020.192813 (access date 30.08.2020).

(Alpatov, 2022a) Alpatov, A.P., Lapkhanov, E.O., Palii O.S. Designing the configuration and selecting the design parameters of drag systems for deorbiting spacecraft created by Pivdenne design office. *Science and Innovation*, 2022. 18(4). P. 55—63.

(Alpatov, 2022b) Alpatov A. P., Kuznetsov O. P., Palii O. S., Lapkhanov E. O. Development of R & D framework for the modernization of the aerodynamic deorbit system for the use on the upper stage of Cyclone-1M launch vehicle. *Science and Innovation*. 2022. 18(6). P. 60—71.

(Alpatov, 2023a) Alpatov A., Dron' M., Golubek A., Lapkhanov E. Combined method for spacecraft deorbiting with angular stabilization of the sail using magnetorquers. *CEAS Space J.* 2023. No. 15. P. 613—625. URL: https://doi.org/10.1007/s12567-022-00469-6 (access date 05.08.2020).

(Alpatov, 2023b) Alpatov A., Lapkhanov E. Features of the development of space-based shading and lighting systems for the earth's surface. *Technical mechanics*. 2023. No. 1. P. 25—39.

(Anderson, 2011) Anderson J. L. NASA's Nanosail-D 'Sails' Home — Mission Complete. November 29, 2011. URL : https://www.nasa.gov/mission_pages/smal.ats/11-148.html (access date 30.04.2020).

(Andrews, 2011) Andrews J., Watry K., Brown K. Nanosat deorbit and recovery system to enable new missions. *25th Annual AIAA/USU Conference on Smal.Satellites*. August 9, 2011. URL: https://digitalcomons.usu.edu/cgi/ viewcontent.cgi?arti-cle=1164&context=smal.at (access date 22.04.2019).

(Atwell, 2000) Atwell W., Badwhar G. A shielding model for an inflatable vehicle, transhab, and the associated astronaut space radiation risk assessment. *33-rd Scientific Assembly of the Committee on Space Research (CoSPAR)* Warsaw, Poland July 16-23, 2000, URL: https://ntrs.nasa.gov/archive/nasa/casi.ntrs.nasa. gov/20100033236.pdf (access date 16.12.2022).

(Babuscia, 2013) Babuscia A., Knapp M., Hicks F. M. et al. InCUBEation: A series of mission for interplanetary exploration using smal.satellite platforms. Presentation A.1.3 on *Interplanetary smal.satellite conference*, 20-21 June 2013 California Institute of Technology, Pasadena, California.

(Bombardelli, 2011) Bombardelli C., Pelaez J. Ion beam shepherd for asteroid deflection. *Journal of Guidance, Control and Dynamics*. 2011. Vol. 34. No. 4. P. 1270—1272.

(Bombardelli, 2012) Bombardelli C., Urrutxua H., Merino M., Ahedo E., Peláez J. Relative dynamics and control of an ion beam shepherd satellite. *Spacefl. Mech*. 2012. Vol. 143. P. 2145—2158.

(Bowman, 2008) Bowman B. R., Tobiska W. K., Marcos F. A., Val.dares C. The JB2006 empirical thermospheric density model. *Journal of Atmospheric and Solar-Terrestrial Physics*. 2008. Vol. 70. Iss. 5. P. 774—793. URL: https://doi.org/10.1016/j.jastp.2007.10.002 (access date 08.08.2020).

(Banichuk, 1997) Banichuk N. V., Karpov I. I., Klimov D. M. Mechanics of large space structures (in Russian). M.: Publishing House «Factorial», 1997. 302 p.

(Bingaman, 2020) Bingaman D. C., Rice C. V., Smith W., Vogel P. G. A Stratospheric Aerosol Injection Lofter Aircraft Concept: Brimstone Angel. *AIAA SciTech Forum*, 6-10 January 2020, Orlando, FL. 2020. P. 1—22. URL: https://doi.org/10.2514/6.2020-0618 (access date 07.03.2023).

(Benvenuto, 2015) Benvenuto R., Salvi S., Lavagna M. Dynamics analysis and GNC design of flexible systems for space debris active removal. *Acta Astronautica*. 2015. Vol. 110. P. 247—265.

(Biktimirov, 2022) Biktimirov S., Belyj G., Pritykin D. Satellite Formation Flying for Space Advertising: From Technical. Feasible to Economical. Viable. *Aerospace*. 2022. Vol. 9. Iss. 8. P. 419. URL: https://doi.org/10.3390/aerospace9080419 (access date 12.03.2023).

(Bloise, 2010) Bloise N., Capello E., Dentis M., Punta E. Obstacle avoidance with potential field applied to a rendezvous maneuver. *Appl. Sci.* 2017. Vol. 7. Iss. 10. P. 1042. URL: https://doi.org/10.3390/app7101042 (access date 14.03.2023).

(Blanchard, 2014) Blanchard B. S., Fabrycky W. J. Systems engineering and analysis. Pearson Education Limited. 2014. 841 p.

(Caparelli, 2001) Caparelli E. C., Tomasi D. An Analytical Calculation of the Magnetic Field Using the Biot Savart Law. *Revista Brasileira de Ensino de Fisica*. Vol. 23. No. 3. 2001. P. 284—288.

(Chulliat, 2020) Chulliat A., Brown W., Alken P., Beggan C., Nair M. & Cox G. et al. The US/UK World Magnetic Model for 2020-2025: Technical Report, National Centers for Environmental Information, NOAA. 2020. URL: https://repository.library.noaa.gov/view/noaa/24390 (access date 29.04.2020).

(COSPAR International…, 2012) COSPAR International Reference Atmosphere — 2012. CIRA 2012. Models of the Earth's Upper Atmosphere. Version: 1.0. July 31, 2012. URL: https://spacewx.com/wp-content/uploads/2021/03/chapters_1_3.pdf (access date 12.08.2020).

(Davidson, 2012) Davidson P., Burgoyne C., Hunt H., Causier M. Lifting options for stratospheric aerosol geoengineering: advantages of tethered bal.on systems. 2012. 370. P. 4263—4300. URL: https://doi.org/10.1098/rsta.2011.0639 (access date 07.03.2023).

(Diamond, 2019) Diamond M. S., Director H. M., Eastman R., Possner A., Wood R. The efficacy of aerosol—cloud radiative perturbations from near-surface emissions in deep open-cell stratocumuli. *AGU Advances*. 2019. Vol. 1, No. 1. 28 p. URL: https://doi.org/10.1029/2019AV000111 (access date 09.03.2023).

(Di Capua, 2011) Di Capua M., Akin D., Davis K. Design, development, and testing of an inflatable habitat element for NASA Lunar Analogue Studies. *41st International Conference on Environmental Systems*. July 2011, Portland, Oregon — 20 p., URL: https://spacecraft.ssl.umd.edu/publications/2011/AIAA-2011-5044.X-Hab.pdf (access date 18.12.2022).

(Dimensions of the payload…) Dimensions of the payload area of the main fairing. "Yuzhnoye" State Design Office. URL: https://old.yuzhnoye.com/ua/technique/launch-vehicles/launch-vehicles/cyclone-1m/ (access date 25.08.2020).

(Dron, 2014) Dron N. M., Khorolskyi P. G., Dubovik L. G. Ways to reduce technogenic pollution of near-Earth outer space (in Russian). *Scientific Bulletin of the National Mining University*. 2014. No. 3. T 141. P. 125—130.

(Dron', 2018) Dron' M., Dreus A., Golubek A., Abramovsky Ye. Investigation of aerodynamics heating of space debris object at reentry to earth atmosphere. *69th International Astronautical Congress*, Bremen, Germany. 01—05 October 2018. Bremen, 2018. IAC-18-A6.1.5. Paper-Nr: IAC-18, A6, IP, 39, x43286. P. 3923—3929.

(Dron', 2019a) Dron' M., Golubek O., Dubovik L., Dreus A., Heti K. Analysis of the Bal.stic Aspects of the Combined Method of Deorbiting Space Objects From the Near-Earth Orbits. *Eastern-European Journal of Enterprise Technologies*. 2019. № Vol. 2. Iss. 5 (98). P. 49—54.

(Dron', 2019b) Dron' N. M., Golubek A. V., Dreus A. Yu., Dubovik L. G. Prospects for the use of a combined method for clearing near-Earth space from large space debris (in Russian). *Space science and technology*. 2019. V. 25. No. 6. P. 61—69.

(Dudziak, 2015) Dudziak R., Tuttle S., Barraclough S. Harpoon technology development for the active removal of space debris. *Advances in Space Research*. 2015. Vol. 56. No. 3. P. 509—527.

(DuPont™ Kapton) DuPont™ Kapton. Summary of Properties. URL: https://www.dupont.com/content/dam/dupont/amer/us/en/ei-transformation/public/ documents/en/EI-10142_ Kapton-Summary-of-Properties.pdf (access date 25.05.2023).

(DuPont™ Kapton FN) DuPont™ Kapton® FN. Polyimide Film. DuPont. URL: https://www.dupont.com/content/dam/dupont/amer/us/en/ei-transformation/public/documents/en/EI-10160-Kapton-FN-Data-Sheet.pdf (access date 27.05.2023).

(Dupuy, 2010) Dupuy C., Le Couls O. Gossamer technology to deorbit LEO non-propulsion fitted satellite. *40th Aerospace mechanisms symposium*, NASA Kennedy space center, may 12-14, 2010. URL: https://core.ac.uk/download/pdf/42754021.pdf (access date 04.05.2021).

(Eickhoff, 2009) Eickhoff J. Simulating spacecraft systems. Springer-Verlag Berlin Heidelberg. 2009. 360 p. URL: https://doi.org/10.1007/978-3-642-01276-1 (access date 15.03.2023).

(Evaporation effects…, 1961) Evaporation effects on materials in space: technical report. Jet propulsion laboratory, California Institute of technology; chief L. D. Jaffe, J. B. Rittenhouse. Pasadena, California, 1961. 22 p. № 32-161.

(Fortescue, 2011) Fortescue P., Stark J., Swinerd G. Spacecraft systems engineering. John Wiley & Sons Ltd. Chichester, 2011. 724 p.

(Freeland, 2014) Freeland R. E., Bard S., Veal G. R., Bilyeu G. D. et al. Inflatable antenna technology with preliminary shuttle experiment results and potential applications. URL: https://trs.jpl.nasa.gov/bitstream/handle/2014/26491/96-1367.pdf?sequence=1&isAllowed=y (access date 20.07.2020).

(Fuglesang, 2021) Fuglesang C., Miciano M. Realistic sunshade system at L1 for global temperature control. *Acta Astronautica*. 2021. No. 186. P. 269—279. URL: https://doi.org/10.1016/j.actaastro.2021.04.035 (access date 12.03.2023).

(Gao, 2021) Gao Sh., Li You, Xue H., Yao Sh. Dynamic Sliding Mode Controller with Variable Structure for Fast Satellite Attitude Maneuver. *Mathematical Problems in Engineering*. 2021. Vol. 21. URL: https://doi.org/10.1155/2021/5539717 (access date 14.03.2023).

(Gaydachuk, 2012) Gaydachuk A. V., Karpikova O. A., Kondratev A. V., Slivinskiy M. V. Honeycomb cores and panel structures for space purposes: monograph. In 2 vol. Vol. 1. Technological imperfections of honeycomb cores and structures; ed. A. V. Gaydachuk. (in Russian) Kharkiv: National Aerospace University named after N.E. Zhukovsky «Kharkiv Aviation Institute», 2012. 279 p.

(Gloyer, 2002) Gloyer P. Aerobracking technology for Earth orbit transfers. P. Gloyer. 16th Annual/USU Conference on Smal.Satellites/ SSC02-VII-2, August 12-15, 2002. URL: http://digitalcommons.usu.edu/cgi/viewcontent.cgi?article=1932&context=smal.at (access date 24.03.2021).

(Golubek, 2020a) Golubek A., Dron' M., Dubovik L., Dreus A., Kulyk O., Khorolskiy P. Development of the combined method to de-orbit space objects using an electric rocket propulsion system. *Eastern-European Journal of Enterprise Technologies*. 2020. Vol 4. No 5 (106). P. 78—87. URL: https://doi.org/10.15587/1729-4061.2020.210378.

(Golubek, 2020b) Golubek A. V., Filipenko I. M., Tatarevskiy K. E. A priori assessment of the accuracy of the launch of space-craft by modern launch vehicles with strapdown inertial navigation system (In Russian). Sub. ed. academ. A. V. Degtyarev National Academy of Sciences. Dnipro: LIRA, 2020. 187 p.

(Gordeev, 2016) Gordeev V. N. Quaternions and biquaternions with applications in geometry and mechanics (in Russian). Kyiv: Publishing house "Steel". 2016. 316 p.

(Han, 2015) Han W., Huang Y., Chen X. Research of impact dynamic modeling of flexible probe-cone docking mechanism based on Kane method. *Archive of Applied Mechanics*. 2015. Vol. 85. No. 2. P. 205—221.

(Handbook…, 1987) Handbook of electrical materials: In 3 vols (in Russian) Vol. 2. Edited by Yu V. Koritsky et al. 3rd ed., revised. Moscow, 1987. 464 p.

(Heaton, 2014) Heaton A. F., Fal.r B. F., Katan C. K. NanoSail-D Orbital and Attitude Dynamics. Advances in Solar Sailing, ed. By M. Macdonald. Springer-Verlag Berlin Heidelberg. 2014. P. 95—113.

(Herbeck, 2002) Herbeck L., Sickinger C., Eiden M., Leipold M. Solar sail hardware developments. *European Conference on Spacecraft Structures: Materials and Mechanical Testing*. Toulouse. 2002. P. 1—10.

(Hoyt, 1998) Hoyt R., Forward R. Application of the terminator tether™ electrodynamic drag technology to the deorbit of constellation spacecraft. In proceedings of *the 34th AIAA/ASME/SAE/ASEE Joint Propulsion Conference and Exhibit*. 1998. P. 1 — 19. URL: https://doi.org/10.2514/6.1998-3491 (access date 30/04/2020).

(Hoyt, 1999) Hoyt R., Forward R. Performance of the Terminator Tether for Autonomous Deorbit of LEO Spacecraft. *AIAA-99-2839 35-th Join Propulsion Conference & Exhibit*. 20 — 24 June. Los Angeles. 1999. P. 1—10. URL: https://doi.org/10.2514/6.1999-2839 (access date 20.03.2021).

(Ivanov, 2019) Ivanov D., Biktimirov Sh., Chernov K., Kharlan A., Monakhova Ul. & Pritykin D. Writing with sunlight: CubeSat Formation Control Using Aerodynamic Forces. *70th International Astronautical Congress (IAC)*, Washington, USA, 21—25 October 2019. P. 1—10.

(Jenkins, 2001) Jenkins C. H. M. Progress in astronautics and aeronautics. Vol. 191. Gossamer spacecraft: membrane and inflatable structures technology for space applications. Reston, Virginia: American institute of aeronautics and astronautics, 2001. 586 p.

(Jensen, 1956) Jensen N. Vapor pressure of plastic materials. Journal of applied physics. 1956. Vol. 27. № 12. P. 1460—1462.

(Kawashima, 2018) Kawashima R., Bak J., Matsuzawa S., Inamori T. Particle Simulation of Plasma Drag Force Generation in the Magnetic Plasma Deorbit. Tokyo University. 2018. URL: www.al.t.utokyo.ac.jp/members/junhwib/docs/2018Kawashima_JSR.pdf (accessed 04.30.2020).

(Kennedy, 2016) Kennedy K., Adams C. ISS TransHab: An Inflatable Habitat. NASA — 2016, URL: https://www.researchgate.net/publication/252368525/download (access date 16.12.2022).

(Kessler, 2010) Donald J. Kessler, Nicholas L. Johnson, J.-C. Liu, Mark Matney. The Kessler Syndrome: Implications to Future Space Operations. *33rd Annual AAS guidance and control conference*. Breckenridge, Colorado. February 6—10, 2010. URL: http://citeseerx.ist.psu.edu/viewdoc/download?doi=10.1.1.394.6767&rep=rep1&type=pdf(access date 04.30.2020).

(Khoroshilov, 2017) Khoroshilov S. V. Synthesis of a robust regulator of the "shepherd with an ion beam" control system (in Russian). *Technical mechanics*. 2017. No. 1. P. 26—39.

(Khoroshilov, 2018) Khoroshilov S. V. The system of controlling the relative motion of the spacecraft for non-contact removal of space debris. *Science and innovation*. 2018. 14(4). P. 5—8.

(Klinkrad, 2006) Klinkrad H. Space debris: Models and risk analysis. Chichester, UK, 2006. 416 p.

(Kondakov, 1975) Kondakov N. I. Logical dictionary-reference (in Russian). Moscow, 1975. 720 p.

(Koshmarov, 1977) Koshmarov Yu. A., Ryzhov Yu. A. Applied rarefied gas dynamics (in Russian). Moscow, 1977. 184 p.

(Kosugi, 2010) Kosugi T. Role of sunshades in space as a climate control option. *Acta Astronautica*. 2010. No. 67. P. 241—253. https://doi.org/10.1016/j.actaastro.2010.02.009 (access date 10.03.2023).

(Kravitz, 2015) Kravitz B., Robock A., Tilmes S., Boucher O., English J. M. & Irvine P. J., et al. The Geoengineering Model Intercomparison Project Phase 6 (GeoMIP6): simulation design and preliminary results. *Geosci. Model Dev.* 2015. No. 8. P. 3379—3392. URL: https://doi.org/10.5194/gmd-8-3379-2015 (access date 08.03.2023).

(Lapkhanov, 2019a) Lapkhanov E. O. Features of the development of means for spacecraft removal from near-Earth operational orbits (in Ukrainian). *Technical mechanics*. 2019. No. 2. P. 16—29.

(Lapkhanov, 2019b) Lapkhanov E. O. Design features of devices with permanent magnets for removal of space debris objects from low Earth orbits (in Ukrainian). *System design and analysis of aerospace engineering characteristics*. 2019. Vol. XXVII. P. 59—70.

(Lapkhanov, 2019c) Lapkhanov E., Khoroshylov S. Development of the aeromagnetic space debris deorbiting system. *Eastern-European Journal of Enterprise Technologies*. 2019. Vol. 5. Iss. 5(101). P. 30 — 37. URL: https://doi.org/10.15587/1729-4061.2019.179382 (access date 29.08.2020).

(Leipold, 1999) Leipold M., Garner C. E., Freeland R., Hermann A., Noca M. & Pagel G. et al. Odissee — a proposal for demonstration of a solar sail in earth orbit. *Acta Astronautica*. 1999. Vol. 45. Iss. 4. P. 557—566.

(Liao, 2009) Liao L., Pasternak I. A review of airship structural research and development. *Progress in aerospace sciences*. 2009. № 45. P. 83—96.

(Lindell, 2006) Lindell M C., Hughes S. J., Dixon M., Willey C. E. Structural analysis and testing of the inflatable re-entry vehicle experiment (IRVE). *Paper AIAA 2006-1699 on 47th AIAA/ASME/ASCE/AHS/ASC Structures, structural dynamics and materials conference*, 1—4 may 2006, Newport, Rhode Island.

(Lovell, 2004) Lovell T.A., Tragesser S. Guidance for Relative Motion of Low Earth Orbit Spacecraft Based on Relative Orbit Elements. *AIAA Paper 2004-4988, presented at the AAS/AIAA Astrodynamics Specialist Conference*, Providence, RI. 2004. URL: https://doi.org/10.2514/6.2004-4988 (access date 18.04.2020).

(Maesen, 2007) Maesen D. S., Van Breukelen E. D., Zandbergen B. T. C., Bergsma O. K. Development of a generic inflatable de-orbit device for cubesats. *58th International astronautic congress*, September 24—28, 2007, Hyderabad, Andhra Pradesh, India, IAC-07-A6.3.06.

(Maslova, 2015) Maslova A. I., Myshchenko A. V., Pirozhenko A. V., Khramov D. A. Studies of the regularities of the dynamics of an electrodynamic space tether system to determine the possibility of creating a highly efficient device for passive removal of space debris from low Earth orbits (in Russian). *Space science and technology*. 2015. Vol.21. No. 1. P. 20—24.

(McCarthy, 2010) McCarthy C. E., Banks B. A., De Groh K. K. MISSE 2 PEACE Polymers Experiment Atomic Oxygen Erosion Yield Error Analysis. NASA/TM—2010-216903. URL: https://core.ac.uk/download/pdf/10556893.pdf (access date 20.05.2023).

(Meteoroid and space…, 2010) Meteoroid and space debris terrestrial environment reference model MASTER-2009 [Electronic resource]. ESA-SD-DVD-02, Release 1.0, December 2010. 1 electronic disc (DVD-R).

(Methewson, 2017) Methewson S. BEAM inflatable space habitat has successful 1st year in orbit. Space.com. — June, 2017. URL: https://www.space.com/37068-beam-inflatable-habitat-first-year-space.html (access date 17.12.2022).

(MMA Design…, 2013) MMA Design. Drag NET De-orbit system. 2013. URL: https://mmadesignllc.com/product/dragnet-de-orbit-system/ (access date 30.04.2020).

(Montenbruck, 2005) Montenbruck O., Gill E. Satellite Orbits: Models, Methods and Applications. 3d edition. Berlin, 2005. 381 p.

(Moody, 2016) Moody C.K., Probe A.B., Masher A., Woodbury T., Saman M. & Davis J. et al. Laboratory Experiments for Orbital Debris Removal. *In: AAS Guidance, Navigation and Control Conference, Breckenridge*, Colorado, USA. 5-10 February. 2016. P. 1—12.

(Mori, 2009) Mori O., Sawada H., Funase R., Endo T., Morimoto M. & Yamamoto T., et al. Development of first solar power sail demonstrator — Ikaros. JAXA Space Exploration Center. Japan. URL: http://issfd.org/ISSFD_2009/AOCSI/Mori.pdf (access date 30.04.2020).

(Mylar…, 2017) Mylar polyester film. Physical-Thermal Properties. URL: https://usa.dupont-teijinfilms.com/wp-content/uploads/2017/01/ Mylar_Physical_Properties.pdf (access date 23.05.2023).

(Myshchenko, 2017) Myshchenko O. V. To determine the length of the cable of the experimental electrodynamic system (in Russian). *Technical mechanics*. 2017. No. 4. P. 55—63.

(Myshchenko, 2018) Myshchenko O. V., Pyrozhenko O. V. Smal.experimental electrodynamic space tether system. Electric model (in Russian). *Space science and technology*. 2018. No. 3. P. 3—10.

(Myshchenko, 2020) Myshchenko O. V., Pyrozhenko O. V. To determine the design parameters of the electrodynamic space cable system (in Russian). *Technical mechanics*. 2020. No. 1. P. 19—30.

(National geospatial-intelligence…, 2008) National geospatial-intelligence agency (NGA) standardization document. Department of defense, World Geodetic System 1984. 2008. 208 p. URL: https://nsgreg.nga.mil/doc/view?i=4085 (last accessed 16.08.2023).

(Nazarenko, 2013) Nazarenko A. I. Modeling of space debris (in Russian). Moscow, 2013. 216 p.

(Nock, 2010) Nock K. T., Gates K. L., Aaron K. M., McRonald A. D. Gossamer orbit lowering device (GOLD) for safe and efficient de-orbit. *AIAA/AAS Astrodynamics specialist conference*, 2—5 August 2010. Toronto, Ontario, Canada, AIAA 2010-782. URL: https://doi.org/10.2514/6.2010-7824 (access date 12.11.2020).

(Overview of…) Overview of materials for Polytetrafluoroethylene (PTFE), Mica Filled. URL: https://www.matweb.com/search/datasheet_print.aspx?matguid=ef394c1e30c54ca8b21836006aee2484 (access date 26.05.2023).

(Palii, 2012) Palii O. S. Methods and means of launching spacecraft from working orbits (state of the problem (in Russian). *Technical mechanics*. 2012. No. 1. P. 94—102.

(Palii, 2014) Palii O. S., Skoryk O. D. Analysis of the possibility of using aerodynamic systems for the introduction of modular large-sized space objects from low Earth orbits (in Russian). *Technical mechanics*. 2014. No. 2. P. 43—51.

(Paliy, 2015) Paliy A. S. Development of the design methodology for aerodynamic systems of spacecrafts deorbiting from near-Earth orbits. *East-European Journal of Enterprises Technologies. Information and control systems*. 2015. No 1. P. 11—15.

(Palii, 2017) Palii A. S. Classifier of the aerodynamic systems of the space technology objects deorbiting from the near-Earth orbits. *Technical Mechanics*. — No 4. 2017. P. 49—54.

(Palii, 2021) Palii O. S. State of the art in the development of orbital industrial platforms. *Technical Mechanics*. 2021. No 3. P. 70— 82.

(Palii, 2022a) Palii O. S. Classification of technological processes for their implementation on the space industrial platform (in Ukrainian). *Technical mechanics*. 2022. No. 2. P. 123—136.

(Palii, 2022b) Palii O. S., Lapkhanov E. O., Svorobin D. S. Model of distributed space power system motion control (in Ukrainian). *Technical mechanics*. 2022. No. 4. P. 35—50.

(Palii, 2023a) Palii O. S. Formation of the design view of the space industrial platform (in Ukrainian). *System design and analysis of the characteristics of aerospace technology*. 2023. Vol. XXXII. P. 78—88.

(Palii, 2023b) Palii O. S. Classification of functional features of the space industrial platform shell. *Technical mechanics*. 2023. No. 2. P. 64—73.

(Pardini, 2009) Pardini C., Hanada T., Krisko P. H. Benefits and Risks of using electrodynamic tethers to deorbit spacecraft. *Acta Astronautica*. Vol. 64, Iss. 5—6. 2009, P. 571—588.

(Patent application for the invention No. WO2012092933) Patent application for the invention No. WO2012092933, IPC7 B64G1/62. Self-deployable deorbiting space structure. Kristensen A. S., Damkilde L. PCT/DK2012/050009; applied 06.01.2012; published 12.07.2012.

(Patent for invention US8979034, 2015) Patent for invention US8979034, IPC B25J9/16; B25J15/00; B25J18/02; B64G1/64; B64G4/00. Sticky boom non-cooperative capture device. Goff J. A, Judson M. I., Hoyt W., Ryan F. P., Bolton W. G. 13/312,984; applied 12.06.2011; published 03.17.2015.

(Patent of Ukraine for invention № 109318, 2015) Patent of Ukraine for invention № 109318, IPC B 64 G 1/62. The method of removing space objects from Earth orbits and the system for its implementation (in Ukrainian). Palii O. S., Alpatov A. P., Skorik O. D. a20131326; applied 14.11.2013; published 10.08.2015, Bull. No. 15. 11 p.

(Patent of Ukraine for invention № 113747, 2017) Patent of Ukraine for invention № 113747, IPC B 64 G 1/62. The method of reducing the ballistic lifetime of space objects in near-Earth orbits and the spacecraft for its implementation (in Ukrainian). Alpatov A. P., Pylypenko O. V., Palii O. S., Skorik O. D., Avdieiev A.M., Masliei V. M., Makarov O. L., Maskalov S. I.; a201407652; applied 07.07.2014; published 10.03.2017, Bul. No. 5. 11 p.

(Patent of Ukraine for invention № 109194, 2015) Patent of Ukraine for invention № 109194, IPC B 64 G 1/62. Aerodynamic system for removing space objects from near-Earth orbits: (in Ukrainian). Alpatov A. P., Palii O. S., Skorik O. D., Avdeev A. M., Baranov E. Yu., Osi-novyi H. H., Shevtsov V. I. a201312759; applied 01.11.2013; published 27.07.2015, Bull. No. 14. 12 p.

(Patent of Ukraine for the invention No. 107880, 2015) Patent of Ukraine for the invention No. 107880, IPC B64G 1/62. The method to remove modular large-sized space objects from near-Earth orbits. Alpatov A. P., Palii O. S., Skoryk O. D. a201309842; applied 08.08.2013; published 25.02.2015, Bull. No. 4.

(Patent of the Ukraine № 125265) Patent of the Ukraine № 125265, IPC B64G 1/00, B64G 1/10, B64G 1/24. Method of orbital flight of a space object: (in Ukrainian). Shuvalov V. O., Degtyarenko P. G., Simanov V. G., Khorolsky P. G., Loboda P. I. u201709603; applied 02.10.2017; published 05.10.2018.

(Patent of the EU for the invention № EP1989112) Patent of the EU for the invention № EP1989112, IPC B64G 1/24. Satellite Air Brake Wing Structure. Peipuda V., Le Couls O. EP07712219A; applied 14.02.2007; published 12.11.2018.

(Patent of the Russian Federation for the invention No. 2463223) Patent of the Russian Federation for the invention No. 2463223, IPC B64G3/00. A method for determining and predicting the motion of a spacecraft in low orbits subject to the influence of braking in the atmosphere. Nazarenko A. I., Klimenko A. G. 2011112179/11; applied 03.30.2011; publ. 10.10.2012, Bull. No. 28.

(Pedley, 2001) Pedley M., Mayeaux B. TransHab Materials Selection. Aerospace Materials, Processes & Environmental Technology. 2001. URL: https://ntrs.nasa.gov/archive/nasa/ casi.ntrs.nasa.gov/20010067265.pdf (access date 12.12.2022).

(Pelton, 2015) Pelton J. N. New solutions for the space debris problem. Springer. 2015. 94 p.

(Pfisterer, 2011) Pfisterer M., Schillo K., Val. C., Lin K.-C, Ham C. The Development of a Propellantless Space Debris Mitigation Drag Sail for LEO Satellites. Space Mission Analysis and Design. 2011. URL: http://www.iiis.org/Chan.pdf (access date 30.04.2020).

(Picone, 2002) Picone J. M., Hedin A. E., Drob D. P., Aikin A. C. NRLMSISE-00 empirical model of the atmosphere: Statistical comparisons and scientific issues. Journal of Geophysical Research. Vol. 107. No. A12. URL: https://agupubs.onlinelibrary.wiley.com/doi/epdf/10.1029/2002JA009430 (access date 10.08.2020).

(Pisarenko, 1988) Pisarenko G. S., Yakovlev A. P., Matveev V. V. Handbook of Strength of Materials (in Russian). 2nd ed. revised and improved. Kyiv, 1988. 736 p.

(Possner, 2018) Possner A., Wang H., Wood R., Caldeira K. and Ackerman T. P. The efficacy of aerosol—cloud radiative pertur-bations from near-surface emissions in deep open-cell stratocumuli. *Atmos. Chem. Phys*. 2018. Vol. 18. No. 23. P. 17475—17488. URL: https://doi.org/10.5194/acp-18-17475-2018 (access date 09.03.2023).

(PW-SAT2…, 2014) PW-SAT2 Critical design review. Project overview. 2014 URL : https://pw-sat.pl/wp-content/uploads/2014/07/PW-Sat2-C-00.00-Overview-CDR.pdf (access date 24.03.2021).

(Rasse, 2014) Rasse B., Damilano P., Dupuy C. Satellite inflatable deorbiting equipment for LEO spacecrafts. *Journal of Space Safety Engineering*. 2014. Vol. 1. No. 2. P. 75—83.

(Roberts, 2002) Roberts P. C. E., Bowling T. S., Hobbs S. E. MUSTANG: A technology demonstrator for formation flying and distributed systems technologies in space. *Proceedings of 5th conference Dynamics and control of systems and structures in space*. Kings College, Cambridge, July 2002. URL: https://dspace.lib.cranfield.ac.uk/ bitstream/handle/1826/881/MUSTANG-formation%20flying%20in%20space-2002.pdf?sequence=1&isAllowed=y (access date 24.03.2021).

(Roddy, 2016) Roddy M., Huang Po-Hao A. Development of a solid-state inflation bal.on for aerodynamic drag assisted deorbit of CubeSats. The University of Arkansas, Fayetteville Arkansas, USA. Published 2016. URL: http://www.unisec-global.org/ddc/pdf/1st/06_MorganRoddy_pre.pdf (access date 22.04.2019).

(Saletta, 2016) Saletta M., Orman-Rossiter K. Inflatable modules could be the future of space habitats. PHYS&ORG — April, 2016, URL: phys.org/pdf379750813.pdf (access date 17.12.2022).

(Sánchez, 2015) Sánchez J-P., McInnes C. R. Optimal Sunshade Configurations for Space-Based Geoengineering near the Sun-Earth L1 Point. *PLoS ONE*. 2015. Vol. 10. No. 8: e0136648. URL: https://doi.org/10.1371/journal.pone.0136648 (access date 10.03.2023).

(Shalin, 1996) Shalin R. E., Efremov I. S., Yarovinskiy Yu. L., Lukin V. I. Experience in design and manufacturing of large-size structures from aluminum-lithium al.ys for rocket-space engineering products (in Russian). Welding production. № 11. 1996. URL: https://viam.ru/sites/default/files/scipub/1996/1996-202092.pdf (access date 14.08.2020).

(Shan, 2018) Shan M., Guo J., Gill E. Review and comparison of active space debris capturing and removal methods. *Progress in Aerospace Sciences*. 2015. Vol. 80. P. 18—32.

(Shuvalov, 2014) Shuvalov V. A., Pismenny N. I., Kochubey G. S., Tokmak N. A. Mass loss of spacecraft polyimide films exposed to atomic oxygen and vacuum ultraviolet radiation (in Russian). Space research. 2014. Vol. 52. No. 2. P. 106—112.

(Shuvalov, 2016) Shuvalov V. A., Tokmak N. A., Pis'mennyi N. I., Kochubei G. S. Dynamic Interaction of a Magnetszed Body with a Rarefied Plasma Flow. *Journal of Applied Mechanics and Technical Physics*. 2016. R.57. №1. P. 145—152.

(Shuvalov, 2018a) Shuvalov V. A., Gorev N. B., Tokmak N. A., Pis'menny N. I., Kochubei G. S. Control of the drag on a spacecraft in the earth's ionosphere using the spacecraft's magnetic field. *Acta Astronautica*. 2018. Vol. 151. P. 717—725.

(Shuvalov, 2018b) Shuvalov V. A., Kuchugurny Yu. P. Experimental substantiation of the concept of an artificial mini-magnetosphere as a means of controlling the movement of spacecraft in the Earth's ionosphere (in Russian). *Space science and technology*. 2018. V. 24. No. 2. P. 43—46.

(Sinn, 2012) Sinn T., Lücking C., Donaldson N. et al. StrathSat-R: Deploying inflatable cubesat structures in micro gravity. *Proceedings of 63rd International Astronautical Congress*. Naples, Italy, 2012. IAC-12-E2.3.7.

(Skorik, 2013) Skorik A. D. Methodology for selecting design parameters of aerodynamic systems for deorbiting space objects from near-Earth orbits. *Technical Mechanics*. 2013. No 3. P. 85—90.

(Smith, 2022) Smith W., Bhattarai U., MacMartin D. G., Lee W. R., Visioni D. & Kravitz B. et al. A subpolar-focused stratospheric aerosol injection deployment scenario. *Environmental Research Communications*. 2022. Vol. 4. No. 9. P. 1—15. URL: https://doi.org/ 10.1088/2515-7620/ac8cd3 (access date 08.03.2023).

(Sobolev, 2017) Sobolev I. A., Leonov V. V., Volkova T. V., Bechasnov P. M. Analysis of the concept of a long-term orbital station for servicing interorbital cargo traffic. *Engineering journal: science and innovation*. 2017, No 4. P. 1—19.

(Space…, 1996) Space Environmental Effects on Spacecraft: LEO Materials Selection Guide. NASA Contractor Report 4661. Part 1. URL: https://ntrs.nasa.gov/api/citations/19960000860/downloads/19960000860.pdf (access date 27.05.2023).

(Space environmental…, 1995) Space environmental effects on spacecraft. LEO materials selection guide: technical report. TRW Space & Electronics Group; chief E. M. Silverman. Redondo Beach, California, 1995. 502 p. NAS1-19291.

(Sproewitz, 2017) Sproewitz T., Seefeldti P., Grundmann J.-T., Spietz P., Toth N. & Hillebrandt M. et al. Design of the Gossamer-1 Deployment Demonstrator. *The Fourth International Symposium on Solar Sail*. 2017. URL: http://www.jsforum.or.jp/ISSS2017/papers/paper/17023_Paper_Mr.%20Tom%20Sproewitz.pdf (access date 30.04.2020).

(State of the Geomagnetic…, 2023) State of the Geomagnetic Field. NOAA. December 2023. URL: https://www.ncei.noaa.gov/sites/g/files/anmtlf171/files/2023-12/WMM_Annual_Report_2023.pdf (access date 30.12.2023).

(State Standard 25645.302-83) State Standard 25645.302-83. Calculations of bal.stic artificial satellites of the Earth. Methodology for calculating solar activity indices (in Russian). Valid from 1985-01-01. Moscow, 1983. 21 p.

(State Standard R 25645.166-2004) State Standard R 25645.166-2004. Earth's upper atmosphere. Density model for bal.stic flight support for artificial earth satellites (in Russian). Valid from 09/03/2004. Moscow, 2004. 28 p.

(Stohlman, 2014) Stohlman O., Schenk M., Lappas V. Development of the Deorbit sail flight model. In proceedings of AIAA Spacecraft Structures Conference, 13-17 January 2014, National Harbor, Maryland. AIAA 2014-1509 URL: http://www.markschenk.com/research/files/AIAA2014_DeorbitSail.pdf (access date 30.04.2020).

(Sutton, 2010) Sutton G. P., Biblarz O. Rocket Propulsion Elements. Eighth Edition. John Wiley & Sons, Inc., 2010. 784 p.

(Svorobyn, 2018) Svorobyn D. S., Fokov A. A., Khoroshilov S. V. Analysis of the feasibility of using an aerodynamic compensator for contactless removal of space debris (in Russian). Aerospace engineering and technology. 2018. No. 6(150). P. 4—11.

(The Echo-I…, 1964) The Echo-I inflation system. Langley research center; chief D. L. Clemmons Jr. Hampton, Virginia, 1964. 56 p. № TN D-2194.

(The Orbital Debris Quarterly News, 2020) *The Orbital Debris Quarterly News*. NASA JSC Houston. 2020. Issue 2. Vol. 24. P 11—12.

(Theresa, 2021) Theresa D. Can A Change In Orbit Save Planet Earth? October 12, 2021. URL: https://bigthink.com/starts-with-a-bang/giant-thruster-migrate-earth/ (access date 06.03.2023).

(Thunnissen, 1991) Thunnissen D. P. Low-Mass Inflation Systems for Inflatable Structures. D. P. Thunnissen, M. S. Webster, C. S. Engelbrecht. Jet Propulsion Lab. 1991. 22 p. URL: http://ntrs.nasa.gov/archive/nasa/ casi.ntrs.nasa.gov/19960054146.pdf (access date 03.12.2014).

(Ti 6Al 4V…) Ti 6Al 4V (Grade 5) Titanium Alloy Data Sheet. URL: https://kyocera-sgstool.co.uk/titanium-resources/titanium-information-everything-you-need-to-know/ti-6al-4v-grade-5-titanium-al.y-data-sheet/#:~:text=Titanium%206al-4v%20has%20a%20density%20of%204.43%20g%2Fcc (access date 14.08.2020).

(Titanium Ti-5…) Titanium Ti-5Al-2Sn-2Zr-4Mo-4Cr (Ti-17) Beta Processed. Matweb. URL: https://www.matweb.com/search/datasheet_print.aspx?matguid=a33b3d2218204cb0b6f84724768a4176 (access date 14.08.2020).

(Titanium Ti-10…) Titanium Ti-10V-2Fe-3Al (Ti 10-2-3) Solution Treated 850°C (1560°F). Matweb. URL: https://www.matweb.com/search/ DataSheet.aspx?MatGUID=e810947a42894199adec39058992b53a&ckck=1 (access date 15.08.2020).

(Titanium IMI…) Titanium IMI 829 (Ti-5.5Al-3.5Sn-3Zr-1Nb-0.25Mo-0.3Si). Matweb. URL: https://www.matweb.com/search/datasheet.aspx?matguid=f76e8131f6fb427ba943a92882273970&n=1 (access date 15.08.2020).

(Upilex…) Upilex. UBE Polyimide Film Exhibits Industry Leading Heat Resistance. URL: https://www.ube.com/upilex/catalog/pdf/upilex_s_e.pdf (access date 20.05.2023).

(US patent for invention № 6830222…, 2004) US patent for invention № 6830222, IPC B64G1/62. Bal.on device for lowering space object orbits. Nock K. T. 10/394,477; appl. 05.21.2003, publ. 14.12.2004.

(US Patent No. 5345238, 1994) US Patent No. 5345238, IPC H1Q15/16. Satellite signature suppression shield. Eldridge M. T., VcKechnie K. H., Helfey R. M. 494278; applied 14/03/90; published 06/09/94.

(US patent for the invention № 6550720) US patent for the invention № 6550720, IPC B64G1/22. Fliter Aerobraking orbit transfer vehicle. DeBra D.B., Gloyer P., Wahl Z., Goldshtein D. 09/925207; applied on August 9, 2001, published on April 22, 2003.

(U.S. Patent for invention No. 6220548) U.S. Patent for invention No. 6220548, IPC7 B 64 G 1/50. Deployed equipment modules for satellite architecture improvement. Hyman N. L. 09/153416; applied 14.09.1998; published 24.04.2001.

(Viquerat, 2014) Viquerat A., Schenk M., Sanders B., Lappas V. Inflatable rigidisable mast for end-of-life deorbiting system. ESA. URL: http://www.markschenk.com/research/files/SSMET2014-InflateSail.pdf (access date 22.04.2019).

(Visagie, 2015) Visagie L. Gossamer sails for satellite de-orbiting, mission analysis and applications. PhD dissertation. Surrey, 2015. 189 p. GU27XH, UK. URL: https://pdfs.semanticscholar.org/cf41/ee46e8bb923bd452459c3f8f4ec412aa2276.pdf (access date 30.04.2020).

(Vitinsky, 1973) Vitinsky Yu. I. Cyclicity and forecasts of solar activity (in Russian). Leningrad, 1973. 258 p.

(Voloshenyuk, 2011) Voloshenyuk O. L., Pirozhenko A. V., Khramov D. A. Space tether systems as a promising area of space engineering and technology (in Russian). *Space science and technology*. 2011. V. 17. No. 2. P. 32—44.

(Wang, 2023) Wang Changqinq, Palii O. S. Mathematical model for determining the design parameters of a deorbit system's aerodynamic elements. *Technical mechanics*. 2023. Vol. 3. P. 35—50. URL: https://doi.org/10.15407/itm2023.03.035

(Williams, 2017) Williams K. NASA's Exo-Brake 'Parachute' to Enable Safe Return for Smal. Spacecraf. 2017. URL: https://www.nasa.gov/directorates/ spacetech/smal.spacecraft/feature/exo-brake_ parachute (access date 30.04.2020).

(Wolanski, 2012) Wolanski P. PW-SAT first polish satellite. *S&T Subcommittee of COPUOS*. 2012. URL: http://www.oosa.unvienna.org/pdf/pres/ stsc2012/tech-44E.pdf (access date 30.04.2020).

(Wood…) Wood R. Marine cloud brightening project. URL: https://faculty.washington.edu/robwood2/wordpress/?page_id=954 (access date 23.03.2023).

(Wormnes, 2013) Wormnes K., Le Letty, R., Summerer L., Schonenborg R., Dubois-Matra O. & Luraschi E. et al. ESA technologies for space debris remediation. *In: 6th European Conference on Space Debris, Darmstadt*, Germany. 22 April, 2013. Vol. 1. P. 1—8.

(Xin, 2011) Xin M., Pan H. Nonlinear optimal control of spacecraft approaching a tumbling target. *Aerospace Science and Technology*. 2011. Vol. 15. No. 2. P. 79—89.

(Yavorsky, 2006) Yavorsky B. M. Detlaf A. A. Lebedev A. K. Reference book on physics for engineers and university students (in Russian). 8th edition revised and corrected. Moscow, 2006. 1056 p.

(Yoshida, 2004) Yoshida K., Nakanishi H., Ueno H., Inaba N., Nishimaki T. & Oda M. Dynamics, control and impedance matching for robotic capture of a non-cooperative satellite. *Advanced Robotics*. 2004. Vol. 18. No. 2. P. 175—198.

(Zbrutskii, 2011) Zbrutskii, A. V., Ganzha, A. P. Navigation of the Earth remote sensing satellite by land surface imagery (in Russian). National technical university "Kyiv Polytechnic Institute" Publishing House, 2011. 160 p.

(Zinner, 2011) Zinner N., Williamson A., Brenner K., Curran J. B., Isaak A. et al. Junk hunter: Autonomous rendezvous, capture and de-orbit of orbital debris. *Revolutionary Aerospace Systems Concepts — Academic Linkage (RASCAL) conference*, 2011. URL: http://rascal.nianet.org/wp-content/uploads/2015/07/2011-RASC-AL-UCB-Tech-Paper.pdf (access date 24.03.2021).

(Zubrin, 2014) Zubrin R. Moving the Earth. *The Space Review*. 2014. URL: https://www.thespacereview.com/article/2547/1 (access date 06.03.2023).

У монографії розглянуто особливості проєктування космічних аеродинамічних систем для пасивного керування космічними апаратами. Однією з цілей використання такої технології є відведення фрагментів космічного сміття з робочих орбіт. Розроблено класифікацію аеродинамічних системи відведення. Класи аеродинамічних систем розподіляються за різними критеріями: ступенем жорсткості аеродинамічного елементу, за способом формоутворення аеродинамічні системи відведення, за ознакою модульності конструкції аеродинамічного елементу, на групи з використанням трансформації елементів конструкції об'єкта залежно від типу матеріалу тощо.

Для наукових і інженерно-технічних працівників, які працюють у галузі ракетно-космічної техніки, а також для аспірантів і студентів відповідних спеціальностей.

Наукове видання

ДЕРЖАВНЕ КОСМІЧНЕ АГЕНТСТВО УКРАЇНИ
НАЦІОНАЛЬНА АКАДЕМІЯ НАУК УКРАЇНИ
ІНСТИТУТ ТЕХНІЧНОЇ МЕХАНІКИ

АЛПАТОВ Анатолій Петрович
ЛАПХАНОВ Ерік Олександрович
ПАЛІЙ Олександр Сергійович

АЕРОДИНАМІЧНІ СИСТЕМИ ПАСИВНОГО КЕРУВАННЯ ОРБІТАЛЬНИМ РУХОМ КОСМІЧНИХ ОБ'ЄКТІВ

Англійською мовою

Переклад *Т.О. Пилипенко*

Редактор *В.К. Рего*

Художнє оформлення *Є.О. Ільницького*
Технічне редагування *Т.М. Шендерович*
Виготовлення ілюстрацій *О.В. Туровського*
Комп'ютерна верстка *С.В. Кубарєва*

Підп. до друку 13.12.2024. Формат 70 × 100/16. Гарн. Minion Pro.
Ум. друк. арк. 13,98. Обл.-вид. арк. 15,13. Тираж 100 прим. Зам. № 7529.

Видавець і виготовлювач Видавничий дім "Академперіодика" НАН України
01024, Київ, вул. Терещенківська, 4

Свідоцтво про внесення до Державного реєстру суб'єктів
видавничої справи серії ДК № 544 від 27.07.2001 р.